Amine-bis(phenolate) Complexes of Chromium for Carbon dioxide/Cyclohexene Oxide Copolymerization and Group(I) and (II) Complexes for the Ring Opening Polymerization of rac-Lactide

by

A Thesis submitted to the

School of Graduate Studies

in partial fulfillment of the requirements for the degree of

Doctor of Philosphy

Chemistry Department

Memorial University of Newfoundland

January 2017

St. John's Newfoundland

ABSTRACT

Finding novel methods for polymer synthesis has been of particular interest as of late from both a chemical and commercial standpoint. This focus stems from the recognized need for biodegradable and biocompatible polymers, originating from renewable resources, and is a legitimate endeavor by society to ease the burden imposed on the environment. Society's conscience also recognizes the great need to utilize the carbon dioxide that is released in the atmosphere and it continues to make noble efforts in order not to contribute further to the greenhouse effect caused by greenhouse gases such as carbon dioxide. Therefore, the use of carbon dioxide as a starting material and the incorporation of it in the product of a chemical synthesis are currently developing research areas. Accordingly, combining the aim of environmentally friendly polycarbonate synthesis with incorporation of carbon dioxide in the polymer chain was the goal of the research conducted in the first part of this thesis. Additionally, biodegradable and biocompatible polylactide from lactide, originating from renewable feedstocks, was produced by biocompatible complexes in the second part.

Polycarbonate synthesis was carried out in the presence of novel chromium(III) catalysts which were synthesized via salt metathesis reactions from tetradentate tripodal amine-bis(phenol) ligands. The complexes were characterized by MALDI-TOF mass spectrometry, UV-Vis and IR spectroscopy, magnetic susceptibility measurement and elemental analysis. The catalyst precursors selectively produced polycarbonates from epoxides and carbon dioxide with high yields and moderate molecular weights. Mechanistic studies revealed a first order dependence on catalyst concentration and that

ring opening of the epoxide was initiated by a nucleophilic species originating either from the complex or from an externally added nucleophile.

Biocompatible magnesium-, lithium-, sodium-, potassium- and calcium complexes of an amino-bis(phenolato) ligand were also prepared and characterized for the synthesis of polylactide, a biodegradable and biocompatible polymer. The magnesium and the sodium complexes in particular showed high catalytic activity and good control over the reaction. The complexes were active even under relatively low catalyst loading (0.1 – 0.2 mol%) and produced polymers of high purity as revealed by NMR, DSC and TGA.

ACKNOWLEDGEMENTS

I express my deepest gratitude to my supervisor, Dr. Christopher M. Kozak, for accepting me as a graduate student and providing guidance throughout my program at Memorial University in his research group. His continuous support, advice and effective suggestions made it possible to conduct my research in both an effective and an enjoyable manner. I will never forget his educational consultations where he taught me how to think critically or how to write in a professional way. His style of teaching and supervision gave me a solid basis to rely on in my future endevours. I also express my special thanks to Dr. Francesca Kerton and my supervisory committee members, Dr. Karen Hattenhauer and Dr. Erika Merschrod who always supported me and also helped me to edit my thesis.

I am also thankful to Dr. Louise N. Dawe and Julie Collins for solving my crystal structures, Dr. Celine Schneider for her help with NMR, Linda Winsor for MALDI training and help, Dave Stirling for making it possible to perform UV-Vis as well as magnetic susceptibility measurements and Nick Ryan for helping me with IR data collection.

I thank NSERC (Dr. Kozak's research grant), Department of Chemistry, School of Graduate Studies (SGS), Graduate Students' Union (GSU) and Memorial University for funding. Their financial support contributed greatly to the successful completion of my studies, alleviating the stress of fiscal obligations.

I would like to thank all the past and present students of the Green Chemistry and Catalysis Group who welcomed me in the group and organized numerous social events to get to know each other. A special thank-you to Justin Bélanger, Rebecca Dean and Nduka Ikpo who were always there whenever I needed help. I also thank Tiber Reardon, Hart Plommer, Yi Liu, Ali Elkurtehi and Dalal Alhashmialameer for their words of encouragement, scientific discussions and/or assistance with my thesis.

Last but not least, I want to express my profound gratitude to my family members, my parents (László and Erzsébet) and my brother (László) who always supported me and also helped me to edit my thesis. I especially thank my husband (Tibor) and my daughters (Kata and Lilien) for all the patience, understanding and encouragement that they offered during my program.

This thesis is dedicated to my father who I admire for his willpower because he has undergone several surgeries and treatments and is still undergoing several therapies and rehabilitation.

Table of Contents

List of Tables

List of Figures

List of Schemes

List of Abbreviations and Symbols

CH_3CN: acetonitrile

et al.: and others

AMM: activated monomer mechanism

E_a: activation energy

Å: Angstrom (10^{-10} m)

ATR: attenuated total reflectance

BASF: Baden Aniline and Soda Factory

BnOH: benzyl alcohol

BPA: bisphenol A

salan: N,N'-bis(phenolato)-1,2-diaminoethane

salen: N,N'-bis(salicylidene)-ethylenediamine

salphen: N,N'-bis(salicylidene)-1,2-diaminobenzene

$PPNN_3$: bis(triphenylphosphoranylidene)iminium azide

PPNCl: bis(triphenylphosphoranylidene)iminium chloride

PPN(2,4-DNP): bis(triphenylphosphoranylidene)iminium 2,4-dinitrophenolate

μ_B: bohr magneton

br: broad

^{n}BuLi: n-Butyllithium

CaH_2: calcium hydride

CO_2: carbon dioxide

CL: ε-caprolactone

C: Celcius

CTA: chain transfer agent

δ: chemical shift

Cl^-: chloride

$CHCl_3$: chloroform

CIM: coordination-insertion mechanism

CLARITY-BPA: Consortium Linking Academic and Regulatory Insights on BPA Toxicity

J: coupling constant (NMR)

CCS: carbon capture and sequestration/storage

cm: centimetre (10^{-2} m)

CHC: cyclohexene carbonate

CHO cyclohexene oxide

(°): degree

DFT: density functional theory

C_6D_6: deuterated benzene

$CDCl_3$: deuterated chloroform

Py-d_5: deuterated pyridine

Tol-d_8: deuterated toluene

CH_2Cl_2: dichloromethane

Et_2Zn: diethyl zinc

DSC: differential scanning calorimetry

DHBA: 2,5-dihydroxybenzoic acid

BDI: β-diketiminate

DMAP: 4-(dimethylamino) pyridine

DMF: dimethylformamide

BHT: 2,6-di-t*ert*-butyl-4-methyl-phenol

d: doublet

dd: double of doublets

μ_{eff}: effective magnetic moment

ESI: electrospray ionization

EtOH: ethanol

EDBP: 2,2'-ethylidene-bis(4,6-di-*tert*-butylphenol)

equiv.: equivalent

ε: molar extinction coefficient ($M^{-1}cm^{-1}$)

FDA: Food and Drug Administration

FTIR: Fourier transform infrared

GPC: gel permeation chromatography

T_g: glass transition temperature

G: gram

X^-: halogen anion

h: hour

OH^-: hydroxyl ion

iROP: immortal ring opening polymerization

IR: infrared

IEA: International Energy Agency

IUPAC: International Union of Pure and Applied Chemistry

in vivo: “in a living organism”

in situ: “in the reaction mixture”

*i*PrOH: isopropyl alcohol

K: Kelvin

kcal: kilocalorie

kg: kilogram

LA: lactide

MS: mass spectrometry

m/z: mass-to-charge ratio

MALDI-TOF: matrix assisted laser desorption/ionization time-of-flight

λ_{max}: maximum wavelength

MeOH: methanol

N-MeIm: 1-methylimidazole

mg: milligram (10^{-3} kg)

mL: millilitre (10^{-3} L)

mmol: millimole (10^{-3} mol)

min: minute

m: multiplet (in NMR)

nm: nanometre (10^{-9} m)

NIEHS: National Institute of Environmental Health Sciences

NMR: nuclear magnetic resonance

Nu: nucleophile

M_n: number average molecular weight

M_w: weight average molecular weight

ORTEP: Oak Ridge thermal-ellipsoid plot program

trans: “on the other side”

cis: “on the same side”

PC: polycarbonate or propylene carbonate

PCHC: poly(cyclohexene carbonate)

ppm: parts per million

Đ: dispersity

PGA: poly(glycolide)

PIB: polyisobutylene

PLA: polylactide

PPC: poly(propylene carbonate)

PO: propylene oxide

rac: racemic

ROP: ring opening polymerization

s: singlet (in NMR)

NaTFA: sodium trifluoroacetate

SQUID: superconducting quantum interference device

$scCO_2$: supercritical carbon dioxide

TBAB: tetrabutylammonium bromide

THF: tetrahydrofuran

TPP: 5,10,15,20 tetraphenylporphyrinato

TGA: thermal gravimetric analysis

t/year: tons per year

Et_3N: triethylamine

TOF: turnover frequency

TON: turnover number

U.S.: United States of America

UV-Vis: ultraviolet-visible

VT: variable temperature

VCHO: 4-vinylcyclohexene oxide

vs.: “versus”

List of Appendices

Chapter 1. Introduction

1.1 Epoxide/CO_2 copolymerization with chromium complexes and mechanistic studies of the reaction

1.1.1 Overview of polycarbonate synthesis

Due to the fact that polycarbonates are durable, transparent, moldable, light and shatter resistant, they are very popular and widely used in the polymer world.[1-4] The conventional synthesis of polycarbonates involves the reaction of Bisphenol A (BPA) with the highly toxic phosgene (Scheme 1-1), which provided the platform so far for the production of the polycarbonate needed for human activities, which is more than 2.5 million metric tons per year.[5]

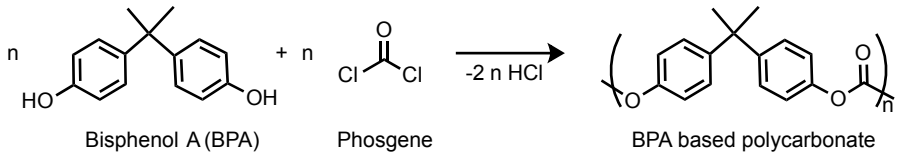

Scheme 1-1 Synthesis of BPA based polycarbonate

Bisphenol A is an organic diphenylmethane molecule, which contains two hydroxyphenyl groups. Its IUPAC (International Union of Pure and Applied Chemistry) name is 4,4'-(propane-2,2-diyl)diphenol. Polycarbonates synthesized from BPA are frequently used as protective lining material in cans, reusable beverage bottles, tableware and storage containers.[6] Concerns were expressed when traces of BPA were found to leach out of the polymers and started to appear as a contaminant even in ground water in parts of the U.S.[5] Numerous studies have been started to investigate the negative effects

of BPA on the endocrine function or the reproductive system of humans.[5] The exposure to BPA – since it is suspected to be an endocrine disruptor – was restricted to 0.05 mg/kg body weight by the European Food Safety Authority in 2006 and it was banned from use in the production of baby bottles in the European Union and Canada in 2010.[7] Recently, several groups who support the production of BPA polycarbonates such as the PlasticsEurope's PC/BPA (Polycarbonate/Bisphenol A) group, an Association of Plastics Manufacturers started to doubt the findings on these negative health effects and claimed that the results could be associated with other factors such as food consumption and lifestyle.[8] According to their website, there are several positive properties of BPA-based polycarbonates. They are very durable, basically unbreakable, resistant to heat and chemicals, transmit light, and are of low weight and high flexibility. The PlasticsEurope PC/BPA group also list the possible health risks associated with BPA, such as it may contribute to the development of type 2 diabetes or act as an endocrine disruptor. At the same time, they include scientific research results concluding that normal day-to-day exposure to BPA is so minimal that it cannot cause any of the listed adverse health effects. Nevertheless, the protesters' main argument is that if a substance poses any risk to human health, its usage should be avoided. To address the controversy around BPA, the U.S. National Institute of Environmental Health Sciences (NIEHS) together with the Food and Drug Administration (FDA) started a chronic toxicity study called Consortium Linking Academic and Regulatory Insights on BPA Toxicity (CLARITY-BPA). The midterm update on the main project was published in July 2015 and the finalized results are expected to be available in 2018.[9] A study on the effects of BPA on spatial navigational learning was already published within the CLARITY-BPA project.[10] In the

end, the controversial situation launched a great number of research opportunities on finding greener and safer alternatives to replace BPA[7] as well as phosgene in polycarbonate synthesis.[11,12] The BPA based polycarbonate synthesis depicted in Scheme 1 carries another health risk, that is, it needs a great amount of dichloromethane (CH_2Cl_2), which is a suspected human carcinogen. Although the CH_2Cl_2 layer is separated from the water after the reaction, it is very difficult to prevent CH_2Cl_2 release to the environment due to its solubility in water (17.5 g/L at 25 °C).[1] Overall, new, greener alternative synthetic routes to produce polycarbonates with the same or similar properties are more than welcome in this field. One possibility is the reaction of epoxides with carbon dioxide.[13]

1.1.2 CO_2 as a feedstock

Concerns have been raised recently on the CO_2 released by burning fossil fuels causing destructive effects to the environment, such as global warming, ocean acidification and rising sea levels.[14] It is well-known that the concentration of CO_2 is continuously increasing in the atmosphere and its rate of increase is about 1.9 parts per million (ppm) per year.[15] An example of this increase was measured at Mauna Loa, Hawaii where in 1958 the concentration of CO_2 was measured as 310 ppm there, which increased to 390 ppm by 2012.[14] The International Energy Agency (IEA) predicts an increase to about 550 ppm by 2050 together with an increase of CO_2 emission (62 billion t/year, in 2012 it was 29 billion t/year) and a temperature increase of about 3 – 4 °C.[16] The increasing concentration of CO_2 coupled with the threatening signs of its

consequences has opened up new areas for research regarding how to decrease the amount of CO_2 released to the atmosphere. One of the possibilities is to sequester CO_2 at the source where it is released, such as a coal burning power plant or a refinery.[17] Moreover, the capture of CO_2 can be directly linked to its application. For example, the sequestered CO_2 as a by-product of ammonia synthesis can be directly used for urea synthesis.[17] Carbon capture and sequestration (CCS), however, has some limitations which require a lot of attention including the transportation of CO_2 and the storage site of the sequestered CO_2 both of which have to be chosen wisely in order to avoid the leakage of CO_2.[14] The direct capture of CO_2 from air has also attracted much attention.[14] For example, direct CO_2 capture with amines requires less energy and thus seems cost-effective. BASF (Baden Aniline and Soda Factory) has already tested a new amine-based state-of-the-art CO_2 capture technology in two pilot plants (Germany and Japan).[18] The results are very promising for post-combustion CO_2 capture and compression with low energy requirement and cost.

Utilization of CO_2 as a chemical feedstock may be an additional means to the decrease in atmospheric CO_2 on the long term, especially if industrial CO_2 is captured and used for reactions.[16,17] A recent study conducted by Stolten and co-workers has evaluated 23 bulk chemicals and 100 fine chemicals with regards to their production from flue gas and a resultant decrease in CO_2 emission.[19] They found that five bulk and five fine chemicals met the very strict selection criteria. The production of the bulk chemicals – formic acid, oxalic acid, formaldehyde, methanol, dimethyl-ether and urea – could contribute to a 0.43% decrease in CO_2 emission in the European Union, which

means a significant decrease in CO_2 released of approximately 20 million tons per year. The production of the fine chemicals – methylurethane, 3-oxo-pentanedioic acid, 2-imidazolidinone, ethylurethane, 2-oxazolidone and isopropyl isocyanate – would result in a lower (0.029%) decrease in greenhouse gases. Still, this study further supported the ongoing research and a foreseeable future where waste/by-product CO_2 is utilized for a wide range of reactions. Several reviews and books have been published already where CO_2 is utilized as a feedstock,[4,15,17,20-22] and all of them mention the importance of catalysis in order to convert the very stable CO_2 into valuable chemicals. Figure 1.1 illustrates the difference between a catalyzed and a non-catalyzed reaction of the same synthesis. Catalysis together with applying starting materials with high free energy, such as epoxides help to lower the activation energy and therefore, the energy requirement needed to convert CO_2 into cyclic or polycarbonates.[13,17,20]

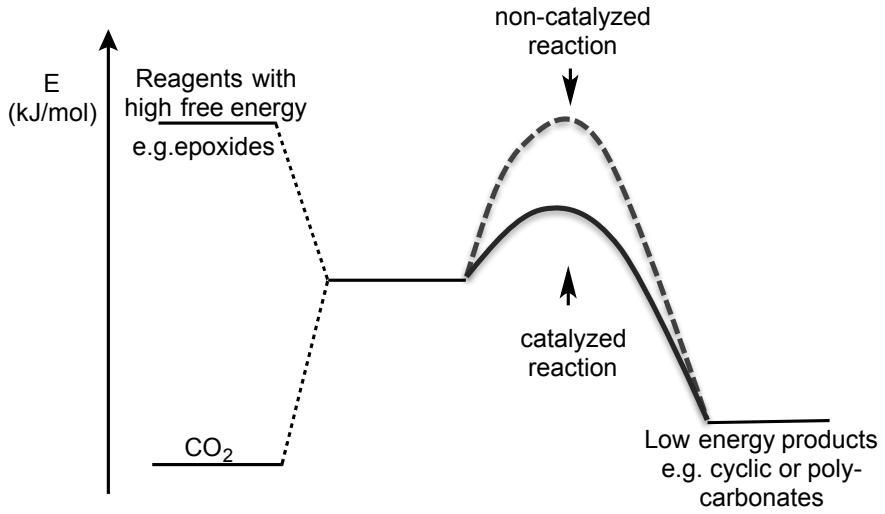

Figure 1.1 General reaction profile for the reaction of CO_2 and high energy reactants to produce low energy products.

1.1.3 Catalytic conversion of carbon dioxide with epoxides

The reaction between epoxides and CO_2 is usually carried out with a suitable epoxide, a Lewis acid catalyst and a nucleophile (Scheme 1-2). The most commonly applied epoxides are propylene oxide (PO), cyclohexene oxide (CHO) and styrene oxide, but the substituted analogues of these epoxides are sometimes tested, for example 4-vinylcyclohexene oxide (VCHO)[23,24] or epichlorohydrin [25-27]. The nucleophile can come from the catalyst or can be added externally as co-catalyst, and can be neutral, such as 4-(dimethyl amino) pyridine (DMAP) and N-methylimidazole (NMeIm) or ionic, such as bis(triphenylphosphine) iminium chloride (PPNCl) and bis(triphenylphosphine) iminium azide ($PPNN_3$) (Figure 1.2).

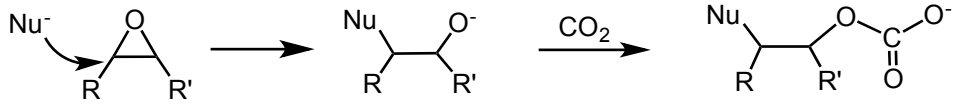

Scheme 1-2 General scheme of the reaction of carbon dioxide with an epoxide.

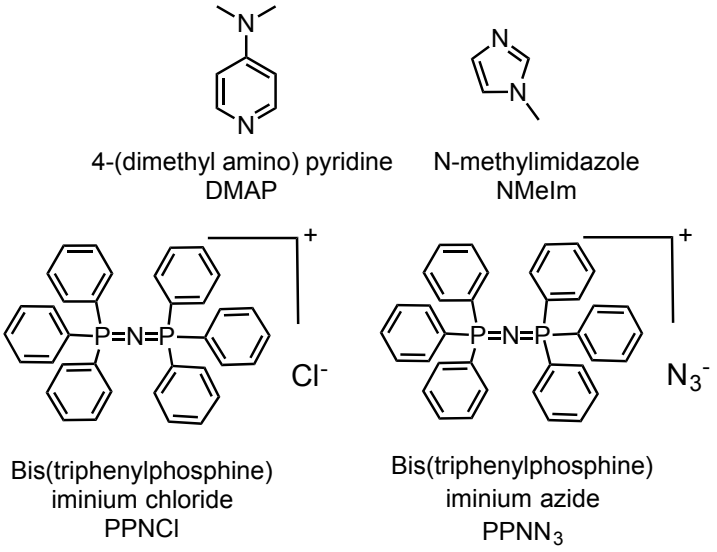

Figure 1.2 Structures of commonly used co-catalysts.

The Lewis acid catalyst may be a complex of a main group element, such as magnesium or aluminum, or a transition metal such as cobalt, chromium, zinc, etc. The reaction, usually but not always, needs high pressures of CO_2 and high temperature depending on the epoxide species, the desired product and the type of catalyst.

1.1.4 Brief history of epoxide/CO_2 copolymerization

The first step in catalyst design for the copolymerization of carbon dioxide and epoxide was taken when Inoue and co-workers successfully used a heterogeneous catalyst obtained using a 1:1 mixture of Et_2Zn and H_2O in 1969.[28] Although the activity of the catalyst was quite low in terms of turn over frequency (0.12 h^{-1}), the fact that the conversion of CO_2 with an epoxide and catalyst could be carried out was a significant discovery in itself and led to the synthesis of numerous, novel catalysts. Another improved system was developed by Soga *et al.* who found that the reaction of a 1:1 mol ratio of $Zn(OH)_2$ with dicarboxylic acids such as glutaric acid showed better activity than the Et_2Zn/H_2O system.[29] Zinc glutarate proved to be the most efficient catalyst, but high catalyst loading was necessary for the reaction resulting in poor reproducibility, most likely due to the presence of excess glutaric acid in the catalyst sample. The structure of zinc glutarate was later elucidated by Darensbourg[30] and Zheng *et al.*[31]

Homogeneous catalysts have the advantage of providing more details about the active sites of the metal and about the mechanism of the reaction. Moreover, product selectivity, molecular weight and molecular weight distribution can usually be controlled more efficiently when homogeneous catalysis is applied. An early example of a

homogeneous system is Inoue's aluminum porphyrin complex (**1.1**, Figure 1.3), (TPP)AlCl (TPP = 5,10,15,20-tetraphenylporphyrinato), with an ammonium or phosphonium bromide co-catalyst.[32] Polymer molecular weights were higher than before, between 3500 g/mol with propylene oxide (PO) and 7300 g/mol with cyclohexene oxide (CHO), and the molecular weight distributions were narrow showing dispersity indices very close to 1.

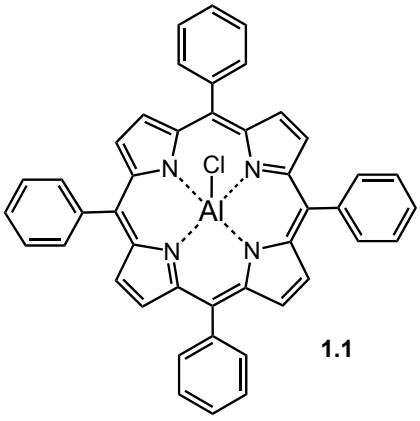

1.1

(TTP)AlCl
TPP = 5,10,15,20-tetraphenylporphyrinato

Figure 1.3 Structure of the Al-porphyrin complex used by Inoue and co-workers.

The next step in catalyst design for CO_2/epoxide copolymerization was the development of Zn-phenoxide catalysts (**1.2**, Figure 1.4) by Darensbourg and Holtcamp.[33] These complexes crystallize with a highly distorted tetrahedral geometry around the zinc centre. Conversions of CHO/CO_2 copolymerization were between 20 – 65% when high temperature (80 °C), high pressure (55 bar) along with long reaction time (69 h) were applied. In addition, the poly(cyclohexene carbonate) (PCHC) contained 9 – 10% undesired polyether linkages.

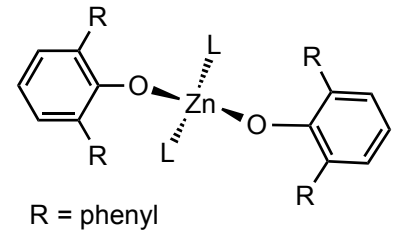

1.2

Figure 1.4 Structure of the Zn-phenoxide complex developed by Darensbourg and Holtcamp.

Later, the same research group further investigated the influence of reaction time, temperature, CO_2 pressure and the substituents on the phenolate moieties of the ligand of complex **1.2**.[34] The yield increased if there were electron-donating groups on the phenolates (R group of **1.2**), with the activity increasing upon going from isopropyl < phenyl < *tert*-butyl < methyl substituents. This is also in good agreement with their findings that less sterically demanding substituents at the 2,6 positions of the phenyl rings, such as methyl groups, enhanced polycarbonate formation, whereas the complex with bulky *tert*-butyl groups was capable of the homopolymerization of cyclohexene oxide. The authors speculated that the metal site was more easily-approachable for the CO_2 to be inserted first when there was no steric hindrance around the zinc centre. They concluded that the catalytic activity toward polycarbonate formation is dependent on both electronic (an electron-rich metal centre) and steric (a less hindered metal site) effects.

The positive effect of electron-donating groups of a pyridine ligand was also observed by Kim, Jang and co-workers when they investigated the activity of pyridine-Zn-halide complexes in cyclic carbonate formation.[35] They found that $[L_2ZnBr_2]$ complexes with electron-donating methyl groups (**1.3b** and **1.3c**, Figure 1.5) showed

higher activity than unsubstituted ones whereas complexes with electron-withdrawing chlorines (**1.3d,** Figure 1.5) showed very little activity.

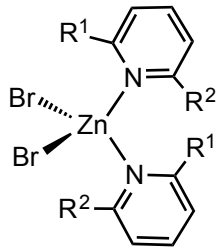

1.3a: $R^1 = R^2 = H$
1.3b: $R^1 = Me$, $R^2 = H$
1.3c: $R^1 = R^2 = Me$
1.3d: $R^1 = Cl$, $R^2 = H$

Figure 1.5 Structures of pyridine Zn-halide complexes synthesized by Kim, Jang and co-workers.

The next major step in catalyst design was the development of *ß*-diiminate Zn-complexes by the Coates research group (Figure 1.6).[36] They observed the highest activity with complex **1.4d** when they added an electron-withdrawing cyano group to the *ß*-diiminate ligand and applied a methyl and an isopropyl group at the phenyl rings. The reaction time was short (10 min) hence the turnover frequency (TOF) was very high (up to 2290 h^{-1}) compared to previously published complexes, but the synthesis of the complex was low-yielding (only 18%) and the conversion of cyclohexene oxide was reported to be approximately 40%.

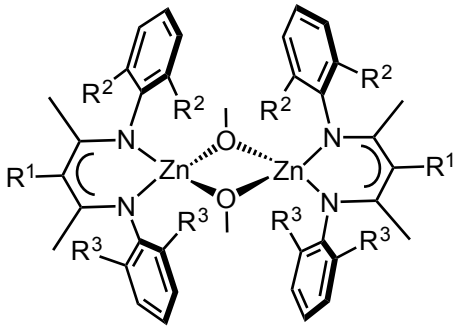

1.4a: R^1 = H, R^2 = R^3 = Et
1.4b: R^1 = CN, R^2 = R^3 = Et
1.4c: R^1 = CN, R^2 = Et, R^3 = *i*Pr
1.4d: R^1 = CN, R^2 = Me, R^3 = *i*Pr

Figure 1.6 Structure of *β*-diiminate Zn-complexes used by the Coates group.

Recently, perhaps the most studied catalysts have been derived from complexes with salicylaldimine (salen) ligands. The Darensbourg group extensively investigated the activity of Cr-salen complexes, which will be discussed in the next section. Besides the salen ligands, complexes with amine-bis(phenolate) ligands have also appeared as good candidates for CO_2/epoxide copolymerization.[37] Since the first appearance of amine-bis(phenol) ligands reported by Spence and co-workers,[38] they have been complexed with various metals, and their structural variation with different metals – including chromium – is studied in detail in a recent review.[39] Cr(III) amine-bis(phenolate) complexes are an ongoing area of investigation by the Kozak group and a discussion of the activity of these complexes is also included in the next section.

1.1.5 Chromium complexes in the copolymerization of carbon dioxide and epoxides

One of the first examples of a chromium complex used for catalyzing CO_2/epoxide copolymerization is a chromium porphyrin complex bearing

pentafluorophenyl substituents in the *meso*-positions reported by Holmes and co-workers (**1.5**, Figure 1.7).[40] With this catalyst, the group was able to obtain poly(cyclohexene carbonate) under supercritical conditions of CO_2. They obtained 90 – 95% carbonate linkages of the polymer with a dispersity less than 1.4 at 2000 psi CO_2 pressure (~ 140 bar), 110 ºC, within 18 h reaction time. The molecular weight of the polymer, however, was relatively low, usually below 4000 g/mol probably due to the high temperature applied (Table 1-1, entry 1). The research group tested the effect of temperature on copolymerization, which had a large effect on molecular weight (9570 g/mol at 110 ºC vs. 800 g/mol at 70 ºC). CO_2 pressure also had a dramatic effect mainly because at lower, CO_2 pressure (5.5 bar), only oligomeric material was obtained with very low yield and CO_2 incorporation. The molar ratio of catalyst to monomer and the reaction time did not have significant influence on the reaction and no further increase in M_n was observed after 8 h reaction time.

The same group later modified the catalyst into a polymer supported porphyrin (**1.6**, Figure 1.7) in order to be able to recycle it.[41] The porphyrin complex was attached to Argogel® chloride beads via an ether linkage. The molecular weights of the polymer produced with the solid supported porphyrin were between 3300 and 7100 g/mol and the dispersity values were between 1.30 and 1.70 (Table 1-1, entry 2) comparable to the results when **1.5** was used. Complex **1.6**, however, proved to be successfully recyclable, although a decrease in polymer molecular weight and yield was observed when it was re-used.

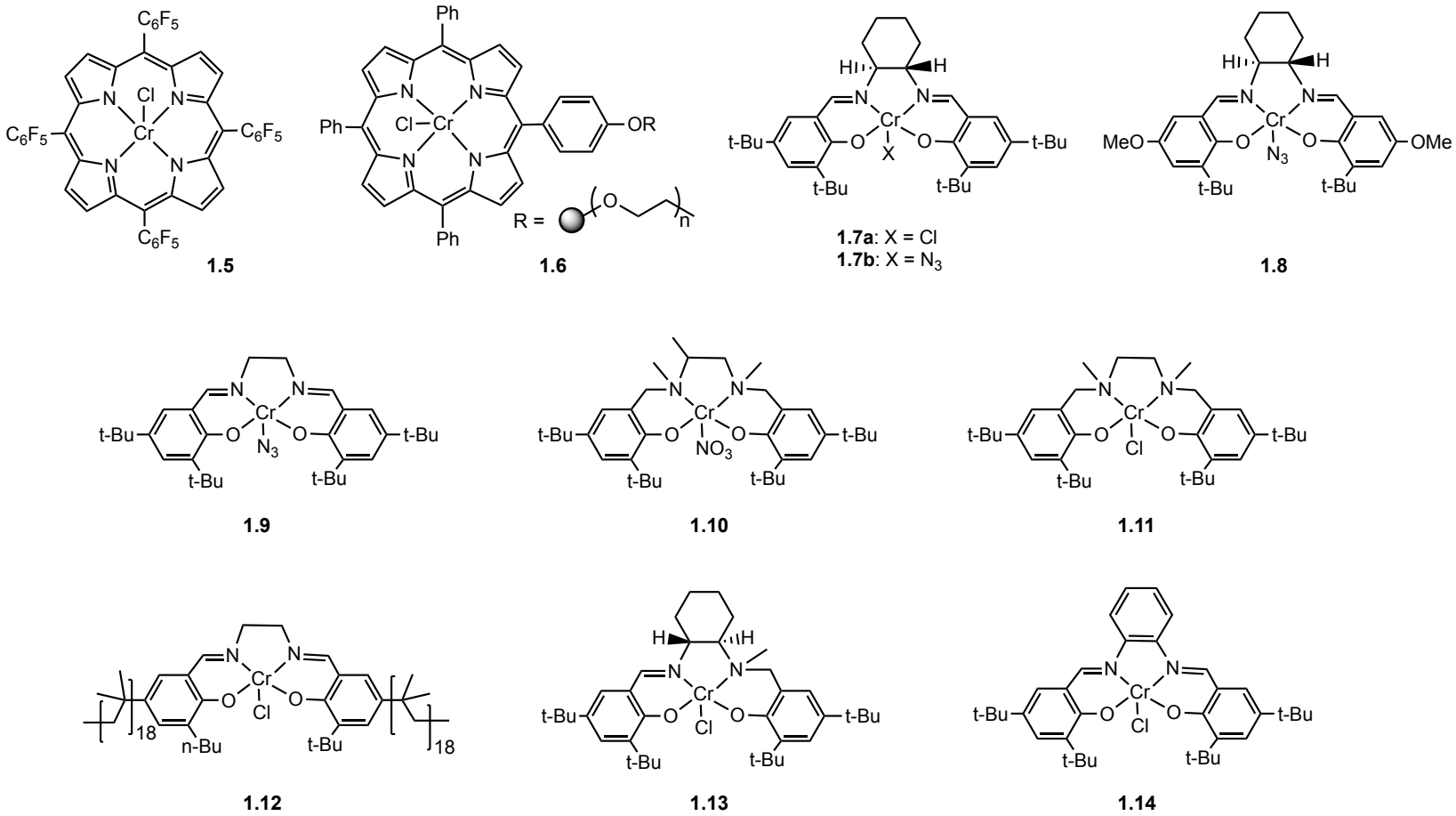

Figure 1.7 Structures of the chromium complexes discussed in Chapter 1, section 1.1.5.

Table 1-1 Results of copolymerization or coupling of CO_2/epoxides of selected complexes. Structures of the complexes are shown in Figure 1.7 and 1.8.

Entry	Complex	Co-catalyst	Mono-mer	Time (h)	Temp. (°C)	CO_2 pressure (bar)	Yield[a] (%)	Select.[b] PCHC or PPC (%)	TOF[c] (h^{-1})	M_n[d] (g/mol)	Đ[d] (M_w/M_n)
1	**1.5**	DMAP	CHO	18	110	140–228	47 – 56	95	34 – 41	< 4000	< 1.40
2	**1.6**	DMAP	CHO	24	90	170	62	> 90	NR[e]	7100	1.70
3	**1.8**	NMeIm	CHO	24	80	55	NR	99	82	NR	NR
4	**1.9**	$PPNN_3$	CHO	24	80	55	NR	99	608	NR	NR
5	**1.10**	$n Bu_4NNO_3$	*rac*-PO	6	50	15	NR	93	152	32 400	1.25
6	**1.11**	$PPNN_3$	CHO	4	60	34	60	NR	405	19 500	1.19
7	**1.13**	PPNCl	CHO	3	70	13	52	99	170	10 200	1.16
8	**1.14**	DMAP	PO	4	75	13	NR	82	154	15 800	1.89
9	**1.15**	–	PO	24	60	40	NR	99	67	70 000	2.00
10	**1.16a**	–	PO	24	60	40	NR	98	82	46 000	3.30
11	**1.16b**	PPNCl	PO	24	60	40	NR	90	55	15 000	1.80
12	**1.17**	PPNCl	CHO	32	80	50	99	NR	15	6550	2.80
13	**1.18**	PPNCl	CHO	6	80	30	NR	72	67	10 900	1.28
14	**1.19**	PPNCl	VCHO	6	90	30	NR	71	71	19 000	1.27
15	**1.20**	$PPNN_3$	CHO	24	60	41	64	76	16	6400	1.42
16	**1.21**	DMAP	CHO	24	60	44	NR	100	17	13 100	1.40
17	**1.21**	$PPNN_3$	PO	24	25	45	NR	93	18	21 100	1.15

[a]Isolated yield. [b]Selectivity determined by ^{1}H NMR. [c]TOF = moles of monomer converted/moles of catalyst/hour. [d]Determined by gel permeation chromatography (GPC). [e]NR = not reported.

The first appearance of chiral salen complexes with manganese can be undoubtedly linked to Jacobsen and co-workers, who designed complexes for asymmetric catalysis.[42] Jacobsen's chiral Mn(III) salen complexes were used in stereoselective epoxidation reactions, where electron donating groups on the catalyst had a positive effect in reaching higher enantioselectivities. This study with Jacobsen's catalyst led to the synthesis of new salen complexes where the ligand was complexed with different metals, including chromium. For example, Jacobsen and co-workers also investigated Cr(III) salen complexes (**1.7a** and **1.7b**, Figure 1.7) in the enantioselective ring opening of epoxides.[43-45] Later, these chromium salen complexes were also studied by other research groups even for different applications. For example, complex **1.7a** with DMAP proved to be an excellent system for the coupling of CO_2 and aziridines to form 5-substituted oxazolidinones.[46] The Jacobsen group's extensive investigation of the asymmetric ring opening of epoxides contributed greatly to its mechanistic understanding and inspired many research groups, including the Darensbourg group, who developed new Cr(III) salen catalysts and tested them for CHO/CO_2 and PO/CO_2 copolymerizations.

The Darensbourg group not only investigated the activity of Cr(III) salen complexes but they also studied the influence of varying the diimine backbone and the phenolate substituents of the salen ligand.[47] They found that bulky substituents such as *tert*-butyl groups on the diimine backbone sterically hindered the accessibility of the metal, which meant a decrease in the rate of copolymerization compared to an unsubstituted diimine backbone. Consequently, they concluded that steric, not electronic,

effects influenced the activity most at the diimine backbone. *Tert*-butyl groups on the phenolate moieties enhanced the solubility of the complex as well as the rate of copolymerization. An increase in activity was observed when a *tert*-butyl group was employed at the *ortho* position and a methoxy group at the *para* position of the phenolate rings. Since the electron-donating ability of the methoxy group had a positive effect on the rate of copolymerization, the Darensbourg group concluded that electronic effects dominated at the phenolates of the complex. The structure of the complex (**1.8**, Figure 1.7) that exhibited the highest activity with the methoxy group at the *para* position and with N-methylimidazole (NMeIm, Figure 1.2) is depicted in Figure 1.7 (Table 1-1, entry 3). The apical anionic ligand is also vital for the activity. Most typically, this ligand is a chloride or an azide, and complexes with the latter showed higher activity (**1.8** and **1.9**, Figure 1.7). Next, the effect of the external nucleophile, or as it is often called, co-catalyst, was tested by the same group. When $PPNN_3$ (Figure 1.2) was used with catalyst **1.9** (Figure 1.7), where the complex had a non-encumbering diimine backbone, Darensbourg and co-workers could achieve a turnover frequency as high as 608 h^{-1} (Table 1-1, entry 4).[48] Putting together all the positive effects tested, one can assume that even higher TOF could be achieved with **1.8** if it is used with $PPNN_3$, but this was not investigated in the Darensbourg group.

Cr(III)-salan (N,N'-disubstituted bis(aminophenoxide)) complexes, with sp^3-hybridized amino donors representing the saturated version of salen complexes (**1.10**, Figure 1.7) were also tested in copolymerization of epoxides and CO_2 by X. B. Lu and co-workers in 2008.[49] These salan complexes were designed to reduce the electrophilicity

of the chromium to a certain extent in order to achieve better stereoregularity in the resulting copolymer. Reducing the Lewis acidity of the chromium was also believed to increase the reaction rate by decreasing the propensity of the growing polymer chain to strongly bind to the chromium centre, thereby forming more active species that can dissociate and take part in polymer chain growth. The best TOF in PO/CO_2 copolymerization was obtained with complex **1.10** (Figure 1.7) and the results are summarized in Table 1-1, entry 5.

In 2009 the Darensbourg group also published their results on the investigation of Cr(III)-salan complexes.[50] With their salan complex (**1.11**, Figure 1.7), they achieved higher TOF and better polymer dispersity (Table 1-1 entry 6) but lower molecular weight compared to the salan complex (**1.10**, Figure 1.7) used in the X. B. Lu group. The Darensbourg group also proposed that the difference between salen and salan complexes might also arise from the different geometry around the chromium. The crystals that they grew out of the reaction mixture showed a dimeric complex with a bridging sulfate group which probably originated from the drying agent sodium sulfate. In this structure one of the phenolate oxygens adopts a *cis* orientation to one of the nitrogens, unlike to the salen ligand where both nitrogens are *trans* to both phenolate oxygens (Figure 1.8). This coordination also results in a *cis* coordination of the anion (SO_4^{2-}) and the neutral (H_2O) ligand *trans* to an oxygen and a nitrogen donor respectively, whereas the anion (N_3) and the vacant coordination site in a 5-coordinate salen complex (which can be filled by the anion of the co-catalyst under catalytic conditions) are *trans* to each other. Another difference between the salen and the salan complexes was observed by the Darensbourg

group.[50] The salan complex exhibited higher solubility as opposed to the salen derivative and so, the complex could be removed from the copolymer more easily. The colour of the polymer produced with the salen complexes was yellow after one methanol purification step, while colourless polymer was obtained when the salan complexes were used.

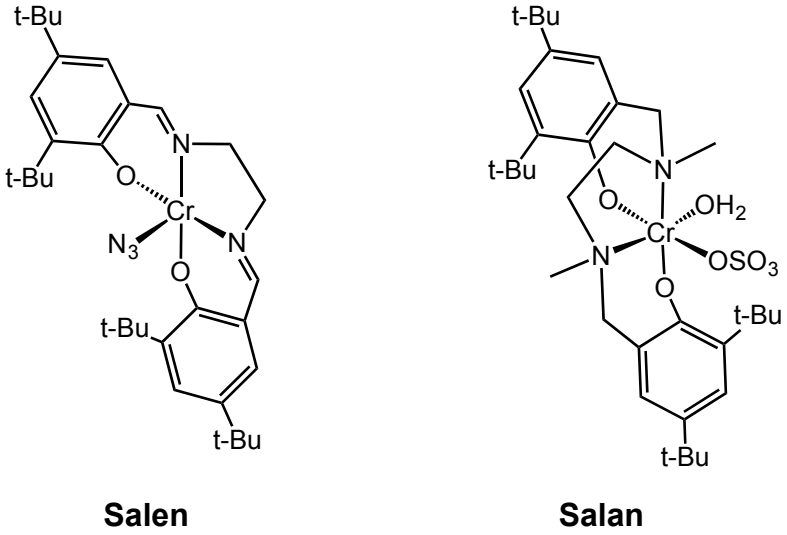

Salen **Salan**

Figure 1.8 Examples of a salen complex and a fragment of a dichromium salan complex showing differences in coordination.

Darensbourg with Bergbreiter later found a solution for removing Cr(III) salen catalysts from the polymer.[51] The modified version of **1.9** contained polyisobutylene (PIB) groups at the *para* positions of the phenolates and a chloride group instead of the azide (**1.12**, Figure 1.7). The non-polar polyisobutylene tag facilitated the dissolution of the complex in the heptane phase of a heptane/CH_3CN mixture, a heptane/DMF mixture or a heptane/EtOH-H_2O mixture affording colourless polymer. The authors compared the activity of the PIB-supported Cr(III) salen complex to its non-supported analogue (similar to **1.9** but with a chloride group instead of the azide) and found no difference

between the two. Although this process definitely means a viable route for removal of the catalyst from the polymer, its drawback lies in the preparation of the complex, which involves at least 4 steps and 5 days to synthesize.

A comprehensive study, which used electrospray ionization (ESI) in combination with tandem mass spectrometry (MS/MS) to study the binding of DMAP to salen and salan complexes revealed that salen complexes generally bind two DMAP molecules, while salan complexes only one.[52] This might be due to the difference in structure as well as in the Lewis acidity of the chromium resulting from the different electron donating ability of the two ligands. The sp^3 hybridized nitrogens result in decreased Lewis acidity at the metal, and hence electrophilicity toward nucleophiles. Structure **1.10** (Figure 1.7), which was also utilized in the study, seems to contain an electronically balanced chromium centre for copolymerization, which is also supported by the very short induction period observed as well as higher reaction (30 times higher) rate as opposed to the reactions catalyzed by the salen derivatives. The mechanistic aspects of this binding ability will be discussed in more details in the next section. It is worth noting that recently a binuclear salan complex showed very good activity in the alternating copolymerization of epoxides and cyclic anhydrides.[53]

Half saturated chromium salalen complexes – where both sp^2 hybridized and sp^3 hybridized nitrogens are present – were synthesized by the Nozaki group.[54] The copolymerization results of their best performing salalen complex (**1.13**, Figure 1.7) can be found in Table 1-1, entry 7. The authors reported that **1.13** was very active even under atmospheric pressure of CO_2, which was attributed to the flexibility of the salalen

complex giving rise to an easier coordination to chromium of a bidentate carbonate chain end rather than with the rigid salen complexes where conformational change would be required for a bidentate carbonate binding.

A salen Cr(III) complex with a fully conjugated backbone (a salphen-type complex) (**1.14**, Figure 1.7) was prepared by Rieger and co-workers to compare its activity for CO_2/PO reaction to the non-conjugated analogue (**1.7a**).[55] The research group tested the effect of DMAP loading and found that with 2 equiv. of DMAP, selectively cyclic propylene carbonate (PC) was isolated exclusively, whereas with 0.5 equiv. of DMAP predominantly poly(propylene carbonate) (PPC) was observed. Using 1 equiv. of DMAP resulted in the mixture of the two products with **1.14**, whereas still only cyclic product was obtained with **1.7a**. They found that **1.14** was more selective toward polymer formation and that the product contained higher percentage of carbonate linkages (91% with **1.14** vs. 76% with **1.7a**). The results obtained with **1.14** with 0.5 equiv. of DMAP are found in Table 1-1, entry 8. Interestingly, recently, a Zn(salphen) catalyst was found highly active in the synthesis of organic carbonates.[56]

In 2010 the Rieger group synthesized modified monomeric (**1.15**, Figure 1.9) and a similarly flexibly linked dimeric (**1.16a**, Figure 1.9) chromium salphen-type complexes, where the spacer linker was a four-membered linear hydrocarbon chain.[57] The complexes were tested both in β-butyrolactone polymerization and PO/CO_2 copolymerization. They found that the activity of **1.16a** remained unaffected even under a high [PO]:[Cr] ratio of 20 000:1 (Table 1-1, entry 10), whereas complex **1.15** lost its activity under these conditions. Table 1-1, entry 9 contains the results obtained with **1.15**

at a [PO]:[Cr] ratio of 2000:1. The high activity of **1.16a** supports the group's proposed bimetallic initiation pathway, which will also be discussed in the next section in detail. Kinetic investigations of the catalytic activities of mononuclear **1.15** and dinuclear **1.16b** (with a six-membered hydrocarbon chain, Figure 1.8) were also performed by Rieger and co-workers in 2011.[58] This study revealed that the addition of 0.5 equiv. PPNCl to the reaction mixture enhanced the selectivity toward PPC formation with **1.16b** (Table 1-1, entry 11) compared to when no co-catalysts were added. At the same time, the addition of 0.5 equiv. PPNCl to the monomeric **1.15** ensured that it could keep its activity even at a high [PO]:[Cr] ratio of 20 000:1 as opposed to the previously observed loss of activity when **1.15** was applied without any co-catalysts.[57]

Duchateau, Gambarotta and co-workers have recently showed interest in quite different chromium complexes with iminopyrrole, aminopyrrole, and aminophosphine ligands including one heterobimetallic complex with both Cr and Zn atoms.[59] Their goal was to prepare robust catalysts that had little affinity toward leaching out as well as to prevent backbiting and thus cyclic carbonate formation during the reactions. They tested eight different complexes in CHO/CO_2 copolymerization and found that the products consisted of mainly low molecular weight oligomers and the conversions were generally low as well. Their best performing complex, **1.17**, Figure 1.9, though, exhibited the highest (99%) conversion of CHO and produced a copolymer with moderate molecular weight (6550 kg/mol) when the reaction time was increased to 32 h but the dispersity was rather high (M_w/M_n = 2.8) and the TOF decreased to 15 h^{-1} (Table 1-1, entry 12).

Based on the positive effect observed with electron-donating methoxy groups with salen complexes (discussed earlier with **1.8**), the newest approach to investigate the effect of even more electron donation to the chromium centre is to replace one ([ONSO]-type) or both ([OSSO]-type) of the nitrogens with soft sulfur(s) resulting in a complex similar to a half saturated salalen ([ONSO]) or a saturated salan ([OSSO]). The first modification with one sulfur atom has been published by the Darensbourg group.[60] They studied four different [ONSO]-type complexes and complex **1.18** (Figure 1.9) produced the highest molecular weight polymer with the highest conversion and selectivity toward PCHC (for details see Table 1-1, entry 13). The authors found that the electron withdrawing phenylene backbone had a positive effect on the reaction. One of the complexes was compared to a salalen analogue and it proved to be inferior in terms of TOF and selectivity toward PCHC formation (87%), while the salalen complex was exclusively selective (100%) toward polymer formation. The research group reasoned that this might be due to the electron donation of the sulfur, and that the growing polymer chain could not be kept close enough to the metal centre to avoid polymer chain dissociation and the possibility of backbiting. This also explained why electron withdrawing groups were beneficial for polymer selectivity in this case because they helped balance the excessive electron donation of the sulfur. It is then evident from this study that the electron donation of the sulfur is too much to maintain product selectivity and, as a matter of fact, it did not mean an improvement in catalysis in this field.

B. Liu and X. Li undertook the synthesis of chromium complexes with [OSSO]-type ligands where they replaced both nitrogens with sulfurs.[24] They concluded that

complex **1.19** with an ethylene backbone had the best properties for 4-vinylcyclohexene oxide (VCHO)/CO_2 copolymerization. The reason for the choice of the monomer VCHO was that it was less studied than other monomers and contains a functional group for post synthetic modification. The results that they obtained with **1.19** were very similar to the results obtained with **1.18** (Table 1-1, entry 13 and 14). The selectivity toward polymer production, TOF and dispersity remained practically the same but higher molecular weight polymer was produced with **1.19** (19 000 g/mol) than with **1.18** (10 900 g/mol). Comparing **1.19** (Table 1-1, entry 14) to its salan analogue (**1.11**, Table 1-1, entry 6), **1.19** also proved to be inferior in activity, probably due to the soft electron releasing sulfur donors resulting in a weaker interaction between the growing polymer and the chromium, however, the monomers were different (CHO vs. VCHO). The studies of these [ONSO] and [OSSO]-type complexes contributed significantly to the knowledge in the field of epoxide/CO_2 copolymerization greatly in that they highlighted the need for careful choice of catalytic conditions and appropriately (electronically and sterically) tuned metal complexes in order to achieve high product selectivity, activity and conversion.

Amine-bis(phenolate) ligands represent a promising class of ligands for catalysis because of their flexible structure and tunable properties.[39] They have the ability to adopt different coordination arrangements around the metal centre. For example, a chromium complex of a tetradentate amine-bis(phenolate) ligand bearing a tetrahydrofuranyl group at the central N-donor showed a structure where the phenolate oxygens were *trans* to each other (**1.20**, Figure 1.9) when a THF solvento adduct was prepared.[37] On the other

hand, when a similar complex formed a chloride-bridged dimer in the absence of exogenous THF or other Lewis basic solvent, the phenolate oxygens were situated *cis* to each other (**1.21**, Figure 1.9).[61] Similar flexibility was thought to be the reason behind the enhanced catalytic activity of chromium salan complexes discussed earlier. Nevertheless, complexes with tetradentate amine-bis(phenolate) ligands have the freedom to orient the incoming nucleophile *cis* to the anionic ligand and *trans* to either a phenolate oxygen or to a neutral donor (pyridyl or furfuryl).[62] The potential that amine-phenolates have favourable properties for catalysis was also shown by a recent computational DFT study on Fe(III) amino trisphenolate complexes which were more effective for the cycloaddition reaction of epoxides with CO_2 than Zn(salphen) complexes.[63] The activity of **1.20** was investigated by the Kozak group[64] and its best results are summarized in Table 1-1, entry 15. The activity exhibited by **1.21** proved to be superior to that of **1.20** in terms of selectivity toward polymer formation and molecular weight. (Table 1-1, entry 16 and 17). It is worth noting here that the best activity was obtained by **1.21** when 0.5 equiv. of the co-catalyst was used, and 2 equiv. inhibited the reaction. Generally, increasing the reaction time proved to be beneficial for higher conversion and molecular weight. When **1.21** was employed in PO/CO_2 copolymerization, the selectivity between polymer and cyclic carbonate could be switched based on the temperature applied. At temperature applied with 25 °C allowing exclusive isolation of PPC, and 60 °C selective for cyclic propylene carbonate. This observation is consistent with previous research and it is most likely due to the small difference in the activation barrier (E_a = 32.9 kJ/mol was calculated for salen complexes) between the formation of PPC and PC.[30,48] This difference is not that significant, and it is easy to overcome, consequently, usually a

mixture of polymer and cyclic product is formed when higher temperature is applied. The difference is much bigger (E_a = 86.1 kJ/mol for salen complexes) when CHO is used, therefore usually PCHC is produced at higher temperature.

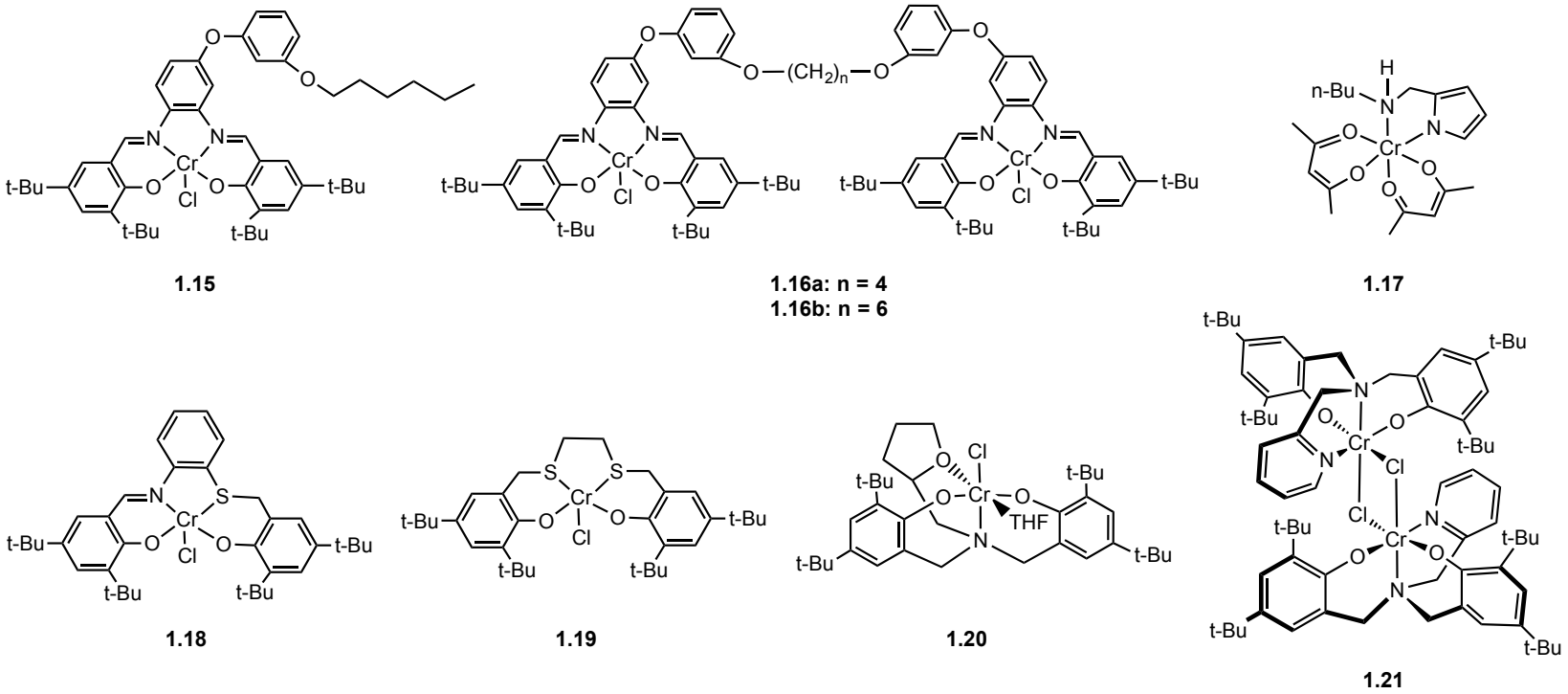

Figure 1.9 Structures of the chromium complexes discussed in Chapter 1, section 1.1.5.

1.1.6 Mechanistic studies of epoxide/CO_2 copolymerization

Mechanistically, there are three main possibilities for the initiation step, the ring opening of the epoxides, toward the preparation of both cyclic carbonate and polycarbonate.[62,65,66] Scheme 1-3 represents these pathways, namely a) bimetallic, b) monometallic intramolecular and c) monometallic intermolecular pathways. In a bimetallic initiation (Scheme 1-3 a)), ring opening of a metal bound epoxide is initiated by a nucleophile that is bound to and is activated by a second metal centre. With the addition of an external nucleophile, species with two coordinated nucleophiles may also exist and can initiate ring opening. Chronologically, the bimetallic pathway was one of the earliest proposed mechanisms that gave insights of the initiation. So, this pathway will be discussed first in this section followed by the monometallic pathways (Scheme 1-3 b) and c)).

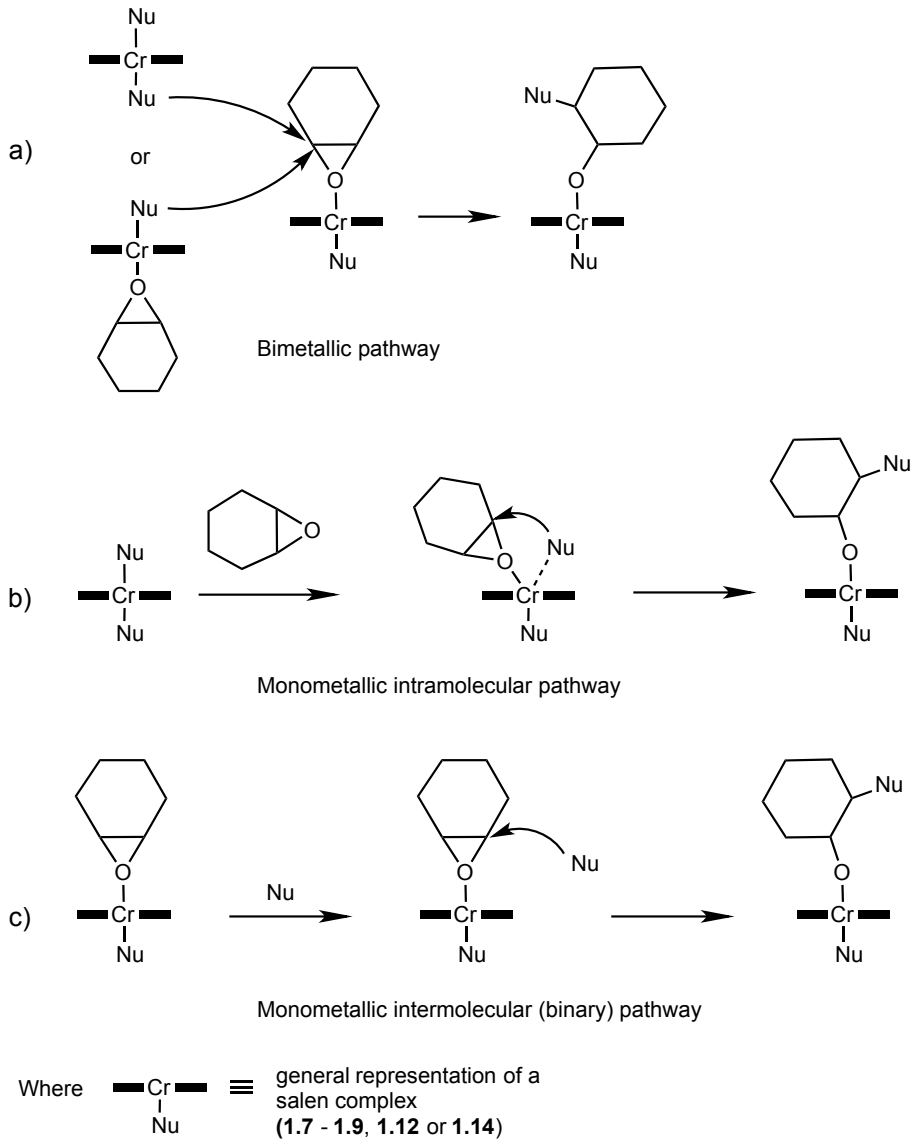

Scheme 1-3 General representation of the three major ring opening pathways.

1.1.6.1 Bimetallic initiation pathway

The bimetallic ring opening was proposed by Jacobsen and co-workers in one of their first studies.[44] The Jacobsen group proposed a mechanism with complex **1.7b** (Figure 1.7) where two epoxide-bound complexes act in a concerted mechanism in the ring opening of cyclopentene oxide (Scheme 1-4).

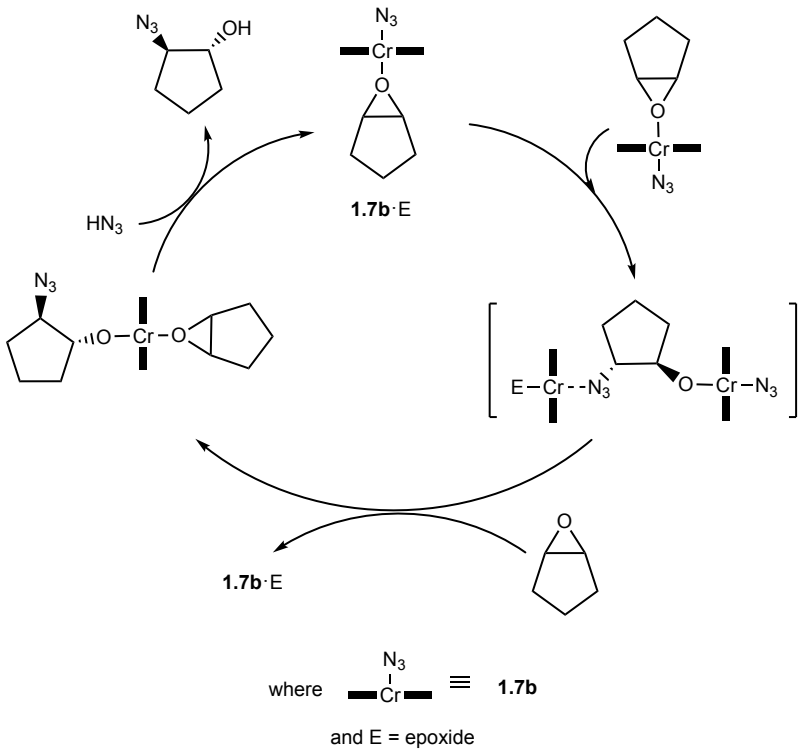

Scheme 1-4 Bimetallic ring opening of cyclopentene oxide proposed by Jacobsen and co-workers.

This type of ring opening is also called second order initiation because the initial reaction rate then depends on two metal complexes. Similar second order initiation was proposed by the Darensbourg group for salen complexes with neutral co-catalysts, such as DMAP.[67] They proposed that epoxide ring opening occurs via a second-order process described in Scheme 1-5, similar to the initiation proposed by the Jacobsen group. After the initial ring opening, however, the reaction was determined to be first order in metal concentration.[68] When DMAP is present, equilibrium is formed between epoxide-bound and the DMAP-bound species (Scheme 1-5 **A** and **B**). Copolymer formation from these species then may occur but represents a minor pathway (Scheme 1-5 **C**). Rather, CO_2 addition helps to establish a second equilibrium by forming a zwitterionic species where

CO_2 is incorporated between the chromium and the nitrogen of DMAP (Scheme 1-5 **D**). This complex is not stable enough and is easily displaced by another DMAP molecule to start the cycle again until all the DMAP present is "activated" (Scheme 1-5 **E**). This activation process might be the explanation for the longer initiation period exhibited with DMAP as opposed to the ionic PPN salts, as well as for the faster propagation rate when excess DMAP is present.[47] Copolymer formation according to Scheme 1-5 **F** represents the major route as revealed by the authors.

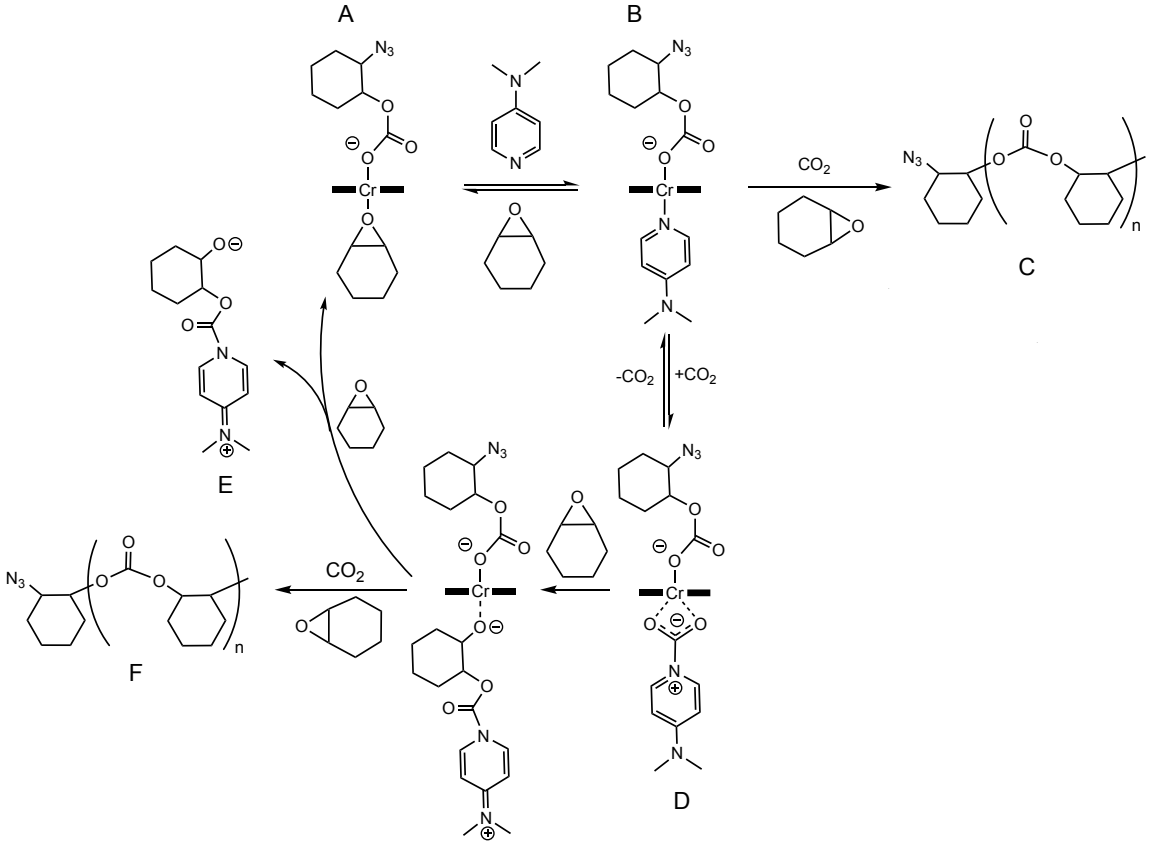

Scheme 1-5 Chain propagation reaction with salen complexes and DMAP proposed by Darensbourg and co-workers.

Bimetallic initiation was also proposed by Rieger and co-workers during the investigation of mono-and dinuclear chromium complexes (**1.15** and **1.16b**, Figure 1.9).[58]

Kinetic investigations with the help of attenuated total reflectance infrared spectroscopy (ATR IR) revealed a reaction order of 1.69 with respect to catalyst concentration for the monometallic **1.15** and an order of 1.2 for the bimetallic **1.16b**. It is worth noting that these complexes are active without the addition of any co-catalysts and the kinetic investigations were carried out solely with the complexes. The research group attributed the higher value (1.69) to a more complex, bimetallic initiation pathway with the monometallic complex (**1.15**, Figure 1.9) accompanied by monometallic rate-determining steps. In the case of **1.16b**, on the other hand, intramolecular initiation is more likely occurring indicating closer to a first order dependence on catalyst concentration accompanied by bimetallic intermolecular initiation to a certain degree. They also investigated the activity of the two complexes under high epoxide:catalyst ratio ([PO]:[cat] = 20 000:1) and they found that **1.15** lost its activity under this condition as opposed to **1.16b**. This was also attributed to the necessity for having two metals within one complex, where the two chromiums are flexibly linked, and close proximity of the two is ensured in order to maintain activity in a highly diluted system. This is also consistent with the bimetallic initiation, that is, for the ring opening two metal complexes are needed except that **1.16b** itself contained two chromium centres and a suitably flexible linker allowing intramolecular bimetallic initiation. The group also examined the effect of co-catalyst and found that in the presence of DMAP or NMeIm **1.16b** became inactive, probably because these N-heterocyclic neutral bases competitively coordinate to the metals and inhibit monomer coordination. 0.5 equiv. of PPNCl, however, had a positive effect on copolymerization, plus **1.15** regained its activity under the highly diluted system ([PO]:[cat] = 20 000:1). So, the authors proposed that without any co-

catalysts mainly bimetallic processes dominate, whereas monometallic intermolecular (binary) initiations occur when PPNCl is present.

Mechanistic investigations of a dizinc acetate macrocyclic complex catalyzed CHO/CO_2 copolymerization also revealed a first order dependence both on catalyst and CHO concentration despite the complex containing two zinc atoms.[69] Williams and co-workers proposed a mechanism based on their results where one polymer chain is grown per complex and the two metals act in synergism to accommodate epoxide coordination, ring opening and chain propagation. The growing polymer chain is switching metals after each epoxide ring opening according to the reaction depicted in Scheme 1-6. Initiation starts with a nucleophilic attack of an acetate on a coordinated CHO (Scheme 1-6 **B**). This is a slow process which corresponds to the ~30 min initiation time observed by the group. This forms species **C** in Scheme 1-6, which is considered to be the active species. The next step, CO_2 insertion occurs very fast leading to species **D**, which was supported by the zero order dependence on [CO_2] determined by the group. After the formation of species **F**, chain propagation occurs via consecutive CO_2 and CHO insertions. Polyether formation is also possible if there is another CHO incorporation after species **F** is formed. It is also possible that the alkoxide species in **F** backbites itself at the carbon of the carbonyl group forming cyclic cyclohexane carbonate. Polyether formation is negligible in this system (between 2 – 5%) and cyclic carbonate formation can also be suppressed if the temperature is kept at or lower than 80 °C according to the authors.

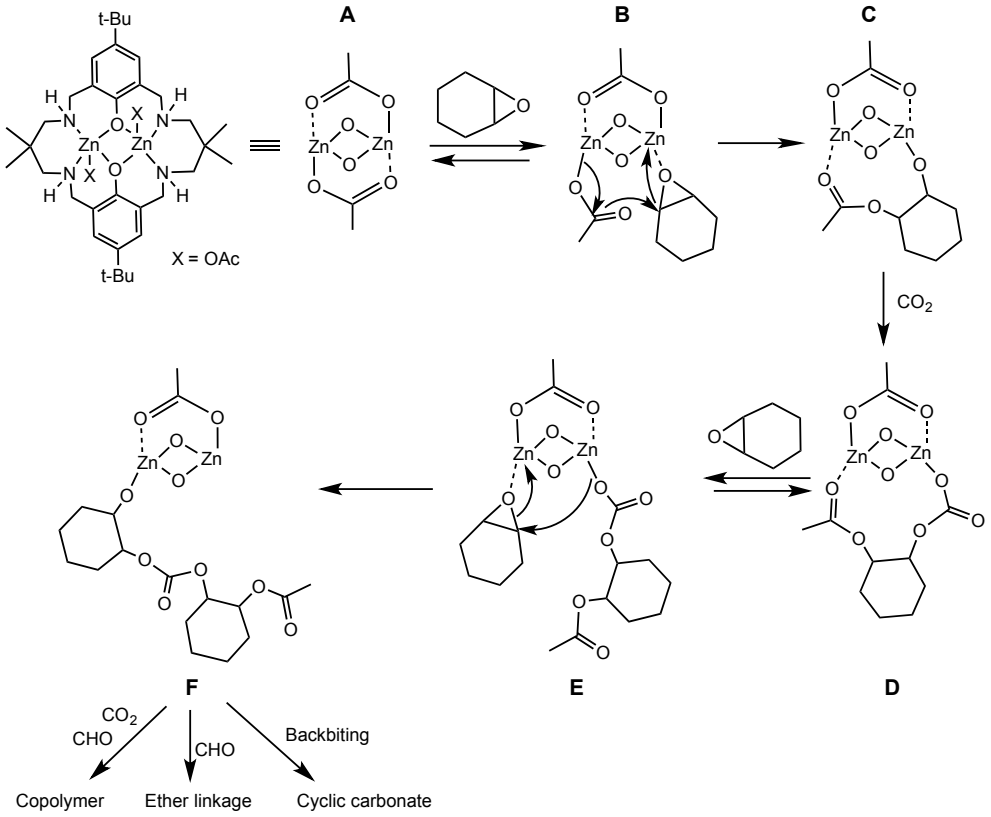

Scheme 1-6 Initiation and chain propagation with Zn macrocyclic complexes proposed by Williams and co-workers.

1.1.6.2 Monometallic intramolecular initiation pathway

The monometallic intramolecular pathway (Scheme 1-2 b) is more likely to occur when ionic co-catalysts are applied, however, this pathway is thought to be thermodynamically disfavoured.[65] The Darensbourg group proposed an intramolecular ring opening with salen complexes together with ionic co-catalysts, such as PPNCl (Scheme 1-7).[67] The co-catalyst, X^- binds to the metal centre weakening the Cr – Nu^- bond due to the increased electron density, which then provides an opportunity for the incoming epoxide to coordinate to chromium. The metal – Nu^- bond becomes weaker and the metal – X^- bond stronger, which helps the ring opening of the epoxide. After the ring

opening an alkoxide is formed and the metal – X bond becomes weaker again so the CO_2 insertion can take place forming the carbonate species.

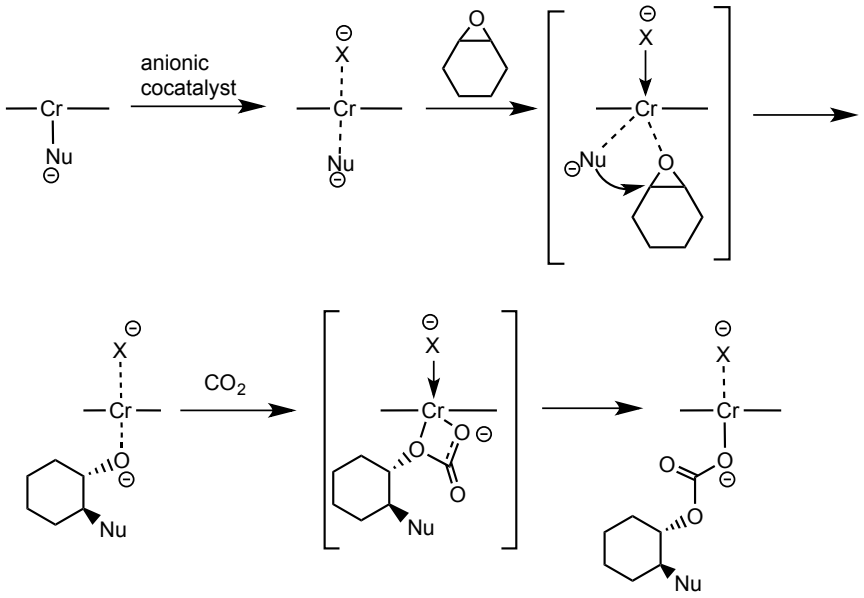

Scheme 1-7 Monometallic intramolecular ring opening with salen complexes and anionic co-catalysts proposed by Darensbourg and co-workers.

1.1.6.3 Monometallic intermolecular pathway

When the Shi research group studied binaphthyldiamino salen-type Zn, Cu and Co complexes in the ring opening of epoxides with CO_2 to yield cyclic carbonates, it was speculated that bimetallic initiation is less likely to occur with their sterically congested complexes.[70] Their hypothesis, that close proximity of the epoxide and co-catalyst bound species was not favoured, was evidenced by an isotope labeling study. They synthesized and carried out the reaction with a deuterated epoxide, *trans*-deuterioethene oxide. The analysis of the products gave information on not only a monometallic intermolecular initiation pathway but also the order of the reaction steps. It was the added Lewis base, triethylamine (Et_3N), that initiated ring opening of a coordinated epoxide followed by

CO_2 insertion. The carbonate species then dissociated from the metal centre and formed cyclic carbonate via backbiting leaving an empty coordination site for the next epoxide. The hypothesis that Et_3N reacted first with CO_2 and the resulting carbamate species initiated epoxide ring opening could be ruled out with the help of this study.

For the monometallic intermolecular initiation an externally added co-catalyst is often needed. This system is called a binary system referring to the two species necessary for the initiation. This type of initiation was also proposed by Rieger and co-workers when investigating mono-and dinuclear Cr(III) salen complexes with PPNCl.[58] In addition, Nozaki and co-workers had very similar observations with mono-and dinuclear Co-salen complexes. Bimetallic initiation was the most plausible pathway when no co-catalysts were used, whereas the binary pathway dominated when co-catalysts were present.[71]

1.1.7 Co-catalyst effect

Darensbourg and co-workers extensively studied the effect of co-catalysts with salen complexes and found that with the use of ionic PPNCl, the reaction rate was linear until the reaction mixture became highly viscous from the polymer formed, no initiation period was observed and the reaction continued until all the CHO was consumed.[67] The best rate of CHO/CO_2 copolymerization was obtained when the complex-to-labile anion (sum of anions of the metal and the added co-catalyst) ratio was 1:2 and no further increase was observed at higher co-catalyst concentration. Thus, if the metal complex possesses a chloride ligand, a 1:1 catalyst:PPNCl ratio is ideal.

In another study, when excess PPNX salt was used with salen complexes in PO/CO_2 copolymerization, exclusively cyclic carbonate was formed.[72] The excess anion was proposed to displace the coordinated alkoxide (resulting from ring opening of the epoxide), which then formed cyclic carbonate via backbiting.

The absence of an induction period for Darensbourg's catalysts partnered with PPN salts differs when N-containing heterocyclic bases, for example DMAP, were used. These co-catalysts always exhibited an induction period and the length of induction was dependent on DMAP loading. The reason for this was attributed to the time needed for DMAP reaction with CO_2 to give carbamate as the initiating nucleophile (Scheme 1-5), which was discussed in Section 1.1.6.1.

The effect of co-catalyst loading was also studied by the Rieger group. In their study the authors were able to control the selectivity of polymer or cyclic carbonate formation by simply increasing the DMAP concentration from one equivalent to two relative to catalyst concentration.[55] They achieved 80% conversion of cyclic propylene carbonate at 13 bar CO_2 pressure, at 75 °C with a TOF of 602 h^{-1} in 2 h with **1.15** (Figure 1.7). The proposed model for the cyclic carbonate formation is illustrated in Scheme 1-8. In this reaction, an alkoxide end of the growing polymer is formed when the chain is displaced from the metal centre by another DMAP molecule. The alkoxide end attacks the carbonyl carbon and this backbiting leads to cyclic propylene carbonate and a polymer chain with a new alkoxide end. Cyclic carbonate production could be somewhat slowed down when higher CO_2 pressure was applied, as a rapid CO_2 insertion converted the alkoxide end into a carbonate, which then did not allow backbiting. This theory was

supported by a reaction carried out at 35 bar CO_2 pressure, which resulted in 60% polypropylene carbonate and 29% cyclic carbonate as opposed to the 38% cyclic product at 13 bar.

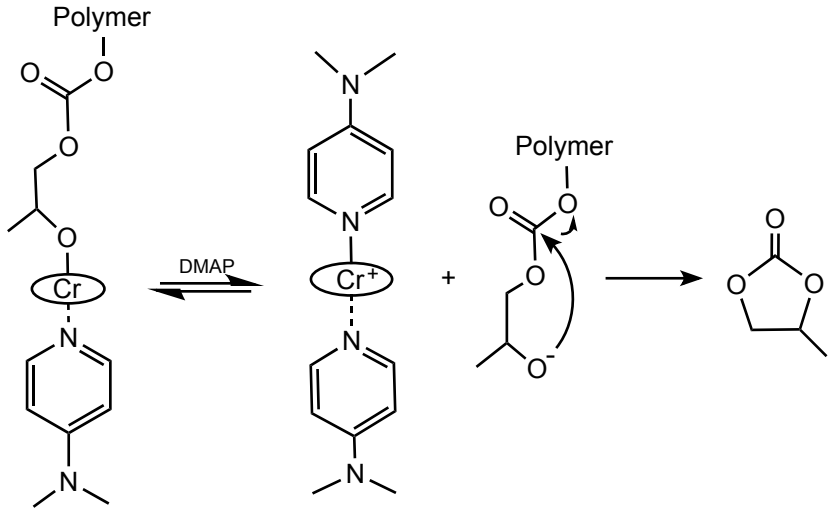

Scheme 1-8 Proposed mechanism for cyclic carbonate formation by Rieger and co-workers.

Based on co-catalyst loading, Kleij and Pescarmona could switch the selectivity of polymer/cyclic carbonate formation with iron(III) tris(phenolate) complexes.[73] 1 equiv. of co-catalyst favoured exclusively polymer formation, whereas applying 10 equiv. resulted in exclusively cyclic carbonates.

In conclusion, more than one equiv. of co-catalyst relative to catalyst loading usually results in either cyclic carbonate formation, or retardation/inhibition of the catalytic activity.

1.1.8 Computational studies

It is worth noting that computational studies contribute a great deal to the mechanistic understanding of epoxide/CO_2 copolymerization. It is becoming more and more widespread to interpret experimental results and reveal important details computationally. In this subsection, only three examples will be mentioned as the detailed aspects of this area are outside of the scope of this thesis.

One of the important questions that was answered through computational studies is how the displacement of a chloride ligand by an epoxide is possible. In an elegant computational study by Darensbourg and Yeung,[74] several bond strengths were calculated, which revealed that epoxides (metal – epoxide: 16 – 19 kcal/mol) bind to the metal as strongly as chlorides (metal – chlroride: ~ 19 kcal/mol), which makes the exchange possible.

Another DFT study revealed that catalyzed coupling or copolymerization of CO_2 with alkyl-substituted terminal epoxides are controlled by steric factors, while reactions with vinyloxirane and styrene oxide are controlled by electronic factors.[63] The study also explains why ring opening occurs via a nucleophilic attack at the methine carbon and not the less hindered methylene carbon of styrene oxide.

Computational studies support the phenomenon observed experimentally that polyether formation is usually negligible for reactions catalyzed by chromium and cobalt complexes.[74] For polyether linkages to occur, a polymeric alkoxide species needs to ring open a metal-bound epoxide. Although this reaction has a low energy barrier of ~ 6

kcal/mol, the displacement of a strongly bound alkoxide by an epoxide is not favoured. Besides, the alkoxide species is easily carboxylated (carboxylation was calculated to be exothermic by 6 – 8 kcal/mol) and so, polyether linkages are usually not observed or negligible. The easy carboxylation of the alkoxide species also contributes to why formation of cyclic carbonate species is less likely to occur via alkoxide backbiting as opposed to carbonate backbiting revealed by the same study. In addition, the interaction between the metal-bound alkoxide and the carbon of the nearest carbonate group is very weak due to the significantly lower nucleophilicity of the metal bound alkoxide, which is also sterically more hindered than the carbonyl oxygen of a metal-bound carbonate. Consequently, the interaction between the carbonyl oxygen and the methylene carbon of the nearest epoxide unit of the polymer chain is stronger and so, this pathway for cyclic carbonate formation is more viable.

1.1.9 Objectives

The objectives of the first part of this thesis focused on the synthesis of new Cr(III) amine-bis(phenolate) complexes in order to synthesize catalysts with an electronically and sterically favourable ligand system to give high activity in epoxide/CO_2 copolymerization. Another aim was to gain mechanistic insights for the initiation of the reaction using MALDI-TOF MS and *in situ* ATR FTIR spectroscopy. The reaction order with respect to catalyst concentration could be determined and the initiation of the reaction was investigated. The effect of varying the co-catalyst loading was also studied.

1.2 Polylactide synthesis with alkali and alkaline earth metal complexes and mechanistic considerations of ring opening polymerization

1.2.1 Introduction

Polylactide is one of the most appealing alternative biopolymers because it is both bio-based and biodegradable.[75] The biodegradation (microbial and enzymatic) of PLA has been extensively studied showing very promising results and a dependence on molecular weight, crystallinity, stereoregularity and composition of the polymer.[76] The total life cycle of polylactide is shown in Figure 1.10. Fermentation of starch containing biomass, for example sugar beet or corn, produces lactic acid. Condensation of lactic acid, including removal of the by-product of water, yields oligomeric lactic acid, which is then depolymerized through internal transesterification to yield lactide, the monomer for ROP.[77] The ring opening of lactide is usually initiated by a suitable catalyst to form possibly high molecular weight polylactide which can biodegrade via hydrolytic degradation of labile aliphatic ester linkages. The end products of the degradation are water and carbon dioxide, which can be metabolized by the environment via photosynthesis to produce biomass and the cycle starts again.[78]

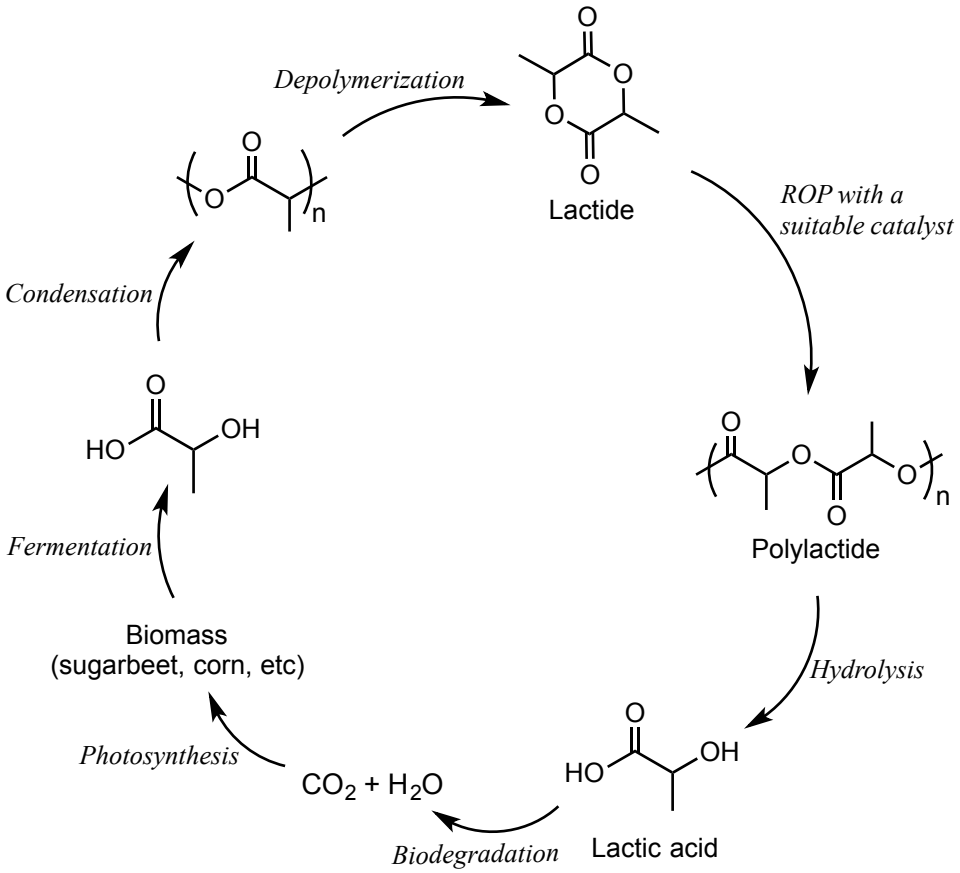

Figure 1.10 Life cycle of polylactide.

Lactide is formed from lactic acid in three stereoisomers: L-lactide, D-lactide and meso-lactide (Figure 1.11). The racemic mixture of L-lactide and D-lactide is called *rac*-lactide or, sometimes, it is referred to as D,L-lactide.

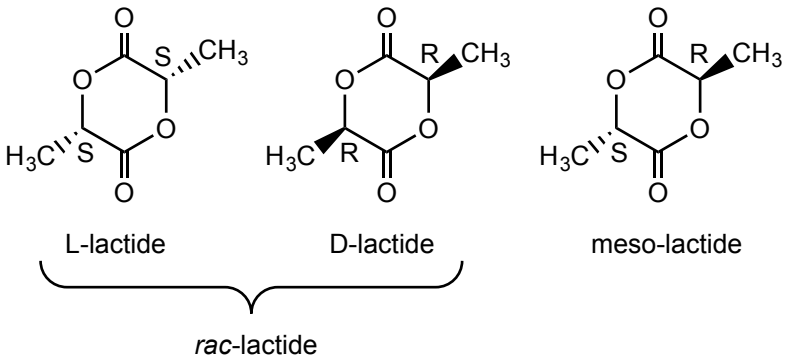

Figure 1.11 Three isomers of lactide.

Polylactide (PLA) has numerous applications, such as disposable tableware, food packaging, compost bags, drink containers, or pillow liners.[77-79] PLA along with poly(glycolide) (PGA) and poly[D,L-(lactide-co-glycolide)] also find many biomedical applications because they are biocompatible with the human body and are biodegraded *in vivo*.[80] For example, they are used in tissue engineering, gene therapy, regenerative medicine,[81] sutures, stents, dental implants or bone screws and pins.[80] These biopolymers also find use in certain disposable medical devices, like syringes, injection pipes, surgical gloves and pads, plus other medical devices like implants forming *in situ*.[81] In addition, PLA, PGA and their copolymer are good candidates for drug delivery systems where the slow release of the drugs is ensured by the slow biodegradation of the polymer.[81,82] PLA fibers may find other applications potentially, such as upholstery, disposable garments, feminine hygiene products and nappies.[77,83]

Currently, PLA is produced by NatureWorks (USA) on a large scale of up to 140 000 tons/year.[84] It is also produced in other countries such as Japan, Korea, China and Belgium, plus, there are new companies emerging for PLA production because they want to modify the quality of the PLA suitable for their own needs (i.e. Arterial Remodeling Technologies in France).[84]

In order to maintain biocompatibility for the production of PLA, biocompatible metal complexes for the ring opening of lactide are preferred over transition metal complexes that are often associated with toxicity. Biocompatable metal complexes include those containing alkaline (Li, Na, K) and alkaline earth (Ca and Mg) metals. In

the next section, these complexes, with special emphasis on amine-bis(phenolato) complexes, will be reviewed.

1.2.2 Li, Na and K complexes in the ring opening polymerization of lactide

Group I metal complexes in ROP of lactide were reviewed by the Williams group in 2008.[85] The authors argued that one of the disadvantages of Li complexes was their tendency to form aggregates. For example, Lin and co-workers synthesized penta- and hexanuclear Li aggregates supported by a 2,2'-ethylidene-bis(4,6-di-*tert*-butylphenol) (EDBP-H_2) ligand and investigated the factors affecting their aggregation.[86] The research group found that hexanuclear complexes in the presence of excess coordinating solvents, such as THF, yield a mixture of penta-and hexanuclear complexes. One example, **1.22**, of a pentanuclear Li-aggregate is depicted in Figure 1.12. This complex was tested in the ROP of L-lactide and proved to be very efficient (Table 1-2, entry 1). The [L-lactide]:[catalyst] ratio was based on the complex and not the number of lithiums it contained and the research group speculated that there was only one active site per complex. Still, molecular weights were lower than the expected calculated molecular weights.

Later, the same group was able to avoid aggregation by synthesizing a dinuclear Li complex with benzyl-alcohol (**1.23a** and **1.23b**, Figure 1.12).[87] In these structures of **1.23a** and **1.23b**, each lithium is three coordinate with one benzyl alcohol (**1.23a**) or *para*-(chloromethyl)-benzyl alcohol (**1.23b**) occupying the third coordination site of each lithium, while one of the phenolate oxygens stays protonated. Both **1.23a** and **1.23b** are

efficient for L-lactide polymerization and the results are summarized in Table 1-2, entries 2 and 3. In addition, generally polymer molecular weights increased with increasing [monomer]:[catalyst] ratio showing better control over the reaction than with **1.22**. These complexes already contain the alcohol that is usually added to the reaction mixture, and the polymer chains contain benzylalcoxyl (**1.23a**) or p-(chloromethyl) benzyl ester (**1.23b**) end groups while there are hydroxyl groups at the other terminus of the polymer chain as revealed by NMR studies. This indicates the coordinated alcohol fragments still function as chain transfer agents/initiators during ROP.

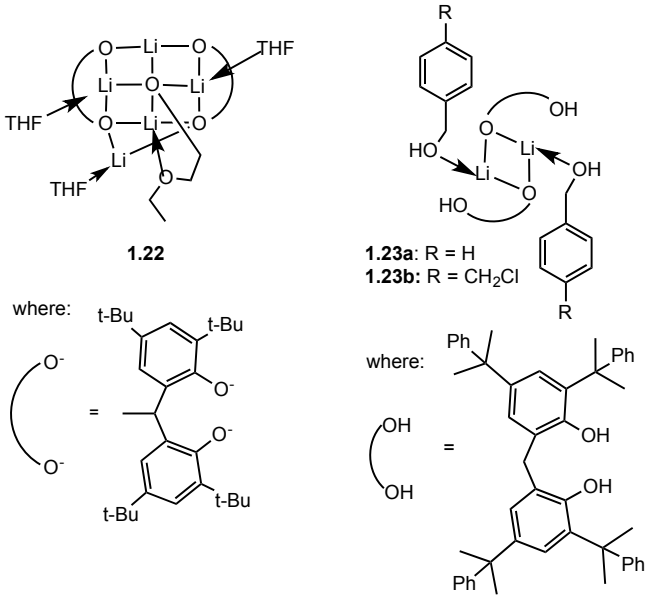

Figure 1.12 Li-complexes of EDBP-H_2 ligands.

Table 1-2 Results of ROP of lactide with selected complexes

Entry	Comp-lex	Solvent	ROH	Monomer (LA)	[LA]:[M]:[ROH][b]	Time	Temp. (°C)	Conver-sion (%)	M_n[d] (calc'd) (g/mol)	M_n[e] (GPC) (g/mol)	Đ[e] (M_w/M_n)
1	**1.22**	DCM	–	L-LA	100:1:0[c]	3 h	0	94	13 500	6300	1.07
2	**1.23a**	DCM	BnOH[a]	L-LA	100:1:1	7 h	0	88	6500	7600	1.07
3	**1.23b**	DCM	*p*-Cl-BnOH[a]	L-LA	100:1:1	6.5 h	0	91	6700	7100	1.10
4	**1.24**	DCM	BnOH	L-LA	100:1:1	20 min	26.5	92	13 300	12 400	1.09
5	**1.26**	Tol.[g]	BnOH	*rac*-LA	100:1:1	120 min	26	99	14 400	5 500	1.80
6	**1.27**	DCM	BnOH	L-LA	200:1:2	35 min	0	96	13 900	14 500	1.08
7	**1.28a**	Tol.	MeOH[h]	L-LA	200:1:2	8 min	20	98	14 100[f]	23 100	1.11
8	**1.29a**	THF	–	L-LA	200:1:0	36 h	60	93	13 600	11 400	1.28
9	**1.29b**	THF	–	L-LA	200:1:0	36 h	60	83	12 100	10 600	1.24
10	**1.30**	DCM	BnOH	*rac*-LA	250:1:1	5 min	25	94	34 100	22 400	1.36
11	**1.31**	Tol.	–	L-LA	100:1:0	36 h	90	79	11 400	13 500	1.44
12	**1.32**	Tol.	–	*rac*-LA	50:1:0	15 min	27	98	7100	45 200	1.73
13	**1.34**	Tol.	–	ε-CL	200:1:0	12 h	60	40	9100	20 000	1.30
14	**1.36**	DCM	BnOH[a]	L-LA	100:1:1	3.5 h	0	92	6700	7000	1.06
15	**1.38a**	Tol.	BnOH	L-LA	100:1:1	5 min	25	92	13 300	15 600	1.10
16	**1.38b**	Tol.	BnOH	L-LA	100:1:1	10 min	25	95	13 800	14 800	1.08
17	**1.39**	Tol.	BnOH	L-LA	120:0.6:1	20 min	20	95	16 400	58 800	1.31
18	**1.40**	Tol.	BnOH	L-LA	100:0.1:1	2 min	20	96	13 800	23 600	1.12
16	**1.41**	Tol.	BnOH	L-LA	100:0.1:1	4 min	20	93	13 400	17 200	1.25

[a]Benzyl-alcohol (BnOH) or *para*-(chloromethyl)benzyl alcohol (*p*-Cl-BnOH) are included in the structures of the complexes. [b]Ratios are indicated as per metal. [c]Ratios are indicated as per complex. [d]Calculated from MW(LA) × ($[LA]_0/[BnOH]_0$) × conversion + MW(ROH).[e]GPC calibrated with polystyrene standards using the correction factor of 0.58. [f]Calculated from MW(LA) × ($[LA]_0/2[MeOH]_0$) × conversion. [g]Tol. = Toluene [h]Methanol (MeOH) (2 equiv./metal) is part of the complex.

Huang and Chen were able to synthesize tetranuclear Li complexes with amine-bis(phenol) ligands.[88] One of the complexes with a pyridyl group is depicted as **1.24** in Figure 1.13. This ladder-like complex exhibited two Li···H–C interactions between each of the otherwise three-coordinate Li atom and one of the hydrogens of each of the closest *tert*-butyl group. Recrystallization of species **1.24** in diethyl ether resulted in complex **1.25** (Figure 1.13), a partially hydrolyzed dinuclear species where two lithium atoms were removed by most likely a small amount of moisture. This way a 1:1 ratio of ligand to metal was ensured, where two mononuclear complexes were bridged via intermolecular hydrogen bonding. Ring opening polymerization of L-lactide was completed within 20 min with **1.24** (for details, please see Table 1-2, entry 4). Thus, amine-bis(phenol) ligands are good candidates to control the aggregation of the complexes when they are complexed with lithium and maintain good activity at the same time. Another example of a Li-amino-bis(phenolato) complex is **1.26** which was prepared by the Kozak group.[89] This complex with a tetrahydrofurfuryl amino nitrogen donor is also tetranuclear and also possesses a ladder-like core similar to **1.24**. With **1.26**, very high conversions were achieved within 120 min (see Table 1-2, entry 5) but the dispersity values were quite high (between 1.8 and 2.5).

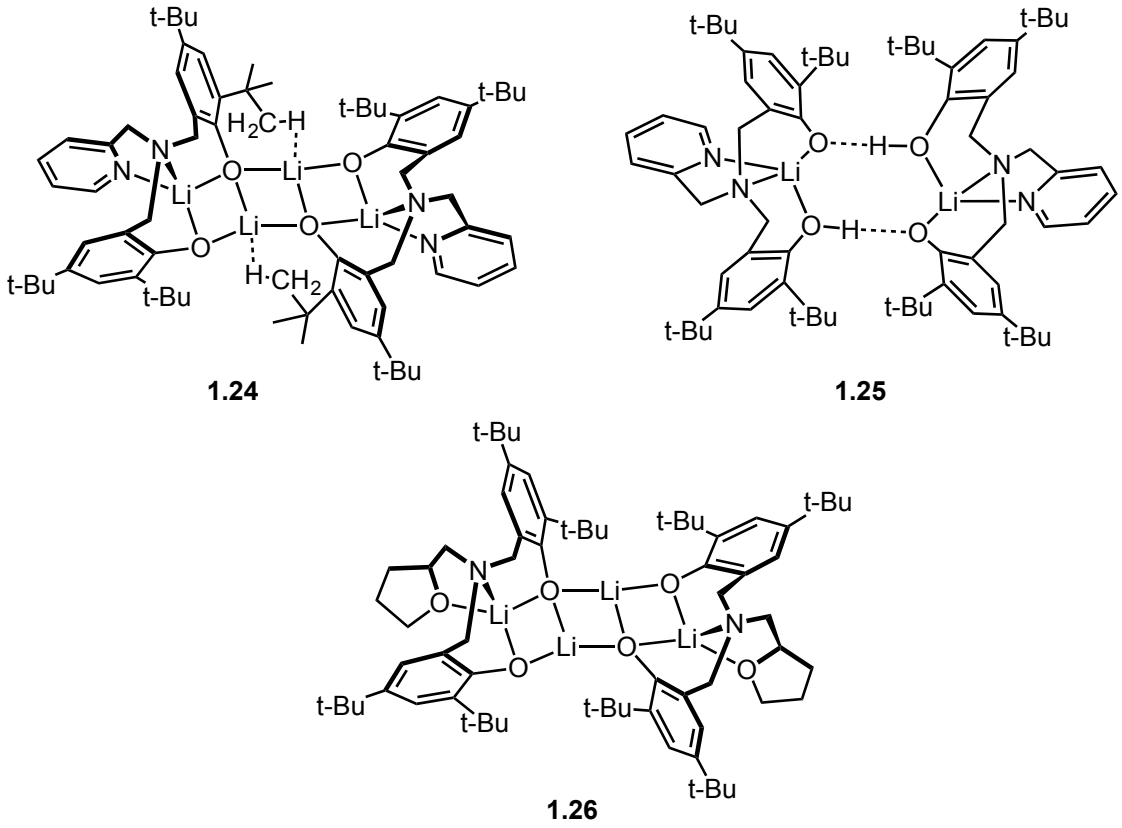

Figure 1.13 Structures of the Li-complexes reported by Huang and Chen (**1.24** and **1.25**) and Kozak and co-workers (**1.26**).

Lin and co-workers prepared a series of Li and Na complexes supported by bulky OOO-tridentate bis(phenolate) ligands.[90] Interestingly, the number of metal atoms involved in a complex could be controlled based on the stoichiometry of the reagents and the type of the solvent used. For example, a mononuclear sodium complex was obtained when THF was used, but dinuclear and tetranuclear complexes were obtained when toluene and diethyl ether were used, respectively. The dinuclear sodium complex is shown as **1.27** in Figure 1.14. This complex was prepared with a stoichiometric amount of $Na(N(Si(CH_3)_3)_2$, and only one phenol group per ligand was deprotonated, which was attributed to partial hydrolysis. Table 1-2, entry 6 shows that the calculated and observed

(by GPC) molecular weights are in good agreement and the dispersity of the polymer is quite low, which shows very good control over the reaction.

EDBP-H_2 has become a very attractive ligand recently (see also **1.22**). Mainly because it has no toxicity and has been approved as an antioxidant in polymer packaging by the U.S. Food and Drug Administration.[91-93] Miller and co-workers reported a monosodium complex of EDBP-H_2, which contains two methanol and two THF molecules coordinated to the sodium centre.[92] The EDBP-H_2 ligand became monodeprotonated exhibiting H-bonding with the protonated oxygen (**1.28a**, Figure 1.14). Interestingly, upon crystallization both of the methanols are lost and bimetallic crystals form with hydrogen bonding between two monosodium complexes (**1.28b,** Figure 1.14), which is another example of the tendency to form dimeric species via hydrogen bonding similar to the observation of Lin and co-workers[88] (**1.25**, Figure 1.13). The results exhibited by **1.28a** in L-LA polymerization can be found in Table 1-2 entry 7. The calculated molecular weight was based on the two methanol molecules that the complex contained, hypothesizing that both initiate polymerization and can propagate a chain. The measured molecular weight, however, proved to be approximately twice the calculated one (Table 1-2, entry 7) suggesting the possibility of only one chain growing per complex despite the presence of two methanols.

Tang and co-workers designed a new bulky ligand derived from EDBP-H_2 and coordinated it to sodium and potassium (**1.29a** and **1.29b**, Figure 1.14).[91] Ring opening polymerization of L-lactide was performed without the addition of any alcohol, but the reaction time was rather long, 36 h (Table 1-2, entries 8 and 9). The sodium complex

proved to be more efficient resulting in better conversions and lower dispersity values, which was attributed to the stronger Lewis acidity of sodium than potassium and thus for easier lactide coordination.[91]

Tetrametallic lithium and sodium complexes supported by tetradentate amino-bis(phenolato) ligands where the nitrogen donors originate from a homopiperazinyl group were prepared by the Kerton group.[94] All of the complexes exhibited very good activity in *rac*-lactide polymerization under melt and solution conditions with or without BnOH. Regarding reaction rate the sodium complexes proved to be better than the lithium analogues under alcohol-free conditions. The observed molecular weights showed good correlation with the expected calculated molecular weights and the polymers obtained were of low dispersity (between 1.10 and 1.41). The structure of the best performing complex (**1.30**) and the results obtained with it can be found in Figure 1.14 and Table 1-2, entry 10 respectively.

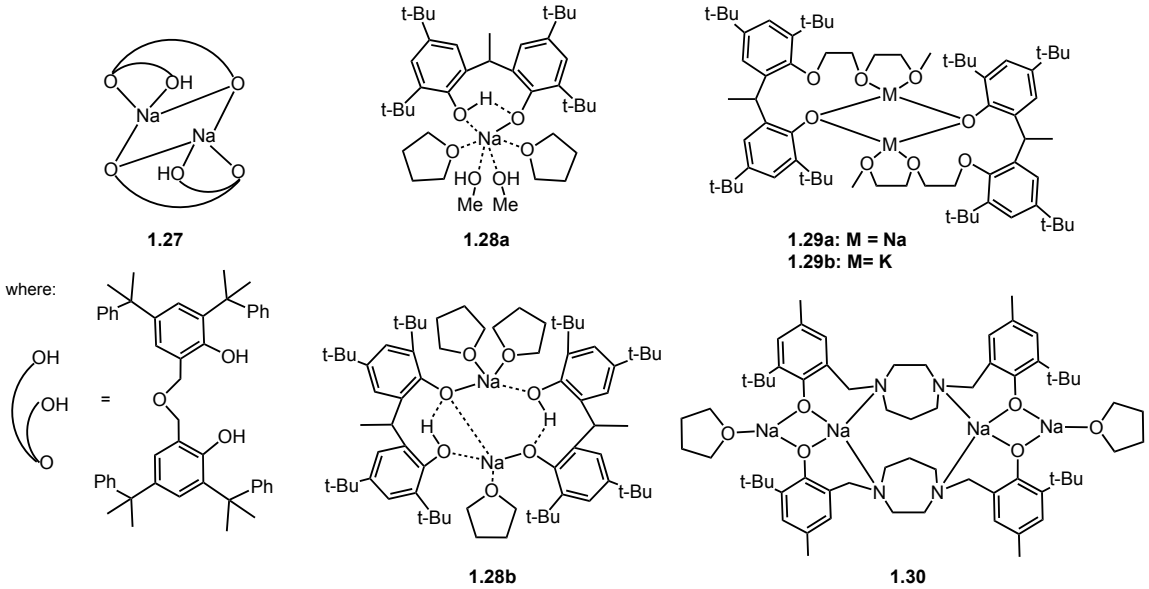

Figure 1.14 Structures of the sodium and potassium complexes published by Lin, Miller, Tang and Kerton.

Another potassium complex with an EDBP-H_2 ligand was prepared by Tang, Wu and co-workers.[95] The dimeric structure of the complex (**1.31**, Figure 1.15) is formed via a p–π interaction between a potassium of one complex and a phenyl ring of the ligand of another. Complex **1.31** was able to catalyze the ring opening polymerization of L-lactide in toluene at 90 °C without any alcohol added (Table 1-2, entry 11). When the authors compared **1.31** to EDBP-Na (**1.28a**), they found that EDBP-Na proved to be more efficient in terms of reaction time, conversion and dispersity (entry 7 vs. entry 11 in Table 1-2).

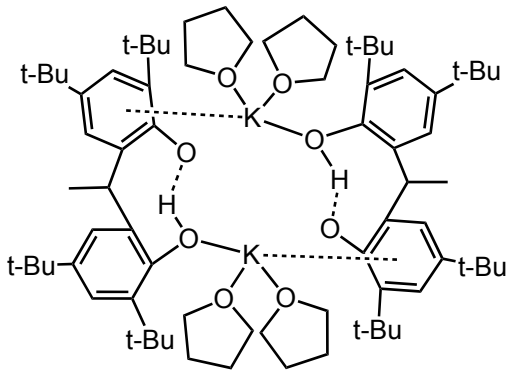

1.31

Figure 1.15 The structure of the complex prepared by Tang, Wu and co-workers.

The Kozak group also reported a bis(phenolato) potassium complex and its activity for ROP of *rac*-LA.[96] The tetrametallic complex **1.32** (Figure 1.16) showed a non-centrosymmetric structure with seven THF molecules coordinated to four potassium ions. Two of the potassium ions exhibited p–π interactions with the neighbouring phenyl rings. The complex showed good activity in *rac*-lactide polymerization with or without benzyl-alcohol (see Table 1-2, entry 12). The calculated molecular weights were much lower than the observed molecular weights when no BnOH was present, showing lack of control and side reactions.

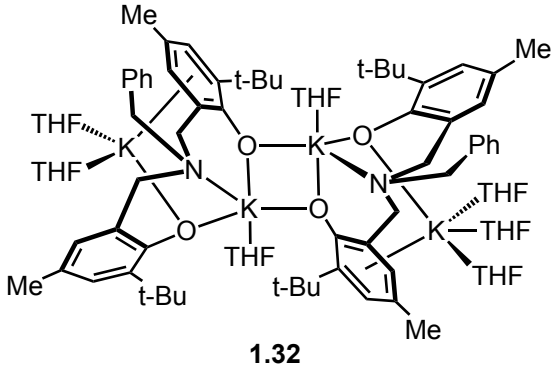

1.32

Figure 1.16 Structure of the complex reported by the Kozak group.

In general when comparing the activity of alkali metal complexes mentioned in this section, a reactivity order of Na > K ≥ Li can be established based on the observations of the different research groups.

1.2.3 Mg and Ca complexes in the ring opening polymerization of lactide

Magnesium and calcium complexes also play an important role in catalyst design because, similar to alkali metals, they are also biocompatible and non-toxic in the form of their salts.[97,98] Mg and Zn complexes were reviewed earlier by Tolman and co-workers[99] and alkaline earth metals by Dove and Stanford[100] as well as by Chishom and Zhou[101]. The Hayes group also published a detailed review on Mg, Ca and Zn complexes for lactide polymerization in 2009.[102] So, this section will focus on the complexes that were either published after these publications or were not included in the reviews.

In 2006 Bochmann and co-workers prepared tetradentate Mg and Ca complexes supported by an amino-(bis)phenolato ligand.[103] Although crystals suitable for X-ray diffraction were not obtained for the Mg complex, the research group proposed a monometallic structure for it (**1.33**, Figure 1.17). **1.33** may also exist as a dimer based on the four *tert*-butyl group environments observed by ^{1}H NMR. The crystal structure of the Ca complex (**1.34**, Figure 1.17) showed a geometry where both Ca atoms were coordinated to two oxygens and two nitrogens of one ligand, and the bridging oxygen of another ligand. In addition, there was an intramolecular Ca···H–C agostic interaction between a hydrogen of a *tert*-butyl group and the Ca resulting in six-coordinate calciums. The calcium complex, **1.34**, proved to more active in ε-caprolactone (CL) polymerization

than **1.33** but long reaction times were still needed for moderate conversions (Table 1-2, entry 13). The better activity with **1.34** was attributed to the higher Lewis acidity of calcium, which can facilitate easier CL coordination and activation for ring opening.

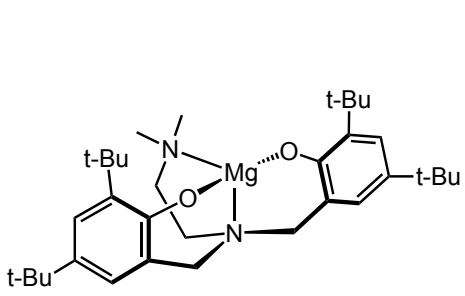

1.33

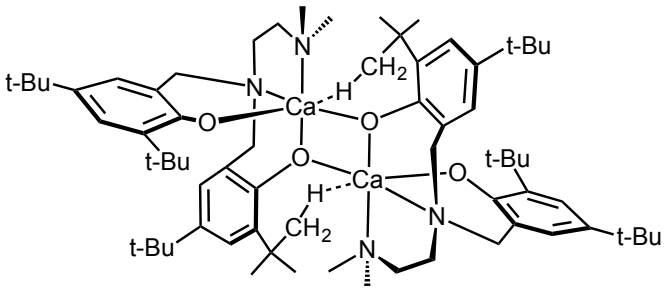

1.34

Figure 1.17 Structures of the complexes prepared by Bochmann and co-workers.

Another Mg complex with a bulky N,N'-bis(2-hydroxy-3,5-tert-butyl)-N,N'-dimethylethane-1,2-diamine ligand was prepared by Davidson and O'Hara in 2006 (**1.35**, Figure 1.18).[104] Unfortunately, the polymerization of CL or L-LA was not successful either at ambient temperature or at 110 °C with **1.35**. The inefficiency of the complex was speculated to be due to the steric hindrance of the bulky ligand as well as to the stability of the dimer not being able to provide an empty coordination site for the cyclic ester.

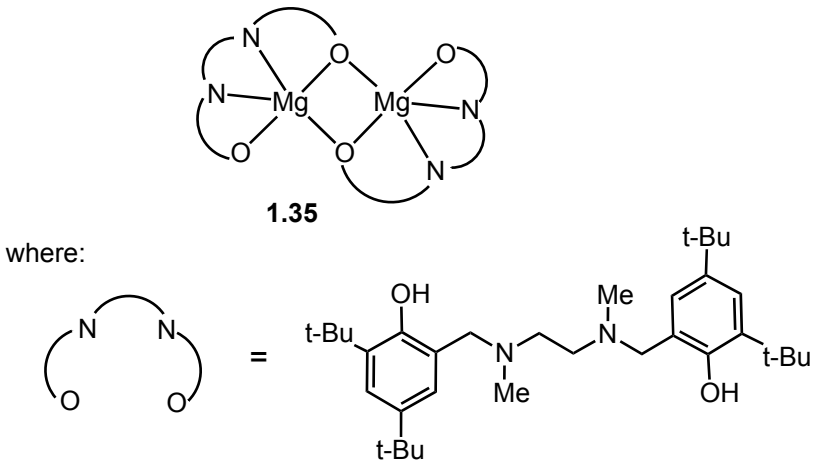

Figure 1.18 The structure of the Mg complex prepared by Davidson, O'Hara and co-workers.

A series of NNO-tridentate Schiff-base magnesium alkoxides was synthesized by Lin and co-workers in 2009.[105] These complexes were penta-coordinated dimers bridging via the oxygens of the benzyl alkoxides. The research group found that the substituent at the *para* position of the phenoxy group had a significant effect on the reactivity. An electron donating methoxy group increased the reactivity dramatically as opposed to no substituents (i.e. only H) or an electron withdrawing chloride or bromide. The structure of the most active complex, **1.36**, is depicted in Figure 1.19 and its polymerization results are in Table 1-2, entry 14.

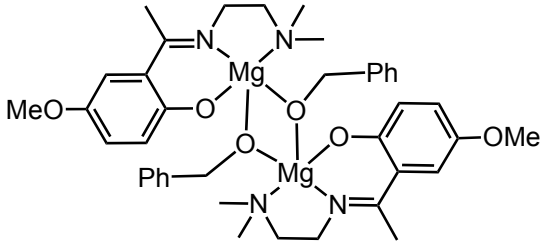

Figure 1.19 The structure of the Mg complex prepared by Lin and co-workers.

A dinuclear tetradentate Mg complex, similar to **1.35**, was synthesized by Sobota and co-workers in 2010.[106] The structure of the complex (**1.37**) is shown in Figure 1.20. Both magnesiums are penta-coordinate and adopt an almost identical geometry between a trigonal bipyramid and a square pyramid with τ parameters of 0.41 and 0.39. This complex was also inefficient in lactide polymerization, similar to **1.35**. The research group attributed this to the stability of the dimer and it not being able to dissociate and provide an empty coordination site for lactide coordination.

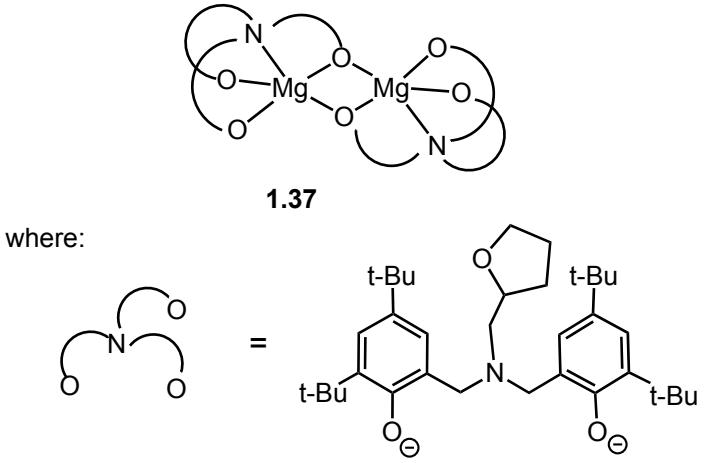

Figure 1.20 The structure of the Mg complex prepared by Sobota and co-workers.

Seeing the stability and inactivity of the dimeric species, next, the same research group next undertook the synthesis of monometallic Mg complexes with bidentate ligands speculating that they would be more open for lactide coordination and polymerization (**1.38a** and **1.38b**, Figure 1.21).[106]

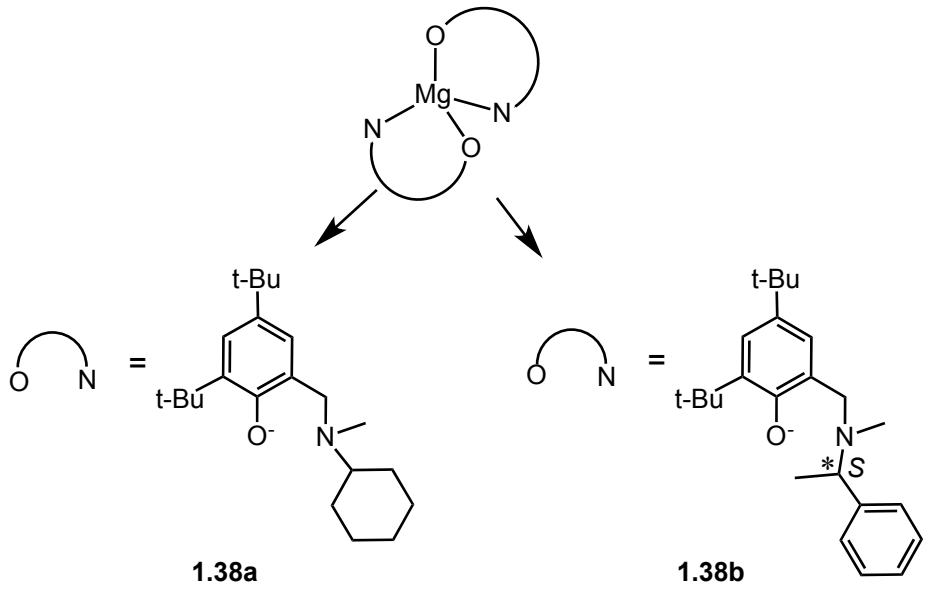

Figure 1.21 Structures of the monometallic Mg complexes prepared by Sobota and co-workers.

These complexes were indeed effective in the ring opening polymerization of L-lactide at room temperature but only with the addition of benzyl-alcohol. The polymerization was well-controlled with polymers of low dispersity (Table 1-2 entries 15 and 16).

In an elegant study, the Miller group prepared a series of alkali and alkaline earth metal complexes of 2,6-di-*tert*-butyl-4-methyl-phenol (BHT) and EDBP-H_2 ligands and compared their activity in 2012.[93] The choice of BHT was based on its non-toxicity as demonstrated by its approval by the U.S. Food and Drug Administration as an antioxidant and can be added directly to food.[93] In general, the complexes with the BHT ligand were more efficient than the complexes with the EDBP-H_2 ligand. The structures of the Mg- and Ca-BHT (**1.39** and **1.40**) and the Ca-EDBP (**1.41**) complexes can be found in Figure 1.22. Of all the nine complexes synthesized, the Mg complex **1.39**

proved to be the slowest. Comparing the activity of the alkaline earth metal BHT complexes to alkali metal BHT complexes, the reactivity order of Na >> Li > Ca >> Mg was established by the authors.

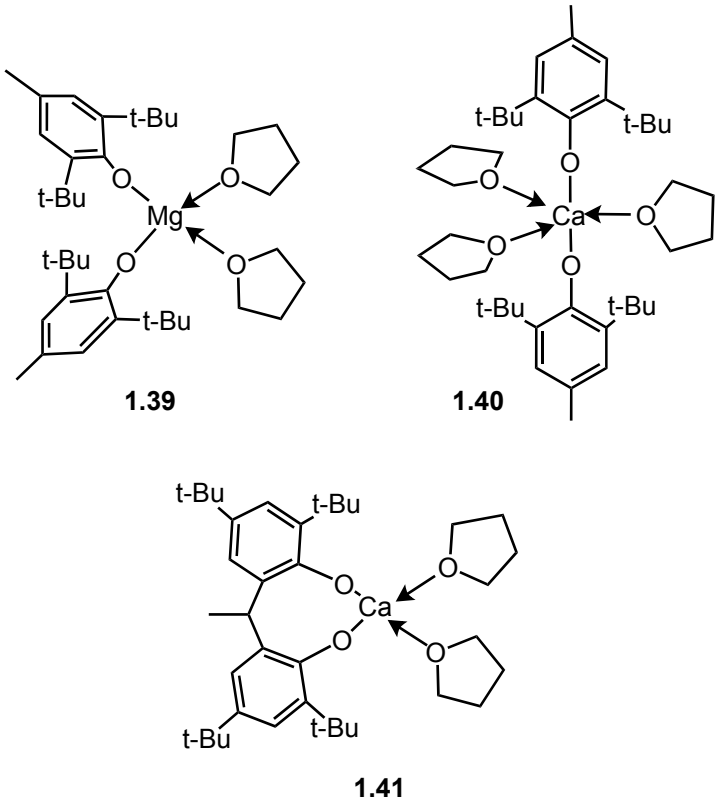

Figure 1.22 The structures of the Mg and Ca complexes prepared by the Miller group.

It is worth noting here that recently, a new trend has emerged in PLA synthesis, where the ring opening polymerization of lactide with biocompatible metal complexes and the potential application of the produced PLA in drug delivery and controlled drug release are combined. For example, alkoxy-butyl magnesium complexes supported by drug chelating agents were synthesized and tested in L-lactide polymerization by Sobota and co-workers.[107,108] The obtained PLA were end-capped with the drugs, resulting in PLA-drug conjugates which have good potential in biomedical applications.

1.2.4 Mechanistic considerations in lactide polymerization

Catalyzed homogeneous ring opening polymerization of lactones in general is a viable and preferred method to obtain polyesters because it allows the reaction to be performed in a controlled manner, especially if the polymerization has a living or immortal characteristic.[80] The thermodynamic driving force behind the reaction is the ring strain that is released upon ring opening of the cyclic lactones allowing the unfavourable entropy to be overcome.[80,85,109] The definitions of living and immortal polymerizations and the difference between the two were first described by Inoue, when he investigated Al-porphyrins in epoxide/carbon dioxide copolymerization.[110,111] In a system that exhibits living character, explained by Inoue, there are no chain transfer and termination reactions. As a result, identical polymer chain lengths, and thus, a very narrow molecular weight distribution are achieved. In the absence of the termination step, the polymer chains just await for additional monomers or termination. So, the living character can be justified by an additional supply of monomer, which can restart the polymerization. The immortal character of a catalyst system is characterized by a rapid exchange between the metal alkoxide and an alcohol. The alcohol behaves as a chain transfer agent, which in other cases causes broadening of the molecular weight distribution. However, in an immortal system, the dispersity remains very narrow. Additionally, the molecular weight of the polymer decreases because the number of the growing chains increases according to the sum of the number of the molecules of the initiator and that of the alcohol.[111]

The living and immortal character in the ring opening polymerization of lactones were further studied by Carpentier, Sarazin and co-workers. They added that "classical living" polymerization can be carried out with a suitable catalyst without any alcohol present, where then the number of active sites is equal to the number of catalyst molecules which, hence, are called initiators.[112] In the immortal ring opening polymerization (abbreviated as iROP), on the other hand, a catalyst and a nucleophile act together as initiator and chain transfer agent (CTA). The number of the growing polymer chains in this case is equal to the amount of CTA added. For both living and immortal ROP, initiation (ring opening of the first lactone) must be faster than propagation and termination should be minimal. For iROP, the reversible chain transfer reactions must also be faster than propagation.

There are two main mechanisms that are characteristic of ROP of lactones with metal catalysts: the coordination-insertion mechanism (CIM) and the activated monomer mechanism (AMM). The general mechanism of CIM is depicted in Scheme 1-9. In this reaction a nucleophile is already included in the complex as an alkoxide ligand, which can be formed via the addition of alcohol if the original complex was not an alkoxide (the reaction at the top of Scheme 1-9). Any excess alcohol present acts as CTA generating active growing polymer chains. The number average molecular weight is then equal to the monomer to CTA ratio. According to the CIM, the alkoxide species initiates the ring opening and the monomer is inserted in the metal – alkoxide bond. The monomer is ring opened via an oxygen-acyl cleavage. The growing polymer chain remains attached to the

metal centre throughout the propagation and the reaction follows a controlled living polymerization under optimal conditions.

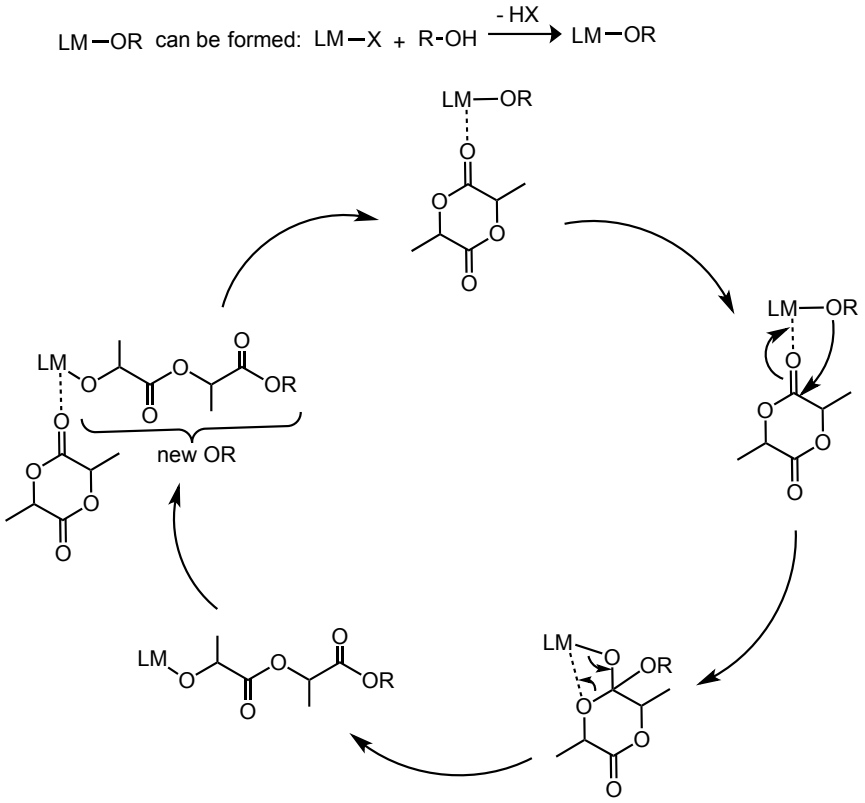

Scheme 1-9 General reaction scheme of the coordination-insertion mechanism (CIM) for the ring opening of lactide.

In the activated monomer mechanism, the nucleophile is not part of the complex (Scheme 1-10). The monomer is activated by a Lewis acidic metal centre first. Then the electrophilic carbon of the carbonyl group is attacked by an external nucleophile, usually an alcohol, and the monomer is ring opened via an oxygen-acyl cleavage.

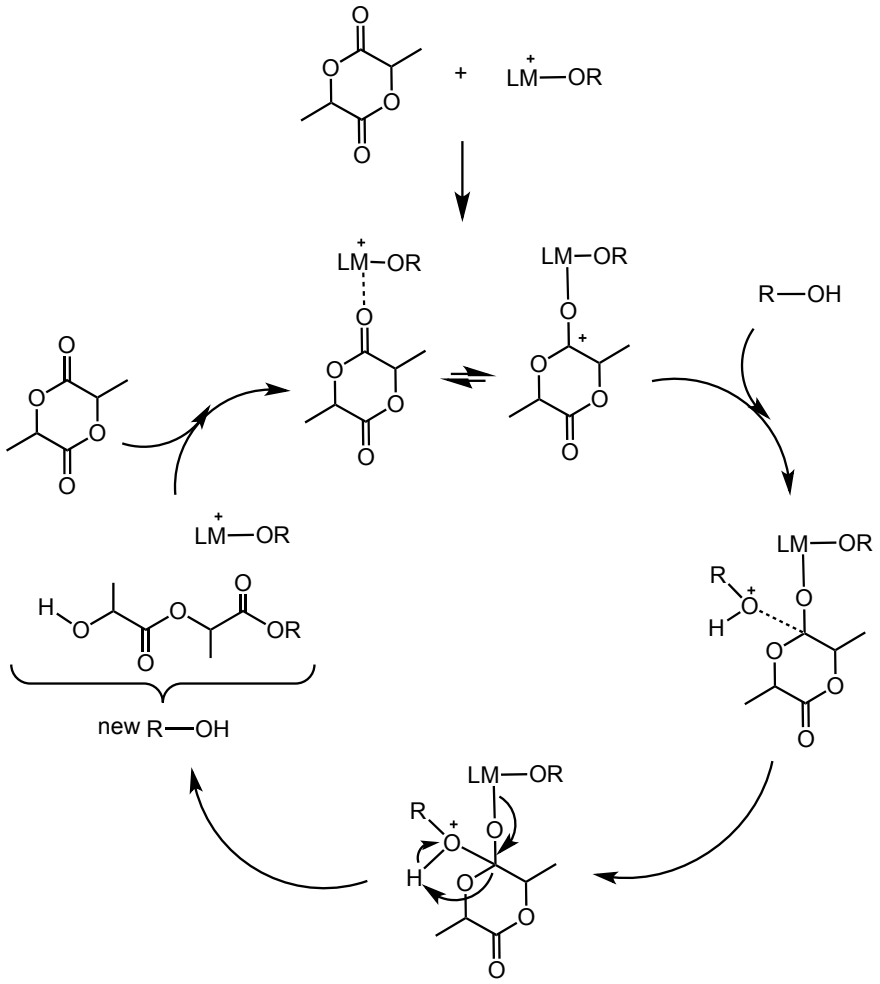

Scheme 1-10 General reaction scheme of the activated monomer mechanism (AMM) for the ring opening of lactide. The + charge indicates formal charge.

Ring opening polymerization with alkali metal phenolate complexes often follows the CIM[113] and there are several examples in the literature where CIM was proposed to occur.[89,94,114] However, sometimes the possibility of the AMM mechanism cannot be excluded. Evidence toward AMM was found by the Carpentier group when alkali aminoether-phenolate complexes were applied in lactide polymerization.[115] The research group systematically followed the reaction between their Li complex, lactide and BnOH in stoichiometric amounts via ^{1}H NMR. First, stoichiometric amounts of the

complex and BnOH were monitored. No change occurred within 45 min and the ^{1}H NMR showed only a mixture of BnOH and complex. Next, a 1:1:1 mixture of complex, BnOH and L-LA was monitored. The lactide monitored was transformed into the ring opened product with a benzyl and a hydroxyl end group and no change in the chemical shifts of the complex was detected. In order to support the hypothesis of an AMM, a 1:1:2 mixture of complex, BnOH and L-LA was monitored next. The findings were in good agreement with the research group's hypothesis, that is, the two equivalents of L-LA were totally consumed into benzyl and hydroxyl group end capped species again and so, the ring opening was initiated by a nucleophilic attack by BnOH. Based on these results and end group analysis, the research group proposed that the reaction followed the activated monomer mechanism. In addition, a detailed kinetic model was developed by Sarazin and co-workers in 2014[116] to describe immortal polymerization that even took fast reversible chain transfers into account, which was missing from previous models.

1.2.5 Objectives

The objective of the second part of the thesis was to synthesize earth abundant and biocompatible alkali and alkaline earth metal complexes for the ring opening polymerization of lactide. The goal was to achieve a good control over the reaction parameters such as molecular weight as well as dispersity. Another aim was to extend ring opening polymerization to melt and microwave assisted conditions beside polymerization in solution. Some mechanistic studies were also undertaken.

1.3 References

1. S. Fukuoka; M. Kawamura; K. Komiya; M. Tojo; H. Hachiya; K. Hasegawa; M. Aminaka; H. Okamoto; I. Fukawa; S. Konno *Green Chem.* **2003**, *5*, 497-507.

2. B. Rieger; A. Kuenkel; G. W. Coates; R. Reichardt; E. Dinjus; T. A. Zevaco; Editors *Synthetic biodegradable polymers. [In: Adv. Polym. Sci., 2012; 245]*; Springer GmbH, 2012.

3. G. A. Luinstra *Polym. Rev.* **2008**, *48*, 192-219.

4. M. Taherimehr; P. P. Pescarmona *J. Appl. Polym. Sci.* **2014**, *131,* 1-17.

5. Y. Gibert; S. Sassi-Messai; J.-B. Fini; L. Bernard; D. Zalko; J.-P. Cravedi; P. Balaguer; M. Andersson-Lendahl; B. Demeneix; V. Laudet *BMC Dev Biol* **2011**, *11*, 4.

6. C. Bolognesi; L. Castle; J.-P. Cravedi; K.-H. Engel; P. Fowler; R. Franz; K. Grob; R. Gurtler; T. Husoey; W. Mennes; M. R. Milana; A. Penninks; F. Roland; V. Silano; A. Smith; M. d. F. T. Pocas; C. Tlustos; F. Toldra; D. Wolfle; H. Zorn *EFSA J.* **2015**, *13*, 3978/3971-3978/3922.

7. A. M. Nelson; T. E. Long *Polym. Int.* **2012**, *61*, 1485-1491.

8. European Information Centre on Bisphenol A, Information provided by PlasticsEurope's PC/BPA-group, available from: http://www.bisphenol-a-europe.org [Accessed: June 2016].

9. J. J. Heindel; R. R. Newbold; J. R. Bucher; L. Camacho; K. B. Delclos; S. M. Lewis; M. Vanlandingham; M. I. Churchwell; N. C. Twaddle; M. McLellen; M. Chidambaram; M. Bryant; K. Woodling; G. Gamboa da Costa; S. A. Ferguson; J. Flaws; P. C. Howard; N. J. Walker; R. T. Zoeller; J. Fostel; C. Favaro; T. T. Schug *Reprod. Toxicol.* **2015**, *58*, 33-44.

10. S. A. Johnson; A. B. Javurek; M. S. Painter; M. R. Ellersieck; T. H. Welsh, Jr.; L. Camacho; S. M. Lewis; M. M. Vanlandingham; S. A. Ferguson; C. S. Rosenfeld *Horm. Behav.* **2016,** *80*, 139 - 148.

11. T. Sakakura; K. Kohno *Chem. Commun.* **2009**, 1312-1330.

12. W. B. Kim; U. A. Joshi; J. S. Lee *Ind. Eng. Chem. Res.* **2004**, *43*, 1897-1914.

13. J. Langanke; A. Wolf; M. Peters *Carbon Dioxide Utilisation*; Elsevier: Amsterdam, 2015, p 59-71.

14. A. Goeppert; M. Czaun; G. K. Surya Prakash; G. A. Olah *Energy Environ. Sci.* **2012**, *5*, 7833-7853.

15. G. Centi; S. Perathoner; Editors *Green Carbon Dioxide: Advances in CO_2 Utilization*; John Wiley & Sons, Inc., 2014.

16. P. Markewitz; W. Kuckshinrichs; W. Leitner; J. Linssen; P. Zapp; R. Bongartz; A. Schreiber; T. E. Mueller *Energy Environ. Sci.* **2012**, *5*, 7281-7305.

17. M. Peters; B. Koehler; W. Kuckshinrichs; W. Leitner; P. Markewitz; T. E. Mueller *ChemSusChem* **2011**, *4*, 1216-1240.

18. S. Rigby; G. Modes; S. Jovanovic; J. Wei; K. Tanaka; P. Moser; T. Katz; John Wiley & Sons, Inc.: 2014, p 193-226.

19. A. Otto; T. Grube; S. Schiebahn; D. Stolten *Energy Environ. Sci.* **2015**, *8*, 3283-3297.

20. T. Sakakura; J.-C. Choi; H. Yasuda *Chem. Rev.* **2007**, *107*, 2365-2387.

21. M. Aresta; A. Dibenedetto; A. Angelini *Chem. Rev.* **2014**, *114*, 1709-1742.

22. P. Styring; E. A. Quadrelli; K. Armstrong; Editors *Carbon Dioxide Utilisation: Closing the Carbon Cycle*; Elsevier: Amsterdam, 2015.

23. N. Yi; J. Unruangsri; J. Shaw; C. K. Williams *Faraday Discuss* **2015**, *183*, 67-82.

24. G. Si; L. Zhang; B. Han; H. Zhang; X. Li; B. Liu *RSC Adv.* **2016**, *6*, 22821-22826.

25. D. Alhashmialameer; J. Collins; K. Hattenhauer; F. M. Kerton *Catal. Sci. Technol.* **2016**, *6*, 5364-5373.

26. P. Sudakar; D. Sivanesan; S. Yoon *Macromol. Rapid Commun.* **2016**, *37*, 788-793.

27. G.-P. Wu; S.-H. Wei; W.-M. Ren; X.-B. Lu; T.-Q. Xu; D. J. Darensbourg *J. Am. Chem. Soc.* **2011**, *133*, 15191-15199.

28. S. Inoue; H. Koinuma; T. Tsuruta *J. Polym. Sci.* **1969**, *7*, 287-292.

29. K. Soga; E. Imai; I. Hattori *Polym. J.* **1981**, *13*, 407-410.

30. D. J. Darensbourg *Inorg. Chem.* **2010**, *49*, 10765-10780.

31. Y. Q. Zheng; J. L. Lin; H. L. Zhang *Z. Kristallogr. - New Cryst. Struct.* **2000**, *215*, 535-536.

32. T. Aida; M. Ishikawa; S. Inoue *Macromolecules* **1986**, *19*, 8-13.

33. D. J. Darensbourg; M. W. Holtcamp *Macromolecules* **1995**, *28*, 7577-7579.

34. D. J. Darensbourg; M. W. Holtcamp; G. E. Struck; M. S. Zimmer; S. A. Niezgoda; P. Rainey; J. B. Robertson; J. D. Draper; J. H. Reibenspies *J. Am. Chem. Soc.* **1999**, *121*, 107-116.

35. H. S. Kim; J. J. Kim; S. D. Lee; M. S. Lah; D. Moon; H. G. Jang *Chem. Eur. J.* **2003**, *9*, 678-686.

36. D. R. Moore; M. Cheng; E. B. Lobkovsky; G. W. Coates *Angew. Chem. Int. Ed.* **2002**, *41*, 2599-2602.

37. R. K. Dean; S. L. Granville; L. N. Dawe; A. Decken; K. M. Hattenhauer; C. M. Kozak *Dalton Trans.* **2010**, *39*, 548-559.

38. C. J. Hinshaw; G. Peng; R. Singh; J. T. Spence; J. H. Enemark; M. Bruck; J. Kristofzski; S. L. Merbs; R. B. Ortega; P. A. Wexler *Inorg. Chem.* **1989**, *28*, 4483-4491.

39. O. Wichmann; R. Sillanpää; A. Lehtonen *Coord. Chem. Rev.* **2012**, *256*, 371-392.

40. S. Mang; A. I. Cooper; M. E. Colclough; N. Chauhan; A. B. Holmes *Macromolecules* **2000**, *33*, 303-308.

41. L. M. Stamp; S. A. Mang; A. B. Holmes; K. A. Knights; Y. R. de Miguel; I. F. McConvey *Chem. Commun.* **2001**, 2502-2503.

42. E. N. Jacobsen; W. Zhang; M. L. Guler *J. Am. Chem. Soc.* **1991**, *113*, 6703-6704.

43. L. E. Martinez; J. L. Leighton; D. H. Carsten; E. N. Jacobsen *J. Am. Chem. Soc.* **1995**, *117*, 5897-5898.

44. K. B. Hansen; J. L. Leighton; E. N. Jacobsen *J. Am. Chem. Soc.* **1996**, *118*, 10924-10925.

45. E. N. Jacobsen *Acc. Chem. Res.* **2000**, *33*, 421-431.

46. A. W. Miller; S. T. Nguyen *Org. Lett.* **2004**, *6*, 2301-2304.

47. D. J. Darensbourg; R. M. Mackiewicz; J. L. Rodgers; C. C. Fang; D. R. Billodeaux; J. H. Reibenspies *Inorg. Chem.* **2004**, *43*, 6024-6034.

48. D. J. Darensbourg *Chem. Rev.* **2007**, *107*, 2388-2410.

49. B. Li; G. P. Wu; W. M. Ren; Y. M. Wang; D. Y. Rao; X. B. Lu *J. Polym. Sci., Part A: Polym. Chem.* **2008**, *46*, 6102-6113.

50. D. J. Darensbourg; M. Ulusoy; O. Karroonnirum; R. R. Poland; J. H. Reibenspies; B. Çetinkaya *Macromolecules* **2009**, *42*, 6992-6998.

51. C. Hongfa; J. Tian; J. Andreatta; D. J. Darensbourg; D. E. Bergbreiter *Chem. Commun.* **2008**, 975-977.

52. D. Y. Rao; B. Li; R. Zhang; H. Wang; X. B. Lu *Inorg. Chem.* **2009**, *48*, 2830-2836.

53. J. Liu; Y.-Y. Bao; Y. Liu; W.-M. Ren; X. B. Lu *Polym. Chem.* **2013**, *4*, 1439-1444.

54. K. Nakano; M. Nakamura; K. Nozaki *Macromolecules* **2009**, *42*, 6972-6980.

55. R. Eberhardt; M. Allmendinger; B. Rieger *Macromol. Rapid Commun.* **2003**, *24*, 194-196.

56. M. Taherimehr; A. Decortes; S. M. Al-Amsyar; W. Lueangchaichaweng; C. J. Whiteoak; E. C. Escudero-Adan; A. W. Kleij; P. P. Pescarmona *Catal. Sci. Technol.* **2012**, *2*, 2231-2237.

57. S. I. Vagin; R. Reichardt; S. Klaus; B. Rieger *J. Am. Chem. Soc.* **2010**, *132*, 14367-14369.

58. S. Klaus; S. I. Vagin; M. W. Lehenmeier; P. Deglmann; A. K. Brym; B. Rieger *Macromolecules* **2011**, *44*, 9508-9516.

59. J. Gurnham; S. Gambarotta; I. Korobkov; L. Jasinska-Walc; R. Duchateau *Organometallics* **2014**, *33*, 4401-4409.

60. B. Han; L. Zhang; S. J. Kyran; B. Liu; Z. Duan; D. J. Darensbourg *J. Polym. Sci., Part A: Polym. Chem.* **2016**, *54*, 1938-1944.

61. R. K. Dean; K. Devaine-Pressing; L. N. Dawe; C. M. Kozak *Dalton Trans.* **2013**, *42*, 9233-9244.

62. R. K. Dean; L. N. Dawe; C. M. Kozak *Inorg. Chem.* **2012**, *51*, 9095-9103.

63. F. Castro-Gomez; G. Salassa; A. W. Kleij; C. Bo *Chem. Eur. J.* **2013**, *19*, 6289-6298.

64. H. Chen; L. N. Dawe; C. M. Kozak *Catal. Sci. Technol.* **2014**, *4*, 1547-1555.

65. S. Klaus; M. W. Lehenmeier; C. E. Anderson; B. Rieger *Coord. Chem. Rev.* **2011**, *255*, 1460-1479.

66. P. P. Pescarmona; M. Taherimehr *Catal. Sci. Technol.* **2012**, *2*, 2169-2187.

67. D. J. Darensbourg; R. M. Mackiewicz *J. Am. Chem. Soc.* **2005**, *127*, 14026-14038.

68. D. J. Darensbourg; J. C. Yarbrough *J. Am. Chem. Soc.* **2002**, *124*, 6335-6342.

69. F. Jutz; A. Buchard; M. R. Kember; S. B. Fredriksen; C. K. Williams *J. Am. Chem. Soc.* **2011**, *133*, 17395-17405.

70. Y.-M. Shen; W.-L. Duan; M. Shi *J. Org. Chem.* **2003**, *68*, 1559-1562.

71. K. Nakano; S. Hashimoto; K. Nozaki *Chem. Sci.* **2010**, *1*, 369-373.

72. D. J. Darensbourg; A. L. Phelps *Inorg. Chem.* **2005**, *44*, 4622-4629.

73. M. Taherimehr; S. M. Al-Amsyar; C. J. Whiteoak; A. W. Kleij; P. P. Pescarmona *Green Chem.* **2013**, *15*, 3083-3090.

74. D. J. Darensbourg; A. D. Yeung *Polym. Chem.* **2015**, *6*, 1103-1117.

75. L. S. Nair; C. T. Laurencin *Prog. Polym. Sci.* **2007**, *32*, 762-798.

76. Y. Tokiwa; B. P. Calabia *Appl. Microbiol. Biotechnol.* **2006**, *72*, 244-251.

77. K. Madhavan Nampoothiri; N. R. Nair; R. P. John *Bioresour. Technol.* **2010**, *101*, 8493-8501.

78. S. Dutta; W.-C. Hung; B.-H. Huang; C.-C. Lin *Adv. Polym. Sci.* **2012**, *245*, 219-283.

79. V. Siracusa; P. Rocculi; S. Romani; M. Dalla Rosa *Trends Food Sci. Technol.* **2008**, *19*, 634-643.

80. C. K. Williams *Chem. Soc. Rev.* **2007**, *36*, 1573-1580.

81. H. Tian; Z. Tang; X. Zhuang; X. Chen; X. Jing *Prog. Polym. Sci.* **2012**, *37*, 237-280.

82. A. Weisman; B. Chou; J. O'Brien; K. J. Shea *Adv. Drug Delivery Rev.* **2015**, *90*, 81-100.

83. O. Avinc; A. Khoddami *Fibre Chem.* **2010**, *42*, 68-78.

84. S. Slomkowski; S. Penczek; A. Duda *Polym. Adv. Technol.* **2014**, *25*, 436-447.

85. R. H. Platel; L. M. Hodgson; C. K. Williams *Polym. Rev.* **2008**, *48*, 11-63.

86. B.-H. Huang; B.-T. Ko; T. Athar; C.-C. Lin *Inorg. Chem.* **2006**, *45*, 7348-7356.

87. A. K. Sutar; T. Maharana; S. Dutta; C.-T. Chen; C.-C. Lin *Chem. Soc. Rev.* **2010**, *39*, 1724-1746.

88. C. A. Huang; C. T. Chen *Dalton Trans.* **2007**, 5561-5566.

89. R. K. Dean; A. M. Reckling; H. Chen; L. N. Dawe; C. M. Schneider; C. M. Kozak *Dalton Trans.* **2013**, 3504-3530.

90. Y. Huang; Y.-H. Tsai; W.-C. Hung; C.-S. Lin; W. Wang; J.-H. Huang; S. Dutta; C.-C. Lin *Inorg. Chem.* **2010**, *49*, 9416-9425.

91. L. Chen; L. Jia; F. Cheng; L. Wang; C.-c. Lin; J. Wu; N. Tang *Inorg. Chem. Commun.* **2011**, *14*, 26-30.

92. H.-Y. Chen; J. Zhang; C.-C. Lin; J. H. Reibenspies; S. A. Miller *Green Chem.* **2007**, *9*, 1038-1040.

93. H.-Y. Chen; L. Mialon; K. A. Abboud; S. A. Miller *Organometallics* **2012**, *31*, 5252-5261.

94. D. Alhashmialameer; N. Ikpo; J. Collins; L. N. Dawe; K. Hattenhauer; F. M. Kerton *Dalton Trans.* **2015**, *44*, 20216-20231.

95. X. Pan; A. Liu; X. Yang; J. Wu; N. Tang *Inorg. Chem. Commun.* **2010**, *13*, 376-379.

96. L. N. Saunders; L. N. Dawe; C. M. Kozak *J. Organomet. Chem.* **2014**, *749*, 34-40.

97. R. Jefferson; *Patty's Toxicology*, **2012**, *1*, 935-947.

98. M. S. Hill *Annu. Rep. Prog. Chem., Sect. A: Inorg. Chem.* **2013**, *109*, 18-27.

99. B. J. O'Keefe; M. A. Hillmyer; W. B. Tolman *J. Chem. Soc. Dalton Trans.* **2001**, 2215-2224.

100. M. J. Stanford; A. P. Dove *Chem. Soc. Rev.* **2010**, *39*, 486-494.

101. M. H. Chisholm; Z. P. Zhou *J. Mater. Chem.* **2004**, *14*, 3081-3092.

102. C. A. Wheaton; P. G. Hayes; B. J. Ireland *Dalton Trans.* **2009**, 4832-4846.

103. Y. Sarazin; R. H. Howard; D. L. Hughes; S. M. Humphrey; M. Bochmann *Dalton Trans.* **2006**, 340-350.

104. M. G. Davidson; M. D. Jones; D. Meng; C. T. O'Hara *Main Group Chem.* **2006**, *5*, 3-12.

105. W. C. Hung; C. C. Lin *Inorg. Chem.* **2009**, *48*, 728-734.

106. J. Ejfler; K. Krauzy-Dziedzic; S. Szafert; L. B. Jerzykiewicz; P. Sobota *Eur. J. Inorg. Chem.* **2010**, 3602-3609.

107. T. Han; J. Utko; L. B. Jerzykiewicz; P. Sobota *Dalton Trans.* **2011**, *40*, 12660-12662.

108. T. Han; R. Petrus; D. Bykowski; L. Jerzykiewicz; P. Sobota *Organometallics* **2015**, *34*, 4871-4880.

109. O. Nuyken; S. D. Pask *Polymers* **2013**, *5*, 361-403.

110. T. Aida; S. Inoue *Acc. Chem. Res.* **1996**, *29*, 39-48.

111. S. Inoue *J. Polym. Sci., Part A: Polym. Chem.* **2000**, *38*, 2861-2871.

112. N. Ajellal; J.-F. Carpentier; C. Guillaume; S. M. Guillaume; M. Helou; V. Poirier; Y. Sarazin; A. Trifonov *Dalton Trans.* **2010**, *39*, 8363-8376.

113. Y. Sarazin; J.-F. Carpentier *Chem. Rev.* **2015**, *115*, 3564-3614.

114. N. Ikpo; C. Hoffmann; L. N. Dawe; F. M. Kerton *Dalton Trans.* **2012**, *41*, 6651-6660.

115. Y. Sarazin; S.-C. Rosca; D.-A. Rosca; V. Dorcet; J.-F. Carpentier; F. M. Kerton; C. M. Kozak *Dalton Trans.* **2013**, 9361–9375.

116. L. Wang; V. Poirier; F. Ghiotto; M. Bochmann; R. D. Cannon; J.-F. Carpentier; Y. Sarazin *Macromolecules* **2014**, *47*, 2574-2584.

Co-Authorship Statement

Chapter 2: Cyclohexene Oxide/Carbon Dioxide Copolymerization by Chromium(III) Amino-bis(phenolato) Complexes and MALDI-TOF MS Analysis of the Polycarbonates

This chapter contains the results published in the full article "Cyclohexene Oxide/Carbon Dioxide Copolymerization by Chromium(III) Amino-bis(phenolato) Complexes and MALDI-TOF MS Analysis of the Polycarbonates", *Polymer Chemistry*, **2015**, *6*, 6305–6315.

Authors: Katalin Devaine-Pressing, Louise N. Dawe and Christopher M. Kozak.

The first author (Katalin Devaine-Pressing) contributed 90% of the content of the article as the main researcher including: performing all the experimental research, collecting data, and writing parts of the paper (including creating ORTEP images, results and discussion and the experimental sections).

The co-author, Louise N. Dawe was the crystallographer on the paper at Memorial University and collected XRD data and solved the structure for complexes **2.1**·THF, **2.2**·THF and **2.1**·DMAP.

The corresponding author (Christopher M. Kozak), my supervisor, was the principal investigator of this research. He developed novel ideas, designed experiments and assisted with writing and submitting the manuscript.

Chapter 2. Cyclohexene Oxide/Carbon Dioxide Copolymerization by Chromium(III) Amine-bis(phenolate) Complexes and MALDI-TOF MS Analysis of the Polycarbonates

2.1 Introduction

As it was highlighted in Chapter 1, the copolymerization of carbon dioxide (CO_2) and epoxides has recently become a growing area of interest for several reasons. Most importantly, the reaction is an appealing alternative to the traditional method of polycarbonate synthesis, which involves the use of the endocrine disruptor Bisphenol-A and highly toxic phosgene.[1-4] Furthermore, the high free energy of epoxides drives the reaction forward to convert the very stable CO_2.[5] Another advantage is that CO_2 is incorporated into the product, which is favorable not only with respect to the atom economy of the reaction, but also because CO_2 is a readily available, non–toxic and low–cost feedstock.[6] Also, CO_2 can be considered a renewable resource,[7] so its utilization is preferred over dwindling fossil fuels that are still the main basis for commercial polycarbonate synthesis.[8]

In order to carry out and control the CO_2/epoxide copolymerization reaction, an efficient catalyst system is needed.[9] Recently, a large number of complexes have been developed as active catalyst precursors for the copolymerization of CO_2 and epoxides. For example, complexes with Zn,[10-12] Al,[13] Co,[14-21] Fe,[22,23] Mg,[24] and Cr[25-42] have proven to be active in CO_2/epoxide copolymerization. Many catalyst systems require a suitable

ionic or neutral nucleophilic co-catalyst (Chapter 1, Figure 1.2, Section 1.1.3), the most broadly used include methylimidazole (*N*-MeIm), 4-(*N,N*-dimethylamino)pyridine (DMAP) and bis(triphenylphosphoranylidene)ammonium (PPN^+) salts, such as PPN-chloride, azide, or 2,4-dinitrophenolate (PPNCl, $PPNN_3$ PPN(2,4-DNP)).

The mechanism of CO_2/epoxide coupling and copolymerization, particularly the role of the co-catalyst, has been studied by several groups.[34,43-48] For chromium salen complexes, Darensbourg found that the anionic nucleophiles of PPN^+ salts do not exhibit initiation periods, unlike the neutral co-catalysts studied (N-heterocyclic amines or phosphines). This was proposed to be due to the fast formation of active, anionic six-coordinate $[(salen)Cr(N_3)X]^-$ derivatives.[34] Studies of the binding of DMAP to salen and salan Cr(III) complexes using electrospray ionization mass spectrometry showed that coordination of two DMAP molecules to the Cr center of the salen complex is possible, even under low DMAP to Cr ratios.[44] It was proposed that the stability of the six-coordinate $[salenCr(DMAP)_2]^+$ ions is a cause for the long initiation time for this catalyst system. In comparison, no induction period was observed for the *salan* analogue, which also showed a much lower propensity for bis-DMAP adduct formation, requiring much higher DMAP:Cr ratios to observe the presence of $[salanCr(DMAP)_2]^+$ ions. The difference in the geometry of the two complexes was speculated as the reason for the difference in DMAP binding. The time needed for the active species to form was ascribed to the slow dissociation of DMAP from the Cr-center of the salen complex to generate a vacant site allowing coordination of the epoxide for subsequent ring opening.

The activity of amine-bis(phenolato) chromium(III) complexes for the copolymerization of epoxides and CO_2[49-51] and the binding ability of DMAP to several derivatives of these ligands using matrix assisted laser desorption/ionization time-of-flight (MALDI-TOF) mass spectrometry were previously reported.[52] When used with DMAP, these amine-bis(phenolato) Cr(III) complexes showed good activity with over 80% conversion of cyclohexene oxide to poly(cyclohexene carbonate) (PCHC) with nearly quantitative carbonate linkages giving polymers with molecular weights up to 13 100 g/mol. The polymer dispersities were generally low, showing good control of the reaction.

In this chapter, the synthesis and structure of three new amine-bis(phenolato) chromium(III) complexes bearing methoxy groups *para* to the phenolate oxygens, instead of the previously reported *tert*-butyl substituents, and their catalytic activity for CHO/CO_2 copolymerization will be discussed. Furthermore, the effect of three co-catalysts (DMAP, PPNCl and $PPNN_3$) is also studied in detail by end-group analysis of the resulting polymers using MALDI-TOF MS, revealing further insights of the initiation of the polymerization.

2.2 Results and discussion

2.2.1 Synthesis and characterization of chromium complexes

The protio ligands 2-pyridylmethylamino-*N,N*-bis(2-hydroxy-3-*tert*-butyl-5-methoxyphenol) (H_2[**L1**])[53-55] and dimethylethyleneamino-*N,N*-bis(2-hydroxy-3-*tert*-butyl-5-methoxyphenol)[56] (H_2[**L2**]) (Scheme 2-1) were prepared via modified Mannich

condensation and using water in place of methanol as solvent. The amine-bis(phenolato) chromium(III) complexes **2.1** and **2.2** (or their THF adducts, **2.1**·THF and **2.2**·THF) can be synthesized by salt metathesis using the alkali-metallated amine-bis(phenolate)s. The protonated ligands H_2[**L1**] and H_2[**L2**] were reacted with either ^{n}BuLi or NaH at –78 °C in THF to afford the corresponding Li or Na salts, respectively, which were subsequently reacted with $CrCl_3(THF)_3$ at –78 °C in THF (Scheme 2-1).

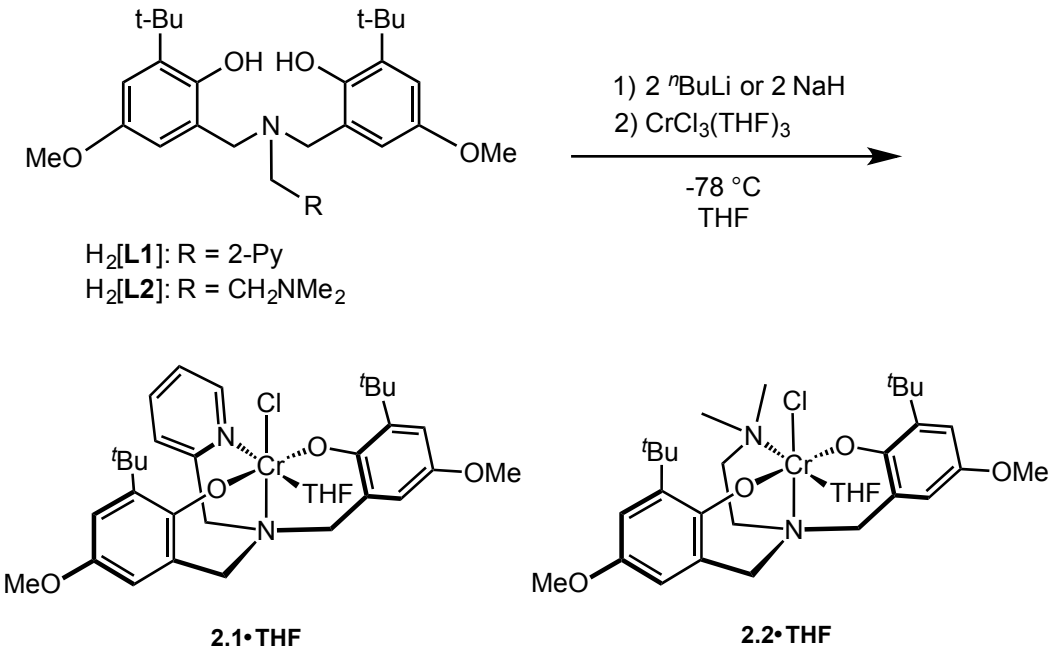

Scheme 2-1 Synthesis of **2.1**·THF and **2.2**·THF

Dark green and purple solids of **2.1** and **2.2**, respectively, were obtained in good yields, regardless of the alkali metal used. Elemental analyses of the purified amorphous materials were most consistent with the THF-free compounds (see Section 2.5), however the structures obtained by single crystal X-ray diffraction showed the crystalline materials are THF adducts (see below). The complexes were further characterized by MALDI-TOF MS, UV-Vis and IR spectroscopy and magnetic susceptibility

measurement. The MALDI-TOF mass spectrum of **2.1** shows a fragment at *m/z* 577.17 corresponding to the $[CrClL1]^{+\bullet}$ ion. The fragment at *m/z* 542.22 represents the $[CrL1]^{+}$ ion after the loss of the chloride.

The experimental isotopic distribution of $[CrClL1]^{+\bullet}$ and $[CrL1]^{+}$ ions are in good agreement with the calculated representations (See Figure B.1 in Appendix B). Two additional peaks are observed at the higher mass region (Figure B.1 and B.2) with the peak at *m/z* 1156.30 corresponding to a dimeric species $[Cr_2L1_2Cl_2]^{+\bullet}$ and the peak at *m/z* 1119.35 representing the fragment ion after chloride loss, $[Cr_2L1_2Cl]^{+}$. The presence of a chloride-bridged dimeric complex is very probable and the structure of such a species was previously reported.[49] The complex is probably formed as a dimer during synthesis, dissociating to monomeric species in the presence of a coordinating solvent such as THF. In the case of complex **2.2**, fragments are observed at *m/z* 522.20 and 557.17, which correspond to the $[CrL2]^{+}$ and $[CrClL2]^{+\bullet}$ ions, respectively (Figure B.3).

Crystals of **2.1**·THF and **2.2**·THF suitable for X-ray diffraction were grown via slow evaporation of toluene/THF solvent mixtures. The molecular structures are shown in Figure 2.1 and crystallographic and structure refinement data are given in Appendix A (Table A-1). As previously observed for other Cr(III)-complexes of amine-bis(phenolato) ligands from our group,[49-51,57] the structure of **2.1**·THF shows a distorted octahedral geometry at the chromium with one THF molecule coordinated to the metal *trans* to the pendant pyridyl donor. The two phenolate oxygens are coordinated *trans* to each other and the chloride group is *trans* to the amine nitrogen. The same geometry was observed

with complex **2.2**·THF. Crystallographic and structure refinement data for **2.2**·THF are also given in Table A-1.

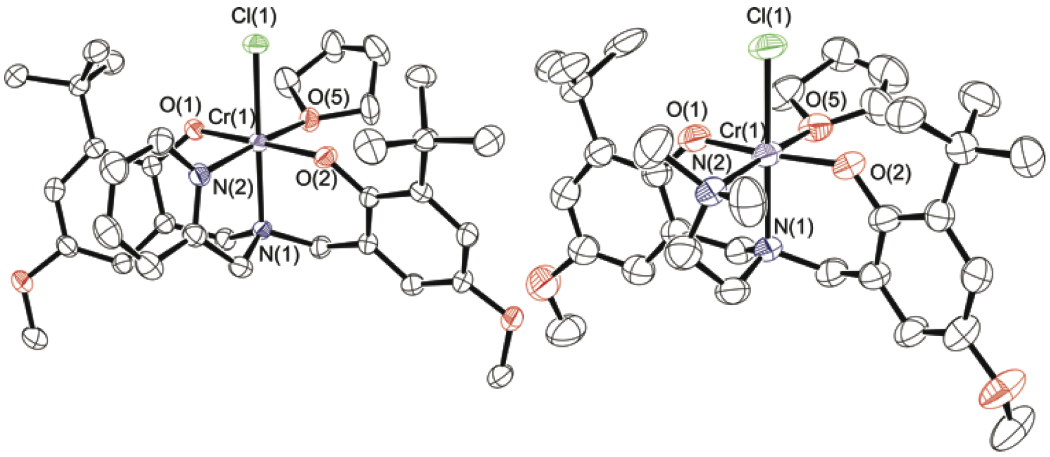

Figure 2.1 Partially labeled molecular structures of **2.1**·THF (left) and **2.2**·THF (right). Thermal ellipsoids are drawn at 50% probability and H atoms are excluded for clarity.

Detailed mechanistic studies previously showed that the first step in obtaining the catalytically active species from the catalyst precursor complexes is the coordination of a nucleophilic co-catalyst to the metal center. Indeed, six-coordinate co-catalyst bound salen chromium(III) complexes have been observed both spectroscopically[44] and structurally.[26,44,58] Similarly, reaction of **2.1**·THF with DMAP allowed isolation of the six-coordinate DMAP adduct, **2.1**·DMAP. The MALDI-TOF mass spectrum of **2.1**·DMAP (Figure B.4) shows the presence of an intense peak at *m/z* 699.23 corresponding to the $[CrClL1DMAP]^{+\bullet}$ ion, indicating that the DMAP is quite strongly bound to the chromium centre.[52] The fragment at *m/z* 664.27 corresponds to the $[CrL1DMAP]^{+}$ ion resulting from chloride loss. The calculated models are in good agreement with the experimentally observed peaks.

Crystals of **2.1**·DMAP were obtained via slow evaporation of an equimolar solution of **2.1**·THF and DMAP in dichloromethane. The molecular structure is shown in Figure 2.2 and a comparison of the bond lengths and angles for the three Cr complexes is given in Table 2-1.

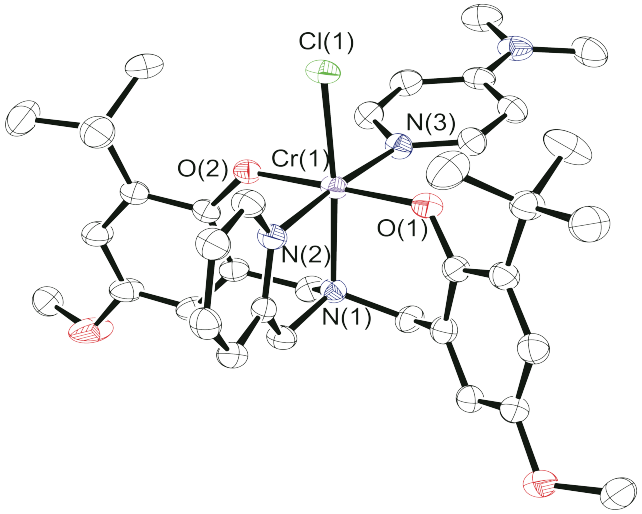

Figure 2.2 Molecular structure of **2.1**·DMAP. Thermal ellipsoids are drawn at 50% probability. H atoms are excluded for clarity.

Table 2-1 Selected bond lengths (Å) and bond angles (°) of **2.1**·THF, **2.2**·THF and **2.1**·DMAP.

	2.1·THF	**2.2**·THF	**2.1**·DMAP
Cr(1)–O(1)	1.943(2)	1.901(3)	1.946(2)
Cr(1)–O(2)	1.912(2)	1.913(3)	1.926(2)
Cr(1)–O(5)	2.074(2)	2.095(3)	-
Cr(1)–N(1)	2.097(2)	2.086(4)	2.129(2)
Cr(1)–N(2)	2.065(3)	2.116(4)	2.088(2)
Cr(1)–N(3)	-	-	2.100(2)
Cr(1)–Cl(1)	2.3463(9)	2.319(2)	2.3386(11)
O(1)–Cr(1)–O(2)	178.17(9)	174.22(13)	178.84(8)
O(1)–Cr(1)–O(5)	86.98(8)	87.38(14)	-
O(2)–Cr(1)–O(5)	91.88(9)	87.26(13)	-
O(1)–Cr(1)–N(2)	89.25(9)	90.23(15)	87.15(9)
O(2)–Cr(1)–N(2)	91.74(10)	95.29(14)	92.86(9)
O(1)–Cr(1)–N(1)	92.09(8)	91.38(13)	91.23(8)
O(2)–Cr(1)–N(1)	86.53(8)	90.92(13)	87.62(8)
O(1)–Cr(1)–N(3)	-	-	89.16(9)
O(2)–Cr(1)–N(3)	-	-	90.78(9)
O(1)–Cr(1)–Cl(1)	91.78(6)	90.21(9)	91.07(6)
O(2)–Cr(1)–Cl(1)	89.67(6)	87.67(9)	90.09(6)
N(2)–Cr(1)–Cl(1)	95.35(7)	94.41(10)	93.49(7)
O(5)–Cr(1)–Cl(1)	90.70(6)	90.52(9)	-
N(3)–Cr(1)–Cl(1)	-	-	89.12(7)

2.1·DMAP contains two strong σ-donor groups (the pendant pyridyl and DMAP) coordinated to the chromium. As a consequence, **2.1**·DMAP contains the most electron-rich chromium centre among these three complexes, and thus shows the longest average interatomic distances – the two exceptions being the Cr(1)–Cl(1) and the Cr(1)–N(2) interatomic distances. The Cr(1)–N(2) bond is, of course, the longest in complex **2.2**·THF, as expected for an sp^3-hybridized amino *N*-donor compared to the pyridine donor in **2.1**·THF and **2.1**·DMAP. Furthermore, the steric influence of the tertiary amine is reflected in the bond angles around the chromium. Both the O(1)-Cr(1)-N(2) and O(2)-Cr(1)-N(2) angles are greater than 90° (90.23(15) and 95.29(14) respectively) in **2.2**·THF

meaning that the phenolate oxygens are pushed away from the tertiary amine. The pushing away of the phenolates by the bulkier amine results in a modest weakening of the bond between THF and Cr, resulting in a longer Cr(1) – O(5) bond length in **2.2**·THF than in **2.1**·THF. Interestingly, this increased steric crowding of the chromium coordination sphere is believed to inhibit binding of more than one DMAP molecule to the metal in dimethylaminoethyl-functionalized amine,[52] however, the influence of the phenolate substituents cannot be ignored.

2.2.2 Copolymerization of cyclohexene oxide with CO_2

The copolymerization of CHO and CO_2 was investigated with complex **2.1**·THF, **2.2**·THF and **2.1**·DMAP (Scheme 2-2).

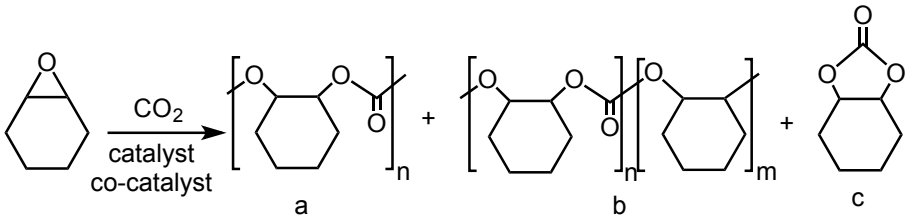

Scheme 2-2 Copolymerization of CHO and CO_2 with the possible products of the reaction: (a) PCHC, (b) polyether formation in the polymer chain and (c) cyclohexene carbonate.

Nucleophilic neutral or ionic co-catalysts are essential for the reaction; therefore, the activity of the complexes was tested with DMAP, PPNCl or $PPNN_3$. Copolymerization results show good conversion of cyclohexene oxide to PCHC

employing **2.1**·THF and **2.1**·DMAP complexes with moderate conversions using **2.2**·THF (Table 2-2). It is worth noting that the catalysts are selective toward polymer formation (Scheme 2-2, product a) as there is no or negligible evidence of either polyether (product b) (3.48 ppm in Figure C.1 in Appendix C) or cyclic carbonate (c) (4.10 ppm in Figure C.1) formation based on ^{1}H NMR spectroscopy (Figures C.1 and C.2). Resonances at 3.58 and 4.41 ppm correspond to the methine protons of the cyclohexane rings of the end groups. The carbonyl region of the ^{13}C NMR spectra shows that the obtained polymers are atactic, containing both syndiotactic and isotactic PCHC (Figure C.3). The maximum conversion achieved was 83% (Table 2-2, entries 5, 6 and 11) at which point only the solid polymer was found in the reaction vessel after opening the reactor. No conversion of CHO was observed in the absence of co-catalysts (Table 2-2, entry 1). Also, complex **2.1**·THF with DMAP did not show any activity toward CHO homopolymerization (entry 2). Overall, very good conversions and yields were obtained at CO_2 pressures of ~ 40 bar, 60 °C and at 0.2 mol% catalyst loading (entries 3, 5 – 7, 10 and 11). The dispersities (M_w/M_n) of the polymers did not change with molecular weight and are generally narrow with values between 1.26 and 1.43. Decreasing the catalyst loading from 0.2 mol% to 0.1 mol% resulted in a decreased conversion as well as molecular weight (entry 4). This is in accordance with previously obtained CHO/CO_2 copolymerization results in our group.[49,51] Comparing the three co-catalysts utilized, there is no significant difference in conversions, molecular weights and dispersities obtained. PPNCl and $PPNN_3$ proved to be only slightly better than DMAP, giving higher conversions, activities and molecular weights when **2.1**·THF was used (entries 3, 5, 6). Carrying out the reaction at room temperature did not produce any polymer product

(entry 8) and shortening the reaction time from 24 h to 5 h also produced lower conversion (entry 9). Complex **2.2**·THF proved to be inferior to complexes **2.1**·THF and **2.1**·DMAP, as it showed low conversions with DMAP and PPNCl co-catalysts, and moderate activity with $PPNN_3$ (entries 12 – 14).

Table 2-2 Results of the copolymerization of CO_2 and CHO

Entry[a]	Cat.	[Cr]:[CHO]:[Co-cat.]	Co-cat.	Time (h)	Temp (°C)	CO_2 Pressure (bar)	% Conversion[b]	%Yield[c]	TON[d]	M_n[e] (g/mol)	M_w/M_n[e]
1	**2.1**·THF	1:500:0	-	24	60	40	0	0	0	ND[f]	ND
2	**2.1**·THF	1:500:1	DMAP	24	60	0	0	0	0	ND	ND
3[g]	**2.1**·THF	1:500:1	DMAP	24	60	42	75 ± 7	72 ± 1	375 ± 35	7100	1.36
4[g]	**2.1**·THF	1:1000:1	DMAP	24	60	40	32 ± 4	29 ± 1	320 ± 40	3700	1.29
5	**2.1**·THF	1:500:1	PPNCl	24	60	44	83	82	415	8100	1.43
6	**2.1**·THF	1:500:1	$PPNN_3$	24	60	42	83	73	415	7500	1.26
7	**2.1**·DMAP	1:500:0	-	24	60	40	81	62	405	7300	1.30
8	**2.1**·DMAP	1:500:0	-	24	25	40	0	0	0	ND	ND
9	**2.1**·DMAP	1:500:0	-	5	60	40	44	25	220	ND	ND
10	**2.1**·DMAP	1:500:1	PPNCl	24	60	40	78	73	390	4900	1.37
11	**2.1**·DMAP	1:500:1	$PPNN_3$	24	60	40	83	73	415	5600	1.32
12[g]	**2.2**·THF	1:500:1	DMAP	24	60	40	12 ± 3	ND	60	ND	ND
13	**2.2**·THF	1:500:1	PPNCl	24	60	40	20	ND	100	ND	ND
14	**2.2**·THF	1:500:1	$PPNN_3$	24	60	40	62	46	310	4300	1.32

[a]All copolymerization reactions were carried out in neat cyclohexene-oxide (4 mL). [b]Calculated by ^{1}H NMR. [c]Yield = moles of isolated product (mass of polymer / molar mass of repeating unit) divided by the moles of starting monomer. [d]Turnover number: moles of repeating units produced per mole of Cr present. [e]Determined by gel permeation chromatography (GPC) in $CHCl_3$, calibrated with polystyrene standards. [f]ND = not determined due to low or no conversion. [g]Based on two runs.

Next, the effect of co-catalyst mixtures on the copolymerization was investigated, thus **2.1**·DMAP was used together with one equiv. of either PPNCl or $PPNN_3$. Interestingly, only a slight decrease in molecular weights could be observed giving 4900 g/mol with PPNCl and 5600 g/mol with $PPNN_3$ (entries 10 and 11) compared to 7300 g/mol using **2.1**·DMAP alone (entry 7). Selectivity toward polymer formation was unaffected by the addition of these salts. Usually, increasing the amount of co-catalyst used can favor the formation of cyclic carbonate over polycarbonate,[23,50] however, cyclic carbonate formation was not observed upon addition of PPNX salts to **2.1**·DMAP (entries 10 and 11). Potentially, molecular weights might be controlled with elevated amounts of co-catalysts. The observed lower molecular weight can be attributed to the increased concentration of co-catalyst that serves to initiate ring-opening of the epoxide fragment, hence an increased concentration of activated epoxide monomer resulting in growth of a larger number of polymer chains. The increased concentration of nucleophilic co-catalysts may also assist the displacement of the polymer chains from the metal center, which can then participate in chain transfer events leading to polymers terminated with the different initiator species.

The effect of methoxy substituents *para* and *tert*-butyl groups *ortho* to the phenoxide group has been investigated for chromium(III) salen complexes.[33] In that study, the rate of copolymer production was increased when these strongly electron donating salen complexes were employed compared to the di-*tert*-butyl analogues. It was proposed that the increased electron-donating ability of the phenolates had a more positive effect on the rate of polymer formation than by modifying the diimine backbone.

The CHO/CO_2 copolymerization activity of the di-*tert*-butyl substituted amine-bis(phenolate) chromium(III) complex bearing a pyridyl side-arm (i.e. a di-*tert*-butyl functionalized analog of complex **2.1**) had previously been reported[49] and described as complex **1.21** in Figure 1.9, Chapter 1, Section 1.1.5. The rate of copolymerization of that complex was compared with **2.1**·THF and **2.1**·DMAP monitored by *in situ* attenuated total reflectance infrared spectroscopy (ATR-IR). The initial rates of CHO/CO_2 copolymerization catalyzed by **2.1**·DMAP, **2.1**·THF and **1.21** (abbreviated as $CrCl[O_2NN']^{BuBuPy}$) are presented in Figure 2.3. DMAP was added as co-catalyst for **2.1**·THF and **1.21**.

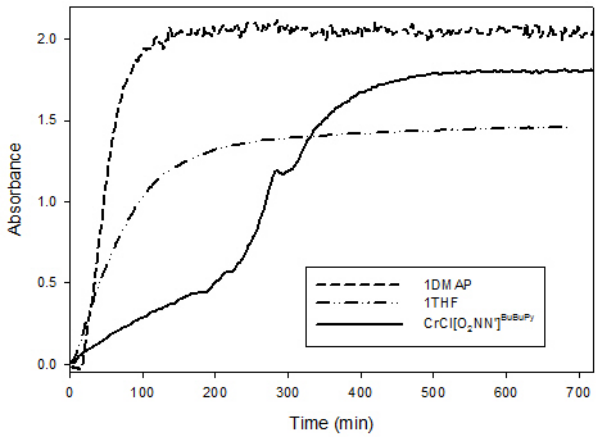

Figure 2.3 First 12 h of the reaction profiles showing the growth of the absorbance of the polycarbonate carbonyl C=O band at 1750 cm^{-1} catalyzed by **2.1**·DMAP (solid line), **2.1**·THF (dashed line) and $CrCl[O_2NN']^{BuBuPy}$ (**1.21**) (dashed-dotted line). Reaction conditions: 40 bar CO_2, 60 °C, [Cr]:[CHO]:[DMAP] = 1:500:1.

The fastest initial reaction rate was exhibited by **2.1**·DMAP followed by **2.1**·THF in the presence of equimolar DMAP. It is also worth noting that signal saturation (reaching a plateau in the absorbance of the polycarbonate *v*(C=O)) was also achieved within the shortest time by **2.1**·DMAP (~ 2 h), whereas **1.21** reached signal saturation

after 8 h. The reaction catalyzed by **1.21** exhibited two stages during the first 6 h. The first stage occurs over 4 h and represents the slowest propagation among the three complexes, while the second stage is faster and lasts for ~ 150 min before signal saturation occurs. In both stages, propagation was slower than for the **2.1**·DMAP and the **2.1**·THF/DMAP catalyzed reactions. Relative reaction rates were calculated based on the propagation in the first hour of the reaction after stabilization of the reaction conditions (~20 min) directly from the change of the carbonyl signal intensity as the slope of the plots (Figure 2.4). The rates of propagation obey the order of **2.1**·DMAP > **2.1**·THF/DMAP > **1.21**/DMAP and are represented in Table 2-3.

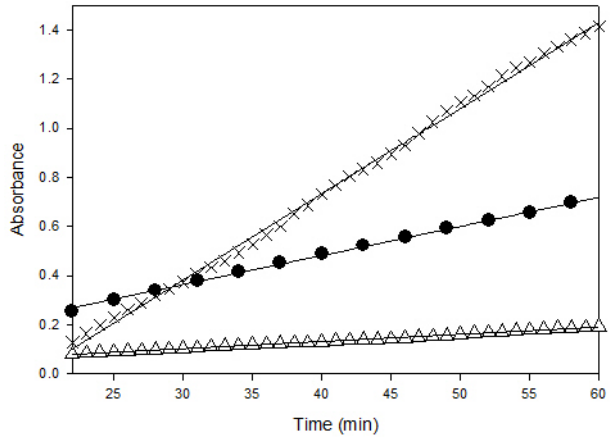

Figure 2.4 Initial rates of reaction profiles during the first hour based on the absorbance of the $\nu_{(C=O)}$ of the polycarbonates. **2.1**·DMAP (×), **2.1**·THF (●), **1.21** (△). Lines represent best fits of a linear model to the observed data (see Table 2-3).

Table 2-3 Relative reaction rates based on the changes in the absorbance at 1750 cm^{-1} corresponding to the $\nu_{(C=O)}$ of the growing polycarbonate chains and R^2 values of the linear regressions.

Complex	Relative reaction rate r_{obs} ($\times 10^{-2}$ min^{-1})	Relative reaction rate r_{obs} ($\times 10^{-4}$ s^{-1})	R^2
2.1·DMAP	3.5 ± 0.026	5.8 ± 0.043	0.9980
2.1·THF	1.2 ± 0.020	2.0 ± 0.033	0.9978
1.21	0.29 ± 0.0032	0.48 ± 0.0053	0.9960

The first 20 min of the reaction exhibit short initiation periods of approximately 8 min for **2.1**·THF/DMAP and approximately 17 min for **2.1**·DMAP (Figure D.1 in Appendix D). These initiation times are in accordance with the initiation periods observed for copolymerization by Cr(III)-salen complexes.[34] The longer initiation with **2.1**·DMAP is possibly due to the relatively strong coordination of DMAP, which results in a more stable complex compared to **2.1**·THF/DMAP. The procedure for use of the **2.1**·THF/DMAP catalyst system involves the addition of DMAP to a solution of **2.1**·THF in CHO where the labile THF could rapidly give rise to an open coordination site, therefore CHO coordination to the chromium center of **2.1** may occur prior to DMAP binding. DMAP coordination to our chromium(III)-complexes was studied in detail previously and the binding of two equivalents of DMAP was observed by MALDI-TOF MS even under equimolar concentrations of chromium complex **2.1** and DMAP.[52] By comparison, **1.21** is THF-free, but exists as a dimer in the solid state and in non-coordinating solvents.[49] The very short initiation time of approximately 5 min. may arise from dissociation of the dimeric complex to monomeric species. This may also serve to explain the two stages of the reaction giving different rates or propagation. Dissociation of the dimer into monomers leads to five-coordinate Cr(III) sites that catalyze

copolymerization according to the rate observed in the first stage (as modeled in Figure 2.4). A faster rate ensues during the second stage, which may be due to DMAP coordination and chloride dissociation. Initiation of epoxide ring opening by chloride nucleophiles is believed to dominate the reaction based on end-group analysis of the polymer by MALDI-TOF MS, where no DMAP-containing end-groups were observed.[49,52] Even for the faster second stage, the rate proved to be slower ($r_{obs} = 0.75 \times 10^{-2}$ min^{-1}, Figure D.2 in Appendix D) than the rates with *para*-methoxy-containing **2.1**·DMAP and **2.1**·THF (3.5×10^{-2} min^{-1} and 1.2×10^{-2} min^{-1} respectively). Rieger and co-workers observed two different rates of propagation after initiation with a dinuclear Cr(III)-salphen type complex (**1.16b**, Chapter 1, Figure 1.9, Section 1.1.5).[59] The first stage was attributed to a heterogeneous phase due to the insolubility of the flexibly linked dinuclear complex, which was followed by a homogeneous stage after dissolution of the complex. Complex **1.21** proved to be highly soluble in CHO, so this is unlikely the cause for the two different rates.

2.2.3 Polymer end group analysis on polymers produced by 2.1·THF and 2.1·DMAP by MALDI-TOF mass spectrometry

MALDI-TOF mass spectrometry is valuable for end-group analysis and the mass spectra of the polymers obtained show multiple end-group series, where repeating units of *m/z* 142 are observed corresponding to the expected cyclohexane carbonate motif. The variety of end groups is a result of different initiation possibilities demonstrated by these catalyst systems, i.e. the chromium chloride-containing catalyst and the additional DMAP, chloride or azide nucleophile. In the next section, first, the end groups of the

polymers produced with **2.1**·DMAP alone and with **2.1**·THF/DMAP will be discussed. Then, the end group analysis of the polymers produced by **2.1**·DMAP and added PPNX salts will follow, revealing more information on the initiation of the copolymerization.

When **2.1**·DMAP was used according to the conditions in Table 2-2, entry 7, the MALDI-TOF mass spectrum of the polymer produced shows two major sets of chains (Figure 2.5). One series possesses chloride and hydroxyl end groups, whereas the other series possesses two hydroxyl group ends, which implies that there is either adventitious water present and/or cyclohexene-1,2-diol is produced during polymerization causing rapid chain transfers.[60] No DMAP end-groups were observed, showing a probable chloride dissociation and initiation, while DMAP stays coordinated.

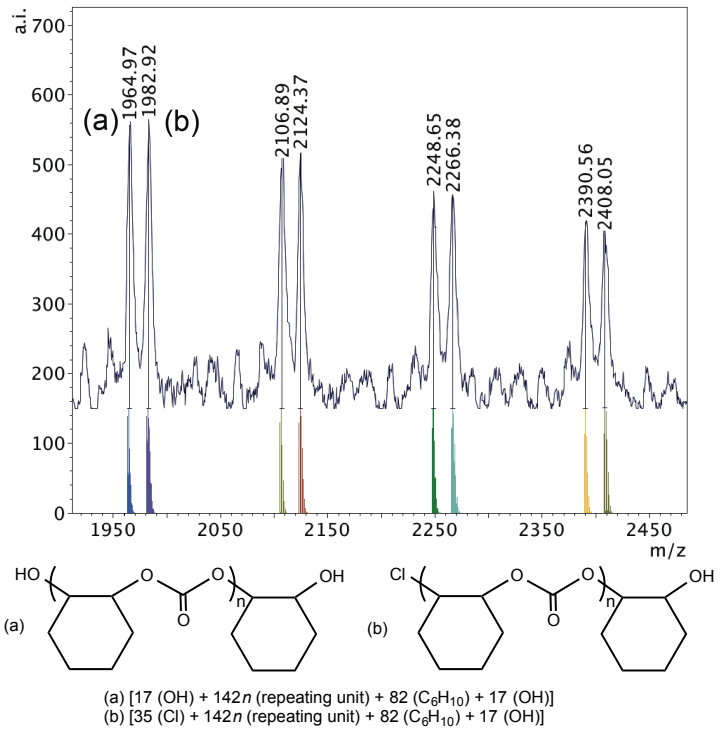

Figure 2.5 MALDI-TOF mass spectrum (*m/z* 1950 – 2450, n = 13 – 17) produced by **2.1**·DMAP according to Table 2-2, entry 7 with calculated masses of fragments shown beneath the observed spectrum and the proposed structures of polymers (a) and (b).

The higher mass region of the MALDI-TOF mass spectrum of the polymer produced by **2.1**·THF according to Table 2-2, entry 3 is shown in Figure 2.6. The polymer consists of only one main chain in the higher mass region (*m/z* 7800 – 8900, inset of Figure 2.6B), which is also chloride initiated and hydroxyl group terminated with a K^+ ion in the chain, also corresponding to chloride initiation again.

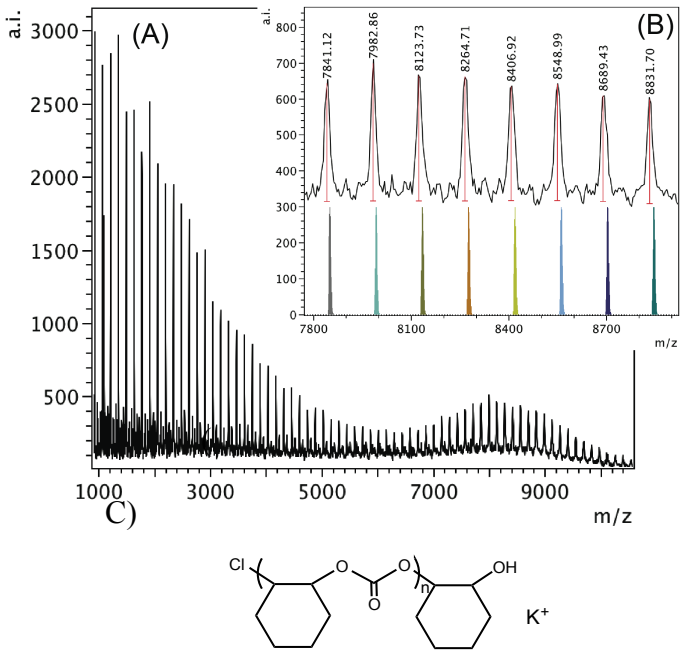

[35 (Cl) + 142*n* (repeating unit) + 82 (C_6H_{10}) + 17(OH) + 39 (K^+)]

Figure 2.6 (A) MALDI-TOF mass spectrum produced by **2.1**·THF according to Table 2-2, entry 3. (B) Higher mass region (*m/z* 7800 – 8900, n = 54 – 61) of the spectrum with calculated masses of fragments shown beneath the observed spectrum. (C) Proposed structure of the high mass polymer.

Inspection of the low molecular weight region of the MALDI-TOF mass spectrum between *m/z* 1900 to 2700, however, reveals the presence of both DMAP and chloride initiated polymer chains (Figure B.5 in Appendix B). Altogether, four different species were detected. Series (a) with the most intense peaks corresponds to a polymer

with DMAP and chloride end groups with one ether linkage in the polymer structure (the ether linkage could be located anywhere in the chain). The presence of DMAP in one end of the polymer end groups indicates that DMAP can also initiate ring opening of the epoxide. Series (b) – the lowest intensity peaks that disappear above *m/z* 2300 – possess DMAP and chloride termini. Series (c) with two hydroxyl group ends is probably the result of chain transfer reactions caused by trace water contamination.[60] Series (d) is represented by chloride and hydroxyl end group-containing polymer, where a sodium ion is also present.

When **2.1**·THF is used with PPNCl, chloride initiation is anticipated as both the complex and the co-catalyst contain chloride groups capable of ring-opening. As shown in Figure 2.7, chloride groups are observed in both of the two sets of polymers detected in the higher mass region.

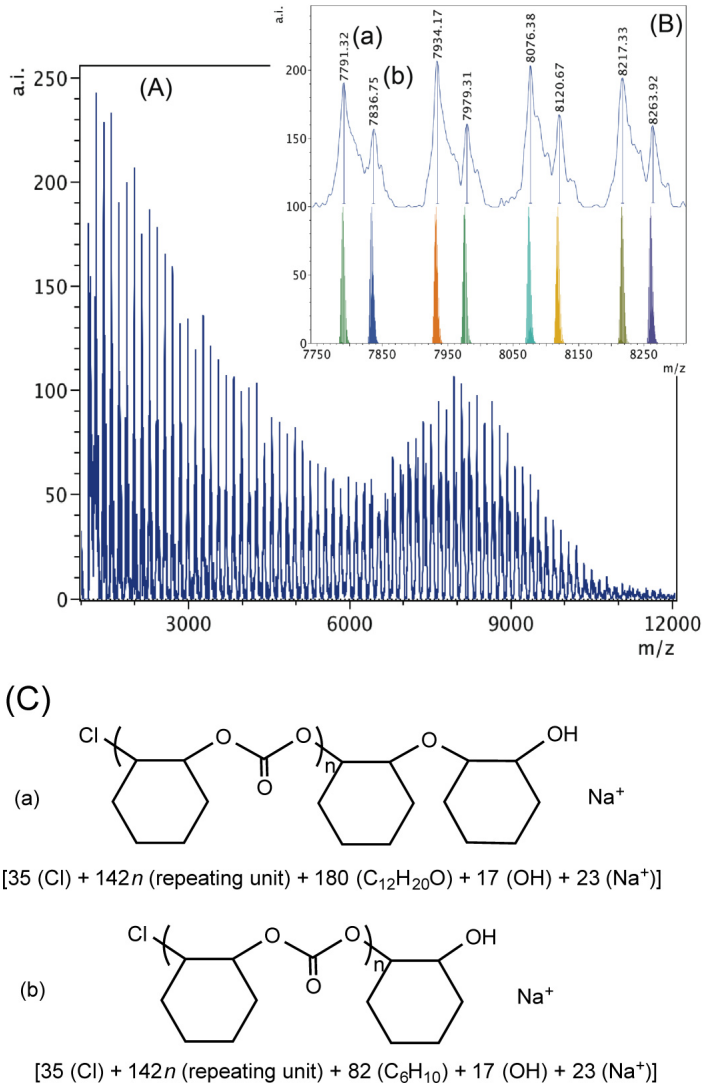

Figure 2.7 (A) MALDI-TOF mass spectrum produced by **2.1**·THF according to Table 2-2, entry 5. (B) Higher mass region (*m/z* 7750 – 8300, n = 53 – 56) of the spectrum with calculated masses of fragments shown beneath the observed spectrum. (C) Proposed structures of the high mass range polymers (a) and (b).

Series (a) and (b) are both hydroxyl group terminated and contain sodium ions. The difference between the two is the presence of an ether linkage incorporated in polymer chain (a). The presence of the chloride end groups in both cases, again, is the indication of initiation by chlorides, which can come from the complex or the added

PPNCl nucleophile. In the lower mass region (Figure B.6 in Appendix B) three sets of polymer chains are observed; series (a) is dihydroxylated, series (b) contains chloride and hydroxyl termini, and series (c) contains chloride end groups. Series (c) could be the result of intermolecular chain transfer of two chains initiated by chloride.[50]

Interestingly, when **2.1**·DMAP is used together with PPNCl, only DMAP initiated polymer chains are observed in both the upper and the lower mass region (Figure 2.8 A). This suggests that the coordinated DMAP is displaced by the anionic chloride and can attack a coordinated cyclohexene oxide. The polymer chain illustrated in the high mass region (Figure 2.8 B) is present over a wide mass range from 2000 – 8000 *m/z* shows initiation by a DMAP molecule and termination by hydrolysis of the metal alkoxide. In the lower mass region (Figure B.7 in Appendix B) we can only see DMAP initiated polymer chains. In series (a) we observe a series with an ether linkage incorporated in the chain terminated by a hydroxyl group, plus a sodium ion.

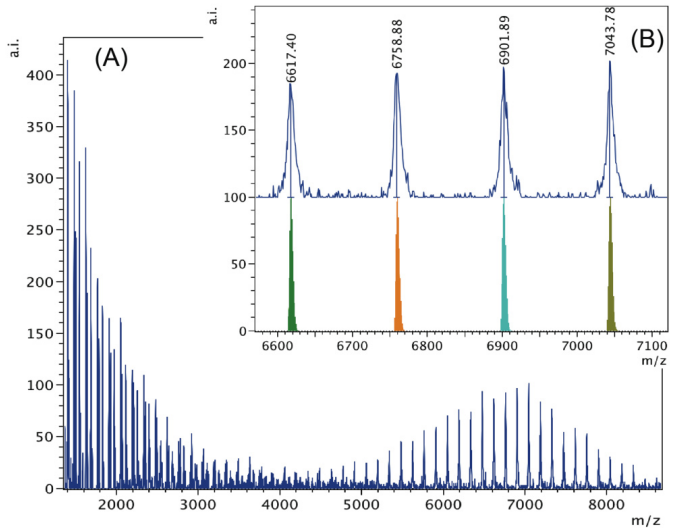

(C)

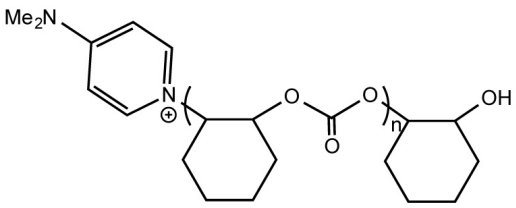

[122 ($C_7H_{10}N_2$) + 142*n* (repeating unit) + 82 (C_6H_{10}) + 17 (OH)]

Figure 2.8 (A) MALDI-TOF mass spectrum of polycarbonate produced by **2.1**·DMAP according to Table 2-2, entry 10. (B) Higher mass region (*m/z* 6600 – 7100, n = 45 – 48) of the spectrum with calculated masses of fragments shown beneath the observed spectrum. (C) Proposed structure of the high mass range polymer.

Series (b) consists of a hydroxyl end group and series (c) of a chloride and DMAP termini with a Na^+ ion. Most likely series (c) represents an intermolecular chain transfer between a DMAP and a chloride initiated polymer chain. This observation is different from the **2.1**·DMAP-catalyzed reaction without any PPNX salt (Table 2-2, entry 7), where there were no DMAP initiated polymer chains found. The difference may be attributed to the elevated amount of chloride ions. When PPNCl is added, there are twice as many chloride ions present coming from both the complex and the PPN^+ salt compared to where there is no PPNCl added. Consequently, the competition for an open

coordination site is higher, which can easily result in DMAP dissociation and incorporation of the polymer chain end.

The spectrum of the polymer obtained when **2.1**·THF was used in the presence of $PPNN_3$ shows high intensity peaks in the high mass region (Figure 2.9). Two sets of polymers can be observed in this region between *m/z* 7400 – 8000. Based on the calculation shown in Figure 2.9 (C), series (a) shows an ether linkage in the polymer chain that was initiated by a nucleophilic attack of an azide group and was terminated by a chloride group. Series (b) is again most likely the result of an intermolecular chain transfer between two polymer chains that were both initiated by azide groups. In the lower mass region, however, azide group-initiated polymer chains are not observed (Figure B.8 in Appendix B). Series (a) with chloride and hydroxyl end groups and series (b) with two hydroxyl termini represent polymers where chain termination and chain transfer could be caused by adventitious water resulting in lower molecular weight polymer chains.

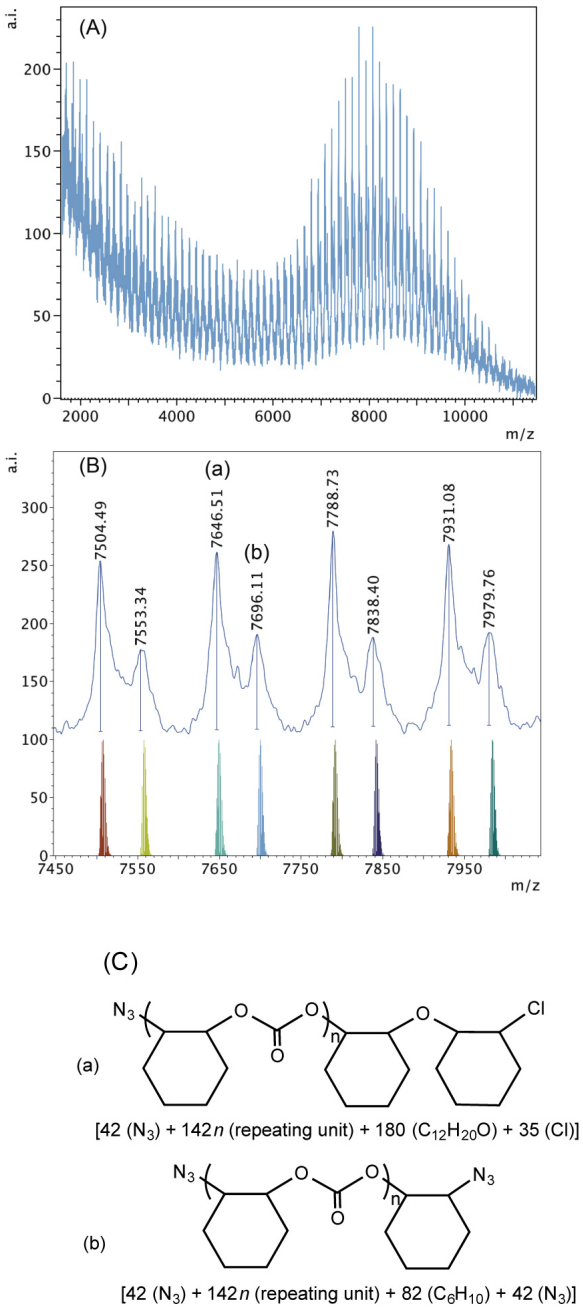

Figure 2.9 (A) MALDI-TOF mass spectrum produced by **2.1**·THF according to Table 2-2, entry 6. (B) Higher mass region (*m/z* 7450 – 8000, n = 51 – 54) of the spectrum with calculated masses of fragments shown beneath the observed spectrum. (C) Proposed structures of the high mass range polymers (a) and (b).

Azide initiated polymer chains were also observed when **2.1**·DMAP was used together with $PPNN_3$ (Figure B.9 in Appendix B and Figure 2.10). In the high mass

region (Figure B.9 in Appendix B) of the spectrum there is only one significant high intensity set of peaks observed, which corresponds to an azide and chloride terminated polymer cationized by Na^+. In the lower mass region, two main sets of polymers can be discerned from the spectrum (Figure 2.10): series (a) possesses azide and chloride groups plus Na^+, and series (b) consists of a DMAP and azide terminated polymer, again, probably due to intermolecular chain transfer.

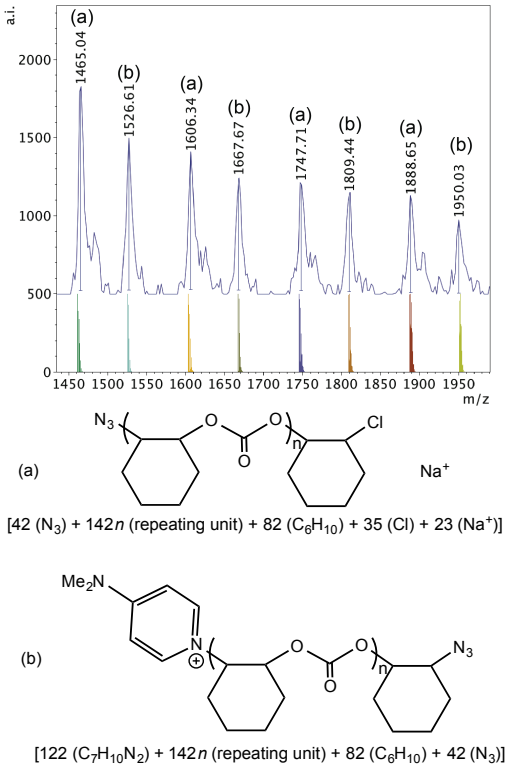

Figure 2.10 Lower mass region (*m/z* 1400 – 2000, n = 9 – 12) of the MALDI-TOF mass spectrum produced by **2.1**·DMAP according to Table 2-2, entry 11, with calculated masses of fragments shown beneath the observed spectrum and the proposed structures of polymers (a) and (b).

2.3 Mechanistic considerations

The presence of the chloride end group indicates chloride initiation, which may occur via an intermolecular or an intramolecular pathway.[49] As calculated in an elegant recent computational study, displacement of the chloride by an epoxide has been shown to be viable based on the bond strengths between chromium and epoxide or chloride with salen complexes.[61] In this manner, one possible pathway can be the replacement of the chloride with an epoxide, which points toward the intermolecular ring opening by the chloride. After the chloride loss, a cationic complex is produced and provides the platform for copolymerization. This possibility of the cationic route is depicted in Scheme 2-3A. Of course, it cannot be excluded that under polymerization conditions the nucleophilic co-catalyst (DMAP) dissociates from the central metal, e.g. in the case of the **2.1**·DMAP/PPNCl system and ring opens a then coordinated epoxide (Scheme 2-3B). In this case, the chlorides of PPNCl compete with the DMAP for coordination to the metal center, leading to a chromium dichloride intermediate.[26] Displacement of one of the chlorides produces a vacant site for epoxide binding and the free DMAP can now serve as nucleophile for epoxide ring-opening. Initiation by a chloride, however, is also possible based on the end group analysis of the **2.1**·DMAP/PPNCl system, where both DMAP and chloride termini were observed in the lower mass region of the MALDI-TOF mass spectrum and likely caused by chain transfer. Several different initiation possibilities were extensively elaborated upon and compiled in reviews.[7,62,63] Based on the observations in this study, it is proposed that it is the monometallic intermolecular

initiation pathway that most likely occurs with these chromium(III)-bis(phenolate) complexes (Scheme 2-3).

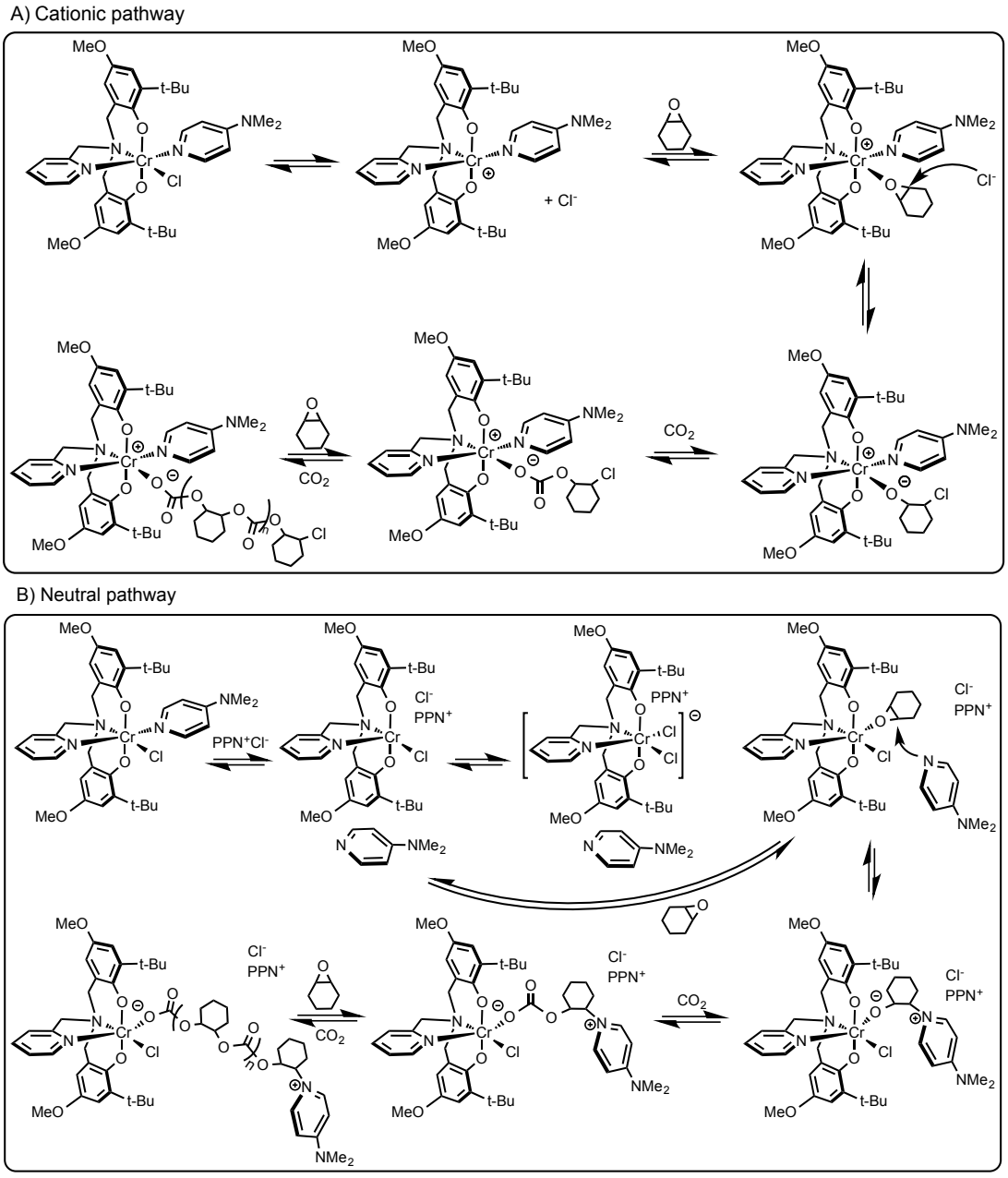

Scheme 2-3 (A) Proposed initiation pathway for the copolymerization of cyclohexene oxide and carbon dioxide with **2.1**·DMAP and (B) with **2.1**·DMAP/PPNCl

2.4 Conclusions

Chromium(III) complexes **2.1**·THF and **2.1**·DMAP show improved catalytic activity over the previously reported complex, **1.21**, in the copolymerization of cyclohexene oxide and CO_2. End group analysis of the polymers obtained by **2.1**·THF and **2.1**·DMAP indicates that ring opening is most probably initiated by the anion of the co-catalyst except when **2.1**·DMAP is used with PPNCl, in which case DMAP dissociation is observed, leading to its role as the epoxide ring-opening nucleophile as shown by polymer end group analysis by MALDI-TOF MS. Based on this end group analysis, we propose that CO_2/epoxide copolymerization catalyzed by chromium (III) amine-bis(phenolate) complexes is initiated by epoxide ring opening by an external nucleophile, that is, an intermolecular pathway. Of course, where a complex contains two nucleophilic groups, for example **2.1**·DMAP, monometallic intramolecular initiation may also be feasible. More details can be revealed by *in situ* monitoring of the copolymerizations with the help of ATR FTIR. Mechanistic studies were designed and performed to obtain more detailed insights of the initiation. The findings of these studies are summarized in Chapter 3.

2.5 Experimental

2.5.1 General experimental conditions

Unless otherwise stated, all manipulations were performed under an atmosphere of dry oxygen-free nitrogen by using standard Schlenk techniques or using an MBraun Labmaster glove box. Cyclohexene oxide was purchased from Aldrich and freshly

distilled from CaH_2 under N_2 atmosphere into an ampule. THF was purified by distillation from sodium/benzophenone ketyl under nitrogen. All other solvents were dried and degassed using an MBraun Manual Solvent Purification System. $CrCl_3(THF)_3$ and $PPNN_3$ were prepared via previously reported methods.[64,65] Although the syntheses of the proligands H_2[**L1**][53-55] and H_2[**L2**][56] were previously reported, modified syntheses in water and full characterization of H_2[**L1**] and H_2[**L2**] are given here. 99.998% (4.8 Supercritical fluid chromatography grade) CO_2 was supplied from Praxair in a high-pressure cylinder equipped with a liquid dip tube. All ^1H and $^{13}C\{^1H\}$ NMR spectra were obtained in $CDCl_3$ purchased from Cambridge Isotope Laboratories, Inc.

2.5.2 Instrumentation

^1H and $^{13}C\{^1H\}$ NMR spectra were recorded on a Bruker AVANCE III 300 MHz spectrometer. All copolymerization reactions were carried out in a 100 mL stainless steel Parr® 5500 autoclave reactor with a Parr 4836 controller. N.B. Caution should be taken when operating such high-pressure equipment. UV-Vis spectroscopy was conducted on a dual-beam Evolution 300 UV-Vis spectrophotometer equipped with a xenon lamp. The samples were diluted to a concentration of 10^{-4} mol/L in dichloromethane. Infrared spectroscopy was conducted on a Bruker Alpha FT-IR spectrometer equipped with a single bounce diamond ATR module. Melting points were measured on a Standford Research Systems MPA100 OptiMelt Automated Melting Point System. Magnetic measurements were carried out using a Johnson-Matthey magnetic susceptibility balance. Elemental analysis was performed at Guelph Chemical Laboratories, Guelph, ON,

Canada. Gel permeation chromatography (GPC) analysis was performed at 35 °C on a Viscotek VE 2001 GPCMax equipped with a Viscotek VE 3580 RI Detector, Phenogel narrow-bore 5 μm 100 Å and 5 μm Linear(2) columns (300 x 4.60 mm), and a 5 μm guard column. Samples were prepared at a concentration of 2 mg/mL and left to equilibrate for ~ 16 h. The samples were filtered through 0.2 μm syringe filters before analysis. The GPC columns were eluted with HPLC grade chloroform at a flow rate of 0.30 mL/min with a 100 μL injection volume. Eight polystyrene standards were used in making the calibration curve, bracketing molecular weights ranging from 1050 to 400,000 Da. No further corrections were performed on the molecular weights obtained. MALDI-TOF mass spectrometry was performed by using an Applied Biosystems 4800 MALDI- TOF/TOF Analyzer equipped with a reflectron, delayed extraction and high performance nitrogen laser (200 Hz operating at 355 nm). Anthracene was used as the matrix for analysis of **2.1**·THF, **2.2**·THF and **2.1**·DMAP. The matrix and complex were dissolved separately in toluene at concentrations of 10 mg/mL. The matrix and chromium complex solutions were combined in a 1:1 ratio and the mixture was spotted on the MALDI plate and left to dry. Samples were prepared in the glove box and sealed under nitrogen in a plastic bag for transport to the spectrometer. For polymer analysis, either 2,5-dihydroxybenzoic acid (DHBA) or 1,8,9-trihydroxyanthracene was used as the matrix with sodium trifluoroacetate (NaTFA) as cationizing agent. The matrix was dissolved in THF at a concentration of 10 mg/mL and ~ 2 mg of NaTFA was added to the solution in the case of 1,8,9-trihydroxyanthracene. The polymer was dissolved at a

concentration of 1 mg/mL. The matrix and polymer solutions were mixed together in a 3:1 ratio and this mixture was spotted on the MALDI plate and left to dry.

2.5.3 Synthesis of the amine-bis(phenol) H_2[L1] and H_2[L2]

H_2**[L1]**: Aminomethylpyridine (6.65 g, 0.0615 mol) was slowly added to a vigorously stirred mixture of 3-tert-butyl-5-hydroxyanisole (22.17 g, 0.123 mol) and formaldehyde (9.16 mL of a 37% aqueous solution, 0.123 mol) in deionized water (100 mL) in a round bottom flask equipped with a magnetic stir bar. This mixture was heated to reflux and stirred overnight. Upon cooling, a large quantity of white solid formed. The solvent was decanted and the solid was washed with cold methanol then recrystallized from a chloroform/methanol solvent mixture to give a white crystalline powder (25.06 g, 82% yield). Anal. Calcd. For $C_{30}H_{40}N_2O_4$: C 73.14, H 8.18, N 5.69. Found: C 72.88, H 7.90, N 5.53. ^{1}H NMR (300 MHz, 298 K, $CDCl_3$, δ): 10.30 (br s, #17, 2H), 8.69 (ddd, $^3J_{HH}$ = 5.03 Hz, $^4J_{HH}$ = 1.79, $^5J_{HH}$ = 0.93 Hz, Py: #16, 1H), 7.70 (ddd, $^3J_{HH}$ = 7.69 Hz, $^3J_{HH}$ = 7.69 Hz, $^4J_{HH}$ = 1. 79 Hz, Py: #15, 1H), 7.29 (ddd, $^3J_{HH}$ = 7.69 Hz, $^4J_{HH}$ = 5.01 Hz, $^5J_{HH}$ = 1.05 Hz, Py: #14, 1H), 7.12 (dt, $^3J_{HH}$ = 7.80 Hz, $^4J_{HH}$ = 1.05 Hz, Py: #13, 1H), 6.83 (d, $^4J_{HH}$ = 3.08 Hz, Ar: #7, 2H), 6.51 (d, $^4J_{HH}$ = 3.06 Hz, Ar: #4, 2H), 3.80 (s, #11, 2H), 3.78 (s, #10, 4H), 3.75 (s, #6, 6H), 1.40 (s, #1, 18H). ^{13}C{^{1}H} NMR (75.5 MHz, $CDCl_3$, 298K, δ): 155.99 (#9); 151.96 (#5) 150.38 (#8),

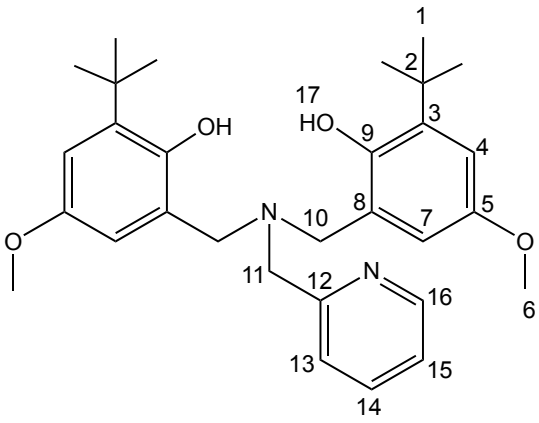

148.37 (#13), 139.06 (#12), 137.68 (#14), 124.18 (#16), 122.85 (#3); 122.81 (#15), 113.72 (#7); 112.54 (#4); 56.44 (#11); 55.91 (#6); 55.12 (#10), 35.28 (#2), 29.66 (#1).

H_2[**L2**]: N,N-dimethylethylenediamine (5.42 g, 0.0615 mol) was slowly added to a vigorously stirred mixture of 3-*tert*-butyl-4-hydroxyanisole (22.17 g, 0.123 mol) and formaldehyde (9.16 mL of a 37% aqueous solution, 0.123 mol) in deionized water (100 mL). This mixture was heated to reflux and stirred overnight. Upon cooling, a large quantity of dark orange product formed. The solvent was decanted and the solid was washed with cold methanol, then recrystallized from a chloroform/methanol mixture to give a white powder (14.06 g, 48% yield). Anal. Calcd. for $C_{28}H_{44}N_2O_4$: C: 71.15, H: 9.38, N: 5.93. Found: C: 71.11, H: 9.14, N: 5.67. ^{1}H NMR (300 MHz, 298 K, $CDCl_3$): δ 9.40 (br s, #14, 2H), 6.80 (d, $^4J_{HH}$ = 3.08 Hz, #7, 2H), 6.48 (d, $^4J_{HH}$ = 3.06 Hz, #4, 2H), 3.74 (s, #6, 6H), 3.57 (s, #10, 4H), 2.56, (d, $^3J_{HH}$ = 2.34 Hz, #11 and #12, 4H), 2.27 (s, #13, 6H), 1.38 (s, #1, 18H). ^{13}C{^{1}H} NMR (75.5 MHz, $CDCl_3$, 298K, δ): 151.66 (#9), 149.86 (#8), 138.66 (#5), 123.18 (#3), 113.39 (#7), 112.76 (#4), 56.39 (#10), 55.86 (#6), 55.84 (#11), 49.21 (#12), 44.89 (#13), 35.22 (#2), 29.58 (#1). M.p.: 148.9 °C – 151.1 °C.

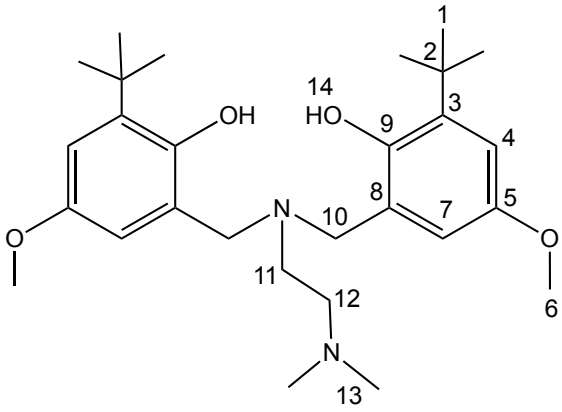

2.5.4 Syntheses of chromium complexes

2.1: *Method A*: H_2[**L1**] (3.00 g, 6.10 mmol) was dissolved in THF (~50 mL) and cooled to -78 °C. ^{n}BuLi (1.6 M in hexanes, 11.16 mL, 17.86 mmol) was added dropwise to give a red solution, which was warmed to room temperature and further stirred for 2 h. This solution was transferred via cannula to a suspension of $CrCl_3(THF)_3$ (2.26 g, 6.03 mmol) in THF (~40 mL) cooled to –78 °C to give a dark brown mixture. Upon warming to room temperature and stirring for 24 h the solids dissolved and the color darkened to dark brown. The solvent was removed in vacuo and the solid residue was extracted into toluene. As the complex was sparingly soluble in toluene, the extraction was carried out by repeated addition of toluene to the solids. The extraction was stopped when the color of the toluene solution became very light brown. The remaining solids were filtered through Celite and the extracts combined. The solvent was removed *in vacuo* and the product was washed with pentane and dried to yield 2.81 g of green powder. Yield: 80%. Anal. Calcd for $C_{30}H_{38}ClCrN_2O_4$ (**2.1**): C 62.33, H 6.63, N 4.85. Anal. Calcd for $C_{34}H_{45}ClCrN_2O_5$ (**2.1**·THF): C 62.91, H 6.99, N 4.32. Found: C 62.04, H 6.48, N 4.79. MS (MALDI-TOF) m/z (%, ion): 577.15 (100, [CrCl[**L1**]$^+$], 542.19 (86.80, Cr[**L1**]$^+$). UV-Vis (CH_2Cl_2) λ_{max} in nm (ε in L·mol^{-1}·cm^{-1}): 228 (18 320), 311 (6280), 395 (1080), 562 (580), 752 (220) (Figure E.1 in Appendix E). IR (cm^{-1}): 2920.87 (alkane C – H stretch), 1610.70 (C = C phenyl stretch), 1462.96 and 1422.18 (sp^3 C – H bending), 1258.60 (C – N stretch), 1206.55 and 1052.22 (C – O stretches), 789.60 (sp^2 C – H bending) (Figure F.1 in Appendix F). μ_{eff} (solid, 27 °C) = 3.27 μ_B.

2.1:*Method B*: H_2[**L1**] (3.00 g, 6.09 mmol) was dissolved in THF (~50 mL). THF was also transferred to a Schlenk flask containing NaH (0.58 g, 24.36 mmol). The ligand solution was transferred dropwise by cannula to the Schlenk flask containing the NaH suspension, which was cooled to –78 °C. The mixture was warmed to room temperature and further stirred for 2 h. This mixture was then cannula filtered to a suspension of $CrCl_3(THF)_3$ (2.26 g, 6.09 mmol) in THF (~40 mL) cooled to – 78 °C giving a dark brown mixture. Upon warming up to room temperature and stirring for 24 h the solids dissolved and the colour darkened to deep dark brown. The solvent was removed in vacuo and the solid residue was extracted into toluene. As the complex was sparingly soluble in toluene, the extraction was carried out by repeated addition of toluene to the remaining solids as well as filtration through Celite. The extraction was stopped when the colour of the toluene solution became very light brown. The solvent was then removed in vacuo and the product was washed with pentane and dried to yield 2.75 g of green powder. Yield: 78%. Anal. Calcd for $C_{30}H_{38}ClCrN_2O_4$ (**2.1**): C 62.33, H 6.63, N 4.85; Anal. Calcd for $C_{34}H_{45}ClCrN_2O_5$ (**2.1**·THF): C 62.91, H 6.99, N 4.32. Found: C 62.49, H 6.37, N 4.59. MS (MALDI-TOF) m/z (%, ion): 577.15 (100, [CrCl[**L1**]$^+$], 542.19 (86.80, Cr[**L1**]$^+$). Crystals were grown from a toluene/THF mixture via slow evaporation at –35 °C.

2.2: *Method A*: H_2[**L2**] (3.00g, 6.35 mmol) was dissolved in THF (~50 mL) and cooled to -78 °C. ^{n}BuLi (1.6 M in hexanes, 7.90 mL, 12.64 mmol) was added dropwise to give a yellow solution, which was warmed to room temperature and further stirred for 2 h. This solution was transferred via cannula to a suspension of $CrCl_3(THF)_3$ (2.23 g,

6.00 mmol) in THF (~ 40 mL) cooled to -78 °C to give a dark purple mixture. Upon warming to room temperature and stirring for 16 h the solids dissolved and the colour darkened to deep dark purple. The solvent was removed in vacuo and the solid residue was extracted into toluene. The mixture was filtered through Celite and the solvent was removed in vacuo. The product was washed with pentane and dried to yield 2.77 g of purple powder. Yield: 83%. Anal. Calcd for $C_{28}H_{42}ClCrN_2O_4$ (**2.2**): C 60.26, H 7.59, N 5.02. Anal. Calcd for $C_{32}H_{49}ClCrN_2O_5$ (**2.2**·THF): C 61.09, H 7.85, N 4.45. Found: C 60.30, H 7.38, N 4.74. MS (MALDI-TOF) m/z (%, ion): 557.23 (66.73, [CrCl[**L2**]$^+$], 522.26 (81.17, Cr[**L2**]$^+$). Crystals were grown a toluene/ THF mixture via slow evaporation at –35 °C. UV-Vis (CH_2Cl_2) λ_{max} in nm (ε in L·mol^{-1}·cm^{-1}): 228 (13 280), 302 (6250), 397 (680 sh), 478 (420), 687 (140) (Figure E.2 in Appendix E). IR (cm^{-1}): ~ 3300 (broad O – H stretch), 2951.28 (alkane C – H stretch), 1602.80 (C = C phenyl stretch), 1462.93 (sp^3 C – H bending), 1270.50 (C – N stretch), 1201.63 and 1061.53 (C – O stretches), 819.70 (sp^2 C – H bending) (Figure F.2 in Appendix F). μ_{eff}(solid, 27 °C) = 3.48 μ_B.

2.2: *Method B*: The synthesis was carried out the same way as described in Method B for complex **2.1** but using H_2[**L2**] to give 3.47 g of purple powder. Yield: 98%.

2.1·**DMAP**: 0.3000 g CrCl[**L1**] with 0.0634 g DMAP (1:1 mol ratio) was dissolved in ~ 8 mL dichloromethane (DCM). The solution was stirred for ~ 15 min. then it was filtered through glass fiber. Crystals were grown via slow evaporation at –35 °C. After crystallization, the solvent was removed in vacuo and the crystalline solid was used

for copolymerization reactions. Anal. Calcd. for $C_{37}H_{48}ClCrN_4O_4$: C 63.46, H 6.91, N 8.00. Found: C 63.32, H 6.72, N 7.75. MS (MALDI-TOF) *m/z* (%, ion): 699.23 (66.11, [CrCl[**L1**]DMAP]$^{+\bullet}$), 664.27 (33.34, [Cr[**L1**]DMAP]$^{+\bullet}$) (Figure B.4 in Appendix B). UV-Vis (DCM) λ_{max} in nm (ε in $L \cdot mol^{-1} \cdot cm^{-1}$): 227 (35 600), 232 (29530), 257 (30 270), 280 (30 550), 286 (30 210), 315 (8820 sh), 409 (980 sh), 547 (200), 693 (140) (Figure E.3 in Appendix E). IR (cm^{-1}): ~ 3300 (broad O – H stretch), 2947.61 (alkane C – H stretch), 1615.35 (C = C phenyl stretch), 1419.56 (sp^3 C – H bending), 1261.41 (C –N stretch), 1061.03 and 1014.46 (C – O stretches), 808.04 (sp^2 C – H bending) (Figure F.3 in Appendix F). μ_{eff} (solid, 27 °C) = 3.31 μ_B.

2.5.5 Copolymerization procedure

The appropriate amount of catalyst and co-catalyst were added to the monomer in a glove box. The reactant solution was stirred for ~ 5 min, then transferred via a long-needled syringe to a Parr autoclave, which was pre-dried under vacuum overnight at 80 °C. The autoclave then was charged with the appropriate pressure of CO_2 and left to stir at the desired temperature and time period. After the appropriate time the autoclave was cooled in an ice bath and vented in the fume hood. An aliquot was taken immediately after opening the reactor for the determination of conversion by NMR. The copolymer was extracted with dichloromethane and re-precipitated in cold acidic methanol. For reactions done in the presence of PPNCl and $PPNN_3$, the catalyst and co-catalyst were first combined in ~ 4 mL of CH_2Cl_2 in the glove box, stirred for ~ 15 min and then dried in vacuo. This way the otherwise insoluble onium salts could be dissolved in

cyclohexene oxide. The remaining procedure was followed in the same manner as described above.

2.5.6 *In situ* monitoring of the copolymerization by IR spectroscopy

In situ monitoring was carried out using a 100 mL stainless steel reactor vessel (Mettler-Toledo) equipped with a silicon sensor (SiComp), motorized mechanic stirrer and a heating mantle. The silicon sensor was connected to a ReactIR 15 base unit through a DS silver-halide Fiber-to-Sentinel conduit. The reactor vessel was cleaned and heated under vacuum at 80 °C overnight before experiments. In a glove box the appropriate amount of complex and DMAP (where needed) were weighed and then dissolved in 5 g CHO. The mixture was stirred for about 15 min., after which the vial cap was replaced with a septum. The reaction solution was transferred into a 5 mL syringe with a cannula needle attached. The syringe was transferred out of the glove box and the solution was injected into the vessel through a port. Then the vessel was pressurized with 40 bar CO_2. Heating and stirring were started and the reaction was monitored for the allotted time.

2.5.7 X-ray crystallographic experimental

Diffraction data for complex **2.1**·THF, **2.2**·THF and **2.1**·DMAP were collected on a Rigaku Saturn70 CCD area detector with a SHINE optic Mo-Kα radiation and solved on an AFC8-Saturn 70 single crystal X-ray diffractometer from Rigaku, equipped with an X-stream 2000 low temperature system. Crystallographic and structure refinement data are given in supporting information. The data were processed using

CrystalClear[66] software and corrected for Lorentz and polarization effects and absorption.[67] Neutral atom scattering factors for all non-hydrogen atoms were taken from the International Tables for X-ray Crystallography.[68] The structure was solved by direct methods using SIR92[69] and expanded using Fourier techniques.[70] All non-hydrogen atoms were refined anisotropically. Hydrogen atoms were refined using a riding model. Anomalous dispersion effects were included in Fcalc;[71] the values for Δf' and Δf'' were those of Creagh and McAuley.[72] The values for the mass attenuation coefficients are those of Creagh and Hubbell.[73] All calculations were performed using the CrystalStructure[74] crystallographic software package except for refinement, which was performed using SHELXL-97.[75] Disordered lattice solvent for **2.2**·THF was removed through applying Platon's Squeeze[76] procedure. Structural illustrations were created using ORTEP-III (v.2.02) for Windows.[77]

2.6 References

1. T. Sakakura; J.-C. Choi; H. Yasuda *Chem. Rev.* **2007**, *107*, 2365-2387.

2. A. M. Nelson; T. E. Long *Polym. Int.* **2012**, *61*, 1485-1491.

3. S. Fukuoka; M. Kawamura; K. Komiya; M. Tojo; H. Hachiya; K. Hasegawa; M. Aminaka; H. Okamoto; I. Fukawa; S. Konno *Green Chem.* **2003**, *5*, 497-507.

4. W. B. Kim; U. A. Joshi; J. S. Lee *Ind. Eng. Chem. Res.* **2004**, *43*, 1897-1914.

5. D. J. Darensbourg *Inorg. Chem.* **2010**, *49*, 10765-10780.

6. D. J. Darensbourg *Chem. Rev.* **2007**, *107*, 2388-2410.

7. M. R. Kember; A. Buchard; C. K. Williams *Chem. Commun.* **2011**, *47*, 141-163.

8. M. Tolinski *Plastics and Sustainability : Towards a Peaceful Coexistence Between Bio-Based and Fossil Fuel-Based Plastics*; Wiley-Scrivener: Hoboken, NJ, USA, 2011.

9. G. W. Coates; D. R. Moore *Angew. Chem. Int. Ed.* **2004**, *43*, 6618-6639.

10. K. Nakano; T. Hiyama; K. Nozaki *Chem. Commun.* **2005**, 1871-1873.

11. H. Sugimoto; A. Ogawa *React. Funct. Polym.* **2007**, *67*, 1277-1283.

12. N. Ikpo; L. N. Saunders; J. L. Walsh; J. M. B. Smith; L. N. Dawe; F. M. Kerton *Eur. J. Inorg. Chem.* **2011**, 5347-5359.

13. D. J. Darensbourg; D. R. Billodeaux *Inorg. Chem.* **2005**, *44*, 1433-1442.

14. X. B. Lu; L. Shi; Y. M. Wang; R. Zhang; Y. J. Zhang; X. J. Peng; Z. C. Zhang; B. Li *J. Am. Chem. Soc.* **2006**, *128*, 1664-1674.

15. G. P. Wu; S. H. Wei; W. M. Ren; X. B. Lu; T. Q. Xu; D. J. Darensbourg *J. Am. Chem. Soc.* **2011**, *133*, 15191-15199.

16. X. B. Lu; W. M. Ren; G. P. Wu *Acc. Chem. Res.* **2012**, *45*, 1721-1735.

17. J. Yoo; S. J. Na; H. C. Park; A. Cyriac; B. Y. Lee *Dalton Trans.* **2010**, *39*, 2622-2630.

18. K. Nakano; S. Hashimoto; K. Nozaki *Chem. Sci.* **2010**, *1*, 369-373.

19. C. E. Anderson; S. I. Vagin; W. Xia; H. Jin; B. Rieger *Macromolecules* **2012**, *45*, 6840-6849.

20. L. N. Saunders; N. Ikpo; C. F. Petten; U. K. Das; L. N. Dawe; C. M. Kozak; F. M. Kerton *Catal. Commun.* **2012**, *18*, 165-167.

21. M. Reiter; P. T. Altenbuchner; S. Kissling; E. Herdtweck; B. Rieger *Eur. J. Inorg. Chem.* **2015**, *2015*, 1766-1774.

22. A. Buchard; M. R. Kember; K. G. Sandeman; C. K. Williams *Chem. Commun.* **2011**, *47*, 212-214.

23. M. Taherimehr; S. M. Al-Amsyar; C. J. Whiteoak; A. W. Kleij; P. P. Pescarmona *Green Chem.* **2013**, *15*, 3083-3090.

24. M. R. Kember; C. K. Williams *J. Am. Chem. Soc.* **2012**, *134*, 15676-15679.

25. K. Nakano; M. Nakamura; K. Nozaki *Macromolecules* **2009**, *42*, 6972-6980.

26. D. J. Darensbourg; A. I. Moncada *Inorg. Chem.* **2008**, *47*, 10000-10008.

27. P. Chen; M. H. Chisholm; J. C. Gallucci; X. Zhang; Z. Zhou *Inorg. Chem.* **2005**, *44*, 2588-2595.

28. R. L. Paddock; S. T. Nguyen *J. Am. Chem. Soc.* **2001**, *123*, 11498-11499.

29. S. Mang; A. I. Cooper; M. E. Colclough; N. Chauhan; A. B. Holmes *Macromolecules* **2000**, *33*, 303-308.

30. D. J. Darensbourg; J. C. Yarbrough *J. Am. Chem. Soc.* **2002**, *124*, 6335-6342.

31. D. J. Darensbourg; J. C. Yarbrough; C. Ortiz; C. C. Fang *J. Am. Chem. Soc.* **2003**, *125*, 7586-7591.

32. R. Eberhardt; M. Allmendinger; B. Rieger *Macromol. Rapid Commun.* **2003**, *24*, 194-196.

33. D. J. Darensbourg; R. M. Mackiewicz; J. L. Rodgers; C. C. Fang; D. R. Billodeaux; J. H. Reibenspies *Inorg. Chem.* **2004**, *43*, 6024-6034.

34. D. J. Darensbourg; R. M. Mackiewicz *J. Am. Chem. Soc.* **2005**, *127*, 14026-14038.

35. D. J. Darensbourg; R. M. Mackiewicz; D. R. Billodeaux *Organometallics* **2005**, *24*, 144-148.

36. B. Li; R. Zhang; X. B. Lu *Macromolecules* **2007**, *40*, 2303-2307.

37. X. Q. Xu; C. M. Wang; H. R. Li; Y. Wang; W. L. Sun; Z. Q. Shen *Polymer* **2007**, *48*, 3921-3924.

38. B. Li; G. P. Wu; W. M. Ren; Y. M. Wang; D. Y. Rao; X. B. Lu *J. Polym. Sci., Part A: Polym. Chem.* **2008**, *46*, 6102-6113.

39. D. J. Darensbourg; S. B. Fitch *Inorg. Chem.* **2009**, *48*, 8668-8677.

40. D. J. Darensbourg; M. Ulusoy; O. Karroonnirum; R. R. Poland; J. H. Reibenspies; B. Çetinkaya *Macromolecules* **2009**, *42*, 6992-6998.

41. D. J. Darensbourg; R. R. Poland; A. L. Strickland *J. Polym. Sci., Part A: Polym. Chem.* **2012**, *50*, 127-133.

42. L. P. Guo; C. M. Wang; W. J. Zhao; H. R. Li; W. L. Sun; Z. Q. Shen *Dalton Trans.* **2009**, 5406-5410.

43. D. Adhikari; S. T. Nguyen; M.-H. Baik *Chem. Commun.* **2014**, *50*, 2676-2678.

44. D. Y. Rao; B. Li; R. Zhang; H. Wang; X. B. Lu *Inorg. Chem.* **2009**, *48*, 2830-2836.

45. Y. L. Xiao; Z. Wang; K. L. Ding *Macromolecules* **2006**, *39*, 128-137.

46. G. A. Luinstra; G. R. Haas; F. Molnar; V. Bernhart; R. Eberhardt; B. Rieger *Chem. Eur. J.* **2005**, *11*, 6298-6314.

47. M. H. Chisholm; Z. P. Zhou *J. Am. Chem. Soc.* **2004**, *126*, 11030-11039.

48. M. Cheng; D. R. Moore; J. J. Reczek; B. M. Chamberlain; E. B. Lobkovsky; G. W. Coates *J. Am. Chem. Soc.* **2001**, *123*, 8738-8749.

49. R. K. Dean; L. N. Dawe; C. M. Kozak *Inorg. Chem.* **2012**, *51*, 9095-9103.

50. R. K. Dean; K. Devaine-Pressing; L. N. Dawe; C. M. Kozak *Dalton Trans.* **2013**, *42*, 9233-9244.

51. H. Chen; L. N. Dawe; C. M. Kozak *Catal. Sci. Technol.* **2014**, *4*, 1547-1555.

52. C. M. Kozak; A. M. Woods; C. S. Bottaro; K. Devaine-Pressing; K. Ni *Faraday Discuss.* **2015**, *183*, 31-46.

53. S. Menage; G. Gellon; J.-L. Pierre; D. Zurita; E. Saint-Aman *Bull. Soc. Chim. Fr.* **1997**, *134*, 785-791.

54. K. Devaine-Pressing; J. H. Lehr; M. E. Pratt; L. N. Dawe; A. A. Sarjeant; C. M. Kozak *Dalton Trans.* **2015**, *44*, 12365-12375.

55. S. Heidari; E. Safaei; A. Wojtczak; P. Cotic; A. Kozakiewicz *Polyhedron* **2013**, *55*, 109-116.

56. L. M. Alcazar-Roman; B. J. O'Keefe; M. A. Hillmyer; W. B. Tolman *Dalton Trans.* **2003**, 3082-3087.

57. R. K. Dean; S. L. Granville; L. N. Dawe; A. Decken; K. M. Hattenhauer; C. M. Kozak *Dalton Trans.* **2010**, *39*, 548-559.

58. D. J. Darensbourg; A. I. Moncada; W. Choi; J. H. Reibenspies *J. Am. Chem. Soc.* **2008**, *130*, 6523-6533.

59. S. Klaus; S. I. Vagin; M. W. Lehenmeier; P. Deglmann; A. K. Brym; B. Rieger *Macromolecules* **2011**, *44*, 9508-9516.

60. F. Jutz; A. Buchard; M. R. Kember; S. B. Fredriksen; C. K. Williams *J. Am. Chem. Soc.* **2011**, *133*, 17395-17405.

61. D. J. Darensbourg; A. D. Yeung *Polym. Chem.* **2015**, *6*, 1103-1117.

62. P. P. Pescarmona; M. Taherimehr *Catal. Sci. Technol.* **2012**, *2*, 2169-2187.

63. S. Klaus; M. W. Lehenmeier; C. E. Anderson; B. Rieger *Coord. Chem. Rev.* **2011**, *255*, 1460-1479.

64. J. H. So; P. Boudjouk *Inorg. Chem.* **1990**, *29*, 1592-1593.

65. K. D. Demadis; T. J. Meyer; P. S. White *Inorg. Chem.* **1998**, *37*, 3610-3619.

66. J. W. Pflugrath *Acta Crystallogr., Sect. D.* **1999**, *55*, 1718-1725.

67. A. C. Larson *Crystallographic Computing*; Munksgaard: Copenhagen, 1970.

68. D. T. Cromer; J. T. Waber *International Tables for X-ray Crystallography*; The Kynoch Press: Birmingham, England, 1974; Vol. IV.

69. A. Altomare; G. Cascarano; C. Giacovazzo; A. Guagliardi; M. Burla; G. Polidori; M. Camalli *J. Appl. Cryst.* **1994**, *27*, 435.

70. P. T. Beurskens; G. Admiraal; G. Beurskens; W. P. Bosman; R. de Gelder; R. Israel; J. M. M. Smits *DIRDIF99*; University of Nijmegen: Netherlands, 1999.

71. J. A. Ibers; W. C. Hamilton *Acta Crystallogr.* **1964**, *17*, 781.

72. D. C. Creagh; W. J. McAuley *International Tables for Crystallography*; Kluwer Academic Publishers: Boston, 1992; Vol. C, Table 4.2.6.8, pp. 219-222.

73. D. C. Creagh; J. H. Hubbell *International Tables for Crystallography*; Kluwer Academic Publishers: Boston, 1992; Vol. C, Table 4.2.4.3, pp. 200-206.

74. *CrystalStructure 3.7.0: Crystal Structure Analysis Package*, Rigaku and Rigaku/MSC, The Woodlands, TX, 2000-2005.

75. *SHELX-97-Programs for crystal structure determination (SHELXS) and refinement (SHELXL)*, University of Gottingen, Gottingen, Germany, 1997.

76. A. L. Spek *J. Appl. Cryst.* **2003**, *36*, 7-13.

77. L. J. Farrugia *J. Appl. Cryst.* **2012**, *45*, 849-854.

Co-Authorship Statement

Chapter 3: Mechanistic Studies of DMAP-initiated Cyclohexene oxide/CO_2 Copolymerization by a Chromium(III) Pyridylamine-bis(phenolate) Complex

This chapter contains the results of the accepted, in press article "Mechanistic Studies of DMAP-initiated Cyclohexene-oxide/CO_2 Copolymerization by a Chromium(III) Pyridylamine-bis(phenolate) Complex", *ChemSusChem*, **2017**, DOI:10.1002/cssc.201601641.

Authors: Katalin Devaine-Pressing and Christopher M. Kozak.

The first author (Katalin Devaine-Pressing) contributed 90% of the content of the article as the main researcher including: performing all experimental research, collecting data, and writing parts of the paper (including the results and discussion and experimental sections).

The corresponding author (Christopher M. Kozak), my supervisor, was the principal investigator of this research. He developed novel ideas, designed experiments and assisted with writing and submitting the manuscript.

Chapter 3. Mechanistic Studies of DMAP-initiated Cyclohexene oxide/CO_2 Copolymerization by a Chromium(III) Pyridylamine-bis(phenolate) Complex

3.1 Introduction

The copolymerization or coupling of carbon dioxide (CO_2) and epoxides continues to be a rapidly growing focus of research. The reaction is an appealing alternative to the traditional method of polycarbonate synthesis, which involves the use of diols such as the suspected endocrine disruptor Bisphenol A and highly toxic phosgene.[1-4] Since the utilization of CO_2 requires a high energy input to compensate for its thermodynamic stability, using the high free energy of epoxides drives the reaction forward in an atom efficient manner to give either cyclic or polycarbonates,[5-7] but the mechanical properties and applications of these CO_2/epoxide-derived polycarbonates are often different from BPA-derived plastics.[2]

Numerous catalyst systems have been developed for CO_2/epoxide copolymerization over the last 40 years that exhibit varying degrees of control, reaction rates, versatility in choice of epoxide and activity under acceptable pressures of CO_2, and there are many excellent reviews covering this field.[6-12] For the majority of homogeneous catalysts, suitable ionic or neutral nucleophilic co-catalysts are required and the most broadly used include methylimidazole (*N*-MeIm), 4-dimethylaminopyridine (DMAP) and bis(triphenylphosphoranylidene)ammonium (PPN^+) salts, such as PPN chloride, azide, or 2,4-dinitrophenoxide (PPNCl, $PPNN_3$ PPN(2,4-DNP)).

The mechanism of CO_2/epoxide coupling and copolymerization, particularly the role of the co-catalyst, has been studied by several groups.[13-20] Darensbourg found that chromium salen complexes paired with anionic nucleophiles of PPN^+ salts do not exhibit initiation periods, whereas neutral co-catalysts (N-heterocyclic amines or phosphines) do. The fast formation of active, anionic, six-coordinate $[(salen)Cr(N_3)X]^-$ derivatives was cited as the reason.[17] DMAP binding to chromium(III) salen and salan complexes was studied using electrospray ionization mass spectrometry.[15] This report showed that even under low DMAP to Cr ratios, coordination of two DMAP molecules to the salenCr(III) fragment was possible, and the stability of the six-coordinate $[salenCr(DMAP)_2]^+$ ions led to long initiation times. The salanCr(III) complex, on the other hand, showed no induction period, possibly as a result of the lower tendency for bis-DMAP adduct formation due to steric differences to the salen analog.

The activity of chromium amino-bis(phenolate) complexes[21] and pyridyl-amine(bis) phenolate complexes[22-25] for the copolymerization of epoxides with CO_2 with ionic or neutral nucleophilic co-catalysts were previously reported. The difference in reaction rate between **2.1**·THF and **2.1**·DMAP was demonstrated and compared to the rate with **1.21** in Chapter 2 (Figure 2.4 and Table 2-3 in Section 2.2.2). The difference in the initiation between **2.1**·THF and **2.1**·DMAP is also illustrated in Figure D.3 in Appendix D, where longer (~17 min) initiation but faster propagation rate ($3.5 \pm 0.026 \times 10^{-2}$ min^{-1}) was observed with **2.1**·DMAP than with **2.1**·THF (~5 min initiation and $1.2 \pm 0.020 \times 10^{-2}$ min^{-1}). Both **2.1**·DMAP and **2.1**·THF exhibited much shorter initiation periods than complex **1.21**, which also had an observed reaction rate one order of

magnitude slower than for **2.1**·DMAP. MALDI-TOF MS analysis of the polycarbonates suggests that the initiation most likely occurs via a monometallic intermolecular pathway where ring opening of the epoxide is initiated by a nucleophilic species (either the chloride ion from the Cr-complex or the added co-catalyst). Based on this observation, it was hypothesized that the reaction was probably first order with respect to catalyst concentration. To confirm this hypothesis, kinetic studies of CHO/CO_2 copolymerization were carried out using **2.1**·DMAP, the system that exhibited the fastest propagation rate. The effect of increasing the co-catalyst loading on the copolymerization rate as well as its influence on polymer end groups was investigated. The findings of these studies are discussed here.

3.2 Results and discussion

3.2.1 Determination of the reaction order of catalyst concentration

To determine the reaction order with respect to catalyst concentration, four different concentrations of the catalyst precursor **2.1**·DMAP were applied: 0.50 mol%, 0.25 mol%, 0.17 mol% and 0.10 mol%, while the initial concentration of CHO and CO_2 pressure were kept constant. To ensure the total homogeneity of the reaction mixture and to be able to accurately follow the reaction via *in situ* attenuated total reflectance infrared spectroscopy (ATR-FTIR), 5 mL of dichloromethane was added to each reaction mixture. This prevented polymer precipitation on the ATR window and ensured sufficient coverage of the sensor. The addition of a solvent is a commonly applied method with ATR-FTIR monitoring[26-28] and is especially advantageous for aliquot

sampling. However, its use is not a requirement and depends on the measurement of interest.[13] It is worth noting here that the addition of solvent in our case had a negative influence in monomer to polymer conversion resulting in 19% conversion in the presence of co-solvent compared to 75% conversion in neat CHO at 0.10 mol% catalyst loading. This can be attributed to the dilution of the activated nucleophilic species and the metal centre, thus inhibiting propagation,[13] and lower monomer concentration. The slowing of the reactions in the presence of solvent proved to be advantageous for accurately determining the initial reaction rates.

The first 100 minutes of the reaction profiles showing the growth of the absorbance of the polycarbonate carbonyl C=O band at 1750 cm^{-1} band are represented in Figure D.4 in Appendix D and the observed initial reaction rates after the initiation periods are in Figure 3.1. Initial rates were determined based on the linear propagation following the initiation period at each catalyst concentration. (Figure 3.1 and Figure D.4). The absorbance values have not been normalized in Figure 3.1 and as the overall spectrum baseline varies between each experiment, there is no correlation among the different catalyst loading studies with respect to absorbance and the absolute concentration of polycarbonate. Plots of normalized absorbance vs. time following temperature stabilization and initiation periods for the different catalyst loading levels are given in Figure D.5 in Appendix D. The observed initial rates calculated from the lines of best fit are compiled in Table 3-1. As expected, rates increased with increasing catalyst concentration.

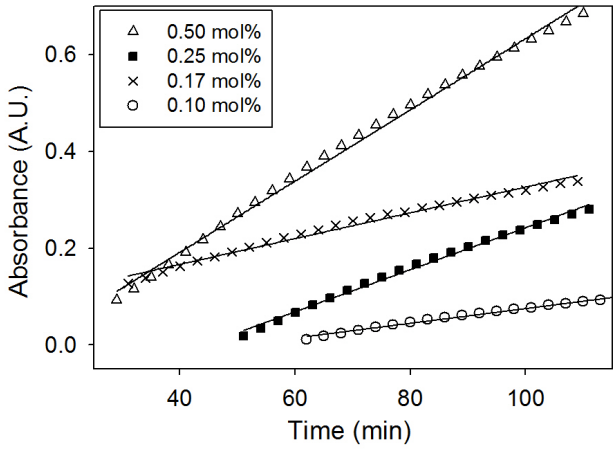

Figure 3.1 Initial rates of reaction profiles based on the absorbance at 1750 cm^{-1} ($\nu_{(C=O)}$) of the polycarbonates with **2.1**·DMAP loadings of 0.5 mol% (△), 0.25 mol% (■), 0.17 mol% (×) and 0.1 mol% (○). Lines represent best fits of a linear model to the observed data (see Table 3-1).

Table 3-1 Relative reaction rates based on the changes in the absorbance at 1750 cm^{-1} corresponding to the $\nu_{(C=O)}$ of the growing polycarbonate chains with different catalyst concentration and R^2 values of the linear regressions.

[cat] (mol%)	Relative reaction rate r_{obs} ($\times 10^{-3}$ min^{-1})	R^2
0.50	7.4 ± 0.094	0.9958
0.25	4.3 ± 0.074	0.9945
0.17	2.7 ± 0.060	0.9874
0.10	1.5 ± 0.037	0.9895

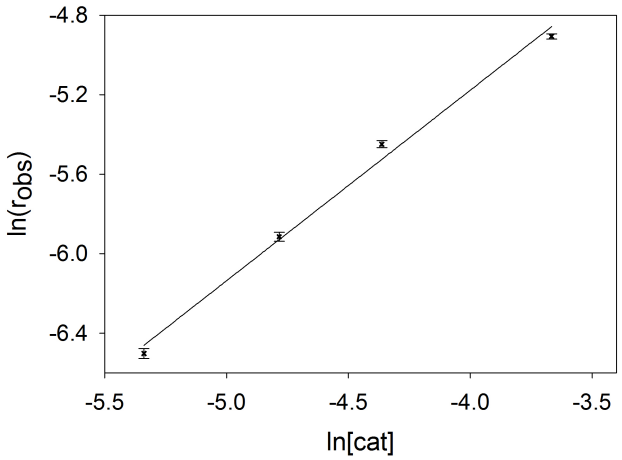

Figure 3.2 Logarithmic plot of the initial rates versus catalyst concentration

Plot of $\ln(r_{obs})$ against ln[cat] (Figure 3.2) shows a linear relationship giving a reaction order of 0.96 (R^2 = 0.9927), showing a first order dependence on catalyst concentration. This observation is in good agreement with the previously proposed mechanism[22] indicating there is only one complex participating in the ring opening of the epoxide followed by one propagating polymer chain per chromium complex. The mechanism suggested in a previous report from our group proposes a monometallic intermolecular initiation where an external or chromium-bound nucleophile initiates ring opening of a coordinated epoxide. However, **2.1**·DMAP contains two metal-bound nucleophilic species (DMAP and chloride ligands), therefore, the possibility of a monometallic intramolecular initiation cannot be excluded.

A reaction order of 1.61 was determined for a binary CoX-salen/$^{n}Bu_4NX$ (X = 2,4-dinitrophenoxide) system, whereas an order of 1.01 was obtained for a bifunctional Co^{III}-salen complex where one quaternary ammonium salt was appended to a phenolate ring of the salen ligand.[13] This report proposed a mainly monometallic intramolecular initiation for the bifunctional system, whereas a monometallic intermolecular ring opening by an external nucleophile was suggested for the binary system. The difference in mechanism was attributed to the appended quaternary ammonium salt, which was believed to keep the dissociated anionic carboxylated polymer chain in close proximity to the cobalt centre, thereby allowing propagation to occur in a well-controlled manner depending only on catalyst concentration. In the binary system, the counter cations of the quaternary ammonium salt and the dissociated carbonate polymer anions may become distant from the cobalt centre, especially in a dilute solution. As a result, the reaction

order is dependent on the propagating species consistent with co-catalyst concentration, as well as on the activated epoxide species with regards to complex concentration. Ren and Lu reported the reaction orders for CO_2/epoxide copolymerization by a Co(DNP)-salen complex with a sterically hindered neutral external nucleophile, 7-methyl-1,5,7-triazabicyclo[4.4.0]dec-5-ene (MTBD) and for a TBD-appended bifunctional Co^{III}-salen system.[13] The values were 1.55 for the binary system and 0.98 for the bifunctional one, which are similar to the observed values using the anionic 2,4-dinitrophenoxide nucleophiles with quaternary ammonium salts. In another study, mono- and dinuclear chromium salphen complexes were compared in propylene oxide/CO_2 copolymerization by Rieger and co-workers.[26] They found that initiation was more complex with their mononuclear complex giving a reaction order of 1.69, whereas they obtained two values in the case of their flexibly linked dinuclear complex (**1.16b**, Figure 1.9, Chapter 1), 0.85 and 1.23, both being closer to first order rather than second order dependence. The two stages observed with the dinuclear complex were attributed to the existence of an initial heterogeneous stage due to the insolubility of the complex in epoxide and dichloromethane, followed by a homogeneous stage after the total dissolution of the complex. The higher value for the mononuclear-complex initiated polymerization was attributed to a considerable intermolecular bimetallic initiation accompanied by intramolecular initiation to a small extent, whereas intramolecular ring opening dominates with the flexibly-linked dinuclear catalyst. A linear relationship between reaction rate and catalyst concentration was found with a dizinc acetate complex coordinated with a macrocyclic ligand by the Williams group.[28] Based on their findings, they proposed a mechanism where there is only one active site per bimetallic complex,

therefore one polymer chain growing per complex even though there are two zinc centres present. The propagating chain possibly migrates to the other Zn centre after every CHO insertion, which also explains the high activity of this complex. The second acetate group maintains its position ensuring that both Zn centres keep their octahedral coordination as well as their neutral charge balance. The mechanism of the reaction was also discussed in Chapter 1, Section 1.1.6.1, Scheme 1.6.

The presence of DMAP end groups observed by MALDI-TOF MS studies (see Section 3.2.3) suggests the **2.1**·DMAP/CHO/CO_2 system undergoes DMAP-initiated ring opening of a coordinated cyclohexene oxide (either inter- or intramolecularly), followed by CO_2 insertion and chain propagation. This pathway also represents the possible mechanism of cyclic carbonate formation in solution where a carbonate polymer chain end backbites leading to shorter chain lengths and cyclic cyclohexene carbonate formation. The probability of a carbonate chain end backbiting is higher in solution than in neat epoxide, mainly because the mobility of polymer species is enhanced in a less viscous medium.[13] Also, higher DMAP loading may favour dissociation of the growing polymer chain, thus leading to increased probability of backbiting.

Copolymerization results of this reaction series (Table 3-2) show a decreasing trend in conversion and yield of recovered polymer as catalyst loading decreases. The yields reported are for polymer obtained through its precipitation from the crude reaction mixture and careful washing to remove catalyst or catalyst decomposition products. Possible by-products include cyclic carbonates, short chain oligomers, polyethers and cyclohexane diol, but none of these could be observed by ^{1}H NMR of the crude reaction

mixtures resulting from these catalytic conditions.[22] A maximum turn over number (TON) of 468 is achieved at 0.17 mol% catalyst loading, where an acceptably high conversion (78%) is also maintained. The lowest M_n value was obtained with 0.10 mol% catalyst concentration probably due to the highly diluted reaction mixture and, consequently, low conversion.

Table 3-2 Effect of catalyst concentration on CHO/CO_2 copolymerization.

Entry[a]	[Cr] (mol×L^{-1})	% Conver-sion[b]	% Yield[c]	TON[d]	M_n[e] (cal'd) (g/mol)	M_n[f] (GPC) (g/mol)	Đ[f] (M_w/M_n)
1	0.50	99	58	198	28 100	12 800	1.10
2	0.25	94	75	376	53 400	14 000	1.14
3	0.17	78	57	468	66 500	14 600	1.13
4	0.10	19	8	190	27 000	9 200	1.08

[a]All copolymerization reactions were carried out in cyclohexene-oxide (5 mL) and CH_2Cl_2 (5 mL). [b]Calculated by ^{1}H NMR. [c]Yield = moles of isolated product (mass of polymer/molar mass of repeating unit) divided by the moles of starting monomer. [d]Turnover number: moles of repeating units produced per moles of Cr present. [e]Molecular weight calculated from [CHO]/[Cr] × % conversion × 142.15 g × mol^{-1}. [f]Molecular weights (g × mol^{-1}) determined by triple detection gel permeation chromatography (GPC) in tetrahydrofuran using a dn/dc value determined individually for each polymer (values between 0.0752 – 0.0887 mL × g^{-1}).

3.2.2 The effect of co-catalyst loading

The effect of the amount of DMAP co-catalyst on reaction rate was investigated with **2.1**·DMAP. **2.1**·DMAP already contains one equivalent of the neutral co-catalyst. Reactions were carried out using the complex on its own, then with one additional equiv. of DMAP (i.e. two equiv. DMAP per chromium) and four equiv. of added DMAP (i.e. five equiv. DMAP per chromium). Figure 3.3A depicts the first 5 h of the reactions. After the initiation period, the propagation rate increases with increased DMAP loading.

The initiation period, however, follows the reverse order (Figure 3.3B), which is the longest (~ 45 min, Table 3-3) when 5 equiv. DMAP are present, and shows multiple rate changes during this time period. This may indicate the presence of equilibria between active and catalytically inactive species during the initiation period. The values of the initial reaction rates are summarized in Table 3-3.

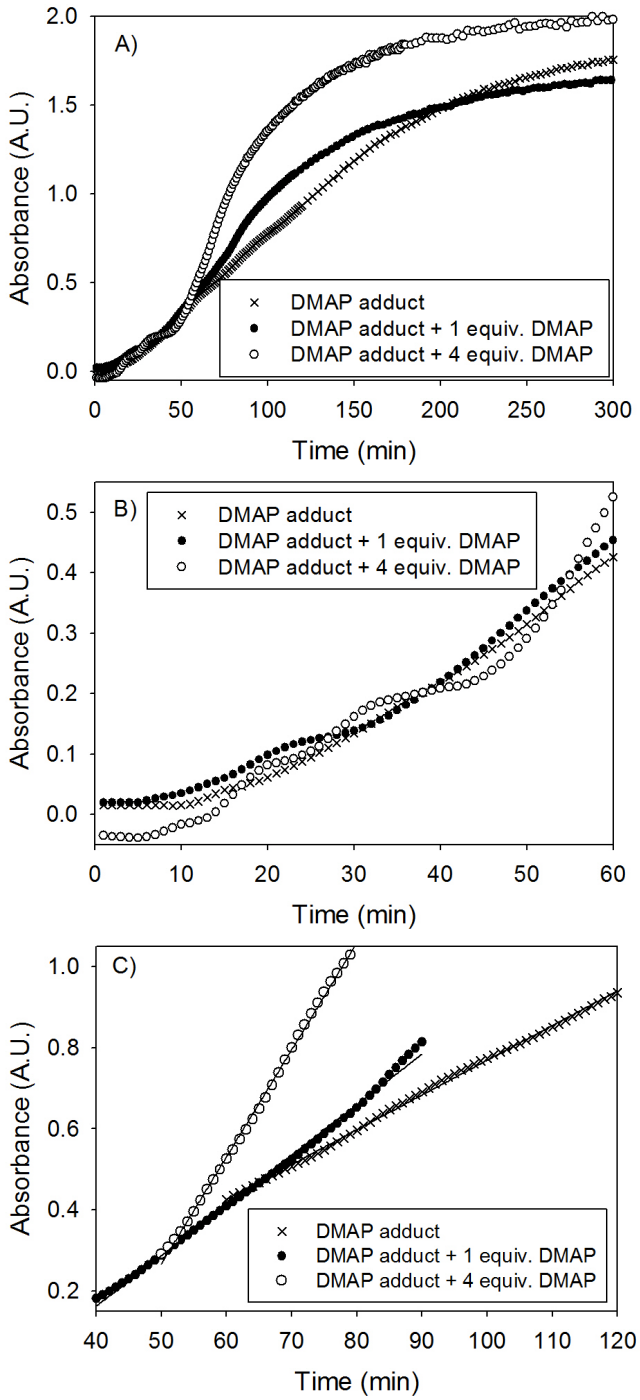

Figure 3.3 A) First 5 h B) first hour of the reaction profiles showing the growth of the absorbance of the polycarbonate carbonyl C=O band at 1750 cm^{-1} catalyzed by **2.1**·DMAP with different amounts of DMAP present: 1 equiv. DMAP (×), 2 equiv. DMAP (●), 5 equiv. DMAP (○) (Reaction conditions: 40 bar CO_2, 60 °C, 24 h). C) Initial rates of reaction profiles following initiation periods based on the absorbance of the $\nu_{(C=O)}$ of the polycarbonates.

Table 3-3 Relative reaction rates based on the changes in the absorbance at 1750 cm^{-1} corresponding to the $\nu_{(C=O)}$ of the growing polycarbonate chains with different amounts of co-catalyst, R^2 values of the linear regressions and initiation time values.

[Cr]:[CHO]:[DMAP]	Relative reaction rate r_{obs} ($\times 10^{-2}$ min^{-1})	R^2	Initiation period (min)
1:500:1	0.86 ± 0.0041	0.9987	17
1:500:2	1.24 ± 0.0102	0.9969	38
1:500:5	2.64 ± 0.0190	0.9985	45

The rate of copolymerization was found to increase with increased co-catalyst loading. For salen complexes, the activity typically plateaus with elevated amounts of co-catalyst, or increases the rate of back-biting side reactions forming cyclic carbonates.[29-34] 0.5 Equiv. of co-catalyst was found to improve polymer selectivity and activity even with mono- and dinuclear cobalt salen complexes.[35] The **2.1**·DMAP/CHO/CO_2 system, however, shows that with up to 5 equiv. of DMAP the conversion of CHO did not decrease (Table 3-4, entries 1 – 3) but very high DMAP loadings (30 equiv.) led to deactivation of the catalyst (entry 4). Previously, elevated amounts of DMAP inhibitied the activity of **1.21**,[24] and Kleij, Pescarmona and co-workers showed that selectivity between cyclic and polycarbonate formation using iron-tris(phenolate) complexes could be controlled by varying co-catalyst loadings.[36] Darensbourg showed copolymerization of 2-(3,4-epoxycyclohexyl)trimethoxysilane (TMSO) with CO_2 was fastest with 3 equiv. of DMAP,[17] but further increasing the DMAP concentration also led to cyclic TMSO carbonate formation. Cyclic cyclohexene carbonate formation was also observed in the **2.1**·DMAP/CHO/CO_2 system when 2 or 5 equiv. of DMAP was applied, but the amount was negligible compared to the amount of polymer formed and the existence of the cyclic product was detected only by using sensitive ATR FTIR monitoring (weak peak at 1810

cm^{-1}, Figure 3.4). ^{1}H NMR of the polymer obtained with 5 equiv. of DMAP showed 0.3% trans cyclic carbonate (4.01 ppm) formation whereas no trans cyclic carbonate was detected when 1 or 2 equiv. of DMAP was used. *Trans*-cyclohexene carbonate is typically formed via back-biting of the polymer whereas *cis*-cyclohexene carbonate forms from the reaction of CHO and CO_2 via a double inversion pathway. The majority of the cyclic carbonate product observed via ATR-FTIR is then the *cis* product for which the chemical shift of the methine protons is buried under the peak of the methine protons of the polymer (4.63 ppm).

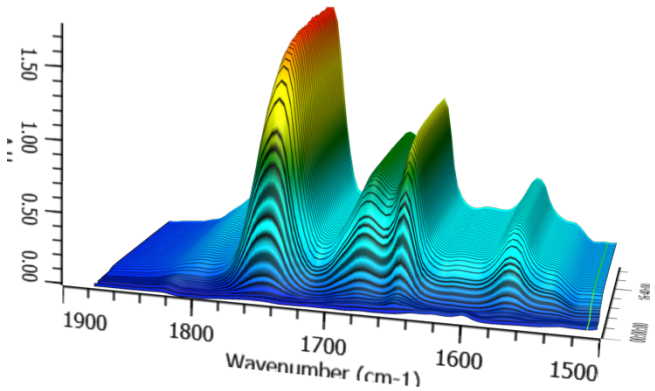

Figure 3.4 Three dimensional surface diagram of the copolymerization of CHO/CO_2 catalyzed by **2.1** and 5 equiv. DMAP at 60 °C and 40 bar CO_2.

Table 3-4 Effect of DMAP loading on CHO/CO_2 copolymerization.

Entry[a]	[Cr]:[CHO]:[DMAP]	% Conversion[b]	%Yield[c]	TON[d]	M_n[e] (cal'd) (g/mol)	M_n[f] (g/mol)	Đ[f]
1	1:500:1	81	62	405	57 600	24 400	1.05
2	1:500:2	81	63	405	57 600	20 000	1.12
3	1:500:5	83	55	415	59 000	24 600	1.05
4	1:500:30	0	0	0	ND[g]	ND	ND

[a]All copolymerization reactions were carried out in neat cyclohexene-oxide (5 g). [b]Calculated by ^{1}H NMR. [c]Yield = moles of isolated product (mass of polymer / molar mass of repeating unit) per mol of monomer. [d]Turnover number: moles of repeating units produced per mole of Cr. [e]Molecular weight calculated from [CHO]/[Cr]/[DMAP] × %

conversion × 142.15 g × mol^{-1}. [f]Molecular weights (g × mol^{-1}) determined by triple detection gel permeation chromatography (GPC) in tetrahydrofuran using a dn/dc value determined individually for each polymer (values between 0.0752 – 0.0887 mL × g^{-1}). [g]ND = not determined.

If the number of active species formed increases with increased DMAP loading, and if polymer chain growth occurs at each active species, then a decrease in molecular weight is expected. A slight molecular weight decrease was observed previously when PPNCl and $PPNN_3$ were utilized together with **2.1**·DMAP.[22] When the amount of DMAP is increased, however, the molecular weights remain effectively unchanged (between 20 000 and 25 000 g/mol). The observed molecular weights are typically lower than calculated, particularly when no excess DMAP is added. This is generally attributed to the formation of solid polymer, increasing the viscosity of the reaction mixture thus inhibiting chain propagation, and resulting in a narrow molecular weight distribution. Another possible explanation, which may contribute to lower than expected molecular weights, is that not all of the active species can sustain chain propagation, thus undergoing chain backbiting leading to cyclic cyclohexene carbonate formation. The effect of the increased amount of DMAP in epoxide/CO_2 copolymerization was also investigated with Cr-salen complexes by Rieger and co-workers, who were able to switch the selectivity between polycarbonate and cyclic carbonate products depending on DMAP loading.[34] They found that 0.5 equiv. of DMAP was ideal for polymer formation, whereas for cyclic cyclohexene carbonate, 2 equiv. of DMAP was needed. In a previous study by the Kozak group, complex **1.21** showed excellent activity with 0.5 equiv. of DMAP and gave no polymer or cyclic carbonate with 2 equiv. of DMAP.[24] This suggests that **1.21** follows a different mechanism of initiation or is more susceptible to blockage of

the active site by DMAP coordination,[23] given that good yields of polymer are obtained by **2.1**·DMAP even with 5 equiv. of DMAP. Besides the dimeric nature of **1.21**, which most likely dissociates under catalytic conditions, the different substituents at the phenolate rings may impart a difference in catalytic behaviour. Influences on catalytic activity arising from the electronic effects of the phenolate substituents have been observed for salen complexes, where changing one of the *tert*-butyl groups to a more electron-donating methoxy group provides a more electron-rich but still balanced chromium centre.[37] The electron-donating influence of the methoxy substituent has similarly been observed,[22,23] namely whereas **1.21** has two *tert*-butyl groups, **2.1**·DMAP bears a *tert*-butyl group ortho to the phenolate oxygen, and a methoxy group in a para position. Specifically, two DMAP molecules may bind sufficiently strongly to chromium in **1.21** that no vacant site is open for epoxide coordination.[23] Similar inhibition of activity through coordinative saturation by DMAP has been reported by others.[34] The more electron-rich metal centre in **2.1**·DMAP results in sufficiently stable coordination of DMAP to be observed in the solid state,[22] but not too strong to prevent formation of a vacant site for CHO coordination and copolymerization.

3.2.3 MALDI-TOF analysis of the polymers obtained with different DMAP loadings

Figure 3.5 shows the MALDI-TOF mass spectrum of the polymer obtained according to the conditions in Table 3-4, entry 1. The lower mass region of the spectrum was obtained in both linear and reflectron mode (Figure 3.5B). In the higher resolution reflectron mode, three different species were detected in the lower mass region, and all of

them were DMAP initiated (Figure 3.5C). Species (a) contains an ether linkage and is terminated by a hydroxyl group, species (b) is also hydroxyl terminated and species c) contains a chloride end group resulting from chain-transfer. In the higher mass region only species (b) was observed, as expected for DMAP initiated copolymerization and termination by hydrolysis.

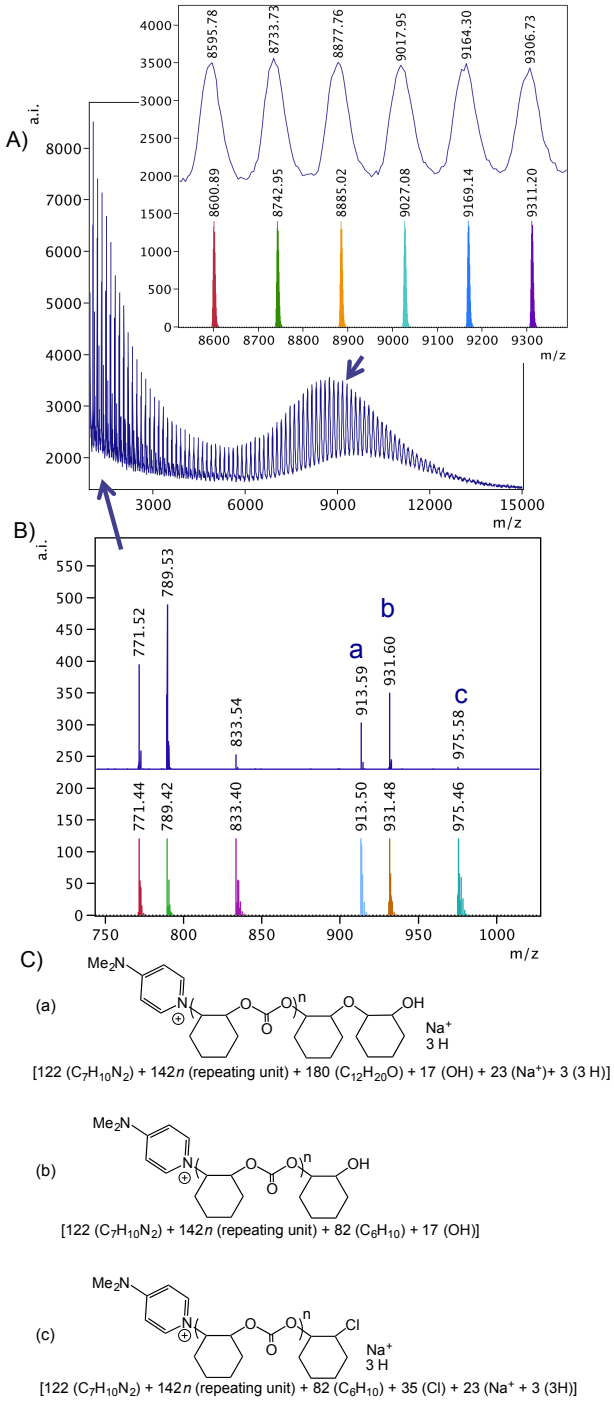

Figure 3.5 A) MALDI-TOF mass spectrum of the polymer obtained according to the conditions in Table 3-4, entry 1, inset: expanded higher mass region (*m/z* 8600 – 9400) with calculated masses of fragments shown beneath the observed spectrum. B) Lower mass (oligomer) region (*m/z* 750 – 1000, n = 3 – 5) of the spectrum in reflectron mode. Calculated masses of the fragments are represented beneath the observed reflectron mode spectrum. C) Proposed structures of the lower mass polymer fragments.

Four different polymer fragments were detected in the MALDI-TOF mass spectrum of the polymer obtained according to the conditions of Table 3-4, entry 2 (Figure 3.6.). Series (a) and (b) both have DMAP and hydroxyl termini and an ether linkage, and series (a) contains a Na^+ ion whereas (b) a K^+ ion. Series (c) has an ether linkage and two chloride termini, indicating chain transfer. Series (d) describes the typical chloride initiated and hydroxyl terminated product.

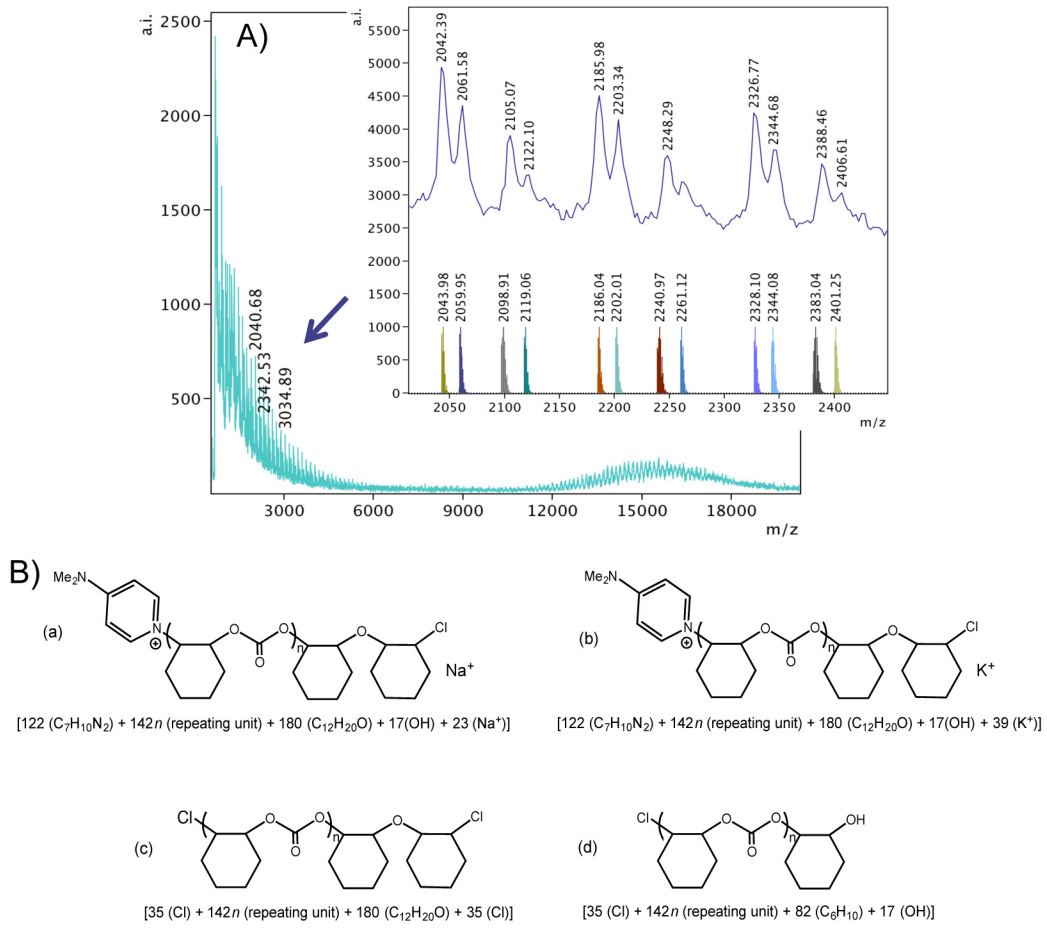

Figure 3.6 A) MALDI-TOF mass spectrum of the polymer obtained according to the conditions in Table 3-4, entry 2, inset: expanded lower mass region (*m/z* 2000 – 2500, n = 13 – 15) of the spectrum with calculated masses of the fragments shown beneath the observed spectrum. B) Proposed structures of the lower mass polymer fragments.

Figure 3.7 shows the MALDI-TOF mass spectrum of the polymer obtained in the presence of 5 equiv. DMAP per chromium (Table 3-4, entry 3). Here again, two of the three series, (a) and (b), are DMAP initiated. Series (a) has an ether linkage with a chloride chain end, (b) has DMAP at both termini and contains a Na^+, which also might be due to chain transfer during polymerization. Series (c) is chloride initiated and hydroxyl terminated with a Na^+ ion present.

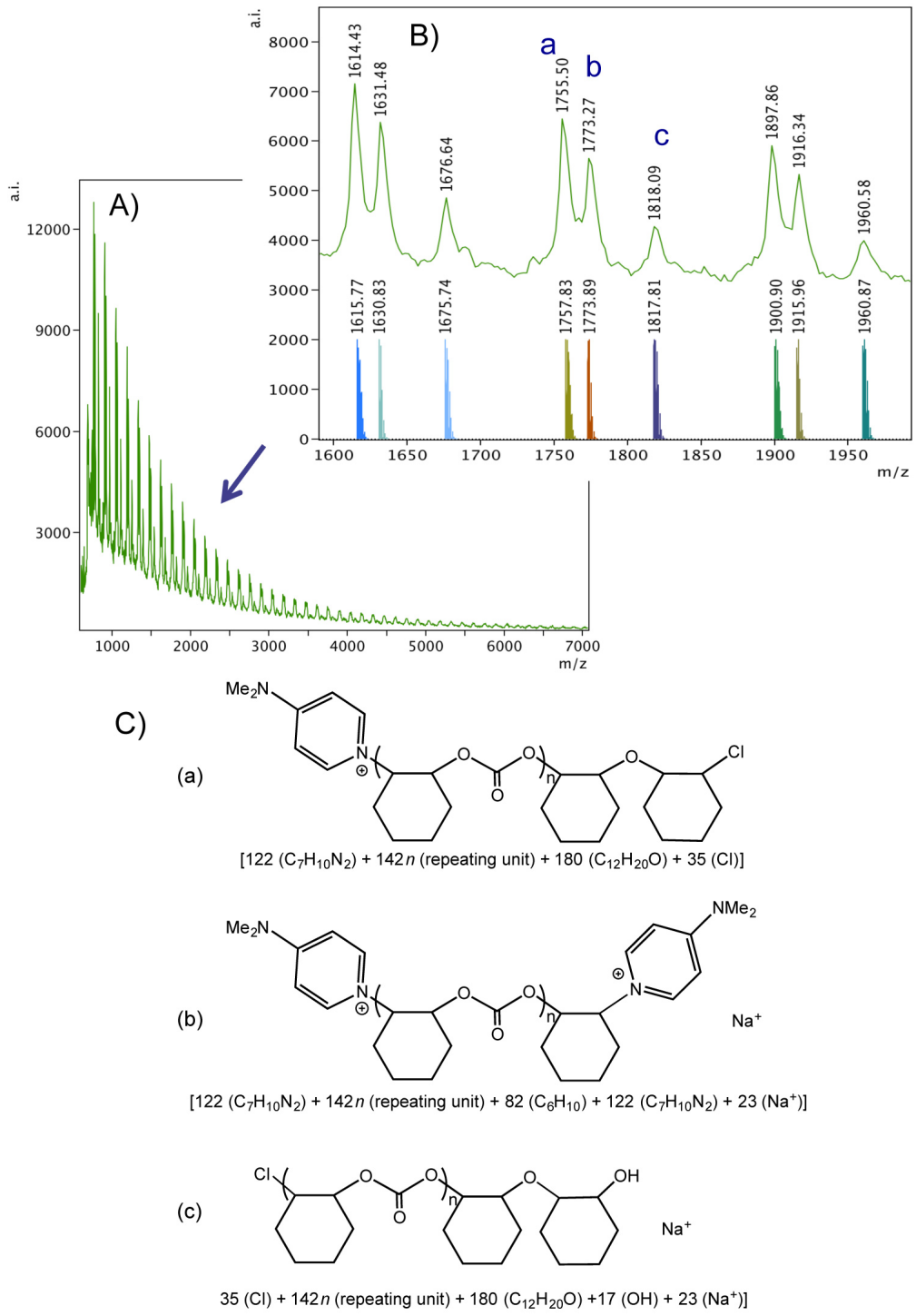

Figure 3.7 A) MALDI-TOF mass spectrum of the polymer obtained according to the conditions in Table 3-4, entry 3. B) Expanded lower mass region (*m/z* 1600 – 2000, n = 10 – 12) of the spectrum with calculated masses of the fragments shown beneath the observed spectrum. C) Proposed structures of the polymer fragments.

The presence of DMAP end groups in all three cases is not surprising, especially with elevated amounts of DMAP present and confirms DMAP is, in addition to the endogenous chloride of the chromium complex, also capable of initiating the epoxide ring-opening. In a scenario where a chloride ring-opens an epoxide and is incorporated as the chain end, and the growing polymer chain dissociates from the chromium, DMAP may also initiate epoxide ring-opening and consequently may be incorporated in the chain end. As both chloride and DMAP termini are observed, it is possible that both processes occur simultaneously. Moreover, the presence of species (b), Figure 3.7, where there are two DMAP termini, indicates a higher degree of chain transfer reactions when the amount of DMAP is increased. Chain transfer is commonly believed to arise from the presence of water, which reacts with the epoxide to form a diol, which in turn serves as the chain transfer agent. This also leads to the occurance of ether linkages. Chain transfer to diol leads to larger than expected polymer molecular weights, effectively doubling the chain length of polymers formed by the original initiating group. The dispersities, observed are narrow in all cases and suggest the rate of chain transfer is faster than the rate of propagation. Similar behaviour has been previously observed by Williams and co-workers.[38]

3.2.4 Investigation of the initiation of CHO/CO_2 copolymerization with DMAP via ATR FTIR spectroscopy

In 2005 Darensbourg and Mackiewicz proposed a possible initiation of CHO/CO_2 copolymerization by a chromium(III) salen complex (**1.9** in Chapter 1, Figure 1.7, Section 1.1.5) and DMAP.[17] They monitored the reaction in a control experiment

between the complex, 50 equiv. DMAP and 55 bar of CO_2 via *in situ* ATR FTIR spectroscopy and detected several new vibration bands at 2097 and 2018 cm^{-1} after 90 min. The new bands were assigned to the vibrations of CO_2 in a zwitterionic carbamic complex where CO_2 has inserted between the chromium and DMAP. Another new peak at 1650 cm^{-1} was assigned to the "activated" DMAP vibration ($\nu_{C=C}$) of the same complex. When epoxide was present, the peaks at 2097 and 2018 cm^{-1} disappeared but the peaks at 1680 and 1650 cm^{-1} persisted. An initiation period was attributed to this DMAP activation until all the free DMAP was consumed, that is, activated (Scheme 3-1). They also supported this by the disappearance of the free DMAP band at 1599 cm^{-1}, which also occurred within the same initiation time.

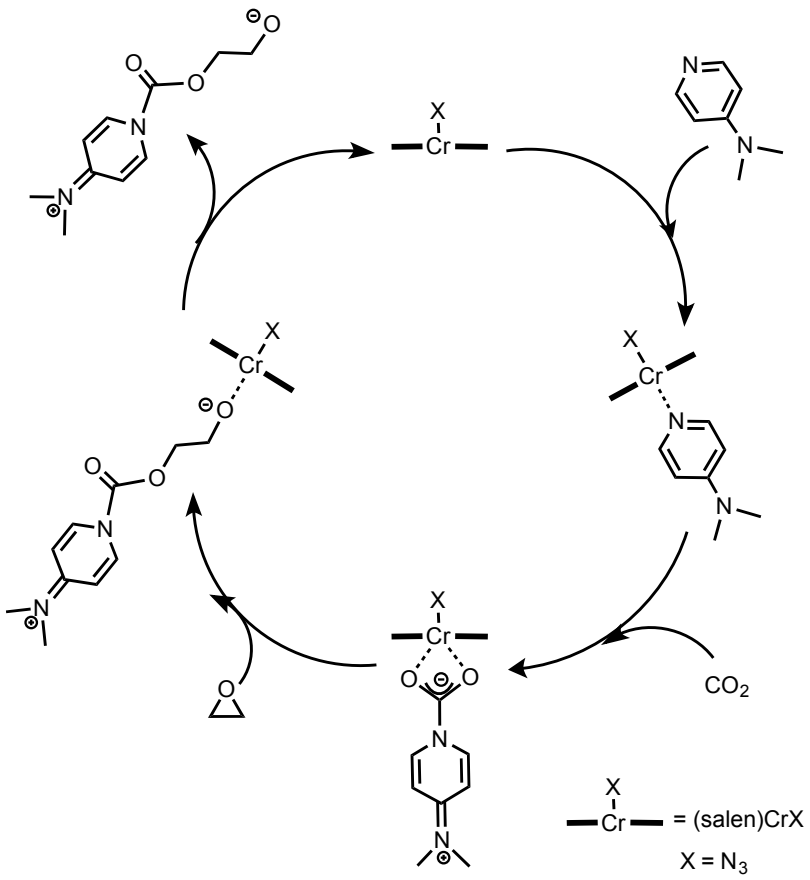

Scheme 3-1 Proposed mechanism of DMAP activation by Darensbourg and co-workers.

In the work of Darensbourg and Mackiewicz, DMAP is not the only nucleophilic group present. The presence of the azide groups complicates interpretation of the IR data because the bands at 2097 and 2018 cm^{-1} may also be attributed to an organic azide stretching frequencies as well. Crystallographic evidence was obtained by Jacobsen when they investigated the asymmetric ring opening of cyclopentene oxide using chromium salen complexes.[39] The crystal structure shows that the azide group initiated the ring opening and became incorporated in the ring opened cyclopentene oxide. In the study by Jacobsen and co-workers, the azide stretching frequency of the salen complex at 2053 cm^{-1} was replaced by a new band at 2095 cm^{-1} of the organic azide with the ring opened

epoxide. The same shift was also found later by Darensbourg and Moncada when they followed the ring opening of propylene oxide, oxetane and cyclohexene oxide by azide via FTIR spectroscopy.[40] In all three cases, the vibration of the azide of the complex at 2047 cm^{-1} shifted to 2100 cm^{-1} when an epoxide was present, therefore, conclusive identification of peaks in the IR spectra is challenging.

In order to see whether a similar DMAP activation is possible with chromium(III) amine-bis(phenolate) complexes, **2.1**·THF with 50 equiv. DMAP and 40 bar CO_2 was subjected to *in situ* ATR FTIR spectroscopy monitoring. The full spectra of the monitoring at three different time intervals are demonstrated in Figure 3.8 and the expanded region between 2200 and 1500 cm^{-1} is in Figure 3.9.

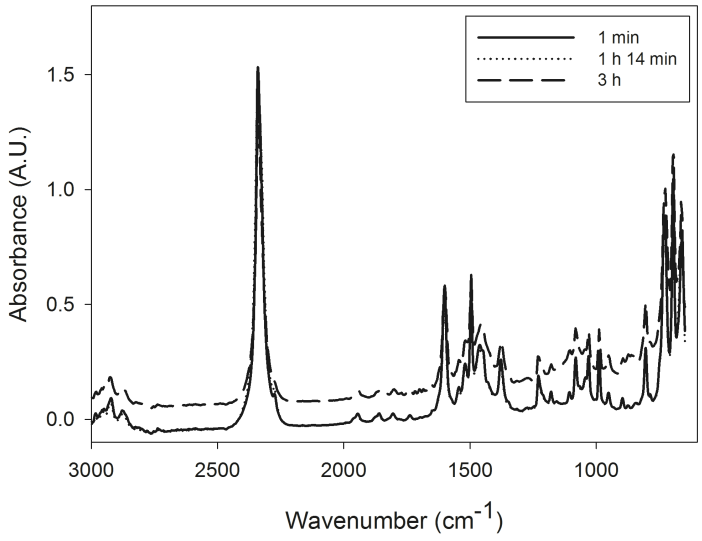

Figure 3.8 Full spectra obtained by ATR IR at 1 min, 1 h 14 min and 3 h of the system of **2.1**·THF + 50 equiv. DMAP and 40 bar CO_2. Note: data collected at 1 min and at 1h 14 min are entirely coincident.

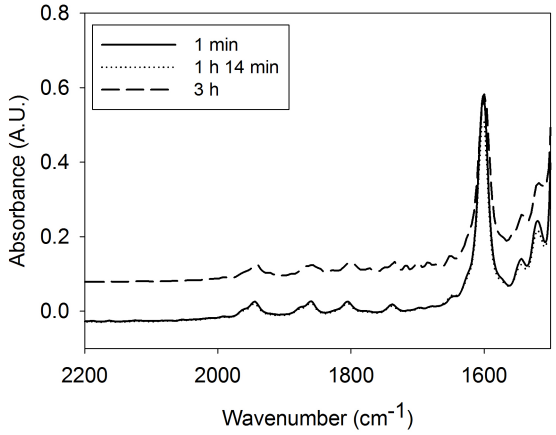

Figure 3.9 Expanded spectra obtained by ATR FTIR at 1 min, 1 h 14 min and 3 h of the system of **2.1**·THF + 50 equiv. DMAP and 40 bar CO_2. Note: data collected at 1 min and at 1h 14 min are entirely coincident.

There is no change observed after 75 min, the first two spectra (obtained after 1 min and 75 min) are indistinguishable in the figures (the dotted line of the 75 min spectrum is entirely coincident with the 1 min spectrum). The peak at 1600 cm^{-1} corresponding to free DMAP persists throughout the reaction and there are no new peaks arising at 2097 or 2018 cm^{-1}, indicating no reaction between **2.1**·THF, DMAP and CO_2 even after heating. A possible explanation is that no carbamate bands are observed simply because the mechanism wherein the DMAP nucleophile reacts with CO_2 to form a DMAP-carbamate is not applicable to the catalysis by **2.1**. This might be due to the different structure of the salen and the amine-bis(phenolate) complexes. Namely, the salen ligand exhibits a more rigid, planar orientation around the chromium, which is consequently less sterically hindered for the formation of the carbamic species *trans* to the chloride ligand. The structure of **2.1**·THF would direct the formation of the carbamic species *cis* to the chloride group, which may be unfavoured.

3.3 Conclusions

Chromium(III) complexes of pyridylamino-bis(phenolate) ligands bearing enhanced electron-donating phenolate groups possessing t-butyl and methoxy substituents showed excellent activity for selective alternating copolymerization of CO_2 with cyclohexene oxide. Kinetic studies performed by *in situ* infrared spectroscopy on the single component catalyst system **2.1**·DMAP revealed a reaction pathway with first order dependance on catalyst concentration. These are the first data of this sort for a chromium system for CO_2/epoxide reactions. Comparison with the binary catalyst system of salen$Co^{III}X$/nBu_4NX (X = 2,4-dinitrophenoxide), which may be the most similar catalyst for which data has been reported, shows different findings to those for **2.1**·DMAP. Instead, **2.1**·DMAP has a reaction order of 0.96, which is more aligned with that reported for a bifunctional catalyst bearing an appended quaternary ammonium salt.[13] Co-catalyst (DMAP) loading showed reaction rates increase with increased DMAP concentrations, suggesting DMAP also serves as an initiator by way of nucleophilic attack at epoxide to induce ring-opening. This is perhaps surprising as elevated amounts of DMAP co-catalyst have previously been reported to lead to either complete inhibition of catalysis or to increased backbiting resulting in cyclic carbonate formation. Neither conversions of substrate nor selectivity for polycarbonate appeared to diminish with higher loadings of DMAP when used with **2.1**·DMAP in the present study. Reaction rate profiles via *in situ* FTIR spectroscopy, however, suggest longer initiation periods at higher DMAP concentrations, therefore a more complex copolymerization pathway with a nonlinear relationship with respect to DMAP occurs. MALDI TOF MS analysis of the

polymers obtained under different co-catalyst loadings reveal the products of chain transfer events and the presence of DMAP end groups. Although carbamate formation has been observed by others for chromium salen catalysts, no evidence was found for this for **2.1**·DMAP. Therefore, it is most likely DMAP that serves to initiate ring opening of the epoxide via an intramolecular manner and that this is the rate determining step of copolymerization for chromium amine-phenolate catalyst systems.

3.4 Experimental

3.4.1 General experimental conditions

Unless otherwise stated, all manipulations were performed under an atmosphere of dry oxygen-free nitrogen by using standard Schlenk techniques or using an MBraun Labmaster glove box. **2.1**·THF is hygroscopic and will discolour in air over the course of a week (changing from dark green to black). Any noticeable discolouration of **2.1**·DMAP occurs more slowly than for **2.1**·DMAP, but air-free conditions were employed as much as possible to prevent accumulation of moisture. Cyclohexene oxide (CHO) was purchased from Aldrich and freshly distilled from CaH_2 under N_2 atmosphere into an ampule. THF was purified by distillation from sodium/benzophenone ketyl under nitrogen. All other solvents were dried and degassed using an MBraun Manual Solvent Purification System. $CrCl_3(THF)_3$ was prepared via previously reported methods.[41] The synthesis of the proligand H_2[**L1**][42-44] was previously reported. A modified synthesis in water and full characterization of H_2[**L1**] is given in Chapter 2, Section 2.5.3. 99.998% (4.8 Supercritical fluid chromatography grade) CO_2 was supplied from Praxair in a high-

pressure cylinder equipped with a liquid dip tube. All ^{1}H and $^{13}C\{^{1}H\}$ NMR spectra were obtained in $CDCl_3$ purchased from Cambridge Isotope Laboratories, Inc.

3.4.2 Instrumentation

^{1}H and $^{13}C\{^{1}H\}$ NMR spectra were recorded on a Bruker AVANCE III 300 MHz spectrometer. All copolymerization reactions were carried out in a 100 mL stainless steel Mettler Toledo reactor with a React IR 15 base unit. N.B. Caution should be taken when operating such high-pressure equipment. GPC analysis was performed in THF at 25 °C on a Wyatt Triple Detection (triple angle light scattering, viscometry and refractive index) system with Agilent 2600 series sample and solvent handling. The system used two Phenogel 10^3 Å 300 × 4.60 mm columns (molecular weight range of 1 k to 75 kdaltons). Samples were prepared at a concentration of 6 mg/mL and left to equilibrate for ~ 2 h, then filtered through 0.2 μm syringe filters before analysis. The GPC columns were eluted with HPLC grade THF at a flow rate of 0.30 mL/min with a 100 μL injection volume. MALDI-TOF mass spectrometry was performed by using an Applied Biosystems 4800 MALDI- TOF/TOF Analyzer equipped with a reflectron, delayed extraction and high performance nitrogen laser (200 Hz operating at 355 nm). For polymer analysis, 2,5-dihydroxybenzoic acid (DHBA) was used as the matrix. The matrix was dissolved in THF at a concentration of 10 mg/mL. The polymer was dissolved at a concentration of 1 mg/mL. The matrix and polymer solutions were combined in a 3:1 or 4:1 ratio and the MALDI plate was spotted using the dried-droplet method.

3.4.3 Synthesis of chromium complexes

The syntheses of **2.1**·THF and **2.1**·DMAP and **1.21** were previously reported[22,24] and the syntheses of **2.1**·THF and **2.1**·DMAP can also be found in Chapter 2, Section 2.5.4.

3.4.4 *In situ* monitoring of the CHO/CO_2 copolymerizations by IR spectroscopy

In situ monitoring was carried out using a 100 mL Parr Instruments stainless steel reactor vessel with motorized mechanic stirrer and a heating mantle. The vessel was modified with a bottom mounted Mettler Toledo SiComp Sentinel sensor, which was connected to a ReactIR 15 base unit through a DS silver-halide Fiber-to-Sentinel conduit. The reactor vessel was cleaned and heated under vacuum at 80 °C overnight before experiments. In a glove box, the appropriate amount of complex and DMAP (where needed) were weighed and then dissolved in 5 g (8 g for the co-catalyst effect runs) CHO. For the runs with the reaction order determination, 5 mL of dichloromethane was added to the mixture. The reactant solution was stirred for ~ 5 min, then transferred via a long-needle syringe to the reactor vessel. The solution was injected into the vessel through a port, after which the reactor was pressurized with the appropriate pressure of CO_2 and left to stir for the desired time at the desired temperature and pressure. A spectrum was collected every minute for 3 h, then every three minutes for any remaining time (up to 24 h). After the reaction, the autoclave was cooled then vented into a fume hood. An aliquot was taken immediately after opening the reactor for the determination of conversion by NMR. The copolymer was extracted into dichloromethane and

precipitated by addition of cold acidic methanol. The yields reported are for the amount of polymer obtained from precipitation, washing and drying.

3.5 References

1. T. Sakakura; J.-C. Choi; H. Yasuda *Chem. Rev.* **2007**, *107*, 2365-2387.

2. A. M. Nelson; T. E. Long *Polym. Int.* **2012**, *61*, 1485-1491.

3. S. Fukuoka; M. Kawamura; K. Komiya; M. Tojo; H. Hachiya; K. Hasegawa; M. Aminaka; H. Okamoto; I. Fukawa; S. Konno *Green Chem.* **2003**, *5*, 497-507.

4. W. B. Kim; U. A. Joshi; J. S. Lee *Ind. Eng. Chem. Res.* **2004**, *43*, 1897-1914.

5. M. Aresta *Carbon Dioxide as Chemical Feedstock*; Wiley-VCH: Weinheim, 2010.

6. D. J. Darensbourg; S. J. Wilson *Green Chem.* **2012**, *14*, 2665-2671.

7. D. J. Darensbourg *Inorg. Chem.* **2010**, *49*, 10765-10780.

8. G. W. Coates; D. R. Moore *Angew. Chem. Int. Ed.* **2004**, *43*, 6618-6639.

9. M. R. Kember; A. Buchard; C. K. Williams *Chem. Commun.* **2011**, *47*, 141-163.

10. S. Klaus; M. W. Lehenmeier; C. E. Anderson; B. Rieger *Coord. Chem. Rev.* **2011**, *255*, 1460-1479.

11. S. Paul; Y. Zhu; C. Romain; R. Brooks; P. K. Saini; C. K. Williams *Chem. Commun.* **2015**, *51*, 6459-6479.

12. M. Taherimehr; P. P. Pescarmona *J. Appl. Polym. Sci.* **2014**, *131, 41141*, 1-17

13. J. Liu; W. M. Ren; Y. Liu; X. B. Lu *Macromolecules* **2013**, *46*, 1343-1349.

14. D. Adhikari; S. T. Nguyen; M.-H. Baik *Chem. Commun.* **2014**, *50*, 2676-2678.

15. D. Y. Rao; B. Li; R. Zhang; H. Wang; X. B. Lu *Inorg. Chem.* **2009**, *48*, 2830-2836.

16. Y. L. Xiao; Z. Wang; K. L. Ding *Macromolecules* **2006**, *39*, 128-137.

17. D. J. Darensbourg; R. M. Mackiewicz *J. Am. Chem. Soc.* **2005**, *127*, 14026-14038.

18. G. A. Luinstra; G. R. Haas; F. Molnar; V. Bernhart; R. Eberhardt; B. Rieger *Chem. - Eur. J.* **2005**, *11*, 6298-6314.

19. M. H. Chisholm; Z. P. Zhou *J. Am. Chem. Soc.* **2004**, *126*, 11030-11039.

20. M. Cheng; D. R. Moore; J. J. Reczek; B. M. Chamberlain; E. B. Lobkovsky; G. W. Coates *J. Am. Chem. Soc.* **2001**, *123*, 8738-8749.

21. H. Chen; L. N. Dawe; C. M. Kozak *Catal. Sci. Technol.* **2014**, *4*, 1547-1555.

22. K. Devaine-Pressing; L. N. Dawe; C. M. Kozak *Polym. Chem.* **2015**, *6*, 6305-6315.

23. C. M. Kozak; A. M. Woods; C. S. Bottaro; K. Devaine-Pressing; K. Ni *Faraday Discuss.* **2015**, *183*, 31-46.

24. R. K. Dean; L. N. Dawe; C. M. Kozak *Inorg. Chem.* **2012**, *51*, 9095-9103.

25. R. K. Dean; K. Devaine-Pressing; L. N. Dawe; C. M. Kozak *Dalton Trans.* **2013**, *42*, 9233-9244.

26. S. Klaus; S. I. Vagin; M. W. Lehenmeier; P. Deglmann; A. K. Brym; B. Rieger *Macromolecules* **2011**, *44*, 9508-9516.

27. C. E. Anderson; S. I. Vagin; M. Hammann; L. Zimmermann; B. Rieger *ChemCatChem* **2013**, *5*, 3269-3280.

28. F. Jutz; A. Buchard; M. R. Kember; S. B. Fredriksen; C. K. Williams *J. Am. Chem. Soc.* **2011**, *133*, 17395-17405.

29. D. J. Darensbourg *Chem. Rev.* **2007**, *107*, 2388-2410.

30. D. J. Darensbourg; J. C. Yarbrough *J. Am. Chem. Soc.* **2002**, *124*, 6335-6342.

31. D. J. Darensbourg; R. M. Mackiewicz; J. L. Rodgers; A. L. Phelps *Inorg. Chem.* **2004**, *43*, 1831-1833.

32. D. J. Darensbourg; P. Bottarelli; J. R. Andreatta *Macromolecules* **2007**, *40*, 7727-7729.

33. R. L. Paddock; S. T. Nguyen *J. Am. Chem. Soc.* **2001**, *123*, 11498-11499.

34. R. Eberhardt; M. Allmendinger; B. Rieger *Macromol. Rapid Commun.* **2003**, *24*, 194-196.

35. K. Nakano; S. Hashimoto; K. Nozaki *Chem. Sci.* **2010**, *1*, 369-373.

36. M. Taherimehr; S. M. Al-Amsyar; C. J. Whiteoak; A. W. Kleij; P. P. Pescarmona *Green Chem.* **2013**, *15*, 3083-3090.

37. D. J. Darensbourg; R. M. Mackiewicz; J. L. Rodgers; C. C. Fang; D. R. Billodeaux; J. H. Reibenspies *Inorg. Chem.* **2004**, *43*, 6024-6034.

38. M. R. Kember; F. Jutz; A. Buchard; A. J. P. White; C. K. Williams *Chem. Sci.* **2012**, *3*, 1245-1255.

39. K. B. Hansen; J. L. Leighton; E. N. Jacobsen *J. Am. Chem. Soc.* **1996**, *118*, 10924-10925.

40. D. J. Darensbourg; A. I. Moncada *Inorg. Chem.* **2008**, *47*, 10000-10008.

41. J. H. So; P. Boudjouk *Inorg. Chem.* **1990**, *29*, 1592-1593.

42. S. Menage; G. Gellon; J.-L. Pierre; D. Zurita; E. Saint-Aman *Bull. Soc. Chim. Fr.* **1997**, *134*, 785-791.

43. K. Devaine-Pressing; J. H. Lehr; M. E. Pratt; L. N. Dawe; A. A. Sarjeant; C. M. Kozak *Dalton Trans.* **2015**, *44*, 12365-12375.

44. S. Heidari; E. Safaei; A. Wojtczak; P. Cotic; A. Kozakiewicz *Polyhedron* **2013**, *55*, 109-116.

Co-Authorship Statement

Chapter 4: Magnesium Amino-bis(phenolato) Complexes for the Ring-opening Polymerization of *rac*-Lactide

This chapter contains the results published in the full article "Magnesium Amino-bis(phenolato) Complexes for the Ring-opening Polymerization of *rac*-Lactide", *Dalton Transactions,* **2015**, *44*, 12365–12375.

Authors: Katalin Devaine-Pressing, Joshua H. Lehr, Michelle E. Pratt, Louise N. Dawe, Amy A. Sarjeant and Christopher M. Kozak.

The first author (Katalin Devaine-Pressing) contributed 70% of the content of the article as the main researcher including: performing most of the experimental research, collecting data, and writing parts of the paper (including creating ORTEP images, results and discussion and the experimental sections).

The co-author, Joshua H. Lehr was an undergraduate summer student who worked alongside the first author helping in the synthesis of complexes and performing experiments in the melt.

The co-author, Michelle E. Pratt was an undergraduate student who worked alongside the first author and synthesized **4.2** and obtained crystals of **4.2** suitable for XRD.

The co-authors, Louise N. Dawe and Amy A. Sarjeant, the crystallographers on the paper at Memorial University and at Northwestern University, respectively, collected XRD data and solved the structure for complex **4.2**.

The corresponding author (Christopher M. Kozak), my supervisor, was the principal investigator of this research. He developed novel ideas, designed experiments and assisted with writing and submitting the manuscript.

Chapter 4. Magnesium Amino-bis(phenolato) Complexes for the Ring Opening Polymerization of *rac*-Lactide

4.1 Introduction

Polylactide is an excellent example of novel synthetic polymers as was mentioned in Chapter 1. It is biodegradable, biosourced and biocompatible.[1] It is also central to the development of sustainable polymers, an area of critical importance for the design of new materials that reduce environmental and health impacts resulting from their manufacture, use, and their end-of-life properties.[2-5] The array of different metal complexes studied for the ROP of lactide has been described in several reviews[6-9] and examples of metal-containing initiators vary considerably in terms of the metal centre and ligands employed. Complexes of amino-bis(phenolates) exhibit interesting structural and electronic effects, as well as catalytic behaviour; the variety of metal complexes with this ligand class has also been reviewed.[10] Derivatives of this ligand class have been used in main group and d-block metal chemistry, including lithium,[11-19] magnesium,[20-26] calcium,[27] rare-earths,[28,29] zinc,[21,30-38] aluminum,[8,39,40] zirconium[41,42] and titanium.[43] Many of these complexes have been reported to be excellent initiators for the ring-opening polymerization (ROP) of cyclic esters such as lactide and ε-caprolactone. For the ring opening polymerization (ROP) of cyclic esters, earth abundant alkali and alkaline earth metal compounds have become particularly important in the search for efficient, stable, inexpensive and non-toxic catalysts. We have previously reported the structures and catalytic lactide ROP activity of lithium and potassium amino-

bis(phenolato) compounds.[44,45] Magnesium compounds also have great potential as ROP catalysts for the preparation of PLA particularly for biomedical applications, as Mg is a biocompatible and non-toxic metal and thus the residue of these metals in the resulting polylactide is not of great concern.[46,47] Furthermore, magnesium compounds have been shown to elicit high reaction rates for copolymerization of CO_2 and epoxides.[48]

Magnesium complexes reported by Ma and co-workers exhibited some of the highest activities in ROP of cyclic esters by this metal.[49,50] The high activity for the ROP of *rac*-lactide may be due to the monomeric nature of these magnesium bis(silyl)amido complexes supported by tetradentate monophenolate ligands and the presence of a reactive monodentate amido ligand. A TOF of 36 560 h^{-1} was achieved when 10 000 equiv. of *rac*-lactide was converted to polylactide in 15 minutes at 25 °C in the absence of any co-catalyst. One of these complexes showed very high activity even under melt conditions at 110 °C giving 72% conversion with a TOF of 86 880 h^{-1}. Magnesium compounds supported by tridentate monophenolate Schiff-base ligands and benzyl alkoxide also proved active for L-lactide polymerization in CH_2Cl_2 solutions.[22] In both of these cases, it is likely the monodentate amido or alkoxide ligand that serves as the initiation site.

In light of these high activities, the activity of magnesium amino-bis(phenolato) complexes towards ROP of *rac*-lactide under melt conditions and in solution were investigated. Magnesium complexes of aminophenolate ligands have previously been reported by others but their activity for ROP of lactides was not tested or they showed very low or no activity.[51-54] In this chapter, the synthesis and characterization of two new

magnesium-bis(phenolate) complexes that show good lactide ROP activity in both melt and solution conditions are presented.

4.2 Results and discussion

4.2.1 Synthesis and characterization of proligands and magnesium complexes

Tetradentate tripodal amine-bis(phenol) protio ligands (Scheme 4-1) were synthesized *via* a modified Mannich condensation reaction in water.[55] The substituted phenols contained *tert*-butyl groups in the *ortho* positions and methoxy (H_2[**L1**]) or methyl groups (H_2[**L3**]) *para* to the hydroxyl group. The proligands possessed pyridyl (H_2[**L1**]) or dimethylaminoethyl (H_2[**L3**]) groups as the neutral pendant *N*-donors. The synthesis of H_2[**L1**] using a four step procedure[56] and without the addition of any further solvents[57] was previously reported. The synthesis of H_2[**L3**] in methanol was reported by Bochmann and co-workers.[54]

The corresponding protio ligand was reacted with one equivalent of di(*n*-butyl)magnesium in toluene at –78 °C to afford complexes **4.1** and **4.2** (Scheme 4-1). The NMR spectra of complexes **4.1** and **4.2** in non-coordinating solvents revealed that the compounds exist as dimers in solution. The ^{1}H NMR spectrum of **4.2** in C_6D_6 showed two *tert*-butyl environments implying inequivalent phenolates. This was further supported by the existence of four aromatic proton resonances arising from the phenolate rings occupying inequivalent coordination sites at the magnesium centres. The methylene resonances exist as four doublets. Two doublets are expected for a monometallic complex given the diastereotopic environments resulting from coordination to the metal

centre. The existence of the four doublets arises from asymmetric phenolate sites where one phenolate of each ligand occupies a bridging position between two magnesium ions. The solid-state structure of compound **4.2** confirmed the proposed connectivity (see below). In coordinating solvents, such as pyridine or DMSO, the NMR spectra are consistent with monometallic compounds. The ^{1}H NMR spectra of **4.1** in C_6D_6 and toluene-d_8 both showed the presence of several isomers suggesting the existence of dimeric species but also of more than one structural isomer (e.g. *syn* and *anti* oriented pendent donors) present in solution. Similar isomerism has been observed in zirconium amine-tris(phenolates).[58]

MALDI-TOF mass spectrometry (see Figure B.10 and B.11 in Appendix B) showed complexes **4.1** and **4.2** exhibit dimeric structures in the gas phase as well as in solution and the solid state. Peaks at *m/z* 1028.50 (rel. intensity 100%) and *m/z* 514.26 (58%) corresponding to the dimer and monomer fragment ions, respectively, were observed for complex **4.1**. For complex **4.2**, the peak assigned to the dimer at *m/z* 924.52 was very weak (3%) and the peak at *m/z* 462.25 (100%) corresponds to the monomer.

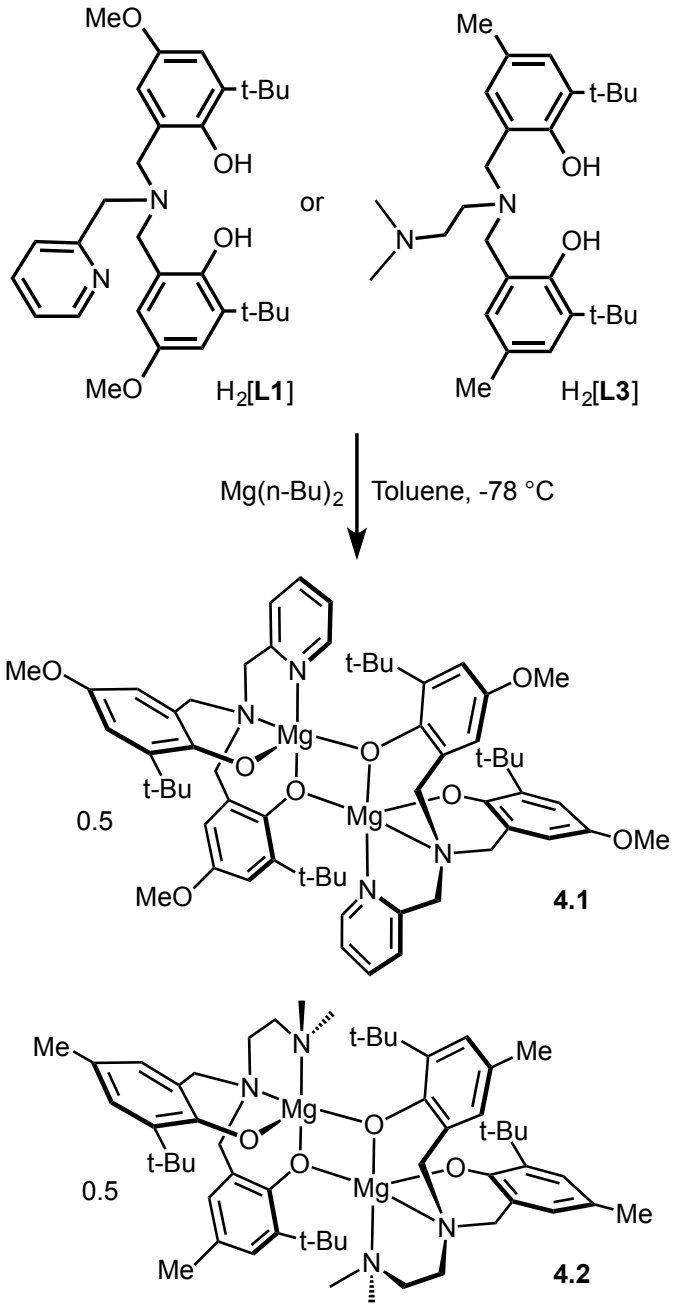

Scheme 4-1 Synthesis of complexes **4.1** and **4.2**.

Colourless crystals of **4.2** suitable for single crystal X-ray diffraction were obtained from saturated toluene solutions at –35 °C. The solid-state molecular structure with selected bond lengths and angles is shown in Figure 4.1. Crystallographic and

structure refinement data can be found in Table A-2 in Appendix A. The dimeric structure with chemically distinct phenolate groups is consistent with the NMR studies discussed above. Each magnesium centre is five-coordinate and bound to two nitrogen donors and three oxygen donors. Four of the coordination sites are occupied by the chelating diamine-bis(phenolate) ligand, while the fifth coordination site is occupied by a bridging phenolate oxygen. The non-planar Mg_2O_2 core exhibits a O(2)-Mg(1)-O(2)*-Mg(1)* torsion angle of 32.69°. The magnesium complexes that show polymerization activity are believed to initiate cyclic ester ring-opening polymerizations through a coordination insertion mechanism;[7,46] therefore, the creation of a vacant site by breaking the Mg_2O_2 ring (in the presence of a polar monomer or a coordinating solvent, for example) may induce activity in these typically inactive bimetallic complexes. NMR studies of monomer formation in the presence of benzyl alcohol (a lactide ROP co-catalyst) are discussed below. The Mg(1)-O(1) bond (1.950(2) Å) in **4.2** is considerably shorter than the Mg(1)-O(2) bond (2.049(2)Å), because of the bridging bonding mode of the O(2) atom. The bond lengths for Mg(1)-N(1) and Mg(1)-N(2) were very similar at 2.243(3) Å and 2.265(3) Å, respectively, and are within the range observed in similar complexes.[51-53]

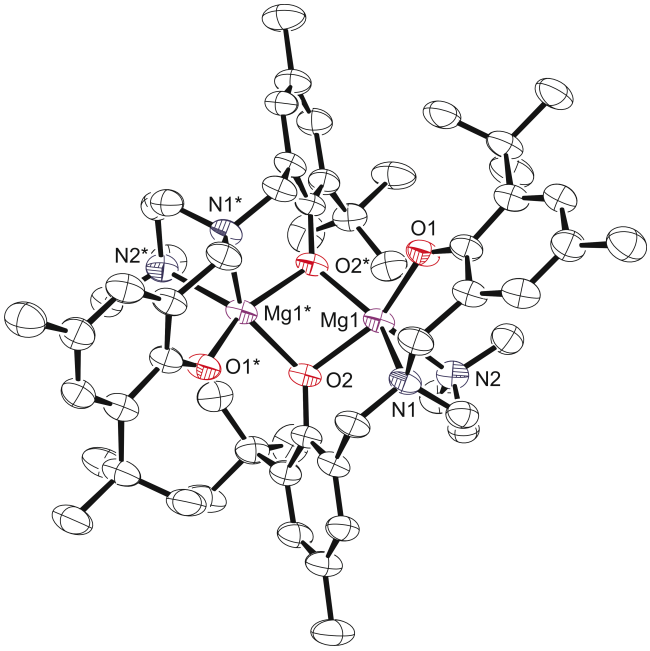

Figure 4.1 Partially labelled molecular structure (ORTEP) of the dimer of complex **4.2**. Thermal ellipsoids are drawn at 50% probability and H atoms are excluded for clarity. Selected bond lengths (Å): Mg(1)-O(1), 1.950(2); Mg(1)-O(2), 2.049(2); Mg(1)-O(2)*, 2.049(2); Mg(1)-N(1), 2.243(3); Mg(1)-N(2), 2.265(3). Bond angles (°): O(1)-Mg(1)-O(2), 153.48(10); O(1)-Mg(1)-N(1), 88.25(9); O(2)-Mg(1)-O(2)*, 74.53(9); Mg(1)-O(2)-Mg(1)*, 95.71(8), O(2)*-Mg(1)-N(1), 140.38(9); O(2)-Mg(1)-N(2), 102.07(9); O(1)-Mg(1)-O(2)*, 91.64(9). *Symmetry operations used to generate equivalent atoms: 1−x, y, ½−z.

A brief comparison of the structural properties of magnesium amine-bis(phenolate) complexes follows. The trigonality index,[59] τ, for **4.2** is 0.27 at both magnesium centres, which more closely approaches a distorted square pyramidal (τ = 0) rather than a trigonal bipyramidal geometry (τ = 1). The related magnesium complex reported by Janas and co-workers differs from **4.2** in that it contains one methyl substituent at the *para* position of the phenolate ring and no substituents at the *ortho* position resulting in a much less sterically encumbered metal site.[51] This is manifested in a rhombic Mg_2O_2 core that is nearly perfectly planar, possessing a sum of angles of 359.9°. The τ values for this compound are 0.35 and 0.61 for Mg(1) and Mg(2),

respectively, indicating geometries around the metal centres that are intermediate to square pyramidal and trigonal bipyramidal.

A similar complex was reported by Sobota and co-workers possessing the tripodal amine-bis(phenolate) ligand, *N,N*-bis(3,5-di-*tert*-butylbenzyl-2-hydroxy)tetrahydro-furfurylamine (**1.37**, Chapter 1, Figure 1.20, Section 1.2.3).[53] A dimeric complex was observed in C_6D_6 solutions and in the solid state, where it displayed a distorted rhombic Mg_2O_2 core whose sum of angles was 346.8°. The structure exhibited τ values for the two pentacoordinate magnesium centres that were almost identical at 0.41 and 0.39, intermediate to trigonal bipyramidal and square pyramidal arrangements, similar to complex **4.2**. This complex, however, also proved to be inactive in ROP of L-lactide at 25 °C in toluene.

A related phenolate-bridged magnesium dimer possessing *N,N'*-bis(2-hydroxido-3,5-di-*tert*-butyl)-*N,N'*-dimethylethane-1,2-diamine ligands was reported by Davidson, O'Hara and co-workers (**1.35**, Chapter 1, Figure 1.18, Section 1.2.3).[52] As in the compound reported by Janas and co-workers, each magnesium ion in this structure possesses different coordination environments with Mg(1) and Mg(2) centres having τ values of 0.32 and 0.25, respectively. A Mg_2O_2 core is also present in this structure with a sum of angles of 357.6°. ^{13}C- and ^{1}H NMR spectra for this compound in aromatic solvents suggested a dimeric structure in solution, similar to complex **4.2**. Two distinct phenolate environments and complicated methylene resonances indicate the dimer remains intact in non-coordinating aromatic solvents. This complex showed no activity in ring opening polymerization of lactide even at 110 °C in solution, which was

attributed to the bulkiness of the ligand and the persistence of the dimeric nature of the complex in non-coordinating, aromatic solvents.

Magnesium *N,N*-bis(3,5,-di-tert-butylbenzyl-2-hydroxy)dimethylethylene-diamine was prepared by Bochmann and co-workers using magnesium bis[bis(trimethylsilyl)amide] (instead of the more commonly used di(*n*-butyl)magnesium) to give a complex that, although not structurally authenticated, is expected to be similar to those discussed above (**1.33**, Chapter 1, Figure 1.17, Section 1.2.3).[54] This complex showed poor activity (only 5% conversion) in the ROP of ε-caprolactone (CL) in toluene at 60 °C for a [CL]:[Mg] ratio of 200:1.

Although the solution-state ROP experiments of the previously reported magnesium-bis(phenolate) complexes were not encouraging, it turned out that under the right conditions compounds **4.1** and **4.2** exhibited good activity. *Rac*-lactide could be polymerized by **4.1** and **4.2** in the bulk at temperatures above 125 °C and, and, in toluene solutions at 90 °C.

4.2.2 Ring opening polymerization in the melt

Melt phase ROP has attracted much interest recently as it offers a viable technique for industry.[60] There are examples for lactide ROP in the melt catalyzed by a variety of metal complexes, such as sulphonamide-supported aluminum complexes,[61] Ni(II) and Ni(II)-Sm(III) salen complexes,[62] aluminum-salen[63] and salen-like[64] complexes, zirconium and hafnium amine tris(phenolate) alkoxides,[65] but solvent-free lactide ROP with an earth-abundant, non-toxic metal initiator at low catalyst loading still

remains a challenge. Magnesium complexes **4.1** and **4.2** were assessed for their capabilities toward the ROP of *rac*-lactide under industrially relevant melt (solvent-free) conditions above 125 °C. The polymerization results are summarized in Table 4-1. Polymerization occurred with or without a co-initiator (benzyl alcohol, BnOH). In general, the polymer molecular weights observed by gel permeation chromatography were lower than expected, likely due to mass transfer issues in the melt. Also, lower molecular weight polymers were obtained when BnOH was used, but the dispersity values were lower indicating a more controlled polymerization. Higher molecular weight and monodisperse polymers were obtained when catalyst loading is decreased. Interestingly, the physical appearance of the polymers was found to depend on whether BnOH was used (which gave thin films) or not (which gave crystalline white solids). The mechanical properties of the polymers are discussed below. Complex **4.1** showed slightly better conversions than complex **4.2**, so **4.1** was chosen to carry out further reactions.

Table 4-1 Solvent-free (melt) *rac*-lactide polymerization by complexes **4.1** and **4.2**

Entry[a]	Complex	Time (min)	T (°C)	[Mg]:[rac-LA] :[BnOH]	Conv. (%)[b]	Activity[c] ($kg \cdot mol^{-1} \cdot h^{-1}$)	M_n[d] (calc'd) (g/mol)	M_n[e] (GPC) (g/mol)	Đ (M_w/M_n)
1	**4.1**	100	125	1:100:0	99	8.56	14 400	20 300	2.74
2	**4.1**	100	125	1:100:1	99	8.56	14 400	11 300	1.77
3	**4.1**	100	125	1:500:0	99	42.8	72 000	36 200	3.01
4	**4.1**	100	125	1:500:1	98	42.4	70 600	9 700	2.01
5	**4.2**	100	125	1:100:0	100	8.65	14 400	16 500	2.40
6	**4.2**	100	125	1:100:1	82	6.23	14 400	7 200	1.54
7	**4.2**	100	125	1:500:0	72	31.1	51 800	30 600	2.72
8	**4.2**	100	125	1:500:1	98	42.4	70 600	2 400	1.25
9	**4.1**	100	125	1:1000:0	93	80.4	133 900	44 900	1.25
10	**4.1**	100	125	1:1000:1	93	80.4	133 900	42 900	1.24
11	**4.1**	180	125	1:1000:0	93	44.7	133 900	74 300	1.05
12	**4.1**	180	125	1:1000:1	89	42.8	128 200	50 100	1.24
13	**4.1**	100	150	1:1000:0	92	79.6	132 500	35 200	1.22
14	**4.1**	100	150	1:1000:1	96	83.0	138 200	70 290	1.08
15	**4.1**	180	150	1:2500:0	16	19.2	57 600	ND[f]	ND

[a]All polymerization reactions were carried out in neat *rac*-lactide (0.5 – 0.6 g), [b]Conversion determined by ^{1}H NMR. [c]Calculated as mass of lactide converted in grams/(mol of Mg × time in h) [d]Calculated from ([LA]/[Mg]) × % conv. × 144.13 $g \cdot mol^{-1}$] [e]Molecular weights ($g \cdot mol^{-1}$) of entries 1 to 8 determined by gel permeation chromatography (GPC) in $CHCl_3$ calibrated against polystyrene standards using the Mark-Houwink correction of 0.58.[66] GPC of entries 9 to 15 were conducted in THF by triple detection. See experimental for full details. [f]ND = Not Determined, yield too low

When the catalyst loading was lowered to 0.1 mol% (entries 9 − 14), lactide conversion remained high translating to an increase in activity with good control as shown by the narrow dispersities of the polymers obtained. Polymerization remained controlled even in the absence of BnOH co-initiator. Highest molecular weights were obtained when the polymerization was run for 180 min (entry 11) or when the temperature was raised to 150 °C (entry 14). Activity was still observed upon further decreasing the catalyst loading to 0.04 mol% at this temperature, but with low conversion (16%) (entry 15).

Kinetic studies performed with **4.1** under conditions given in Table 4-1, entry 3 revealed that the polymerization reached completion in 60 minutes (see Table 4-2). Molecular weights increase with increasing time and conversion and the dispersity values are generally low (1.14 – 1.40). The difference in conversion between entry 5 and 6 is not significant, but the difference in molecular weight is in accordance with the phenomenon observed earlier in Table 4-1, entry 11 that it is favourable to leave the polymerization to occur for longer time to achieve higher molecular weight polymers.

Table 4-2 Time dependence of melt-phase *rac*-lactide polymerization by **4.1**.

Entry[a]	Time (min)	Conv'n (%)[b]	M_n[c] (calc.d)	M_n[d] (GPC)	Đ (M_w/M_n)
1	10	7	5 000	5 400	1.40
2	20	36	25 900	16 600	1.22
3	30	78	56 000	18 100	1.34
4	40	91	65 500	25 100	1.37
5	50	93	67 000	31 400	1.32
6	60	96	69 100	55 100	1.14

[a]All polymerization reactions were carried out in neat *rac*-lactide (0.5 g), 125 °C with [**4.1**]:[LA] = 1:500. [b]Determined by ^{1}H NMR. [c]Calculated from ([LA]/[Mg]) × % conv. × 144.13 g·mol^{-1}) [d]Molecular weights (g·mol^{-1}) determined by triple detection gel permeation chromatography (GPC) in tetrahydrofuran using a dn/dc value of 0.049 mL/g.

The conversion vs. time plot (Figure G.1 in Appendix G) shows that polymerization starts once a homogenous melt is achieved (after 5 minutes at 125 °C) and the rate of conversion remains almost linear for the next 10 min and then accelerates for 5 min before returning to a constant rate. The discontinuity in conversion rate implies an induction period, which could be a result of dimer dissociation in order to form the active species. Solution polymerization kinetics studies (see below) are consistent with this theory. The MALDI-TOF mass spectra of the polymers obtained in the melt in the absence of BnOH showed the presence of both cyclic poly(*rac*-lactide) and linear chains terminated with –OH and carboxylic acid end groups (Figure B.12 and B.13 in Appendix B).

4.2.3 Mechanical properties of the polymers obtained under melt conditions

Polymerizations were performed on a larger scale using 1.0 g (instead of 0.5 g) of *rac*-lactide according to the conditions in entries 3 and 4 of Table 4-1 to investigate the correlation between conversion and isolated yield. The scaled-up reactions improved the recovery of the clean polylactide as determined by ^{1}H NMR. The physical appearance of the polymers obtained with and without added benzyl alcohol is significantly different as a result of the difference in polymer molecular weights obtained (Figure G.2 in Appendix G). Without BnOH, the polymer is obtained as a thin film whereas in the presence of alcohol a crystalline polymer results. Differential Scanning Calorimetry (DSC) and Thermogravimetric Analysis (TGA) were performed on these samples and revealed very similar thermal properties. The midpoint of the glass transition temperature taken from the third heating curve was 52.59 °C for the polymer obtained from entry 3 and 50.86 °C for entry 4, which is expected given the polymer's much lower observed M_n. TGA conducted with a ramp rate of 10 °C/min showed the decomposition temperature of the polymer obtained in the absence of BnOH was 354.5 °C and slightly higher (356.7 °C) for the polymer obtained in presence of BnOH. Slower rates of 5 °C/min resulted in slightly lower decomposition temperatures for both the polymers obtained with BnOH (onset at 340 °C, end at 375 °C) and without BnOH (onset at 344 °C, end at 367 °C (Figures H.1 – H.3 in Appendix H). These decomposition temperatures are higher than expected,[67] but they are similar to carboxylic acid terminated *branched* polymers reported by S. H. Kim and co-workers.[68] It should be noted that the polymers used for

thermal analysis were highly purified by precipitation, centrifugation, decanting of solvents, washing with cold methanol and drying by vacuum oven overnight at 40 °C.

Regarding polymer tacticity, the solvent-free (melt) ROP of *rac*-lactide using **4.1** gives an essentially atactic microstructure of poly(*rac*-lactide). This is not surprising given the achiral ligands used in compounds **4.1** and **4.2** and the poor polymer M_n control. A representative $^1H\{^1H\}$ NMR spectrum of the methine resonances of poly(*rac*-lactide) is given in Figure C4 in Appendix C. Highly isotactic polylactide stereopolymers can be obtained solvent-free at 130 °C using salen aluminum alkoxides at a monomer/initiator molar ratio of 200, but the reaction rates were very slow (95% conversion after 2 days).[69]

4.2.4 Ring opening polymerization in solution

Polymerization at room temperature did not occur in either CH_2Cl_2 or THF with complexes **4.1** and **4.2**. However, upon heating to 90 °C with 1 equivalent of isopropyl alcohol (*i*PrOH) as co-initiator, complex **4.2** exhibited fast propagation in toluene achieving 98% conversion in 12 minutes (Table 4-3, entry 1 and Figure 4.2). Use of *i*PrOH accelerates the polymerization activity compared to using **4.2** alone, but gives lower than expected polymer molecular weights, likely resulting from transesterification. Increasing the amount of *i*PrOH as co-initiator to 10 equivalents with respect to **4.2** resulted in faster reaction rate but much lower molecular weight and narrower dispersity (entry 2). The plot of conversion vs. time (Figure 4.2) indicates an induction period of approximately 7 minutes before the onset of the expected conversion curve. This non-

linearity is apparent when attempting to model the data using a first order kinetics plot over the whole reaction time (Figure G.3 in Appendix G). These observations can be explained if one considers the dimeric form of **4.2** in toluene as being inactive to ROP of *rac*-lactide. Hence, activation of the complex is achieved in the presence of co-initiator, possibly via formation of monomeric alcohol adducts. Once an active species is obtained, ROP proceeds quickly at 90 °C, thus explaining the rapid increase in conversion after 7 minutes and effectively complete consumption of monomer after 12 minutes. This is consistent with the activity vs. *t* plot (Figure G.4 in Appendix G), which shows the highest activity was observed between 9 and 15 min. NMR spectra following the reaction profile are given in Figure C.5 in Appendix C.

The influence of the co-initiator on polymerizations in toluene was investigated. The polymerization without a co-initiator (Table 4-3, entry 3) proceeded very slowly and any conversion of lactide was only observed after 30 min in toluene at 90 °C, which is consistent with a slow initiation period. In the presence of BnOH, however, the reaction proceeded very quickly and achieved 98% conversion within 6 minutes (Table 4-3, entry 4). The polymerization demonstrates first order reaction profiles with respect to [LA] in either the presence or absence of BnOH (Figure 4-3 and Figure G.5 in Appendix G). The observed rate constant, k_{obs}, in the presence of BnOH was 0.828 min^{-1} whereas in the absence of BnOH was 9.87×10^{-2} min^{-1}. When the concentration of BnOH was doubled (Table 4-3, entry 5), the molecular weight of the polymer decreased by half, which suggests a well-behaved *immortal* ROP with rapid, reversible chain transfer between growing PLA fragments and dormant hydroxyl-terminated polylactide chains.[70,71]

Table 4-3 Polymerization of *rac*-lactide by **4.2** in toluene.

Entry[a]	[Mg]:[LA]:[ROH]	Time (min)	Conv'n (%)	M_n[c] (calc.d)	M_n[d] (GPC)	Đ (M_w/M_n)
1	1:100:1 (*i*PrOH)	30	99	14 300	5 700	1.70
2	1:100:10 (*i*PrOH)	3	99	1 400	480	1.42
3	1:100:0	210	100	14 400	46 000	1.26
4	1:100:1 (BnOH)	12	98	14 100	13 900	1.07
5	1:100:2 (BnOH)	7	97	7 200	7 100	1.02

[a]All polymerization reactions were carried out in toluene (10 mL) at 90 °C. [b]Determined by ^{1}H NMR. [c]Calculated from ([LA]/[Mg]/[ROH]) × % conv. × 144.13 g·mol^{-1}) [d]Molecular weights (g·mol^{-1}) determined by gel permeation chromatography (GPC) in $CHCl_3$ calibrated against polystyrene standards using the Mark-Houwink correction of 0.58.[66]

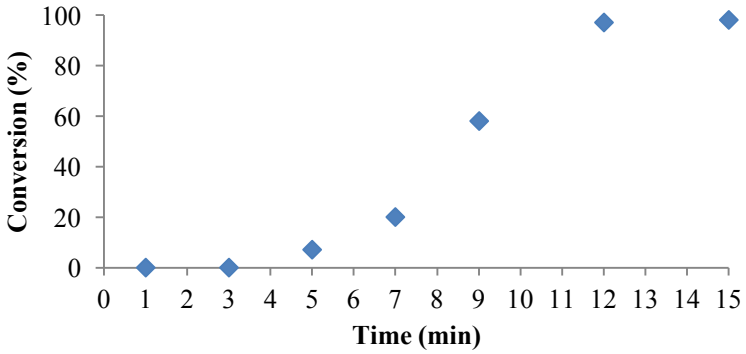

Figure 4.2 Conversion (%) vs. time for the ROP of *rac*-LA initiated by **4.2** under the conditions in Table 4-3, entry 1.

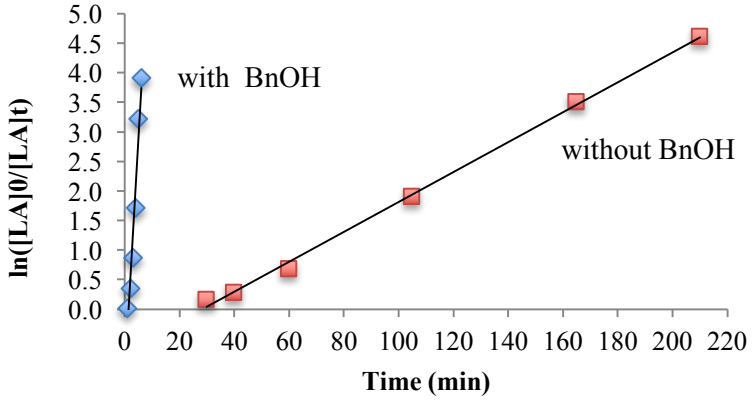

Figure 4.3 Plot of $\ln[LA]_0/[LA]_t$ vs. t, $[LA]_0/[Mg]_0 = 100$, in toluene at 90 °C according to the conditions in Table 4-3, entries 3 and 4.

4.2.5 Mechanistic proposal

Without addition of exogenous alcohol, the ROP of LA is slower in solution than when the alcohol co-initiator is present. Initiation by nucleophilic attack of the phenolate ligand on the monomer has been observed in related lithium-phenolate complexes.[11,45,70] In melt polymerization, however, there is no significant loss of control of the polymerization when conducted in the absence of alcohol co-initiator. The observation in the MALDI-TOF mass spectrum of cyclic polylactide alongside acyclic polymer possessing carboxylic acid and hydroxyl end groups (resulting from hydrolytic quenching of polymerization with acidified methanol) is consistent with phenolate-initiated ROP (Scheme 4-2).

The mechanism of polymerization and the role of the alcohol co-initiator require closer examination, particularly since the majority of binary systems (employing a Lewis acidic metal site and an added alcohol as initiators) hypothesize coordination-insertion mechanisms. Carpentier, Sarazin and co-workers suggest that activated monomer

mechanisms should not be excluded and have performed elegant studies of alkali aminoether-phenolate complexes that provide strong evidence that this mechanism at play under living or immortal ROP conditions of L-LA.[70]

Preliminary stoichiometric studies by ^{1}H NMR spectroscopy of reactions involving complex **4.2**, *rac*-LA and BnOH were conducted in toluene-d_8 at 363 K, i.e. the conditions employed in solution ROP catalysis shown in Table 4-3. The reaction of a 1:1 ratio (per Mg centre) of **4.2** and BnOH was followed by ^{1}H NMR at 363 K. After 10 minutes at this temperature, in addition to those of complex **4.2** alone, new resonances were observed consistent with monomeric Mg compounds (see Figure C.6 in Appendix C for ^{1}H NMR spectra). It is not unequivocal whether the BnOH is coordinated to the metal centre since the benzyl methylene peak is slightly broadened at this temperature, possibly from an exchange process as suggested by the continued presence of dimer in the spectrum. Also, a very small peak at 9.19 ppm could be observed upon expansion of the region of the spectrum, suggesting that the presence of protonated ligand, H_2[**L3**] is negligible.

The reaction of a 1:1:1 mixture of *rac*-LA, **4.2** and BnOH was monitored under the same conditions. Within 10 minutes at 363 K the product of lactide ring-opening, benzyl-2-((2-hydroxypropanoyl)oxy)propanoate or its deprotonated alkoxide form, was observed. It is possible that the ring-opened lactide remains coordinated to the Mg site, since a phenolic –OH resonance is observable at 9.22 ppm indicating protonation of a phenolate oxygen. The proposed mechanism is shown in Scheme 4-3. Based on these

observations, an activated monomer mechanism may be occurring, but further investigation is needed.

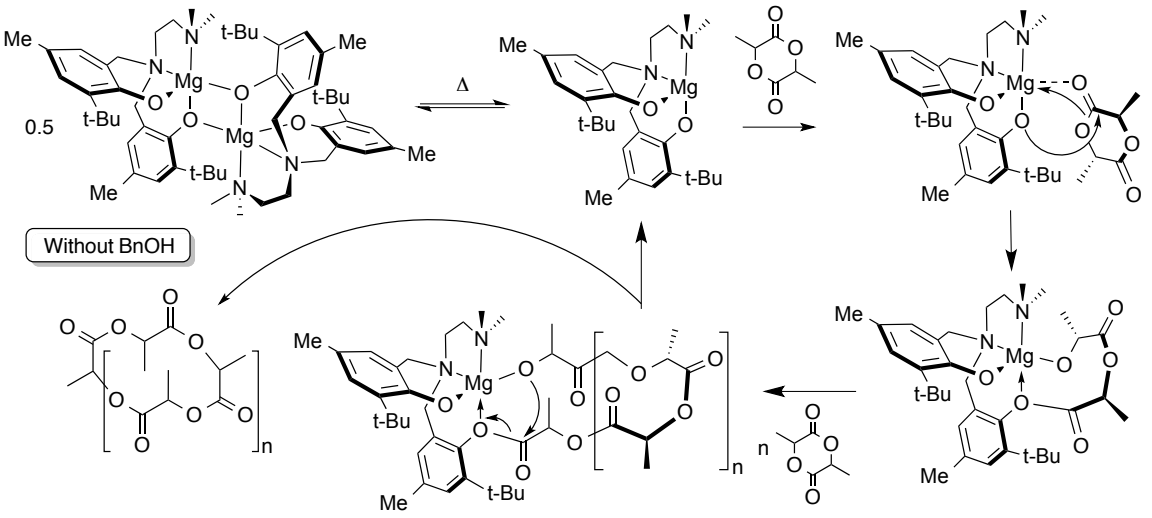

Scheme 4-2 Proposed mechanism for ROP of LA by **4.2** without added alcohol co-initiator. Generation of cyclic polymer is shown, but hydroxyl or carboxylic acid end groups may be obtained by protonolysis.

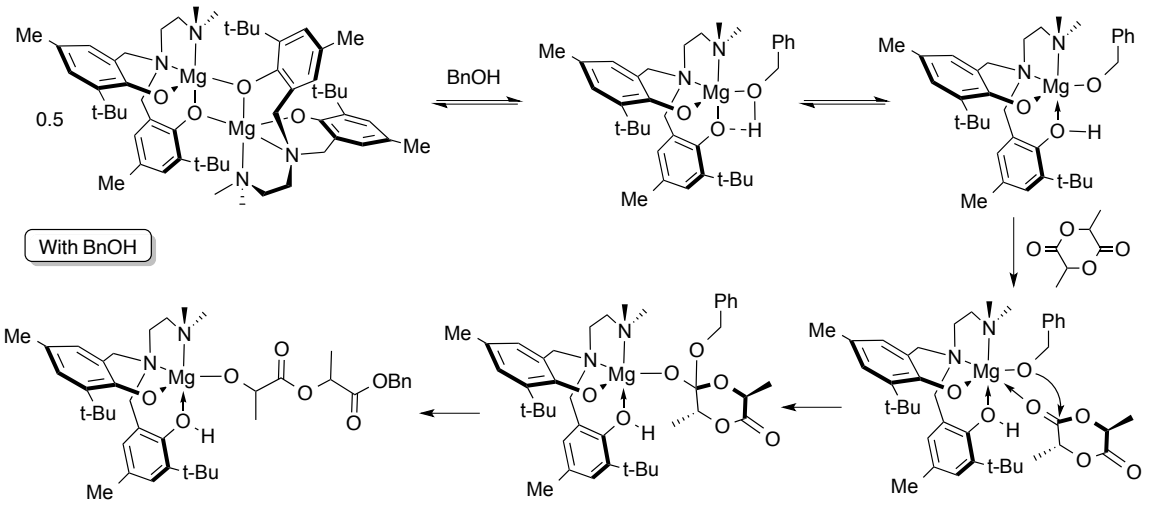

Scheme 4-3 Proposed mechanism for ROP of LA by **4.2** with benzyl alcohol co-initiator.

4.3 Conclusions

Magnesium amine-bis(phenolate) compounds **4.1** and **4.2** showed catalytic activity for the ROP of *rac*-lactide both in toluene solutions and solvent-free (melt) to give atactic poly(*rac*-lactide). Kinetic studies showed that conversion of *rac*-lactide is essentially complete within 60 minutes in the melt at 125 °C, although the resulting polymers exhibit broad dispersities. Solution polymerization studies in toluene at 90 °C indicate long initiation periods in the absence of an alcohol co-initiator, but rapid initiation when a suitable co-initiator is used. Complex **4.2** proved to be an efficient initiator in solution at 90 °C with a [LA]:[Mg] ratio of 100:1 regardless of whether a co-initiator was used or not. Without a co-initiator an initiation period of ~30 min was observed, after which time the propagation showed a slow first order reaction profile with respect to *rac*-lactide concentration and effectively complete conversion within 210 minutes. The polymerization was accelerated significantly by the addition of a co-initiator, either *i*PrOH or BnOH. The highest activity was observed for [LA]:[Mg]:[BnOH] ratios of 100:1:1 at 90 °C in toluene giving 177.3 kg of *rac*-PLA per mol Mg per h (k_{obs} = 1.38 × 10^{-2} s^{-1}). Preliminary mechanistic studies support an activated monomer pathway, but more detailed studies are needed.

4.4 Experimental

4.4.1 General experimental conditions

Unless otherwise stated, all manipulations were performed under an atmosphere of dry, oxygen-free nitrogen by means of standard Schlenk techniques or using an

MBraun Labmaster DP glove box. Anhydrous THF was distilled from sodium benzophenone ketyl under nitrogen. Isopropyl alcohol was dried over calcium oxide, then distilled under nitrogen. Toluene was purified by an MBraun Manual Solvent Purification System. Reagents were purchased either from Aldrich or Alfa Aesar and used without further purification. *Rac*-lactide was purchased from Aldrich or Alfa Aesar and dried over sodium sulphate in THF, recrystallized and stored under an inert atmosphere prior to use. Benzyl alcohol was purchased from Alfa Aesar and dried over activated 4 Å molecular sieves, distilled under reduced pressure and stored under nitrogen in an ampule prior to use.

4.4.2 Instrumentation

MALDI-TOF MS was performed using an Applied Biosystems 4800 MALDI TOF/TOF Analyzer equipped with a reflectron, delayed ion extraction and high performance nitrogen laser (200 Hz operating at 355 nm). Samples were prepared in the glove box and sealed under nitrogen in a Ziploc© bag for transport to the instrument. Anthracene was used as the matrix for compounds **4.1** and **4.2** and 2,5-dihydroxybenzoic acid (DHBA) was used as the matrix for the polymers. The matrix was dissolved in THF at a concentration of 10 mg/mL. Polymer was dissolved in THF at approximately 1 mg/mL. The matrix and polymer solutions were mixed together at ratios of 5 to 1, 4 to 1 or 3 to 1; 1 μL of this was spotted on the MALDI plate and left to dry. Images of mass spectra were prepared using mMass™ software (www.mmass.org).

GPC analysis was performed either in $CHCl_3$ on a Viscotek VE 2001 GPCMax at 35 °C equipped with a Viscotek VE 3580 Refractive Index Detector or in THF at 25 °C on a Wyatt Triple Detection (triple angle light scattering, viscometry and refractive index) system with Agilent 2600 series sample and solvent handling. The Viscotek system used two Phenogel 5μ Linear Mixed Bed 300 × 4.60 mm columns whereas the Wyatt system used two Phenogel 10^3 Å 300 × 4.60 mm columns. Samples were prepared at a concentration of 2 mg/mL in $CHCl_3$ and left to equilibrate for ~2 h. The samples were filtered through syringe filters before analysis and eluted with HPLC grade solvents at flow rates of 0.30 mL/min with 100 μL injection volumes. For conventional calibration, six polystyrene standards (Viscotek) were used in making the calibration curve, bracketing molecular ranges from 1050 to 400 000 Da. A correction factor of 0.58 was used to calculate the M_n value.[66]

NMR spectra were recorded at 300 MHz for ^1H and 75.5 MHz for ^{13}C or at 500 MHz for ^1H NMR kinetic studies. $CDCl_3$, C_6D_6, DMSO-d_6 were purchased from Cambridge Isotope Laboratories and pyridine-d_5 from Aldrich. All deuterated solvents except for DMSO-d_6 used in the analysis of the magnesium complexes were dried over calcium hydride ($CDCl_3$ and pyridine-d_5) or sodium/potassium alloy (C_6D_6), vacuum transferred and stored under nitrogen in ampules fitted with Teflon valves. Elemental analyses were performed at Guelph Chemical Laboratories, Guelph, Ontario, Canada.

Thermogravimetric analysis (TGA) was performed with a TA Instruments Q500. Samples (4 – 15 mg) were loaded onto a platinum pan and subjected to a dynamic high-resolution scan, with an initial heating rate of 5 or 10 °C/min. Each sample was heated

from room temperature to 600 °C. Glass transition (T_g) temperatures were measured using a Mettler Toledo DSC 1 S**TA**R^e System equipped with a Julabo FT 100 immersion cooling system, using R1150 refrigerant in an EtOH bath with a working range of −100 to +20 °C. Samples (~5 mg) were weighed into 40 μL aluminum pans and subjected to three heating cycles. The first heating cycle consisted of heating from 0 to 100 °C at a rate of 10 °C/min, held for 2 min at 100 °C and then cooled back to 0 °C at 10 °C/min. The sample was held at this temperature for 2 min and subjected to a two heating cycles from 0 to 190 °C at a rate of 10 °C/min.

4.4.3 X-ray crystallography

Crystallographic and structure refinement data are given in Table A2. A single crystal of **4.2** was mounted on a glass fibre using Paratone-N oil. All measurements were made on a Rigaku Saturn CCD area detector with graphite monochromated Mo-Kα radiation solved on an AFC8-Saturn 70 single crystal X-ray diffractometer from Rigaku, equipped with an X-stream 2000 low temperature system. Using OLEX2[72], the structure was solved with the ShelXT[73] structure solution program using Direct Methods and refined with the ShelXL[74] refinement package using Least Squares minimisation.

Raw data images from the diffraction experiment were converted from Rigaku format to Bruker format via the program Eclipse (Parsons, Simon. 2010. ECLIPSE – Program for masking high pressure diffraction images and conversion between CCD image formats) for inspection, integration and scaling using APEX2 software (Bruker (2007). APEX2. Bruker AXS Inc., Madison, Wisconsin, USA.) The program Cell Now

(Sheldrick, G. M. (2004). CELL NOW. University of Göttingen, Germany) was used to search for twin domains and returned four twin orientations. Upon inspection of the raw data frames it was determined that these four orientations were not twin domains but rather represented four unique orientations of the crystal for each run of the data collection. This is consistent with reports that the diffractometer used for data collection experienced slippage of the χ axis during data collections, resulting in shifting crystal orientation relative to the goniometer zeroes. Two of the orientations were similar enough that those two runs (Runs 1 and 3) could be integrated using the same orientation matrix. The other two runs were integrated separately, each with its own orientation matrix. After integration, the refined unit cell used for Runs 1 and 3 was used as the true unit cell. All four runs were scaled and corrected for absorption together, using the program SADABS (Bruker (2001). SADABS. Bruker AXS Inc., Madison, Wisconsin, USA) to produce a merged, scaled HKLF file which was used for structure solution.

H-atoms were introduced in calculated positions, and refined on a riding model. All non-hydrogen atoms were refined anisotropically. One of the *t*-butyl groups was disordered with two orientations. These were refined as PARTs witth PART 1 = C26-C28 (and corresponding H-atoms) with occupancy = 0.508(8); PART 2 = C29-C31 (and corresponding H-atoms) with occupancy = 0.492(8). Distance and anisotropic restrains (RIGU and SADI) were applied to this group.

The OLEX2[72] solvent masking routine was applied to recover 56.6 electrons per unit cell in two voids. An area of disperse electron density appeared to be present prior to the solvent masking, however, a good point atom model could not be achieved for this,

and the content was not accounted for in the formula (or resulting intensive properties). The application of the solvent mask gave a good improvement in the data statistics and allowed for a full anisotropic refinement of the framework structure.

4.4.4 Synthesis of compounds

H_2**[L1]**: The synthesis and characterization of this compound can be found in Chapter 2, Section 2.5.3.

H_2**[L3]**: N,N-Dimethylethylenediamine (5.45 g, 61.8 mmol) was slowly added to a vigorously stirred mixture of 2-tert-butyl-4-methylphenol (20.23 g, 123 mmol) and formaldehyde (10.0 mL of a 37% aqueous solution, 0.123 mol) in deionized water (100 mL) in a round bottom flask equipped with a magnetic stir bar. The mixture was heated to reflux and stirred for approximately 24 hours, at which point a large amount of orange-brown solid had formed. The mixture was decanted and the remaining solid residue was washed with ice-cold methanol to yield a white powder. Recrystallization from chloroform produced analytically pure product (yield: 23.8 g, 88%). Spectroscopic characterization was consistent with that previously reported.[54]

4.1: 2.46 g (5.00 mmol) of H_2[**L1**] was dissolved in 100 mL of toluene and cooled to – 78 °C. To this solution was added 5.0 mmol of $MgBu_2$ (5.0 mL of a 1.0 M solution in heptane) via syringe. The solution was warmed to room temperature and stirred overnight. Volatiles were removed *in vacuo* to yield a pale yellow powder. Yield = 2.42 g (94%). Anal. calc'd for $C_{30}H_{38}MgN_2O_4$: C 69.97, H 7.44, N 5.44. Found: C 69.26, H 7.17, N 5.13. The lower than expected %C is attributed to a 5 – 10%

contamination by MgO or $Mg(OH)_2$ (e.g. anal. calc'd for $C_{30}H_{38}MgN_2O_4(MgO_2H_2)_{0.05}$: C 69.58, H 7.42, N 5.41. ^{1}H NMR (300 MHz, 298 K, DMSO-d_6, δ): 8.49 (d, $^3J_{HH}$ = 4.43 Hz, Py: NC*H*, 1H); 7.68 (td, $^3J_{HH}$ = 7.62 Hz, $^4J_{HH}$ = 1.51 Hz, Py: NCHC*H*, 1H); 7.21 (dd, coupling constants could not be determined because of the overlapping residual toluene peaks, Py: NCHCHC*H*, 1H); 7.06 (d, $^3J_{HH}$= 7.8 Hz, Py: NCC*H*, 1H); 6.44 (d, $^4J_{HH}$ = 3.23 Hz, Ar: C*H*CCH$_2$N, 2H); 6.38 (d, $^4J_{HH}$ = 3.23 Hz, Ar: C*H*CCMe$_3$, 2H); 3.76 (d, $^3J_{HH}$ = 11.65 Hz, NC*H*$_2$Ar, 2H); 3.58 (s, NC*H*$_2$Py, 2H); 3.55 (s. OC*H*$_3$, 6H); 3.15 (d, $^3J_{HH}$ = 11.72 Hz, NC*H*$_2$Ar, 2H); 1.29 (s, C(C*H*$_3$)$_3$, 18H). ^{13}C{^{1}H} NMR (75.5 MHz, 298K, DMSO-d_6, δ): 160.71 (*C*OMg); 158.04 (*C*OMe); 148.60 (Ar: *C*CH$_2$N); 145.35 (Py: NC*C*H); 138.46 (Py: N*C*); 136.66 (Py: NCCH*C*H); 130.38 (Py: NCH*C*H); 122.69 (Py: N*C*H); 122.03 (Ar: *C*CMe$_3$); 113.46 (Ar: *C*HCCH$_2$N); 112.94 (Ar: *C*HCCMe$_3$); 60.68 (*C*H$_2$Py); 56.10 (*C*H$_2$Ar); 55.69 (O*Me*); 34.54 (*C*Me$_3$); 29.34 (C*Me*$_3$). MS (MALDI-TOF) *m/z* (%, ion): 514.26 (58, $[M]^+$); 1028.50 (100, $[M]_2^+$).

4.2: 2.21 g (5.0 mmol) of H_2[**L3**] was dissolved in 70 mL of toluene and cooled to – 78 °C. To this solution was added 5.0 mmol of $MgBu_2$ (5.0 mL of a 1.0 M solution in heptane) via syringe, forming a bright yellow solution. The solution was warmed to room temperature and stirred overnight, upon which a large amount of white precipitate formed within a colourless solution. Volatiles were removed *in vacuo*, yielding an analytically pure white powder. Yield = 2.29 g (99%). Recrystallization from toluene at – 35 °C afforded colourless crystals. Anal. calc'd for $C_{34}H_{54}MgN_2O_2$: C 72.64, H 9.14, N 6.05. Found: C 72.38, H 9.09, N 6.22. ^{1}H NMR (300 MHz, 298 K, C_6D_6, δ): 7.29 (m, Ar, 4H); 6.80 (d, $^4J_{HH}$ = 2.35 Hz, Ar, 2H); 6.69 (d, $^4J_{HH}$ = 2.30, Ar, 2H); 4.84 (d, $^2J_{HH}$ =

12.01 Hz, Ar-C*H*(H)-N, 2H); 4.63 (d, $^{2}J_{HH}$ = 12.41 Hz, Ar-C*H*(H)-N, 2H); 2.97 (d, $^{2}J_{HH}$ = 12.38 Hz, Ar-C*H*(H)-N, 2H); 2.63 (d, $^{2}J_{HH}$ = 12.06 Hz, Ar-C*H*(H)-N, 2H); 2.00 – 2.70 (br, *CH*$_2$NMe$_2$, 4H); 2.35 (s, N*Me*$_2$, 6H); 2.31 (s, N*Me*$_2$, 6H); 1.05 – 1.70 (br, *CH*$_2$CH$_2$NMe$_2$, 4H); 1.69 (s, C*Me*$_3$, 18H); 1.65 (s, Ar*Me*, 6H); 1.59 (s, Ar*Me*, 6H); 1.29 (s, CMe$_3$, 18H). ^{13}C{^{1}H} NMR (75.5 MHz, 298K, C_6D_6, δ): 164.59 (*C*-O); 160.09 (*C*-O); 137.80, 136.95, 130.13, 129.61, 128.92, 128.06, 128.74, 125.55, 123.01, 119.89 (All Ar); 65.49 (Ar*C*H$_2$); 64.48 (Ar*C*H$_2$); 60.54 (*C*H$_2$CH$_2$NMe$_2$); 48.69 (*C*H$_2$NMe$_2$); 47.55 (N*Me*$_2$); 47.42 (N*Me*$_2$); 35.12 (*C*Me$_3$); 34.77 (*C*Me$_3$); 32.82 (C*Me*$_3$); 30.34 (C*Me*$_3$); 20.98 (Ar*Me*); 20.90 (Ar*Me*). ^{1}H NMR (300 MHz, 298 K, pyridine-d_5, δ): 7.35 (d, $^{4}J_{HH}$ = 2.45 Hz, Ar, 2H); 6.92 (d, $^{4}J_{HH}$ = 2.51 Hz, Ar, 2H); 4.04 (d, $^{2}J_{HH}$ = 12.49, Ar-C*H*(H)-N, 2H); 3.11 (d, $^{2}J_{HH}$ = 12.51 Hz, Ar-C*H*(H)-N, 2H); 2.75 (br, C*H*$_2$NMe$_2$, 2H); 2.40 (s, N*Me*$_2$, 6H); 2.23 (br, C*H*$_2$CH$_2$NMe$_2$, 2H); 1.97 (s, ArMe, 6H); 1.75 (s, C*Me*$_3$, 18H). ^{13}C{^{1}H} NMR (75.5 MHz, 298 K, pyridine-d_5, δ): 167.80 (*C*-O); 138.71, 132.41, 130.65, 130.08, 126.64 (All Ar); 66.88 (Ar*C*H$_2$); 61.54 (*C*H$_2$CH$_2$NMe$_2$); 51.27 (*C*H$_2$NMe$_2$); 49.51 (N*Me*$_2$); 37.24 (*C*Me$_3$); 32.43 (C*Me*$_3$); 23.05 (C*Me*$_3$). MS (MALDI-TOF) *m/z* (%, ion): 462.25 (100, $[M]^+$); 924.52 (3, $[M]_2^+$).

4.4.5 Polymerization procedure

Melt polymerization: A representative polymerization with a 500:1 [*rac*-lactide]:[**1**] ratio was carried out with 500 mg (3.47 mmol) *rac*-lactide and 3.57 mg (6.93 × 10^{-3} mmol) of complex **4.1** weighed into a 10 mL scintillation vial equipped with a small stir bar in the glove box. The closed vial was taken out of the glove box and placed

into an aluminum block vial holder, which was pre-heated on a hotplate to 125 °C. A typical polymerization was run for 100 minutes. The vial was then placed in an ice bath to halt the reaction and solidify the polymer. The solids were dissolved in dichloromethane or chloroform and the polymer was precipitated with acidified methanol. Centrifugation was applied where needed for better separation of the solids. Solvents were decanted and the white solids (either crystalline or thin film-like) were dried *in vacuo* followed by drying in a vacuum oven at 40 °C overnight.

Solution polymerization: The appropriate amount of complex **4.1** or **4.2** and alcohol (*i*PrOH or BnOH) were placed in an ampule equipped with a PTFE valve. A second ampule was prepared containing a stir bar and the required amount of monomer and toluene (7.50 mL). Both ampules were heated to 90 °C for ~ 30 min, after which time the lactide solution was transferred by cannula to the complex mixture. Timing of the reaction began when all the lactide was transferred. An aliquot of the reaction mixture was taken for ^{1}H NMR analysis at certain time intervals. When the presence of monomer was no longer apparent by ^{1}H NMR, volatiles were removed *in vacuo* and the solid residue was dissolved in CH_2Cl_2 and precipitated using cold methanol. Solvents were decanted and the white solids were dried *in vacuo* followed by drying in a vacuum oven at 40 °C overnight.

4.5 References

1. B. Rieger; A. Kuenkel; G. W. Coates; R. Reichardt; E. Dinjus; T. A. Zevaco; Editors *Synthetic biodegradable polymers. [In: Adv. Polym. Sci., 2012; 245]*; Springer GmbH, 2012.

2. R. T. Martin; L. P. Camargo; S. A. Miller *Green Chem.* **2014**, *16*, 1768-1773.

3. J. M. Becker; A. P. Dove *Green Polymerization Methods: Renewable Starting Materials, Catalysis and Waste Reduction*; 1st ed.; R. T. Mathers, M. A. R. Meier, Eds.; Wiley-VCH: Weinheim, 2011, p 201-220.

4. R. E. Drumright; P. R. Gruber; D. E. Henton *Adv. Mater.* **2000**, *12*, 1841-1846.

5. O. Dechy-Cabaret; B. Martin-Vaca; D. Bourissou *Chem. Rev.* **2004**, *104*, 6147-6176.

6. M. J. Stanford; A. P. Dove *Chem. Soc. Rev.* **2010**, *39*, 486-494.

7. C. A. Wheaton; P. G. Hayes; B. J. Ireland *Dalton Trans.* **2009**, 4832-4846.

8. M. H. Chisholm; Z. P. Zhou *J. Mater. Chem.* **2004**, *14*, 3081-3092.

9. B. J. O'Keefe; M. A. Hillmyer; W. B. Tolman *J. Chem. Soc. Dalton Trans.* **2001**, 2215-2224.

10. O. Wichmann; R. Sillanpää; A. Lehtonen *Coord. Chem. Rev.* **2012**, *256*, 371-392.

11. N. Ikpo; C. Hoffmann; L. N. Dawe; F. M. Kerton *Dalton Trans.* **2012**, *41*, 6651-6660.

12. Y. Huang; Y.-H. Tsai; W.-C. Hung; C.-S. Lin; W. Wang; J.-H. Huang; S. Dutta; C.-C. Lin *Inorg. Chem.* **2010**, *49*, 9416-9425.

13. L. Wang; X. B. Pan; L. H. Yao; N. Tang; J. C. Wu *Eur. J. Inorg. Chem.* **2011**, 632-636.

14. C.-A. Huang; C.-L. Ho; C.-T. Chen *Dalton Trans.* **2008**, 3502-3510.

15. C. A. Huang; C. T. Chen *Dalton Trans.* **2007**, 5561-5566.

16. F. M. Kerton; C. M. Kozak; K. Lüttgen; C. E. Willans; R. J. Webster; A. C. Whitwood *Inorg. Chim. Acta* **2006**, *359*, 2819-2825.

17. B.-T. Ko; C.-C. Lin *J. Am. Chem. Soc.* **2001**, *123*, 7973-7977.

18. W. Clegg; M. G. Davidson; D. V. Graham; G. Griffen; M. D. Jones; A. R. Kennedy; C. T. O'Hara; L. Russo; C. M. Thomson *Dalton Trans.* **2008**, 1295-1301.

19. Z. Janas; T. Nerkowski; E. Kober; L. B. Jerzykiewicz; T. Lis *Dalton Trans.* **2012**, *41*, 442-447.

20. L. E. Breyfogle; C. K. Williams; V. G. Young; M. A. Hillmyer; W. B. Tolman *Dalton Trans.* **2006**, 928-936.

21. J. Ejfler; S. Szafert; K. Mierzwicki; L. B. Jerzykiewicz; P. Sobota *Dalton Trans.* **2008**, 6556-6562.

22. W. C. Hung; C. C. Lin *Inorg. Chem.* **2009**, *48*, 728-734.

23. E. L. Marshall; V. C. Gibson; H. S. Rzepa *J. Am. Chem. Soc.* **2005**, *127*, 6048-6051.

24. Y. Sarazin; V. Poirier; T. Roisnel; J.-F. Carpentier *Eur. J. Inorg. Chem.* **2010**, 3423-3428.

25. A. D. Schofield; M. L. Barros; M. G. Cushion; A. D. Schwarz; P. Mountford *Dalton Trans.* **2009**, 85-96.

26. X. Zhang; T. J. Emge; K. C. Hultzsch *Organometallics* **2010**, *29*, 5871-5877.

27. D. J. Darensbourg; W. Choi; O. Karroonnirun; N. Bhuvanesh *Macromolecules* **2008**, *41*, 3493-3502.

28. H. E. Dyer; S. Huijser; A. D. Schwarz; C. Wang; R. Duchateau; P. Mountford *Dalton Trans.* **2008**, 32-35.

29. A. Amgoune; C. M. Thomas; J.-F. Carpentier *Macromol. Rapid Commun.* **2007**, *28*, 693-697.

30. M. H. Chisholm; J. C. Gallucci; H. H. Zhen; J. C. Huffman *Inorg. Chem.* **2001**, *40*, 5051-5054.

31. C. K. Williams; N. R. Brooks; M. A. Hillmyer; W. B. Tolman *Chem. Commun.* **2002**, 2132-2133.

32. C. K. Williams; L. E. Breyfogle; S. K. Choi; W. Nam; V. G. Young; M. A. Hillmyer; W. B. Tolman *J. Am. Chem. Soc.* **2003**, *125*, 11350-11359.

33. D. J. Doyle; V. C. Gibson; A. J. P. White *Dalton Trans.* **2007**, 358-363.

34. J. D. Farwell; P. B. Hitchcock; M. F. Lappert; G. A. Luinstra; A. V. Protchenko; X.-H. Wei *J. Organomet. Chem.* **2008**, *693*, 1861-1869.

35. G. Labourdette; D. J. Lee; B. O. Patrick; M. B. Ezhova; P. Mehrkhodavandi *Organometallics* **2009**, *28*, 1309-1319.

36. L. Wang; H. Ma *Dalton Trans.* **2010**, *39*, 7897-7910.

37. N. Ikpo; L. N. Saunders; J. L. Walsh; J. M. B. Smith; L. N. Dawe; F. M. Kerton *Eur. J. Inorg. Chem.* **2011**, 5347-5359.

38. V. Poirier; T. Roisnel; J.-F. Carpentier; Y. Sarazin *Dalton Trans.* **2011**, *40*, 523-534.

39. J. Lewinski; P. Horeglad; M. Dranka; I. Justyniak *Inorg. Chem.* **2004**, *43*, 5789-5791.

40. J.-T. Issenhuth; J. Pluvinage; R. Welter; S. Bellemin-Laponnaz; S. Dagorne *Eur. J. Inorg. Chem.* **2009**, 4701-4709.

41. S. Gendler; S. Segal; I. Goldberg; Z. Goldschmidt; M. Kol *Inorg. Chem.* **2006**, *45*, 4783-4790.

42. S. Groysman; E. Sergeeva; I. Goldberg; M. Kol *Inorg. Chem.* **2005**, *44*, 8188-8190.

43. L. M. Broomfield; Y. Sarazin; J. A. Wright; D. L. Hughes; W. Clegg; R. W. Harrington; M. Bochmann *J. Organomet. Chem.* **2007**, *692*, 4603-4611.

44. L. N. Saunders; L. N. Dawe; C. M. Kozak *J. Organomet. Chem.* **2014**, *749*, 34-40.

45. R. K. Dean; A. M. Reckling; H. Chen; L. N. Dawe; C. M. Schneider; C. M. Kozak *Dalton Trans.* **2013**, 3504-3530.

46. R. H. Platel; L. M. Hodgson; C. K. Williams *Polym. Rev.* **2008**, *48*, 11-63.

47. J. H. Khan; F. Schue; G. A. George *Polym. Int.* **2009**, *58*, 296-301.

48. M. R. Kember; C. K. Williams *J. Am. Chem. Soc.* **2012**, *134*, 15676-15679.

49. L. Wang; H. Ma *Macromolecules* **2010**, *43*, 6535-6537.

50. S. Song; H. Ma; Y. Yang *Dalton Trans.* **2013**, *42*, 14200-14211.

51. E. Kober; Z. Janas; T. Nerkowski; L. B. Jerzykiewicz *Dalton Trans.* **2013**, *42*, 10847-10854.

52. M. G. Davidson; M. D. Jones; D. Meng; C. T. O'Hara *Main Group Chem.* **2006**, *5*, 3-12.

53. J. Ejfler; K. Krauzy-Dziedzic; S. Szafert; L. B. Jerzykiewicz; P. Sobota *Eur. J. Inorg. Chem.* **2010**, 3602-3609.

54. Y. Sarazin; R. H. Howard; D. L. Hughes; S. M. Humphrey; M. Bochmann *Dalton Trans.* **2006**, 340-350.

55. F. M. Kerton; S. Holloway; A. Power; R. G. Soper; K. Sheridan; J. M. Lynam; A. C. Whitwood; C. E. Willans *Can. J. Chem.* **2008**, *86*, 435-443.

56. S. Menage; G. Gellon; J.-L. Pierre; D. Zurita; E. Saint-Aman *Bull. Soc. Chim. Fr.* **1997**, *134*, 785-791.

57. S. Heidari; E. Safaei; A. Wojtczak; P. Cotic; A. Kozakiewicz *Polyhedron* **2013**, *55*, 109-116.

58. T. R. Forder; M. F. Mahon; M. G. Davidson; T. Woodman; M. D. Jones *Dalton Trans.* **2014**, *43*, 12095-12099.

59. A. W. Addison; T. N. Rao; J. Reedijk; J. van Rijn; G. C. Verschoor *J. Chem. Soc., Dalton Trans.* **1984**, 1349.

60. A. C. Silvino; D. B. A. T. Martins; A. C. Rodrigues; M. L. Dias *J. Polym. Environ.* **2013**, *21*, 1002-1008.

61. A. D. Schwarz; Z. Chu; P. Mountford *Organometallics* **2010**, *29*, 1246-1260.

62. G. Xiao; B. Yan; R. Ma; W. J. Jin; X. Q. Lu; L. Q. Ding; C. Zeng; L. L. Chen; F. Bao *Polym. Chem.* **2011**, *2*, 659-664.

63. C. Paetz; R. Hagen *Chem. Ing. Tech.* **2014**, *86*, 519-523.

64. M. Bouyahyi; E. Grunova; N. Marquet; E. Kirillov; C. M. Thomas; T. Roisnel; J.-F. Carpentier *Organometallics* **2008**, *27*, 5815-5825.

65. A. J. Chmura; M. G. Davidson; C. J. Frankis; M. D. Jones; M. D. Lunn *Chem. Commun.* **2008**, 1293-1295.

66. J. Baran; A. Duda; A. Kowalski; R. Szymanski; S. Penczek *Macromol. Rapid Commun.* **1997**, *18*, 325-333.

67. K. Jamshidi; S. H. Hyon; Y. Ikada *Polymer* **1988**, *29*, 2229-2234.

68. S.-H. Lee; S. Hyun Kim; Y.-K. Han; Y. H. Kim *J. Polym. Sci. A: Polym. Chem.* **2001**, *39*, 973-985.

69. Z. Zhong; P. J. Dijkstra; J. Feijen *Angew. Chem., Int. Ed.* **2002**, *41*, 4510-4513.

70. Y. Sarazin; S.-C. Rosca; D.-A. Rosca; V. Dorcet; J.-F. Carpentier; F. M. Kerton; C. M. Kozak *Dalton Trans.* **2013**, 9361–9375.

71. N. Ajellal; J.-F. Carpentier; C. Guillaume; S. M. Guillaume; M. Helou; V. Poirier; Y. Sarazin; A. Trifonov *Dalton Trans.* **2010**, *39*, 8363-8376.

72. O. V. Dolomanov; L. J. Bourhis; R. J. Gildea; J. A. K. Howard; H. Puschmann *J. Appl. Crystallogr.* **2009**, *42*, 339-341.

73. G. M. Sheldrick *Acta Crystallogr., Sect. C: Struct. Chem.* **2015**, *71*, 3-8.

74. G. M. Sheldrick *Acta Crystallogr., Sect. A: Found. Crystallogr.* **2008**, *64*, 112-122.

Chapter 5. Lithium, Sodium, Potassium and Calcium Amine-bis(phenolate) Complexes in the Ring-opening Polymerization of *rac*-Lactide

5.1 Introduction

The synthesis of polylactide has been the centre of attention concerning alternative plastics, because it is biodegradable, biocompatible and renewable.[1,2] Its biocompatibility makes it an appealing biomaterial, and so it finds use in biomedical and pharmaceutical applications.[3] Lactide copolymerized with glycolide yields poly(lactic-co-glycolic acid) (PLGA) which has been used as a polymeric matrix for the slow release of drugs[1] and it has also been tested as a polymer base against Staphylococcal α-hemolysin (Hla) toxin.[4] Alkali (Li, Na, K) and alkaline earth metal (Mg, Ca) complexes are ideal candidates for catalysts for ring opening polymerization of lactide as these metals are also biocompatible and do not possess the toxicity concerns of heavy metals if some of the metal remains in the polymer produced. There are several examples of lithium,[5-8] sodium,[9-11] potassium[11-14] and calcium[15-17] complexes in the literature, which were tested mainly in solution for the ring opening polymerization of lactide. In this chapter, the synthesis of new sodium, lithium, potassium and calcium complexes will be discussed and their activity in the ring opening polymerization of *rac*-lactide under melt, microwave assisted melt and solution polymerization conditions.

5.2 Results and discussion

5.2.1 Synthesis and characterization of proligand and the complexes

The tetradentate tripodal amine-bis(phenol) proligand was synthesized *via* a modified Mannich condensation reaction in water.[18] The substituted phenol contained a *tert*-butyl group in the *ortho* position and a methoxy *para* to the hydroxyl group and a pyridyl group as the neutral pendant *N*-donor. The synthesis of H_2[**L1**] was previously reported[19-21] (also see Chapter 2, Section 2.5.3).

H_2[**L1**] was reacted with excess NaH or 2.2 equivalents of ^{n}BuLi in THF to obtain the bimetallic complexes **5.1**·THF and **5.2** (Scheme 5-1). The reaction of H_2[**L1**] with NaH was also performed in toluene giving THF-free **5.1** (Figure C.7 in Appendix C). The reaction in toluene, however, is not preferred because the yield of the reaction proved to be poor (58% vs. 99% in THF) due to the poor solubility of the product in toluene, therefore it was left behind with excess NaH. For extracting the product, THF was still required but the compound thus obtained proved to be THF free. Since the reaction in toluene involves an extra step (dissolution in THF and cannula filtration) and the yield is lower than when **5.1** is synthesized in THF, for the polymerization reactions **5.1**·THF was used (Scheme 5-1).

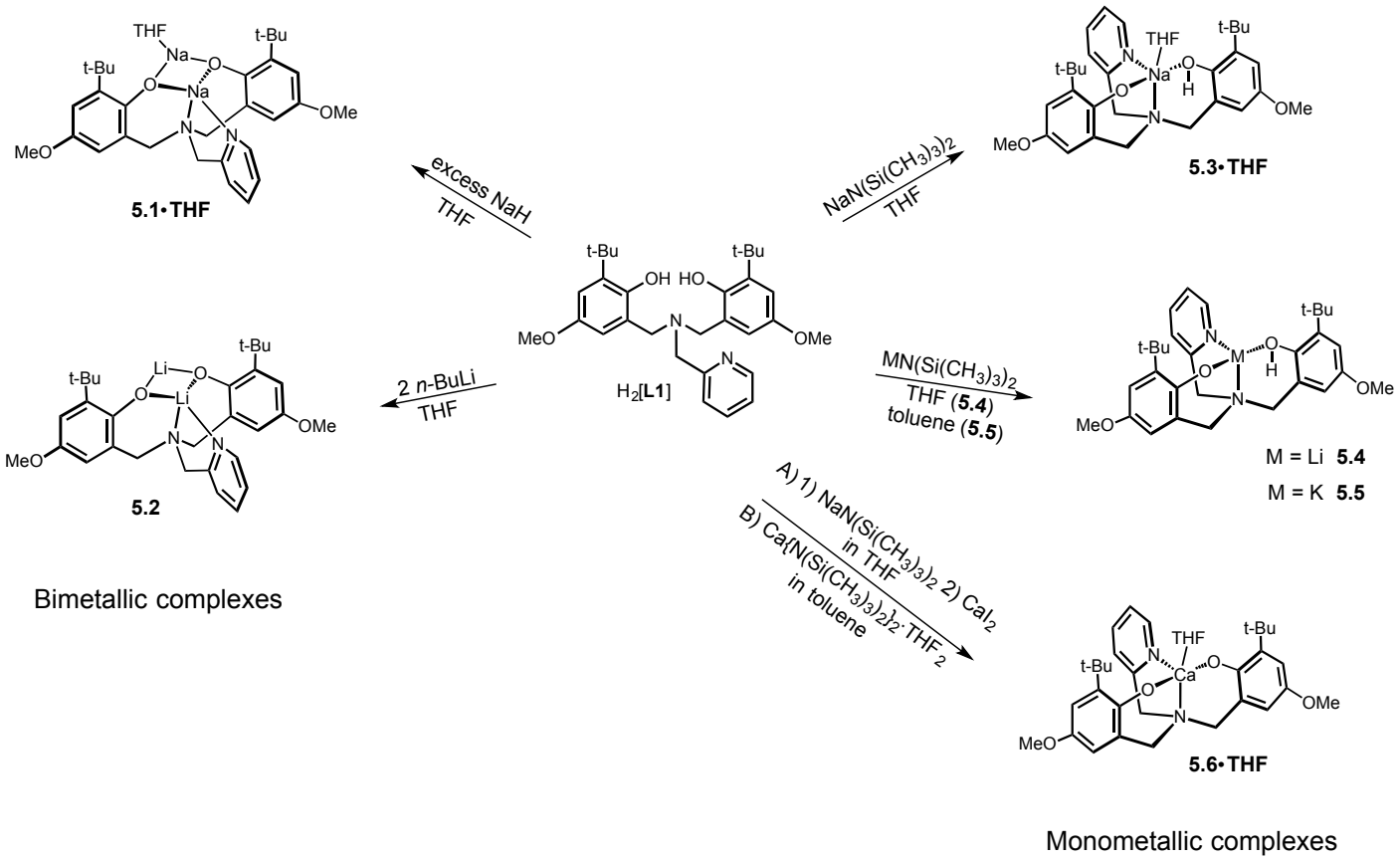

Scheme 5-1 Synthesis of bimetallic complexes **5.1**·THF and **5.2**, and monometallic complexes **5.3**·THF, **5.4**, **5.5** and **5.6**·THF

The structures of dimeric, tetranuclear lithium amino-bis(phenolato) compounds were previously reported.[22] These complexes usually adopt ladder-like[23,24] or boat-like[6] conformations in their cores when bulky substituents are at the *ortho* position of the phenolates, whereas cubanoid or six-membered cores are observed with no substituents at the *ortho* position.[25] As a consequence, it would be possible that with a bulky *tert*-butyl group at the *ortho* position of the phenolates of H_2[**L1**], tetralithium or tetrasodium complexes could be obtained similar to those reported by Lin[9] and co-workers and Thomas and co-workers.[26] However, ^{1}H NMR, ^{7}Li NMR in the case of **5.2**, and MALDI-TOF MS provided evidence toward bimetallic complexes possessing one amine-bis(phenol) ligand molecule involved (**5.1**·THF and **5.2** depicted in Scheme 5-1). ^{1}H NMR spectra gave sharp, well-defined peaks for **5.1** and **5.1**·THF in pyridine-d_5 (py-d_5). The spectrum of **5.1** (Figure C.7 in Appendix C) shows that the sample still contains some toluene (2.24 ppm, 7.19 and 7.30 ppm) but no coordinated THF can be detected as opposed to the spectra of **5.1**·THF, which were obtained both in py-d_5 (Figure C.8 in Appendix C) and DMSO-d_6 (Figure C.9 in Appendix C). A disadvantage of using pyridine is that the solvent peaks coincide with the pyridyl proton resonances of the complex resulting in obstructions (e.g. 7.20 ppm (pyridyl pendant) with 7.22 ppm (py-d_5). The presence of THF in **5.1**·THF was further confirmed by elemental analysis, which showed 0.55 equiv. of THF in the observed composition (see Section 5.3.4). MALDI-TOF MS analysis of **5.1**·THF reveals a protonated molecular ion $[M+H]^+$ at *m/z* 538.13 and a fragment ion after a sodium loss at *m/z* 515.29 (Figure B.14 in Appendix B). Bimetallic **5.2** was also characterized by ^{1}H NMR spectroscopy in three different solvents: py-d_5 (Figure C.10 in Appendix C), DMSO-d_6 (Figure C.11 in Appendix C)

and THF-d_8 (Figure C.12 in Appendix C). The characteristic sign of coordination is usually observed when the methylene protons between the aromatic ring and the amino nitrogen become diastereotopic. Thus, they appear as pairs of doublets at 4.43 and 3.37 ppm in py-d_5 (Figure C.10 in Appendix C), and 4.31 and 3.17 ppm in THF-d_8 (Figure C.12 in Appendix C). In DMSO-d_6 the coupling in the doublets could not be discerned, rather two very broad peaks are present at 3.1 and 4.0 ppm (Figure C.11). Another difference was also observed in DMSO-d_6. The pair of doublets of the two phenolate aromatic proton resonances came very close together and coalesced into one overlapping peak at 6.30 – 6.34 ppm (Figure C.11 in Appendix C). In addition, two proton peaks of the pyridyl pendant became coincident at 6.93 – 6.89 ppm (Figure C.11 in Appendix C). These phenomena are not surprising and are often observed in DMSO-d_6 due to second order resonances.[27,28] The clearest spectrum for **5.2** was thus obtained in THF-d_8 (Figure C.12 in Appendix C). MALDI-TOF MS shows fragment ions at *m/z* 504.24 corresponding to the bimetallic ion of **5.2** and *m/z* 498.24 representing the protonated version of **5.2** after a lithium ion loss (Figure B.15 in Appendix B). Elemental analysis also confirmed the structure of **5.2** (see Section 5.4.4).

Colourless single crystals suitable for X-ray diffraction were obtained from the powder of **5.1**·THF dissolved in a toluene/THF mixture and a toluene/pentane mixture for **5.2** at –35 °C. The crystals obtained were found to be partial hydrolysis products of **5.1**·THF and **5.2**. One of the phenolate oxygens in each compound was found to be protonated leaving only one alkali metal per ligand, giving instead compounds **5.3**·THF (Figure 5.1) and **5.4** (Figure 5.2), not the anticipated structures supported by NMR,

MALDI-TOF MS and elemental analysis. It is believed that partial hydrolysis occurred during crystallization, most likely from adventitious moisture in the solvent. Partial hydrolysis of the phenolate oxygens of a similar Li-complex was also observed by Huang and Chen when crystals of the complex were obtained from diethyl ether, also discussed in Chapter 1 **(1.25** in Figure 1.13, Section 1.2.2).[6] They hypothesized that the two lithium atoms can be easily removed from the tetranuclear complex by moisture resulting in the hydrolysis of one of the phenolate oxygens leaving one Li atom per ligand. Two molecules then arrange in a structure where intermolecular hydrogen bonding is exhibited between the hydrogen of the protonated oxygen of one complex and the non-protonated oxygen of the other, resulting in a dimeric structure. Reacting the ligand with 1.1 equiv. of ^{n}BuLi or with the addition of water both proved to be unsuccessful to obtain this partially hydrolysed product.[6] Layering a water/hexane mixture on top of a diethyl ether solution of a tetranuclear lithium complex, however, was reported to give partial hydrolysis.[6] In another study Lin and co-workers reacted OOO-tridentate bis(phenolate) ligands with $NaN[Si(CH_3)_3]_2$ and observed partially deprotonated compounds or THF adducts of Li and Na complexes depending on the stoichiometry or solvent used.[9] One example of such a complex (**1.27**) is shown in Chapter 1, Section 1.2.2, Figure 1.14. Stabilization of tetraphenolate Li-, Na- and K-complexes via H-bonding was also shown by Wu and co-workers.[11] In addition, Miller, Lin and co-workers prepared a disodium complex of 2,2'-ethylidene-bis(4,6-di-*tert*-butyl-phenol) ($EDBPH_2$) which had a monodeprotonated bis-phenol ligand also upon recrystallization after THF and methanol loss (**1.28b**, Chapter 1, Section 1.2.2, Figure 1.14).[29]

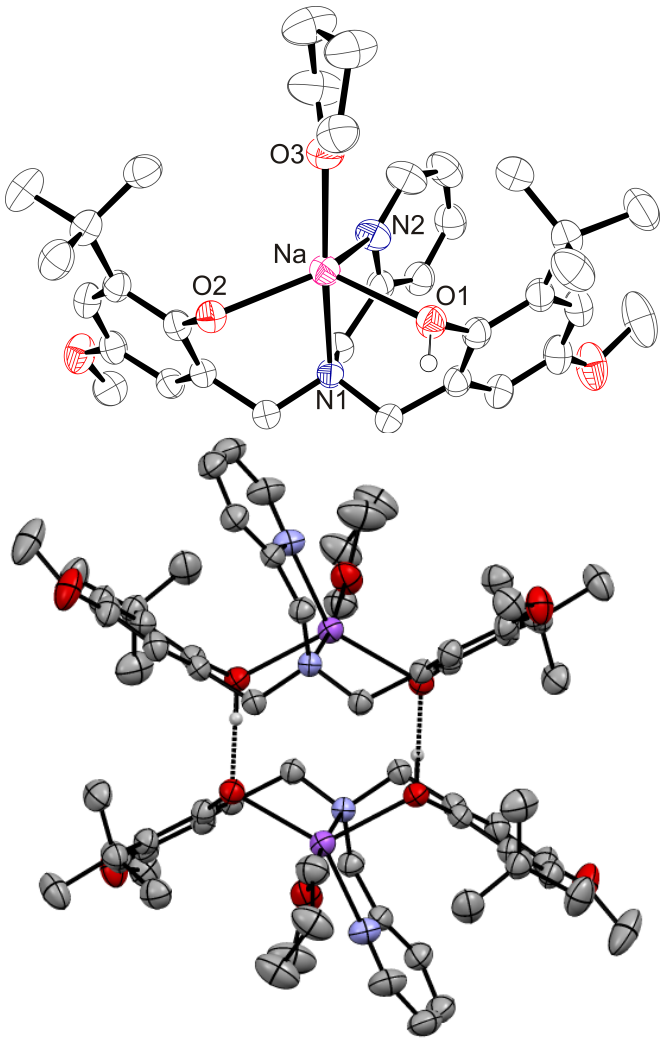

Figure 5.1 Partially labelled molecular structure (ORTEP) of **5.3**·THF and the dimeric structure showing intermolecular H-bonding. Thermal ellipsoids are drawn at 50% probability and H atoms are excluded for clarity (except for the hydrogen atom attached to O1). Selected bond lengths (Å) and angles (°): Na – O1, 2.350(2); Na – O2, 2.329(2); Na – O3, 2.415(2); Na – N1, 2.499(2); Na – N2, 2.483(3); O1 – H1, 0.871(18); H1 – O2`, 1.61(3); O1 – Na – O2: 123.43(7); O1 – Na – O3: 101.09(7); O2 – Na – O3: 104.73(7); O1 – Na – N1: 82.33(7); O2 – Na – N1: 81.39(7); O3 – Na – N1: 169.15(8); O1 – Na – N2: 96.78; O2 – Na – N2: 127.41(8); O3 – Na – N2: 98.07(8); N1 – Na – N2: 71.21(8). Symmetry operations used to generate equivalent atoms: (i) = x, y, z; (ii) = –x+1, y, –z +½.

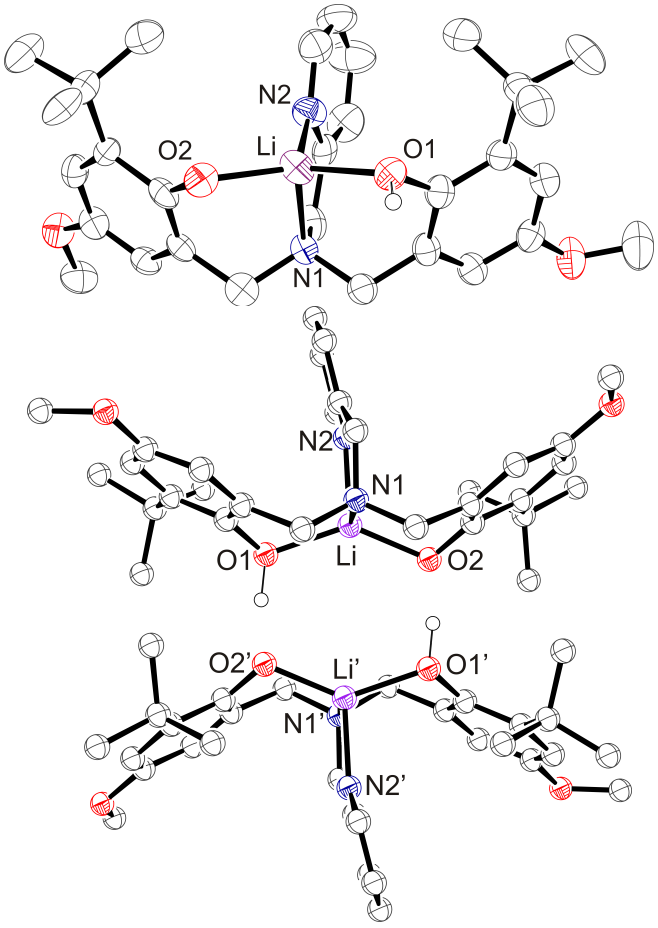

Figure 5.2 Partially labelled molecular structure (ORTEP) of **5.4** and the dimeric structure showing intermolecular hydrogen bonding. Thermal ellipsoids are drawn at 50% probability and H atoms are excluded for clarity (except for the hydrogen atom (H1) attached to O1). Selected bond lengths (Å) and angles (°): Li – O1, 1.932(11); Li – O2, 1.976(12); Li – N1, 2.044(12); Li – N2, 2.000(12); O1 – Li – O2: 137.5(6); O1 – Li – N1: 98.3(5); O2 – Li – N1: 97.7(5); O1 – Li – N2: 105.8(8); O2 – Li – N2: 114.4(6); N1 – Li – N2: 85.9(4). Symmetry operations used to generate equivalent atoms: (i) = x, y, z; (ii) = –x, y+½, –z+½.

The trigonality index,[30] τ, (where $\tau = (\beta - \alpha)/60$) for **5.3**·THF was calculated to be 0.70, which indicates that the geometry around the sodium is closer to trigonal bipyramidal (where $\tau = 1$) than square pyramidal (where $\tau = 0$). This is also supported by the largest angle O3–Na–N2 being 169.15(8)°, which is very close to the ideal 180° for a trigonal bipyramidal geometry. The distorted trigonal bipyramidal geometry is different

from a related Na complex supported by a tetradentate homopiperazinyl amine-bis(phenolato) ligand, where the geometry around the sodium proved to be distorted square pyramidal.[31] The difference probably originates from the different structures of the complexes. The presence of the homopiperazinyl group and the tetrametallic dimeric nature give a more rigid environment for the complex around the sodium as opposed to the monometallic **5.3**·THF. The coordination of the THF is at the apical position most likely to avoid congestion around the central sodium. The bond lengths around the Na centre are between 2.329(2) and 2.499(2) Å and comparable to the bond lengths of similar Na complexes.[8,11,12,31-33] There is also an intramolecular π-π interaction between one of the phenolate rings and the pyridyl group showing a plane centroid to plane centroid distance of 3.6709(19) Å.

The lithium atom of **5.4** is tetracoordinate, where the Li is coordinated to two phenolate oxygens, an amino nitrogen and the nitrogen of the pyridyl group. To distinguish between a tetrahedral or square planar geometry, Houser and co-workers defined a simple equation, based on Addison and Reedijk's τ parameter from which the geometry of a four-coordinate species can be determined using a simple calculation.[34] Based on their equation ($\tau_4 = \{360° - (\alpha + \beta)\}/141°$), the τ_4 value was calculated to be 0.77, implying a geometry closer to a tetrahedral (where $\tau_4 = 1.0$) rather than square planar (where $\tau_4 = 0.0$). Okuniewski and co-workers have recently published a modified calculation of Houser's equation.[35] They argued that the equation published by Houser and others did not distinguish between the two greatest valence angles of the coordination centre. When the equation determined by Okuniewski and co-workers is

used ($\tau_4' = (\beta - \alpha)/(360° - \theta) + (180° - \beta)/(180° - \theta)$), the τ_4' value for **5.4** is 0.69, very close to the τ_4 value, 0.77, calculated based on Houser's equation. Both values support a distorted tetrahedral geometry of the lithium centre of **5.4**. The distorted geometry in a related tetralithium complex was also found by Janas and co-workers[36] as well as in a Li-phenoxo-imine complex Cano, Tabernero and co-workers[8]. The bond distances around the Li atom are between 1.932(11) and 2.044(12) Å, showing good agreement with the distances observed with other lithium complexes in the literature.[6,7,9-11,37]

The monometallic complexes **5.3**·THF, **5.4** and **5.5** were obtained by a rational synthesis by reacting H_2[**L1**] with the corresponding alkali metal bis(trimethylsilyl) amide in THF (**5.3** and **5.4**) or toluene (**5.5**). Contrary to bimetallic **5.1**·THF and **5.2**, where distinct, well-defined, sharp peaks were observed, the ^{1}H NMR spectra of **5.3**·THF resulted in broad peaks both in DMSO-d_6 and py-d_5 (Figures C.13 and C.14 in Appendix C). Similarly complicated spectra were obtained in the case of **5.4** (Figures C.15 – C.16 in Appendix C). Peak broadening may be due to a fluxional process, such as formation and breaking of the hydrogen bonding between the molecules, or a disproportionation process which will be described below. Despite the absence of observable microstructure in the spectra due to this broadening, all the resonances for **5.3**·THF could be assigned. Assigning the ^{1}H NMR spectra of **5.4** in DMSO-d_6 and py-d_5, however, proved to be difficult, therefore, further investigation of this species in other solvents was performed. ^{1}H NMR of **5.4** in THF-d_8 resulted in sharp, assignable peaks but showed the presence of possibly two species (Figure C.17 in Appendix C). One possibility for the observed spectra is chemical equilibrium/disproportionation between **5.4** and **5.2** + H_2[**L1**] in

weakly coordinating solvents such as DMSO-d_6 resulting in broader than expected peaks. In THF-d_8 or py-d_5 both **5.2** and H_2[**L1**] become readily identified (Figures C.17 – C.18). The comparison (Figures C.18 – C.20) of the ^{1}H NMR spectra of **5.2**, **5.4** and the free ligand H_2[**L1**] in THF-d_8 underlines this phenomenon because the spectrum of **5.4** in strongly coordinating solvents shows the presence of an equimolar ratio of **5.2** and the pro-ligand. It is very likely then, that in the absence of a good coordinating solvent such as py-d_5 or THF-d_8, there is a disproportionation making peak assignment difficult. This raises the question of whether **5.4** was indeed genuinely synthesized as a monolithium complex, or whether the reaction of H_2[**L1**] with one equiv. of $LiN(Si(CH_3)_3)_2$ actually creates a mixture of unreacted H_2[**L1**] with **5.2** and the equilibrium between 2 **5.4** ⇌ **5.2** + H_2[**L1**] is solvent dependent. The products obtained by the two methods (2 equiv. ^{n}BuLi with H_2[**L1**] to give **5.2**, and one equiv. $LiN(Si(CH_3)_3)_2$ with H_2[**L1**] to give **5.4**) exhibit different solubilities. While **5.2** is soluble in most common solvents, such as chloroform, dichloromethane, toluene, THF, DMSO and pyridine, **5.4** is only soluble in THF, DMSO and pyridine. The solubility of **5.4** in DMSO also helps distinguish it from being just a mixture of **5.2** and H_2[**L1**], because the pro-ligand, H_2[**L1**], has low solubility in DMSO. If **5.4** was just mixture of pro-ligand and **5.2**, the ligand portion wouldn't dissolve in DMSO, whereas **5.4** showed good total solubility in DMSO-d_6. ^{7}Li NMR provided further insights into the difference between complex **5.2** and **5.4**. ^{7}Li NMR spectra of **5.2** and **5.4** were obtained in three different solvents (Figure 5.3 and Table 5-1, see Figures C.21 – C.23 in Appendix C for full spectra). The concentration of the NMR samples was kept the same (0.1067 mol/L) for all runs (see Section 5.4.6). One broad asymmetric peak was observed in py-d_5 for **5.2** including a shoulder peak. This is consistent with the

structure of **5.2**, as it possesses two distinct Li environments (Scheme 5-1). The existence of the two different lithium environments was further supported by a ^{7}Li NMR spectrum that was run on **5.2** with a lower concentration of 0.0762 mol/L earlier (Figure C.24 in Appendix C). A similar spectrum for an analogous compound with two *tert*-butyl groups at the phenolates and a furfuryl pendant donor was obtained previously in our group in py-d_5.[22] **5.4** exhibited a peak with a much less pronounced a shoulder. In DMSO-d_6, only one very broad peak appeared for each complex, but with different chemical shifts. In THF-d_8, two distinct peaks with similar widths and symmetry were observed for **5.2**, consistent with two different lithium environments. For **5.4** two peaks were found in THF-d_8 as well, but the shape and the intensities of the peaks, however, were different (Table 5-1). The chemical shifts of **5.4** do not show good correlation with the bimetallic **5.2**. It is also possible that some residual $LiN[Si(CH_3)_3]_2$ is still present in the sample and appears as the second peak at 0.66 ppm allowing for further complications regarding spectrum assignment. Kimura and Brown observed one ^{7}Li chemical shift for $LiN[Si(CH_3)_3]_2$ at +0.45 ppm in THF-d_8 relative to aqueous lithium bromide,[38] very close to the observed +0.66 ppm, calibrated against 1.0 M lithium chloride in D_2O. Wannagat also reported that although alkali bis(silyl)amides exist as dimers in nonpolar solvents, they exhibit only a single signal in their ^{7}Li NMR spectra, revealing possible highly symmetric dimeric structures.[39] Unfortunately, no chemical shifts of the amides were reported by the author. Consequently, the origin of the small peak at +0.66 ppm in THF-d_8 may be attributed to a small amount of $LiN[Si(CH_3)_3]_2$ contamination, which was further supported by elemental analysis (see Section 5.4.6 for details).

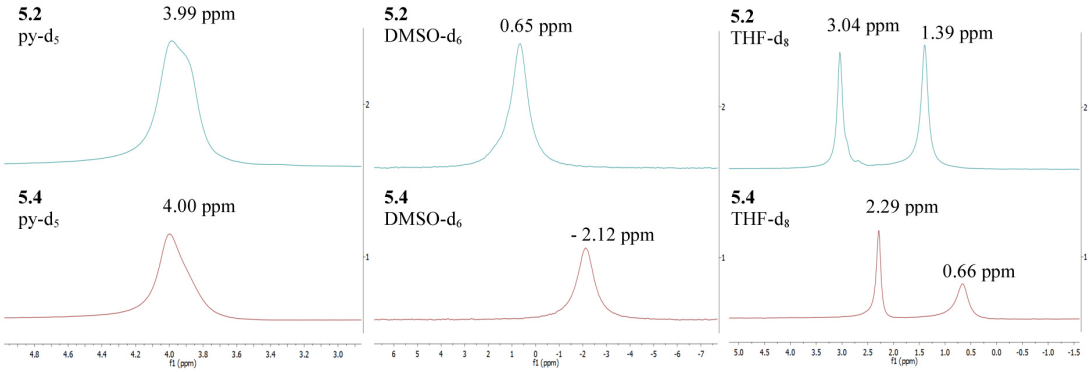

Figure 5.3 ^{7}Li NMR spectra for **5.2** and **5.4** in py-d_5, DMSO-d_6 and THF-d_8.

Table 5-1 ^{7}Li NMR chemical shifts and widths at half height values exhibited by **5.2** and **5.4** in different solvents

	5.2		**5.4**	
	δ	$w_{1/2}$ (Hz)	δ	$w_{1/2}$ (Hz)
Py-d_5	3.99	29.23	4.00	23.79
DMSO-d_6	0.65	95.73	- 2.12	97.72
THF-d_8	1.39	19.03	0.66	31.14
	3.04	14.85	2.29	12.24

Variable temperature ^{1}H NMR (Figure C.25 in Appendix C) and ^{7}Li NMR (Figure C.26 in Appendix C) spectra were also conducted in DMSO-d_6 to investigate whether sharpening of the observed broad peaks would occur upon increasing temperature. Increasing the temperature from 298 K to 378 K caused the peaks of the ^{1}H NMR spectra of **5.4** in DMSO-d_6 to narrow for the methylene as well as the aromatic region supporting again the presence one dominant species, but they were still broader than for **5.2** in the same solvent (Figure C.25 in Appendix C). Nevertheless, the spectrum at 378 K showed that even at high temperature there is considerable fluxionality causing peak broadening. ^{7}Li variable temperature NMR spectra of **5.4** also showed significant narrowing upon increasing the temperature (Figure C.26 in Appendix C).

MALDI-TOF mass spectrum of **5.3**·THF shows an intense peak at *m/z* 514.24, which corresponds to the molecular ion of **5.3** (Figure B.16 in Appendix B). There are additional peaks present at *m/z* 537.23 and *m/z* 559.20 corresponding to a sodium and a disodium adduct of **5.3** (Figure B.14 in Appendix B). The molecular ion of **5.4** is depicted at *m/z* 498.26 in the MALDI-TOF mass spectrum of **5.4** in Figure B17 in Appendix B. There is also a peak arising from the lithium adduct of **5.4** at *m/z* 504.26.

^{1}H NMR spectra of the potassium complex **5.5** (Figure C.27 in Appendix C) and the calcium complex **5.6**·THF (Figures C.28 and C.29 in Appendix C) exhibited well-defined, sharp peaks in DMSO-d_6. The resonances convincingly shifted from the resonances of the free ligand as well. Figure C.27 shows the presence of residual toluene (2.30, 7.18 and 7.25 ppm) in **5.5**, while the presence of THF was detected with **5.6**·THF (1.75 and 3.60 ppm, Figures C.28 and C.29) regardless of whether it was synthesized via route A) or B) (Scheme 5-1). The chemical shifts of the protons of the THF do not differ from the resonances of free THF likely because any coordinated THF can be replaced by DMSO-d_6. When **5.6**·THF was synthesized via route B) (Scheme 5-1), by reaction of H_2[**L1**] with $Ca\{N(Si(CH_3)_3)_2\}_2 \cdot THF_2$ in toluene, THF was still found in the product (Figure C.29) originating from the THF-containing Ca-amide starting material. MALDI-TOF MS supported the compositions of **5.5** (Figure B.18 in Appendix B) and **5.6**·THF (Figure B.19 in Appendix B). The molecular ion of **5.5** was found at *m/z* 530.23, together with its protonated form at *m/z* 531.24. There are also a potassium adduct and a bipotassium adduct of the molecular ion at *m/z* 569.19 and *m/z* 607.14, similar to the MALDI-TOF mass spectrum of **5.3**·THF. The mass spectrum of **5.6**·THF (Figure B.19

in Appendix B) shows radical ions of the dimer of **5.6** (*m/z* 1060.40) and the monomer fragment for **5.6** (*m/z* 530.30) are detected. The calculated isotopic distribution patterns of these peaks match very well with the experimentally obtained isotopic distribution pattern (Insets of Figure B.19).

5.2.2 Ring opening polymerization in the melt

As discussed in Chapter 4, melt phase ROP offers a simple and convenient method to generate PLA on an industrial scale.[40-42] No additional solvent is needed because the molten *rac*-lactide provides the reaction medium as well as the monomer supply for the ROP. Of course, as the polymerization proceeds and the molecular weight of the polymer chains increases, the viscosity of the reaction mixture increases as well until stirring of the molten mixture is no longer possible. The complexity of the reaction gives rise to opportunities for optimizing the conditions and the characterization of the resulting polymers.[40] In Chapter 4, two magnesium-amine-bis(phenolate) complexes were found to give excellent activity for the ROP of *rac*-lactide both in solvent-free/melt conditions and in solvent at 90 °C. Having observed this high activity in the melt, complexes **5.1** – **5.5** were investigated for lactide ROP in the melt.

Initially, complexes **5.1**·THF – **5.6**·THF were screened in the melt at 125 °C for the allotted time to see which provided the best conversion. The results are summarized in Table 5-2. It is worth noting that the monomer/initiator ratio was calculated as *rac*-lactide/complex regardless whether the complex contained two (**5.1**·THF and **5.2**) or one metal (**5.3**·THF – **5.6**·THF). Generally, better conversions were obtained when BnOH

was added as a chain-transfer agent/co-initiator (compare entries 5 and 6, 9 and10, 15 and 16). The monometallic complexes generally exhibited better conversions than the bimetallic ones. In 30 min., 85% conversion was achieved with **5.3**·THF when BnOH was used (entry 6), whereas 66% conversion was observed with the bimetallic analogue **5.1**·THF (entry 2). Interestingly, very high, 95% conversion was also observed with **5.5** within 60 min in the presence of BnOH (entry 16). Without BnOH, the best conversion was achieved with **5.6**·THF within 100 min (95%, entry 19). When the catalyst loading was decreased, the conversion decreased significantly (entries 11 and 12).

Table 5-2 Solvent-free (melt) *rac*-lactide polymerization by complexes **5.1**·THF – **5.6**·THF

Entry[a]	Complex	Time (min)	T (°C)	[LA]:[C] :[BnOH][b]	Conv. (%)[c]
1	**5.1**	30	125	100:1:0	78
2	**5.1**	30	125	100:1:1	66
3	**5.2**	30	125	100:1:0	64
4	**5.2**	30	125	100:1:1	64
5	**5.3**	30	125	100:1:0	48
6	**5.3**	30	125	100:1:1	85
7	**5.4**	30	125	100:1:0	56
8	**5.4**	30	125	100:1:1	49
9	**5.4**	100	125	100:1:0	45
10	**5.4**	100	125	100:1:1	98
11	**5.4**	100	125	500:1:0	8
12	**5.4**	60	125	500:1:1	27
13	**5.5**	30	125	100:1:0	59
14	**5.5**	30	125	100:1:1	48
15	**5.5**	60	125	100:1:0	55
16	**5.5**	60	125	100:1:1	95
17	**5.5**	100	125	500:1:0	< 5
18	**5.5**	60	125	500:1:1	10
19	**5.6**	100	125	100:1:0	95

[a]All polymerization reactions were carried out in neat *rac*-lactide (0.5 g). [b]C = Complex. [c]Conversion determined by ^{1}H NMR.

Based on the high conversion that was exhibited by **5.4** (entry 10), further experiments were carried out with this species to test its activity. A conversion vs. time study was performed and Table 5-3 contains the results of these reactions. The reactions were carried out in separate vials under the same conditions and terminated at the prescribed times. No benzyl alcohol chain transfer agent was added.

Table 5-3 Results of ROP of *rac*-lactide under solvent-free/melt conditions (125 °C) initiated by **5.4** with no added alcohol.

Entry[a]	Time (min)	Conversion[b] (%)	M_n (Calc)[c] (g/mol)	M_n (GPC)[d] (g/mol)	Đ (M_w/M_n)[d]
1	20	29	4 200	10 700	2.00
2	40	32	4 600	15 700	2.23
3	60	39	5 600	12 200	2.24
4	80	46	6 600	14 800	2.13
5	100	61	8 800	9 200	2.70
6	120	77	11 100	14 200	2.17

[a]All polymerization reactions were carried out in neat *rac*-lactide (0.5 g), [LA]:[Li]:[BnOH] = 100:1:0. [b]Conversion determined by ^{1}H NMR. [c]Calculated from ([LA]/[Mg]) × % conv. × 144.13 g·mol^{-1}] [d]Molecular weights (g·mol^{-1}) and dispersity (Đ (M_w/M_n)) determined by gel permeation chromatography (GPC) in $CHCl_3$ calibrated against polystyrene standards using the Mark-Houwink correction of 0.58.[43]

In general, the conversion increases with increasing reaction time. The molecular weights, however, do not show good correlation with the calculated molecular weights indicating unwanted side reactions, such as transesterification or chain transfers, possibly due to adventitious water. This poor control of molecular weight might also be attributed to the absence of benzyl alcohol initiator/chain transfer agent. The calculated molecular weight was closest to the experimentally observed molecular weight with the 100 min reaction, although with the highest dispersity (2.70). Overall, the dispersity ranges between 2.00 – 2.70, which also shows the lack of control over molecular weight without BnOH.

Table 5-4 Results of ROP of *rac*-lactide under solvent-free/melt conditions (125 °C) initiated by **5.4**

Entry[a]	Time	Conversion (%)[b]	M_n (Calc)[c] (g/mol)	M_n (GPC)[d] (g/mol)	Đ (M_w/M_n)[d]
1	40	49	7 100	9 000	2.00
2	80	58	8 400	9 300	1.86
3	100	60	8 600	10 200	1.97
4	120	70	10 100	7 900	1.94

[a]All polymerization reactions were carried out in neat *rac*-lactide (0.5 g), [LA]:[Li]:[BnOH] = 100:1:1. [b]Conversion determined by ^{1}H NMR. [c]Calculated from ([LA]/[Mg]) × % conv. × 144.13 g·mol^{-1}] [d]Molecular weights (g·mol^{-1}) and dispersity (Đ) determined by gel permeation chromatography (GPC) in $CHCl_3$ calibrated against polystyrene standards using the Mark-Houwink correction of 0.58.[43]

The conversion vs. time experiment was repeated using 1 equiv. of BnOH per metal complex. Table 5-4 also shows that the conversion increases with time. Molecular weights are in much better agreement with the calculated molecular weights in the presence of BnOH and they show an increase up to 100 min. A slight decrease in M_n was observed when the reaction was run for more than 100 min., possibly due to the increasing probability of side reactions when the reaction is left to occur for longer time. The dispersity values are lower (1.86 – 2.00) compared to the reactions when no BnOH is used (2.00 – 2.70), but still show poor control. The activity of **5.4** was also tested in the ROP of L-lactide with and without BnOH in two different timed reactions (Figures G.6 and G.7 in Appendix G). These experiments reveal that there was no significant difference in conversion or reaction rate whether or not BnOH was used within 30 min.

5.2.3 Microwave assisted experiments

Microwave assisted polymerization reactions were also carried out to assess whether rapid heating by microwave radiation has any influence on *rac*-lactide polymerization. All the reactions were carried out in neat *rac*-lactide. The microwave automatically applies the appropriate power level to keep the mixture at the desired temperature of 125 °C (Figure G.8 in Appendix G). To get reliable results, the experiments were carried out twice (except for entry 1) and the conversions of these duplicate experiments are summarized in Table 5-5.

Table 5-5 Results of the microwave assisted polymerizations. Conditions: melt, [LA]:[Cat]:[BnOH] = 100:1:0 (entries 1 – 4) or 100:1:1 (entries 5 – 8), where Cat = Catalyst

Entry	Complex	Conversion (Run 1) (%)	Conversion (Run 2) (%)	Average Conversion (%)
1	**5.1**·THF	74	–	74
2	**5.2**	94	85	90
3	**5.3**·THF	24	31	28
4	**5.4**	79	54	67
5	**5.1** (+ 1 eq BnOH)	62	86	74
6	**5.2** (+ 1 eq BnOH)	93	89	91
7	**5.3** (+ 1 eq BnOH)	39	27	33
8	**5.4** (+ 1 eq BnOH)	80	64	72

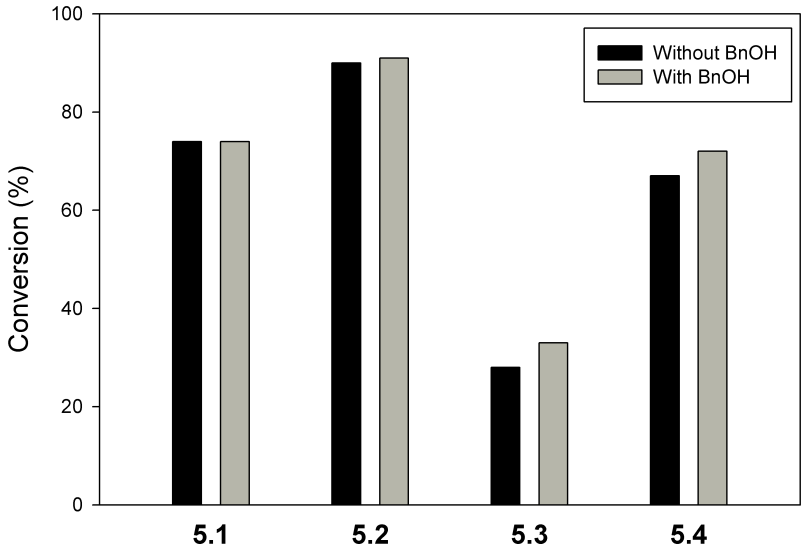

Figure 5.4 Conversion (%) reached by complexes **5.1**·THF – **5.4** in 30 min under microwave assisted, solvent-free conditions. [LA]:[Cat]:[BnOH] = 100:1:1 (right hand side, grey bars) or 100:1:0 (left hand side, black bars)

Figure 5.4 shows the average values of two consequent experiments obtained by complexes **5.1**·THF – **5.4**. The highest conversions were observed with **5.2** (90% and 91%). Although the conversions exhibited by **5.1**·THF and **5.4** were lower (averaging 74% and 67%, respectively), they were still quite high compared to the conversions observed with **5.3**·THF (28% and 33%). After the allotted time, the polymers were purified by precipitation from CH_2Cl_2 by cold acidified methanol. However, the polymers that were produced with complexes **5.1**·THF and **5.3**·THF, unfortunately, could not be precipitated out, possibly because of their lower molecular weights. The polylactides made by complexes **5.2** and **5.4** could be purified without difficulty. Table 5-6 shows the molecular weights and dispersities of the polymers obtained using complex **5.4** with and without BnOH. Again, the conversions are the same, higher molecular weight is obtained without BnOH, but the dispersity values are very similar.

The molecular weights determined by ^{1}H NMR (Figure 5.5) confirmed the polymers produced with **5.1**·THF and **5.3**·THF possessed low molecular weights, therefore were difficult to purify.

Table 5-6 Results of ROP of *rac*-lactide with **5.4** under microwave-assisted solvent-free conditions.

Entry[a]	[LA]:[Li]:[BnOH]	Conversion[b] (%)	Yield[c] (%)	M_n (calc)[d] (g/mol)	M_n (GPC)[e] (g/mol)	Đ (M_w/M_n)[e]
1	100:1:0	79	72	11 400	8 800	2.15
2	100:1:1	80	63	11 500	4 700	2.14

[a]All polymerization reactions were carried out in neat *rac*-lactide (0.5 g) at 125 °C, 30 min. [b]Conversion determined by ^{1}H NMR. [c]Calculated from (mass of polymer isolated/mass of polymer could be obtained theoretically) [d]Calculated from ([LA]/[Mg]) × % conv. × 144.13 g·mol^{-1}] [e]Molecular weights (g·mol^{-1}) and Đ determined by gel permeation chromatography (GPC) in $CHCl_3$ calibrated against polystyrene standards using the Mark-Houwink correction of 0.58.[43]

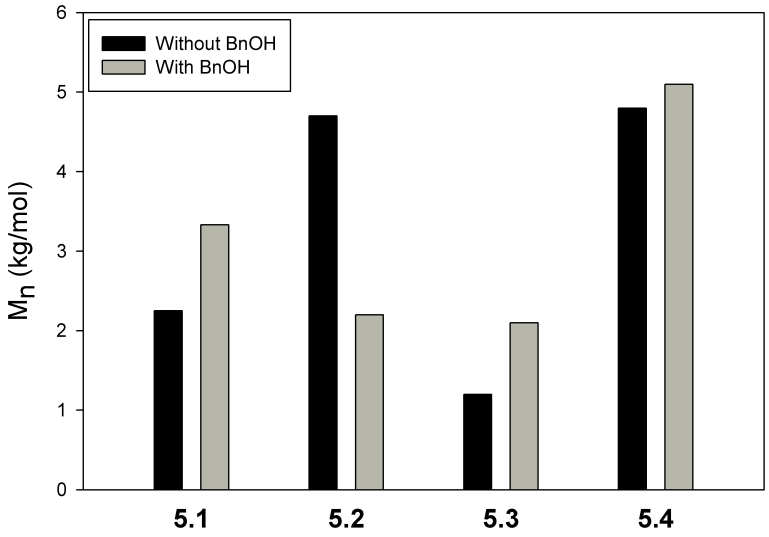

Figure 5.5 Molecular weights determined by ^{1}H NMR for polymers obtained in microwave assisted experiments. Conditions: melt, [LA]:[Cat]:[BnOH] = 100:1:1 (grey bars) or 100:1:0 (black bars).

The highest molecular weights were obtained with the monometallic lithium complex **5.4** regardless of whether BnOH was added or not. Comparing the two solvent-free conditions (melt and microwave), microwave assisted heating did not result in higher conversions, molecular weights or lower dispersity.

5.2.4 ROP of *rac*-lactide in solution

The ring opening activity of the monometallic complexes **5.3**·THF – **5.6**·THF was also tested in solution. Initial tests in CH_2Cl_2 and THF showed no activity by any of the complexes at room temperature. When toluene was used as the reaction medium, however, very fast reactions were observed with **5.3**·THF and **5.5** in the absence of BnOH, but not with **5.4**, which proved to be very slow (Figure 5.6).

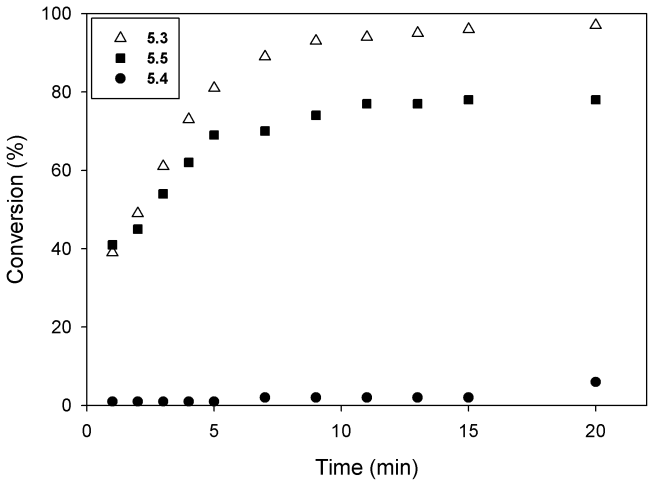

Figure 5.6 Comparison of **5.3**·THF – **5.5** in ROP of *rac*-lactide in toluene at room temperature. [LA]:[M]:[BnOH] = 100:1:0, where M = Na for **5.3**·THF, Li for **5.4**, K for **5.5**.

Very high conversion (94%) was achieved with **5.3**·THF within 11 min when BnOH was not used (Figure 5.6), moderate (77%) with **5.5** within the same time, but

very low (18%) with **5.4** in 90 min. The reaction did go to completion (98%) even with **5.4**, though long reaction time (24 h) was needed. The same reactivity order (Na > Li > Ca > Mg) was observed by the Miller group when they compared Na, Li, Ca and Mg complexes with a 2,6-di-*tert*-butyl-4-methylphenol (BHT) ligand.[44] In a more recent study, Cano and co-workers found that the potassium analogue of the azonaphthoxide complexes proved to be better than the sodium analogue and reported an activity order of K > Na > Li > Ca > Mg > Zn.[45] They attributed the activity order to the generally increasing atomic radius of the alkali, alkaline earth and Zn metals. The reactivity order of Ca > Mg > Zn was also observed by the Chisholm group earlier when bulky trispyrazolylborate complexes were used.[15] Tetrametallic Na diamine-bis(phenolate) complexes also proved to be superior to their lithium analogues reported recently by Kerton and co-workers.[31] When comparing the amine-bis(phenolate) complexes used in this study, a reactivity order of Na > K > Li > Ca > Mg can be concluded. The Na complex proved to be the fastest, followed by potassium and then lithium. The Ca-complex needed the longest time at room temperature (24 h) and the Mg analogue proved to be inactive at room temperature, needing an elevated temperature of 90 °C to react (see Chapter 4, Section 4.2.4).

Table 5-7 summarizes the results of the solution polymerization experiments. When 1 equiv. of BnOH was added, the reaction became even faster with **5.3**·THF and 99% conversion was achieved within only 2 min (Table 5-7, entry 2). The reactions with **5.4** and **5.5** completed in 30 min (Table 5-7, entries 10 and 12), whereas **5.6**·THF needed 240 min to reach 76% conversion with BnOH (Table 5-7, entry 14). Again, a reactivity

order of Na > K > Li can be concluded. The dispersity values are between 1.04 and 1.37 when BnOH is utilized. Without BnOH the dispersity is higher, giving values between 1.27 and 2.65.

Table 5-7 Results of the solution polymerizations by **5.3**·THF – **5.6**·THF.

Entry[a]	Complex	[LA]:[M]:[BnOH]	Temp (°C)	Time (min)	Conversion[b] (%)	M_n (calc)[c]	M_n (GPC)[d]	Đ[d]
1	**5.3**·THF	100:1:1	5	20	99	14 300	12 600	1.20
2	**5.3**·THF	100:1:1	25	2	99	14 300	7 100	1.21
3	**5.3**·THF	100:1:0	25	13	95	13 700	9 500	1.98
4	**5.3**·THF	200:1:1	25	3	99	28 500	10 000	1.31
5	**5.3**·THF	200:1:0	25	20	94	27 000	33 800	1.58
6	**5.3**·THF	200:1:2	25	3	98	14 100	11 300	1.07
7	**5.3**·THF	200:1:5	25	1	98	5 600	7 300	1.37
8	**5.3**·THF	500:1:1	25	2.5	38	27 400	14 600	1.04
9	**5.3**·THF	500:1:0	25	60	99	64 800	18 800	1.27
10	**5.4**	100:1:1	25	30	99	14 300	6 900	1.25
11	**5.4**	100:1:0	25	1 440 (24 h)	98	14 100	18 400	1.60
12	**5.5**	100:1:1	25	30	94	13 500	6 600	1.32
13	**5.5**	100:1:0	25	60	80	11 500	24 000	2.65
14	**5.6**·THF	100:1:1	25	240	76	10 900	8 400	2.42

[a]All polymerization reactions were carried out in toluene (0.8 g *rac*-lactide in 20 mL toluene). [b]Conversion determined by ^{1}H NMR. [c]Calculated from ([LA]/[M]) × % conv. × 144.13 g·mol^{-1}] [d]Molecular weights (g·mol^{-1}) and Đ determined by gel permeation chromatography (GPC) in THF by triple detection. See experimental for full details.

The highest dispersity (2.65) was observed with **5.5** when BnOH was not used. **5.6**·THF also produced highly disperse polylactide (Đ = 2.42) even with BnOH present (entry 14).

The highly active sodium complex **5.3**·THF in toluene was further investigated. A low temperature (5 °C) polymerization was also conducted with **5.3**·THF under the same conditions and was compared to the polymerizations at 25 °C (Table 5-7, entries 1 – 3). Figure 5.7 shows the difference in the initial rates of the polymerization at room temperature and at 5 °C. The reaction at 5 °C became expectedly slower compared to the room temperature run, however, it was still very fast and showed 90% conversion within 9 min (Figure G.9). The k_{obs} value of the 5 °C polymerization (0.325 ± 0.003 min^{-1}) is statistically identical to the k_{obs} value of the polymerization under the same condition but without BnOH (0.334 ± 0.014 min^{-1}).

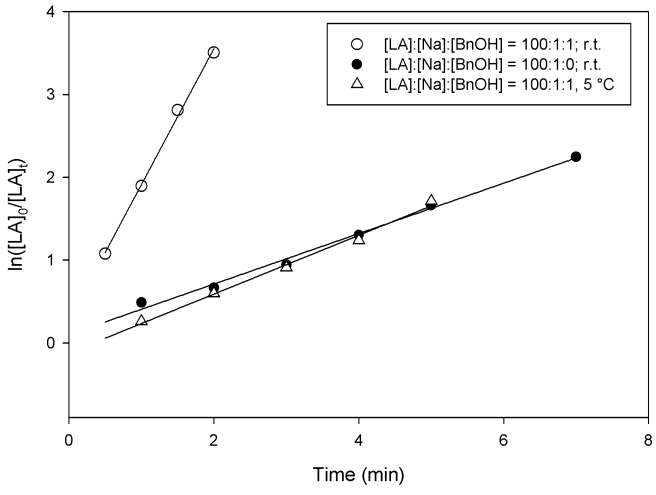

Figure 5.7 Plot of $\ln([A]_0/[LA]_t)$ vs time, [LA]:[Na]:[BnOH] = 100:1:1, 25 °C and at 0 °C and 100:1:0 at 25 °C in toluene. The observed rate constants: k_{obs} (100:1:1, 25 °C) = 1.640 ± 0.060 min^{-1}, R^2 = 0.9997; k_{obs} (100:1:1, 5 °C) = 0.325 ± 0.003 min^{-1}, R^2 = 0.9960; k_{obs} (100:1:0, 25 °C) = 0.334 ± 0.014 min^{-1}, R^2 = 0.9929.

When the *rac*-lactide:metal ratio was changed to 200:1 and 500:1, the initial reaction rate decreased (Figure 5.8) and the time needed to complete the reaction increased (Figure G.10 in Appendix G). Particularly, the reaction with a catalyst loading [LA]:[Na] = 500:1 proved to be slow and achieved 99% conversion after one hour. Table 5-8 contains the observed rate constants for reactions without (entries 1 – 3) and with BnOH (entries 4 – 6).

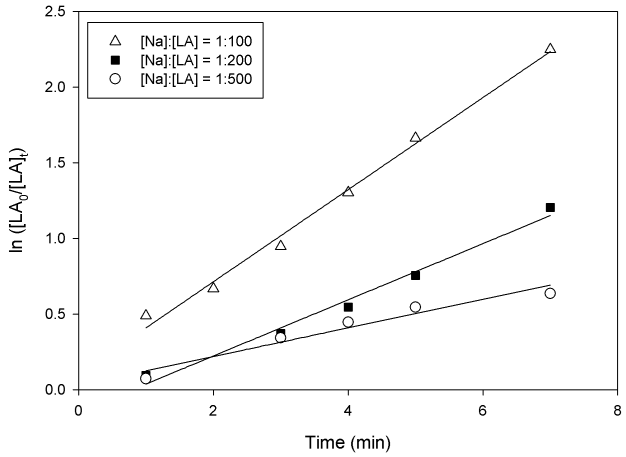

Figure 5.8 $\ln([LA]_0/[LA]_t)$ vs. time plots for the polymerization with complex 5.3·THF with different [LA]:[Na] ratios without BnOH at 25 °C in toluene.

The conversion vs. time plots (Figure G.11 in Appendix G) of the reactions with BnOH show the substrate to catalyst ratio, [LA]:[Na]:[BnOH], of 200:1:1 is very fast and full conversion is reached in 5 min. Reaction using 1 mol% catalyst loading achieved nearly complete conversion at 2 min. Reaching full conversion with the [LA]:[Na]:[BnOH] = 500:1:1 ratio, however, takes more than a day. Figure 5.9 illustrates the difference in reaction rates at different substrate to catalyst ratios.

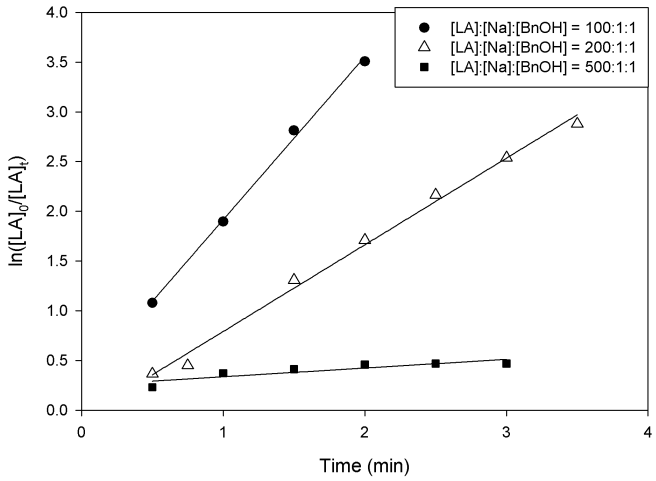

Figure 5.9 $\ln([LA]_0/[LA]_t)$ vs. time plots for the polymerization with complex **5.3**·THF with different [LA]:[Na] ratios with BnOH at 25 °C in toluene.

Table 5-8 Observed reaction rates (k_{obs}) and R^2 values for the linear fits in Figures 5.8 and 5.9.

Entry	[LA]:[Na]:[BnOH]	k_{obs} (min^{-1})	R^2
1	100:1:0	0.3044 ± 0.0128	0.9930
2	200:1:0	0.1856 ± 0.0123	0.9850
3	500:1:0	0.0945 ± 0.0119	0.9470
4	100:1:1	1.6399 ± 0.0602	0.9973
5	200:1:1	0.8717 ± 0.0312	0.9928
6	500:1:1	0.0510 ± 0.0116	0.8785

The different structures of species **5.2** and **5.4** were elucidated with the help of ^{1}H NMR, ^{7}Li NMR and solubility tests earlier in Section 5.2.1. For the ROP of *rac*-lactide in solution, however, **5.3**·THF was used based on its high activity. The same question – similarly to **5.4** earlier – whether it is possible that **5.3**·THF exists as a mixture of **5.1**·THF and H_2[**L1**] was addressed here experimentally. A series of experiments was carried out using a mixture of **5.1**·THF + H_2[**L1**] with and without BnOH. The activity of this mixture was compared to the activity exhibited by **5.3**·THF. Based on the possible equilibrium between 2 **5.3**·THF ⇌ **5.1**·THF + H_2[**L1**],

a mixture of 0.5 equiv. **5.1**·THF and 0.5 equiv. of pro-ligand was used to be able to compare the activity of the mixture of the two to that of **5.3**·THF. Figure 5.10 illustrates the difference between the mixture and the complex regarding both the conversion (Fig. 5.10) and the reaction rate (Fig. 5.11). The reaction rate initiated by **5.3**·THF is significantly faster than the reaction initiated by the mixture of **5.1**·THF and H_2[**L1**] with or without BnOH, and the k_{obs} values are lower by one order of magnitude when the mixture of **5.1**·THF and is H_2[**L1**] used (Table 5-9). Consequently, the catalytic activity of **5.3**·THF was proven to be superior to that of the mixture and the difference is more obvious when BnOH is not used.

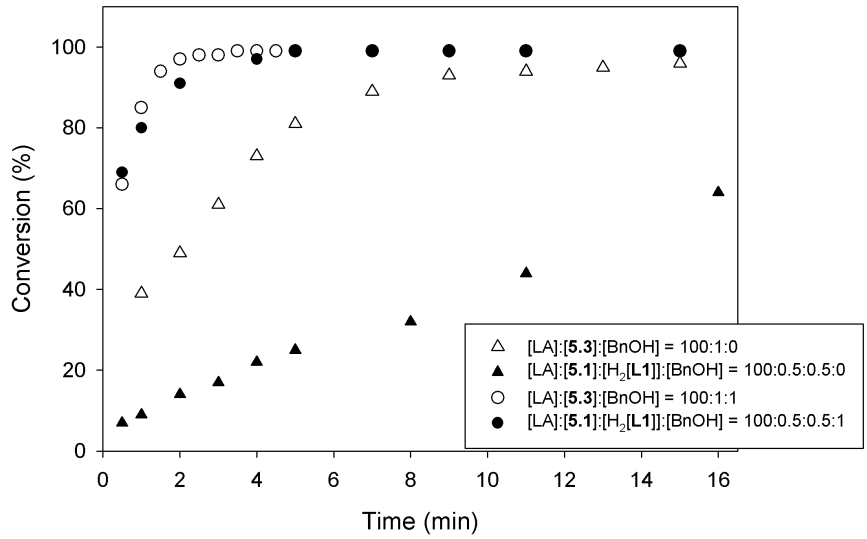

Figure 5.10 Conversion vs. time plots of the ROP of rac-lactide with **5.3**·THF and with **5.1**·THF + H_2[L1] at 25 °C with and without BnOH.

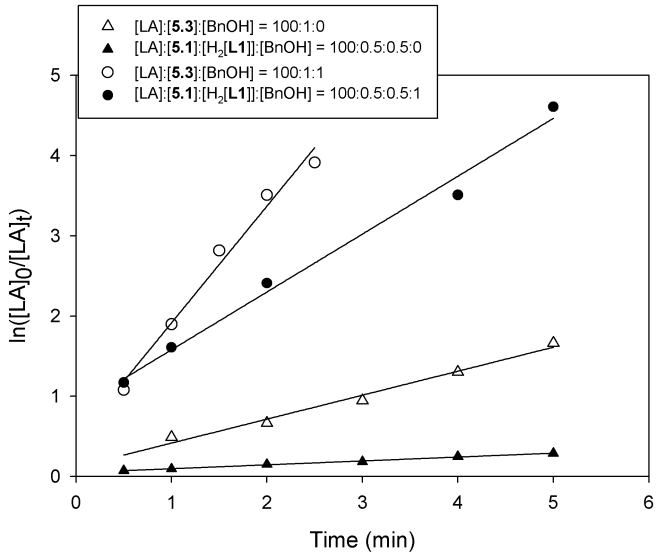

Figure 5.11 ln([LA]$_0$/[LA]t) vs. time plots of the ROP of rac-lactide with **5.3**·THF and **5.1**·THF + H_2[L1] at 25 °C with and without BnOH.

Table 5-9 Observed reaction rates (k_{obs}) and R^2 values for the linear fits in Figure 5.11.

Entry	[LA]:[Na]:[BnOH]	Ratio	k_{obs} (min^{-1})	R^2
1	[LA]:[**5.3**·THF]:[BnOH]	100:1:0	0.299 ± 0.0154	0.9838
2	[LA]:[**5.1**·THF]:[H_2**L1**]:[BnOH]	100:0.5:0.5:0	0.0484 ± 0.00130	0.9961
3	[LA]:[**5.3**·THF]:[BnOH]	100:1:1	1.46 ± 0.112	0.9825
4	[LA]:[**5.1**·THF]:[H_2[**L1**]]:[BnOH]	100:0.5:0.5:1	0.721 ± 0.0789	0.9885

The polymers produced by the mixtures of **5.1**·THF and H_2[**L1**] were also investigated by GPC. The molecular weights and dispersity values being 9 900 g/mol and Đ = 1.05 with BnOH, and 9 100 g/mol and Đ = 1.24 without BnOH. These molecular weights and dispersities are similar to the values obtained by **5.3**·THF (7 100 g/mol, Đ = 1.21 with BnOH and 9 500, Đ = 1.98 without BnOH (Table 5-7, entries 2 and 3). So, there is no significant difference between the **5.1**·THF/H_2[**L1**] mixture and **5.3**·THF with respect to molecular weight, but there is difference in the dispersity of the polymers, which is higher for the polymers produced with **5.3**·THF.

In conclusion, **5.3**·THF exhibited higher activity than the **5.1**·THF/H_2[**L1**] mixture regardless of whether BnOH was used or not, which also helped distinguish it from being just a mixture of **5.1**·THF/H_2[**L1**]. The molecular weights of the polymers obtained with the mixture were very similar to the molecular weights produced with **5.3**·THF. Interestingly, the polymers obtained with the mixture were lower in dispersity compared to the polymers obtained with **5.3**·THF.

5.2.5 MALDI-TOF MS of the polylactides

MALDI-TOF mass spectrometry commonly showed the expected peaks separated by *m/z* 72 corresponding to the repeating unit of half of a lactide molecule. The spectra were obtained in reflectron mode and/or in linear mid or high mass mode. Reflectron mode gives rise to spectra with better resolution and consequently, a very accurate determination of the end groups in the low mass region. On the other hand, linear mode provides the observed polymer fragments in the higher mass region (Figure B.20 in Appendix B). Interestingly, cyclic polymers were always present in the low mass region regardless of whether BnOH was used or not (Figure 5.12 and 5.13). Figure 5.12 demonstrates two species of cyclic product (image B, a and b) corresponding to a sodium and a potassium adduct, whereas only the sodiated species was detected when the conditions of Table 5-7, entry 2 were applied and no BnOH was used (Figure 5.13). The presence of Na^+ and K^+ cations is an artefact of adventitious ions within the mass spectrometer because no cationizing agents were employed. The two cyclic species are characteristic of all the polymers produced by **5.3**·THF (Figures B.21 – B.22 in Appendix B), the mixture of **5.1**·THF and H_2[**L1**] (Figures B.23 – B.24), **5.4** (Figure B.25) and **5.5** (Figure B.26) and they are also

present in the polymer produced by **5.6**·THF, which contains four different species. (Figures B.27 and B.28). Two species correspond to the cyclic products and the other two are linear polymer chains.

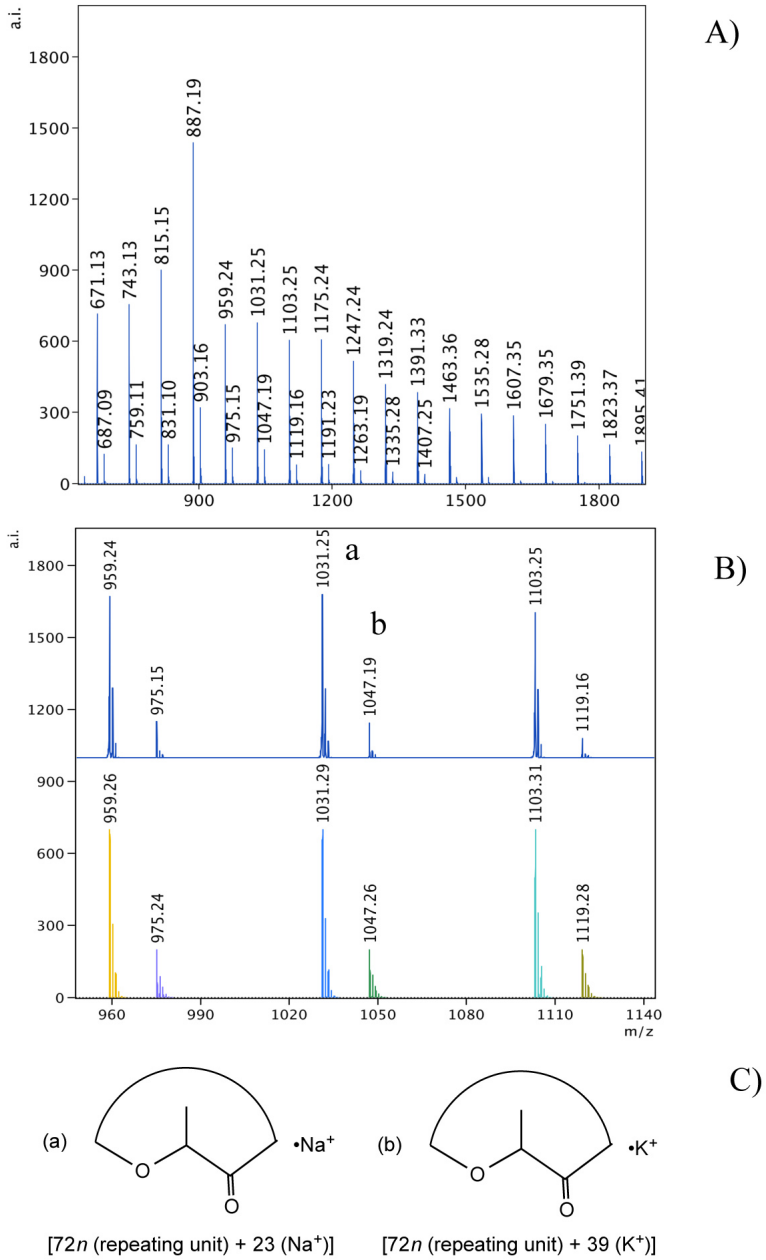

Figure 5.12 A) MALDI-TOF mass spectrum of PLA produced by **5.3**·THF according to the conditions of Table 5-7, entry 2. B) Expanded region of A) (*m/z* 950 – 1140, n = 13 – 15, top part of B)) with modeled calculated polymer peaks (bottom part of B)). C) Possible structures of the polymers based on the calculations shown.

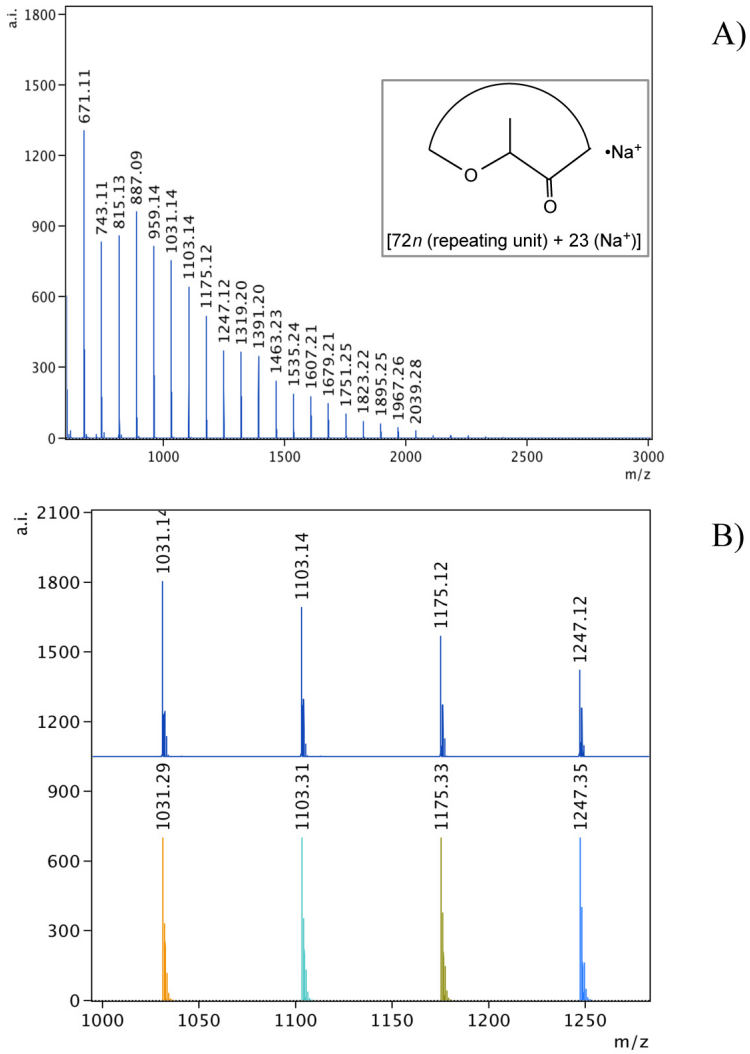

Figure 5.13 A) MALDI-TOF mass spectrum of PLA produced by **5.3**·THF according to the conditions of Table 5-7, entry 3, inset: possible structure of the polymer based on the calculation shown. B) Expanded region of A) (*m/z* 1000 – 1250, n = 14 – 17) (top part of B)) with modeled calculated polymer peaks (bottom part of B)).

5.3 Conclusions

In conclusion, five new alkali (Li, Na, K) and one new alkaline earth metal (Ca) complexes were synthesized, characterized and tested in the ring opening polymerization of *rac*-lactide. All complexes are active in the melt (125 °C) and in solution (25 °C). Microwave assisted heating did not enhance the activity of the complexes. The monometallic lithium complex **5.4** provided the best conversion in the melt phase, whereas the monometallic sodium analogue **5.3**·THF exhibited the

fastest propagation and highest conversion in solution at 25 °C. Based on the solution polymerization results, a reactivity order of Na > K > Li > Ca could be established. The end group analysis of the polymers obtained revealed that mainly cyclic polymers were present in the low mass region regardless whether added alcohol was present or not.

5.4 Experimental

5.4.1 General experimental conditions

Unless otherwise stated, all manipulations were performed under an atmosphere of dry, oxygen-free nitrogen by means of standard Schlenk techniques or using an MBraun Labmaster DP glove box. Anhydrous THF was distilled from sodium benzophenone ketyl under nitrogen. Toluene was purified by an MBraun Manual Solvent Purification System. $HN[Si(CH_3)_3]_2$ was distilled from CaH_2. $KN[Si(CH_3)_3]_2$ was purchased from Aldrich Chemical Company and was used without further purification. $NaN[Si(CH_3)_3]_2$[46] and $Ca\{N(Si(CH_3)_3)_2\}_2{\cdot}THF_2$[47-49] were prepared by previously reported methods. (See ^1H NMR and ^{13}C NMR spectra for $NaN[Si(CH_3)_3]_2$ Figure C.30 and C.31 in Appendix C, for $Ca\{N(Si(CH_3)_3)_2\}_2{\cdot}THF_2$ see Figure C.32 and C.33). *Rac*-lactide was purchased from Alfa Aesar and dried over sodium sulfate in THF, recrystallized from toluene, then sublimed and stored under an inert atmosphere prior to use. Benzyl alcohol was purchased from Alfa Aesar and dried over activated 4 Å molecular sieves, distilled under reduced pressure and stored under nitrogen in an ampule prior to use.

5.4.2 Instrumentation

MALDI-TOF MS was performed using an Applied Biosystems 4800 MALDI TOF/TOF Analyzer equipped with a reflectron, delayed ion extraction and high performance nitrogen laser (200 Hz operating at 355 nm). 2,5-Dihydroxybenzoic acid (DHBA) was used as the matrix for the polymers. The matrix was dissolved in THF at a concentration of 10 mg/mL. Polymer was dissolved in THF at approximately 1 mg/mL. The matrix and polymer solutions were mixed together at ratios of 5 to 1, 4 to 1 or 3 to 1; 1 μL of this mixture was spotted on the MALDI plate and left to dry. Images of mass spectra were prepared using mMass™ software (www.mmass.org).

GPC analysis was performed either in $CHCl_3$ on a Viscotek VE 2001 GPCMax at 35 °C equipped with a Viscotek VE 3580 Refractive Index Detector or in THF at 25 °C on a Wyatt Triple Detection (triple angle light scattering, viscometry and refractive index) system with Agilent 1260 series sample and solvent handling. The Viscotek system used two Phenogel 5μ Linear Mixed Bed 300 × 4.60 mm columns whereas the Wyatt system used two Phenogel 10^3 Å 300 × 4.60 mm columns. Samples were prepared at a concentration of 2 mg/mL in $CHCl_3$ or 6 mg/mL in THF and left to equilibrate for ~2 h. The samples were filtered through syringe filters before analysis and eluted with HPLC grade solvents at flow rates of 0.30 mL/min with 100 μL injection volumes. For conventional calibration, six polystyrene standards (Viscotek) were used in making the calibration curve, bracketing molecular ranges from 1050 to 400 000 Da. A correction factor of 0.58 was used to calculate the M_n values obtained using the Viscotek instrument.[43] For the molecular weights determined by the Wyatt Triple Detection system, 0.49 mL/g was used as the dn/dc value.[50]

All NMR spectra were recorded on an AVANCE III 300. $CDCl_3$, DMSO-d_6, py-d_5 and were purchased from Cambridge Isotope Laboratories. $CDCl_3$ and DMSO-d_6 were dried over calcium hydride, whereas py-d_5 was dried over potassium, vacuum transferred and stored under nitrogen in ampules fitted with Teflon valves. THF-d_8 was purchased in ampules from Cambridge Isotope Laboratories, transferred into a glove box and the solvent was used without further purification. Elemental analyses were performed at Guelph Chemical Laboratories, Guelph, Ontario, Canada or at the Department of Ocean Sciences, Memorial University, St John's, Canada.

5.4.3 X-ray crystallography

Crystallographic and structure refinement data of **5.3**·THF and **5.4** are given in Table A3 in Appendix A. Single crystals of **5.3**·THF and **5.4** were mounted on a glass fibre using Paratone-N oil. All measurements were made on a Rigaku Saturn CCD area detector with a SHINE optic and graphite monochromated Mo-Kα radiation, and equipped with an X-stream 2000 low temperature system. All calculations were performed using the CrystalStructure software package[51] except for refinement, which was performed using SHELXL-97.[52]

For **5.3**·THF, H(2) was introduced in its difference map position and refined with Uiso = 1.5 Ueq of O(2). A distance restraint was applied to the O(2)-H(2) bond. For **5.4**, H(2) was introduced from its difference map position and allowed to refine isotropically and for position. All other hydrogen atoms were introduced in calculated positions and refined on a riding model. All non-hydrogen atoms were refined anisotropically. For **5.3**·THF, a one half-occupancy, disordered THF molecule is present about a two-fold screw axis (the symmetry operation (i) = x, y, z; (ii) = ½-x,

½-y, -z; (iii) 1-x, y, ½-z; (iv) ½+x, ½-y, ½+z must be applied to generate the full molecule.) Similarity restraints were applied to atoms in that molecule. H-atoms for the disordered THF could not be located from difference maps, and could not be satisfactorily introduced by calculation into ideal geometries, and were therefore omitted from the model. They have been included in the formula for the calculation of intensive properties. There is an intramolecular π-π interaction between one of the phenolate rings and the pyridyl pendant within one molecule. Plane to plane angle: 28.04(9)°. Plane centroid to plane centroid distance: 3.6709(19) Å. Plane to plane shift distance: 0.424(4) Å. There is intermolecular π-π interaction between two molecules which are not bonded via hydrogen bonding, that is between the hydrogen bonded dimers. One pyridyl group of such a dimer exhibits π-π interaction with another pyridyl group of another dimer. Plane to plane angle: 4.87(14)°. Plane centroid to plane centroid distance: 3.634(3) Å. Plane to plane shift distance: 0.417(5) Å.

5.4.4 Synthesis of compounds

H_2**[L1]**: Synthesis and characterization can be found in Chapter 2, Section 2.5.3.

5.1·THF: In the glove box, 4.02 g (8.16 mmol) of H_2[**L1**] was placed in a Schlenk flask in the glove box. 0.78 g (33.0 mmol) NaH was added to another Schlenk flask. 50 mL THF was transferred via cannula to each flask. The NaH suspension was cooled to −78 °C and the ligand solution was slowly transferred via cannula to the NaH suspension. Upon warming up to room temperature, the colour of the solution became bright yellow. The mixture was left to stir overnight, then,

filtered by cannula to remove the excess NaH. Volatiles were removed *in vacuo* yielding 4.15 g of beige powder which was washed with pentane. Yield = 99%. Anal. Calcd. for $C_{30}H_{38}N_2Na_2O_4$: C, 67.15; H, 7.14; N, 5.22; (for $C_{30}H_{38}N_2Na_2O_4 \cdot 0.55$ THF: C, 67.11; H, 7.42; N, 4.86). Found: C 67.11, H 7.39, N 4.82. ^{1}H NMR (300 MHz, 295 K, DMSO-d_6, δ): 8.16 (d, $^3J_{HH}$ = 4.08 Hz, Py*H*, 1H); 7.40 (dd, Py*H*, 1H); 7.19 (d, $^3J_{HH}$ = 7.82 Hz, Py*H*, 1H); 7.05 (d, $^4J_{HH}$ = 3.32 Hz, Ar*H*, 2H); 6.70 (d, $^4J_{HH}$ = 3.30 Hz, Ar*H*, 2H); 6.65 (dd, Py*H*, 1H); 4.67 (br s, CH_2, 2H); 4.04 (s, CH_2 (Py), 2H); 3.72 (s, O(CH_3), 6H); 3.30 (br s, CH_2, 2H); 1.59 (s, (CH_3)$_3$, 18H). ^{13}C{^{1}H} NMR (75.5 MHz, 298 K, DMSO-d_6, δ): 165.33 (Ar: *C*ONa); 160.60 (Ar: *C*OMe); 148.82 (Py: NC*C*H); 142.32 (Ar: *C*CH$_2$N); 135.84 (Py: NCCH*C*H); 135.52 (Py: N*C*); 124.23 (Ar: *C*CMe$_3$); 122.44 (Py: NCH*C*H); 120.81 (Py: N*C*H); 115.08 (Ar: *C*HCH$_2$N); 112.87 (Ar: *C*HCCMe$_3$); 62.57 (*C*H$_2$Py); 60.38 (*C*H$_2$Ar); 56.33 (O*Me*); 34.66 (*C*Me$_3$); 29.69 (C*Me*$_3$).

5.2: In the glove box, 2.62 g (5.30 mmol) of H_2[**L1**] was weighed and placed in a Schenk flask, transferred out of the glove box and attached to a Schlenk line. Then ~ 100 mL of THF was cannula transferred into the flask and and the solution was cooled to -78 ºC. ^{n}BuLi (1.6 M, 6.6 mL, 10.56 mmol) was slowly added via cannula. The mixture was left to warm to room temperature resulting in a yellow solution, which was stirred overnight. The volatiles were removed *in vacuo* and the product was washed with cold pentane yielding 2.49 g of light orange powder. Yield = 93%. Anal. Calcd. For $C_{30}H_{38}Li_2N_2O_4$: C 71.42, H 7.59, N 5.55. Found: C 71.27, H 7.88, N 5.34. ^{1}H NMR (300 MHz, 295K, py-d_5, δ): 8.16 (d, $^3J_{HH}$ = 4.64 Hz, Py: NC*H*, 1H); 7.20 (appears a singlet as a shoulder of the 7.22 py-d_5 peak, Py: NCHC*H*, 1H); 7.04 (d, $^4J_{HH}$ = 3.07 Hz, Ar: C*H*CCH$_2$N, 2H); 6.94 (appears d, $^3J_{HH}$ = 7.81 Hz, Py:

NCHCHC*H*, 1H); 6.80 (d, $^{4}J_{HH}$ = 3.08 Hz, Ar: C*H*CCMe$_3$, 2H); 6.75 (dd, coupling constants could not be determined due to overlap with the 6.80 Ar peak. Py: NCC*H*, 1H); 4.43 (d, $^{4}J_{HH}$ = 11.63 Hz, NC*H*$_2$Ar, 2H); 3.89 (s, NC*H*$_2$Py, 2H); 3.70 (s, OC*H*$_3$, 6H); 3.37 (d, $^{4}J_{HH}$ = 11.65 Hz, NC*H*$_2$Ar, 2H); 1.61 (s, C(C*H*$_3$)$_3$, 18H). ^{7}Li NMR (116.7 MHz, 298K, py-d$_5$) 4.37 (overlapping s, 1Li), width at half-height ($w_{1/2}$): 10.9 Hz; 4.25 (overlapping s, 1Li), $w_{1/2}$: 13.0 Hz. ^{13}C{^{1}H} NMR (75.5 MHz, 298 K, py-d$_5$, δ): 163.71 (Ar: *C*OLi); 162.18 (Ar: *C*OMe); 149.08 (Py: NC*C*H); 147.53 (Ar: *C*CH$_2$N); 138.65 (Py: NCCH*C*H); 137.38 (Py: N*C*); 127.57 (Ar: *C*CMe$_3$); 122.40 (Py: NCH*C*H); 122.01 (Py: N*C*H); 114.95 (Ar: *C*HCH$_2$N); 114.61 (Ar: *C*HCCMe$_3$); 68.29 (O*Me*); 63.47 (*C*H$_2$Py); 58.85 (*C*H$_2$Ar); 35.76 (*C*Me$_3$); 30.12 (C*Me*$_3$).

5.3·THF: In the glove box, 1.00 g (2.03 mmol) of H$_2$[**L1**] and 0.37 g (2.03 mmol) of NaN(Si(CH$_3$)$_3$)$_2$ were loaded into one Schlenk flask. The flask was transferred out and attached to a Schlenk line. Then it was cooled down to –20 °C in an ice/NaCl bath. 100 mL of THF was transferred by cannula and the mixture was warmed up to room temperature and stirred for ~ 1 h. Volatiles were removed *in vacuo* yielding 0.56 g of an off white powder. Yield = 54%. Anal. calc'd for C$_{30}$H$_{39}$N$_2$NaO$_4$: C 70.02, H 7.64, N 5.44. Found: C 69.59, H 7.75, N 5.25. ^{1}H NMR (300 MHz, 298 K, DMSO-d$_6$, δ): 12.39 (s, O*H*, 1H); 8.46 (br = broad) br s, Py: NC*H*, 1H); 7.69 (br s, Py: NCHC*H*, 1H); 7.47 (br s, Py: NCCHC*H*, 1H); 7.20 (br s, NCC*H*, 1H); 6.50 (br s, Ar: C*H*CCH$_2$N, 2H); 6.41 (br s, C*H*CCMe$_3$, 1H); 3.70 (s, NC*H*$_2$Py, 2H); 3.60 (s, NC*H*$_2$Ar, 4H); 3.56 (s, O*Me*, 6H); 1.35 (s, C*Me*$_3$, 18H). ^{13}C{^{1}H} NMR (75.5 MHz, 298 K, DMSO-d$_6$, δ): 159.64 (*C*ONa); 152.12 (Ar: *C*OMe); 151.62 (Ar: *C*CH$_2$N); 148.38 (Py: NC*C*H); 137.02 (Py: N*C*); 136.34 (Py: NCCH*C*H); 124.79 (Py: N*C*H); 123.10 (Py: NCH*C*H); 113.24 (Ar: *C*CMe$_3$); 112.31 (Ar: *C*HCH$_2$N); 112.15

(Ar: *C*HCCMe$_3$); 56.98 (*C*H$_2$Py); 56.83 (*C*H$_2$Ar); 55.50 (O*Me*); 34.62 (*C*Me$_3$); 29.58 (C*Me*$_3$).

5.4: In the glove box, 1.50 g (3.05 mmol) of H$_2$[**L1**] and 0.51 g (3.05 mmol) LiN(Si(CH$_3$)$_3$)$_2$ were loaded into one Schlenk flask. The flask was attached to the Schlenk line and cooled down to – 78 °C. 100 mL of THF was transferred to the flask by cannula and the mixture was warmed up to room temperature and stirred overnight. Volatiles from the light yellow solution were removed *in vacuo* to yield 1.14 g of a pale yellow powder. Yield = 75%. Anal. calc'd for C$_{30}$H$_{39}$LiN$_2$O$_4$: C 72.27, H 7.88, N 5.62. Found: C 70.21, H 8.01, N 5.37. The lower than expected %C is attributed to THF and residual LiN[Si(CH$_3$)$_3$]$_2$ contamination (for C$_{30}$H$_{39}$LiN$_2$O$_4$·0.3 THF·0.2 LiN[Si(CH$_3$)$_3$]$_2$: C 70.28, H 8.19, N 5.57). ^{1}H NMR (300 MHz, 378 K, DMSO-d$_6$, δ): 9.69 (br s, O*H*, 1H) 8.21 (br s, Py: NC*H*, 1H); 7.52 (br s, Py: NCHC*H*, 1H); 7.03 (br s, Py: NCHCHC*H* and NCC*H*, 2H); 6.50 (br s, Ar: C*H*CCH$_2$N, 2H); 6.42 (br s, Ar: C*H*CCMe$_3$, 2H); 3.69 (d, s, NC*H*$_2$Py, 2H); 3.64 (s, NC*H*$_2$Ar, 4H); 3.57 (s. OC*H*$_3$, 6H); 1.37 (s, C(C*H*$_3$)$_3$, 18H). (300 MHz, 298 K, THF-d$_8$, δ, (C = corresponding to complex, L = corresponding to ligand)): 10.23 (s, O*H*, 1H, (L)); 8.67 (d, $^3J_{HH}$ = 4.46 Hz, py: NC*H*, 0.67H, (L)); 7.87 (d, $^3J_{HH}$ = 4.65 Hz, py: NC*H*, 1H, (C)); 7.76 (a t, $^3J_{HH}$ = 7.10 Hz, py: NCHC*H*, 0.68H, (L)); 7.35 (a t, two peaks together: py: NCHCHC*H* (L) and py: NCHC*H* (C), 1.68H); 7.25 (d, $^3J_{HH}$ = 7.78 Hz, py: NCC*H*, 0.72H, (L)); 6.89 (d, $^3J_{HH}$ = 7.82 Hz, py: NCHCHC*H*, 1H, (C)); 6.75 (with a minor shoulder at 6.78 ppm, two peaks together: py: NCC*H* (C) and Ar: C*H*CCH$_2$N (L), 2.46H); 6.54 (d, $^4J_{HH}$ = 2.75 Hz, Ar: C*H*CCMe$_3$, 1.43H (L)); 6.47 (d, $^4J_{HH}$ = 3.12 Hz, C*H*CCH$_2$N, 2H (C)); 6.30 (d, $^4J_{HH}$ = 3.08 Hz, C*H*CCMe$_3$, 2H (C)); 4.32 (d, $^4J_{HH}$ = 11.50 Hz, NC*H*$_2$Ar, 2H (C)); 3.84 (s, NC*H*$_2$Py, 1.51H, (L)); 3.76 (s,

two peaks together: NCH_2Py (C) and NCH_2Ar (L), 4.84H); 3.67 (s, OCH_3 (L), 4.58H); 3.50 (s, OCH_3 (C), 6H); 3.18 (d, $^4J_{HH}$ = 11.45 Hz, NCH_2Ar, 2H (C)); 1.43 (s, C(CH_3)$_3$, 18H (C)); 1.38 (s, C(CH_3)$_3$, 14H, (L)).

5.5: In the glove box, 1.97 g (4.00 mmol) of H_2[**L1**] was loaded into a Schlenk flask and dissolved in ~ 70 mL of toluene. KN[Si(CH_3)$_3$]$_2$ (yellow solution in toluene, 0.5 M, 8.0 mL, 4.00 mmol) was slowly via syringe. Upon addition of KN[Si(CH_3)$_3$]$_2$ addition, a white precipitate started to form in the flask turning into a cloudy yellow suspension after complete addition of KN[Si(CH_3)$_3$]$_2$. The mixture was stirred overnight. Volatiles were removed *in vacuo* yielding 2.12 g of a beige product. Yield = 86%. Note: The product is very air sensitive. Exposure of the material to air causes brown discoloration. Anal. Calcd. For $C_{30}H_{39}KN_2O_4$: C 67.89, H 7.41, N 5.28. Found: C 66.19, H 7.71, N 4.81. The lower than expected %C is attributed to toluene and residual KN[Si(CH_3)$_3$]$_2$ contamination (for $C_{30}H_{39}KN_2O_4$·0.8 C_7H_8·0.45 KN[Si(CH_3)$_3$]$_2$: C 66.26, H 7.77, N 4.94). ^{1}H NMR (300 MHz, 295 K, DMSO-d$_6$, δ): 13.41 (s, O*H*, 1H); 8.45 (d, $^3J_{HH}$ = 4.88, NC*H*, 1H); 7.69 (ddd, $^3J_{HH}$ = 7.70, $^4J_{HH}$ = 1.80, NCHC*H*, 1H); 7.59 (d, $^3J_{HH}$ = 7.81, NCCHC*H*, 1H); 7.19 (ddd, coupling constants could not be determined accurately due to interfering residual toluene peaks, Py: NCC*H*, 1H); 6.50 (d, $^4J_{HH}$ = 3.23, Ar: C*H*CCH$_2$N, 2H); 6.38 (d, $^4J_{HH}$ = 3.18, Ar: C*H*CCMe$_3$, 2H); 3.71 (s, NCH_2Py, 2H); 3.63 (s, NCH_2Ar, 4H); 3.56 (s, OCH_3, 6H); 1.37 (C(CH_3)$_3$, 18H). ^{13}C{^{1}H} NMR (75.5 MHz, 298 K, DMSO-d$_6$, δ): 160.57 (Ar: *C*OK); 156.80 (Ar: *C*OMe); 148.22 (Ar: *C*CH$_2$N); 147.10 (Py: NC*C*H); 137.29 (Py: N*C*); 136.09 (Py: NCCH*C*H); 125.64 (Py: NCH*C*H); 123.33 (Py: N*C*H); 121.62 (Ar: *C*CMe$_3$); 113.05 (Ar: *C*HCCH$_2$N); 111.84 (Ar: *C*HCCMe$_3$); 59.64 (*C*H$_2$Py); 55.42 (*C*H$_2$Ar); 54.16 (O*Me*); 34.66 (*C*Me$_3$), 29.62 (C*Me*$_3$).

5.6·THF: *Method A*: In the glove box, 2.50 g (5.07 mmol) of H_2[**L1**] and 1.86 g (10.14 mmol) of $NaN[Si(CH_3)_3]_2$ were loaded into a Schlenk flask, transferred out of the glove box and attached to a Schlenk line. 100 mL of THF was transferred by cannula into the flask to give a yellow solution, which was left to stir overnight. 1.49 g (5.05 mmol) of CaI_2 was placed in another Schlenk flask and the yellow solution containing Na_2[**L1**] was added to it via cannula. The yellow solution was cannula transferred to the flask containing the CaI_2. The mixture was left to stir overnight giving a dark yellow solution. Volatiles were removed *in vacuo* yielding a pale yellow residue, which was extracted into CH_2Cl_2, filtered and dried *in vacuo* yielding 2.99 g of pale green solid, which was identified as **5.6**·1.5 THF. Yield = 92%. Anal. Calcd. For $C_{30}H_{38}CaN_2O_4$: C 63.13, H 6.71, N 4.91. Found: C 61.16, H 7.18, N 4.10. The lower than expected %C is attributed to the presence of THF and residual NaI contamination (e.g. anal. calc'd for $C_{30}H_{38}CaN_2O_4$·1.4 THF·0.45 NaI: C 61.16, H 7.09, N 4.01). ^{1}H NMR (300 MHz, 295K, DMSO-d_6, δ): 8.18 d (Py: NC*H*, 1H); 7.33 ddd (Py: NCHC*H*, 1H); 6.88 ddd (Py: NCCHC*H*, 1H); 6.62 d (Py: NCC*H*, 1H); 6.40 d (Ar: C*H*CCH$_2$N, 2H); 6.32 d (Ar: C*H*CCMe$_3$, 2H); 4.11 d (NC*H*$_2$Ar, 2H); 3.52 s (O*Me*, 6H); 3.44 s (NC*H*$_2$Py, 2H); 2.97 d (NCH2Ar, 2H); 1.22 s (C*Me*$_3$, 18H). ^{13}C{^{1}H} NMR (75.5 MHz, 298 K, DMSO-d_6, δ): 162.60 (Ar: *C*OCa); 159.71 (Ar: *C*OMe); 148.15 (Py: NC*C*H); 144.40 (Py: *C*CH$_2$N); 136.51 (Py: NCCH*C*H); 135.49 (Py: N*C*); 123.21 (Ar: *C*CMe$_3$); 121.24 (Py: N*C*H); 120.40 (Py: NCH*C*H); 114.33 (*C*HCCH$_2$N); 113.32 (*C*HCCMe$_3$); 62.59 (N*C*H$_2$Py); 56.14 (N*C*H$_2$Ar); 56.06 (O*Me*); 34.45 (*C*Me$_3$); 29.46 (C*Me*$_3$).

5.6·THF: *Method B*: In the glove box, 1.025 g (2.03 mmol) $Ca\{N(Si(CH_3)_3)_2\}_2$·THF_2 and 1.00 g (2.03 mmol) of H_2[**L1**] were loaded into a

Schlenk flask. 50 mL toluene was added to the solids and the mixture stirred for 12 h. Volatiles were removed *in vacuo* to give 1.057 g of a yellow residue. Yield: 82%. ^{1}H NMR (300 MHz, 295 K, C_6D_6, δ): 0.37 (s, (CH_3)$_3$, 36H), 1.26 (m, CH_2 (THF), 8H), 3.58 (m, CH_2 (THF), 8H), see Figure C.32 in Appendix C. ^{13}C{^{1}H} NMR (75.5 MHz, 298 K, C_6D_6, δ): 6.25 ((CH_3)$_3$), 25.29 (CH_2 (THF)), 70.11 (CH_2 (THF)), see Figure C.33 in Appendix C.

5.4.5 Polymerization procedure

Melt polymerization: A representative polymerization with a 100:1 [*rac*-lactide]:[**5.1**·THF] ratio was carried out with 500 mg (3.47 mmol) *rac*-lactide and 17.9 mg (3.47×10^{-5} mol) of **5.3**·THF weighed into a 10 mL scintillation vial equipped with a small stir bar in the glove box. The closed vial was removed from the glove box and placed into an aluminum block vial holder, which was pre-heated on a hotplate to 125 °C. A typical polymerization was run for 30, 60 or 100 minutes. The vial was then placed in an ice bath to halt the reaction and solidify the contents. The solids were dissolved in dichloromethane or chloroform and the polymer was precipitated with acidified methanol. Centrifugation was applied where needed for better separation of the solids. Solvents were decanted and the white solids were dried *in vacuo* followed by drying in a vacuum oven at 40 °C overnight.

Solution polymerization: The appropriate amount of **5.3** and alcohol (BnOH) were placed in an ampule equipped with a PTFE valve. A second ampule was prepared containing a stir bar and the required amount of *rac*-lactide and toluene (15 mL). Both ampules were attached to a Schlenk line and then the complex/BnOH solution was transferred by cannula into the lactide solution. Timing of the reaction

began when all the initiator solution was transferred. An aliquot of the reaction mixture was taken for ^{1}H NMR analysis at specified time intervals. When the presence of monomer was no longer apparent by ^{1}H NMR, volatiles were removed *in vacuo* and the solid residue was dissolved in CH_2Cl_2 and precipitated using cold acidified methanol. Solvents were decanted and the white solids were dried *in vacuo* followed by drying in a vacuum oven at 40 °C overnight.

5.4.6 NMR sample preparation for the study by ^{7}Li NMR spectroscopy

The concentration of the samples was kept the same in each case: 0.1067 mol/L. A representative sample preparation: 35 mg (7.0198×10^{-5} mol) of **5.4** was weighed on an analytical balance in the glove box. The mass of 658 μL DMSO-d_6 was calculated based on its density and was weighed on an analytical balance. The solid was added to the solvent and the solution was transferred and sealed in a J. Young NMR tube.

5.5 References

1. S. Dutta; W.-C. Hung; B.-H. Huang; C.-C. Lin *Adv. Polym. Sci.* **2012**, *245*, 219-283.

2. R. H. Platel; L. M. Hodgson; C. K. Williams *Polym. Rev.* **2008**, *48*, 11-63.

3. J. Wu; T.-L. Yu; C.-T. Chen; C.-C. Lin *Coord. Chem. Rev.* **2006**, *250*, 602-626.

4. A. Weisman; B. Chou; J. O'Brien; K. J. Shea *Adv. Drug Delivery Rev.* **2015**, *90*, 81-100.

5. M. L. Hsueh; B. H. Huang; J. C. Wu; C. C. Lin *Macromolecules* **2005**, *38*, 9482-9487.

6. C. A. Huang; C. T. Chen *Dalton Trans.* **2007**, 5561-5566.

7. R. K. Dean; A. M. Reckling; H. Chen; L. N. Dawe; C. M. Schneider; C. M. Kozak *Dalton Trans.* **2013**, 3504-3530.

8. F. M. Garcia-Valle; R. Estivill; C. Gallegos; T. Cuenca; M. E. G. Mosquera; V. Tabernero; J. Cano *Organometallics* **2015**, *34*, 477-487.

9. Y. Huang; Y.-H. Tsai; W.-C. Hung; C.-S. Lin; W. Wang; J.-H. Huang; S. Dutta; C.-C. Lin *Inorg. Chem.* **2010**, *49*, 9416-9425.

10. W.-Y. Lu; M.-W. Hsiao; S. C. N. Hsu; W.-T. Peng; Y.-J. Chang; Y.-C. Tsou; T.-Y. Wu; Y.-C. Lai; Y. Chen; H.-Y. Chen *Dalton Trans.* **2012**, *41*, 3659-3667.

11. J. Zhang; C. Jian; Y. Gao; L. Wang; N. Tang; J. Wu *Inorg. Chem.* **2012**, *51*, 13380-13389.

12. L. Chen; L. Jia; F. Cheng; L. Wang; C.-c. Lin; J. Wu; N. Tang *Inorg. Chem. Commun.* **2011**, *14*, 26-30.

13. X. Pan; A. Liu; X. Yang; J. Wu; N. Tang *Inorg. Chem. Commun.* **2010**, *13*, 376-379.

14. Y. Sun; J. Xiong; Z. Dai; X. Pan; N. Tang; J. Wu *Inorg. Chem.* **2016**, *55*, 136-143.

15. M. H. Chisholm; J. Gallucci; K. Phomphrai *Chem. Commun.* **2003**, 48-49.

16. M. H. Chisholm; J. C. Gallucci; K. Phomphrai *Inorg. Chem.* **2004**, *43*, 6717-6725.

17. Y. Sarazin; R. H. Howard; D. L. Hughes; S. M. Humphrey; M. Bochmann *Dalton Trans.* **2006**, 340-350.

18. F. M. Kerton; S. Holloway; A. Power; R. G. Soper; K. Sheridan; J. M. Lynam; A. C. Whitwood; C. E. Willans *Can. J. Chem.* **2008**, *86*, 435-443.

19. S. Menage; G. Gellon; J.-L. Pierre; D. Zurita; E. Saint-Aman *Bull. Soc. Chim. Fr.* **1997**, *134*, 785-791.

20. S. Heidari; E. Safaei; A. Wojtczak; P. Cotic; A. Kozakiewicz *Polyhedron* **2013**, *55*, 109-116.

21. K. Devaine-Pressing; J. H. Lehr; M. E. Pratt; L. N. Dawe; A. A. Sarjeant; C. M. Kozak *Dalton Trans.* **2015**, *44*, 12365-12375.

22. R. K. Dean; A. M. Reckling; H. Chen; L. N. Dawe; C. M. Schneider; C. M. Kozak *Dalton Trans.* **2013**, *42*, 3504-3520.

23. R. K. Dean; S. L. Granville; L. N. Dawe; A. Decken; K. M. Hattenhauer; C. M. Kozak *Dalton Trans.* **2010**, *39*, 548-559.

24. R. E. Mulvey *Chem. Soc. Rev.* **1998**, *27*, 339-346.

25. Z. Janas; T. Nerkowski; E. Kober; L. B. Jerzykiewicz; T. Lis *Dalton Trans.* **2012**, *41*, 442-447.

26. J. Char; O. G. Kulyk; E. Brule; F. de Montigny; V. Guerineau; T. Roisnel; M. J. L. Tschan; C. M. Thomas *C. R. Chim.* **2016**, *19*, 167-172.

27. D. L. Pavia *Introduction to Spectroscopy*; 4th ed.; Brooks/Cole, Cengage Learning: Australia, Belmont, CA, 2009.

28. J. K. M. Sanders; B. K. Hunter *Modern NMR Spectroscopy: a guide for chemists*; 2nd ed.; Oxford University Press: Oxford Toronto, 1993.

29. H.-Y. Chen; J. Zhang; C.-C. Lin; J. H. Reibenspies; S. A. Miller *Green Chem.* **2007**, *9*, 1038-1040.

30. A. W. Addison; T. N. Rao; J. Reedijk; J. van Rijn; G. C. Verschoor *J. Chem. Soc., Dalton Trans.* **1984**, 1349.

31. D. Alhashmialameer; N. Ikpo; J. Collins; L. N. Dawe; K. Hattenhauer; F. M. Kerton *Dalton Trans.* **2015**, *44*, 20216-20231.

32. Y. Huang; Y.-H. Tsai; W.-C. Hung; C.-S. Lin; W. Wang; J.-H. Huang; S. Dutta; C.-C. Lin *Inorg. Chem.* **2010**, *49*, 9416-9425.

33. H.-Y. Chen; J. Zhang; C.-C. Lin; J. H. Reibenspies; S. A. Miller *Green Chem.* **2007**, *9*, 1038-1040.

34. L. Yang; D. R. Powell; R. P. Houser *Dalton Trans.* **2007**, 955-964.

35. A. Okuniewski; D. Rosiak; J. Chojnacki; B. Becker *Polyhedron* **2015**, *90*, 47-57.

36. Z. Janas; T. Nerkowski; E. Kober; L. B. Jerzykiewicz; T. Lis *Dalton Trans.* **2012**, *41*, 442-447.

37. C.-A. Huang; C.-L. Ho; C.-T. Chen *Dalton Trans.* **2008**, 3502-3510.

38. B. Y. Kimura; T. L. Brown *J. Organometal. Chem.* **1971**, *26*, 57-67.

39. U. Wannagat *Advan. Inorg. Chem. Radiochem.* **1964**, *6*, 225-278.

40. A. C. Silvino; D. B. A. T. Martins; A. C. Rodrigues; M. L. Dias *J. Polym. Environ.* **2013**, *21*, 1002-1008.

41. C. Paetz; R. Hagen *Chem. Ing. Tech.* **2014**, *86*, 519-523.

42. S. Vouyiouka; P. Theodoulou; A. Symeonidou; C. D. Papaspyrides; R. Pfaendner *Polym. Degrad. Stab.* **2013**, *98*, 2473-2481.

43. J. Baran; A. Duda; A. Kowalski; R. Szymanski; S. Penczek *Macromol. Rapid Commun.* **1997**, *18*, 325-333.

44. H.-Y. Chen; L. Mialon; K. A. Abboud; S. A. Miller *Organometallics* **2012**, *31*, 5252-5261.

45. C. Gallegos; V. Tabernero; M. E. G. Mosquera; T. Cuenca; J. Cano *Eur. J. Inorg. Chem.* **2015**, *2015*, 5124-5132.

46. H. Buerger; C. Forker; J. Goubeau *Monatsh. Chem.* **1965**, *96*, 597-601.

47. J. M. Boncella; C. J. Coston; J. K. Cammack *Polyhedron* **1991**, *10*, 769-770.

48. M. Westerhausen *Inorg. Chem.* **1991**, *30*, 96-101.

49. Y. Sarazin; R. H. Howard; D. L. Hughes; S. M. Humphrey; M. Bochmann *Dalton Trans.* **2006**, 340-350.

50. R. Walkenhorst *LC-GC Eur.* **2001**, *14*, 676-678.

51. *CrystalStructure 3.7.0: Crystal Structure Analysis Package*, Rigaku and Rigaku/MSC, The Woodlands, TX, 2000-2005.

52. G. M. Sheldrick *Acta Crystallogr. Sect. A* **2008**, *64*, 112-122.

Chapter 6 Additional and Attempted Experiments, and Suggestions for Future Work

6.1 Introduction

This chapter includes details about additional syntheses and experiments that were performed but for which only preliminary results have been obtained to date. They are included here for the purpose of providing starting points for subsequent researchers in the group who may further develop this chemistry. Two new chromium(III) complexes were synthesized and tested in CO_2/CHO copolymerization but their activity was inferior to the previously synthesized complexes, **2.1**·THF and **2.1**·DMAP. Further modifications of the complexes may influence their catalytic activity. Magnesium complex **4.1** was tested in CHO/CO_2 copolymerization, which was unfortunately unsuccessful. This chapter also includes some suggestions for future students on how to modify the complexes in order to be able to improve their catalytic activity.

6.2 Preparation of new chromium(III) complexes and their activity in CHO/CO_2 copolymerization

6.2.1 Preparation of 6.1·THF and its activity

The protio ligand 2-tetrahydrofurfuryl-methylamino-*N*,*N*-bis(2-hydroxy-3-*tert*-butyl-5-methoxyphenol) (H_2[**L4**]) was prepared via a modified Mannich condensation and using water as the reaction medium instead of methanol. Elemental analysis showed good agreement with the calculated, expected results (see Experimental section). The amino-bis(phenolato) chromium(III) complex **6.1**·THF

can be synthesized the same way as **2.1**·THF and **2.2**·THF (Chapter 2) by salt metathesis using the alkali-metallated amino-bis(phenolate). H_2[**L4**] was reacted with ^{n}BuLi at –78 °C in THF to afford its Li salt, which was then reacted with $CrCl_3(THF)_3$ at –78 °C in THF (Scheme 6-1) to yield a dark green solid.

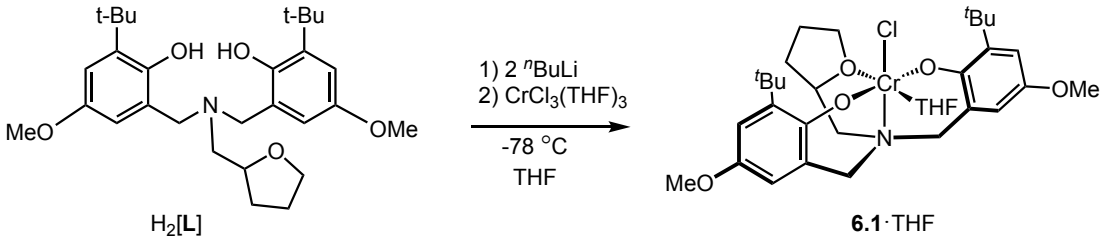

Scheme 6-1 Synthesis of **6.1**·THF.

Crystals of **6.1**·THF suitable for X-ray diffraction were grown via slow evaporation of a toluene/THF solvent mixture. The molecular structure is shown in Figure 6.1 and crystallographic and structure refinement data are given in Table A-4 in Appendix A.

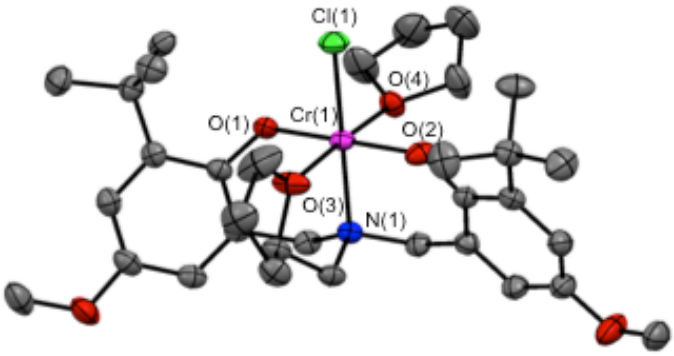

Figure 6.1 Partially labeled molecular structure of **6.1**·THF. Thermal ellipsoids are drawn at 50% probability and H atoms are excluded for clarity.

The distorted octahedral geometry of **6.1**·THF is very similar to the structure of a related chromium(III) complex also bearing a tetrahydrofurfuryl donor, but with two *tert*-butyl groups at the phenolates (complex **1.20**, Figure 1.9, Chapter 1, Section 1.1.5). Complex **1.20** was previously synthesized and characterized by Kozak and co-

workers.[1] The bond distances and angles of **6.1**·THF show good agreement with those of **1.20** (Table 6-1). Comparing the bond lengths of **6.1**·THF to the complexes with the pyridyl donor, the Cr(1)–Cl(1) bond distance in **6.1**·THF (2.3280(18) Å) is shorter than in **2.1**·THF (2.3463(9) Å) and **2.1**·DMAP (2.3386(11) Å) but longer than in **2.2**·THF (2.319(2) Å). The longer Cr(1)–Cl(1) distance might be one of the reasons for the superior activity of **2.1**·THF and **2.1**·DMAP meaning easier chloride dissociation and hence epoxide coordination in copolymerization.

Table 6-1 Selected bond lengths (Å) and bond angles (°) of **6.1**·THF and **1.20**.

	6.1·THF	**1.20**
Cr(1)–O(1)	1.924(2)	1.911(2)
Cr(1)–O(2)	1.913(2)	1.937(2)
Cr(1)–O(3)	2.011(2)	2.020(2)
Cr(1)–O(4)	2.0554(19)	2.048(2)
Cr(1)–N(1)	2.112(2)	2.124(3)
Cr(1)–Cl(1)	2.3280(18)	2.3394(9)
O(1)–Cr(1)–O(2)	178.01(7)	176.39(10)
O(1)–Cr(1)–O(3)	91.02(10)	90.99(10)
O(2)–Cr(1)–O(3)	90.43(10)	92.19(11)
O(1)–Cr(1)–O(4)	86.73(9)	86.81(9)
O(2)–Cr(1)–O(4)	91.69(9)	89.90(9)
O(3)–Cr(1)–O(4)	173.95(7)	175.51(9)
O(2)–Cr(1)–N(1)	87.56(7)	90.70(9)
O(1)–Cr(1)–N(1)	91.35(7)	88.14(9)
O(3)–Cr(1)–N(1)	79.91(7)	80.33(9)
O(4)–Cr(1)–N(1)	94.52(7)	95.78(9)
O(1)–Cr(1)–Cl(1)	91.65(5)	88.88(7)
O(2)–Cr(1)–Cl(1)	89.57(5)	92.65(7)
O(3)–Cr(1)–Cl(1)	95.54(6)	93.22(7)
O(4)–Cr(1)–Cl(1)	90.14(5)	90.79(7)
N(1)–Cr(1)–Cl(1)	174.60(5)	172.78(7)

The complex is different from **2.1**·THF and **2.2**·THF in that instead of two nitrogen donors, there is only one in **6.1**·THF and that the tetrahydrofurfuryl pendant also provides an oxygen donor resulting in four oxygens at the equatorial sites coordinated to the chromium. Copolymerization of CHO/CO_2 was carried out with **6.1**·THF (0.2 mol% catalyst loading) with DMAP as co-catalyst under 40 bar CO_2

and 60 °C for 24 h to compare the activity of **6.1**·THF to **2.1**·THF. The conversion of the reaction was quite low, 31% (Figure C34), as opposed to 82% with **2.1**·THF. **6.1**·THF proved to be inferior, so no further experiments were carried out with it. **1.20** produced 76% conversion with $PPNN_3$ under 41 bar CO_2, 60 °C and 24 h. The molecular weight, however, was quite low (6400 g/mol) and the dispersity value was quite high (1.42).[2] The shape of the reactor vessel seems to influence the outcome of a reaction in terms of activity and conversion.[15] Hence, a vessel with a wider diameter proved to be more beneficial than a vessel of the same volume with a smaller diameter (narrower base). The lower conversion produced by **6.1**·THF was carried out in the reactor with the narrower vessel, therefore, it would be worth repeating the experiment in the reactor with the wider vessel to see whether the shape of the vessel really has a positive effect on the outcome of the reaction.

6.2.2 Preparation of a chromium(III) amine-bis(phenolate) complex with an acetate group (6.2) and its activity for CHO/CO_2 copolymerization

6.2 was prepared by reacting **2.1**·THF with silver acetate (AgOAc) in dichloromethane (CH_2Cl_2) for 3 days according to Scheme 6-2. Upon mixing the solution of **2.1**·THF with the AgOAc solution, a precipitate formed and the mixture became cloudy. Slowly, a grey coloured solid residue appeared inside the flask. After filtering the solution and removing the solvent, a brown crystalline solid was obtained.

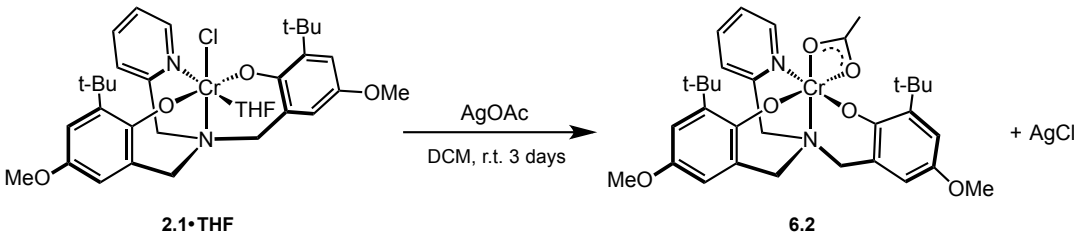

2.1•THF **6.2**

Scheme 6-2 Synthesis of **6.2**.

Unfortunately, crystals suitable for X-ray diffraction could not be obtained and the results of the elemental analysis of **6.2** did not support the structure, either. MALDI-TOF MS, however, showed a convincing spectrum with the highest intensity peak corresponding to the molecular ion of **6.2**. The full spectrum is shown in Figure 6.2 with an expanded region of the main peaks.

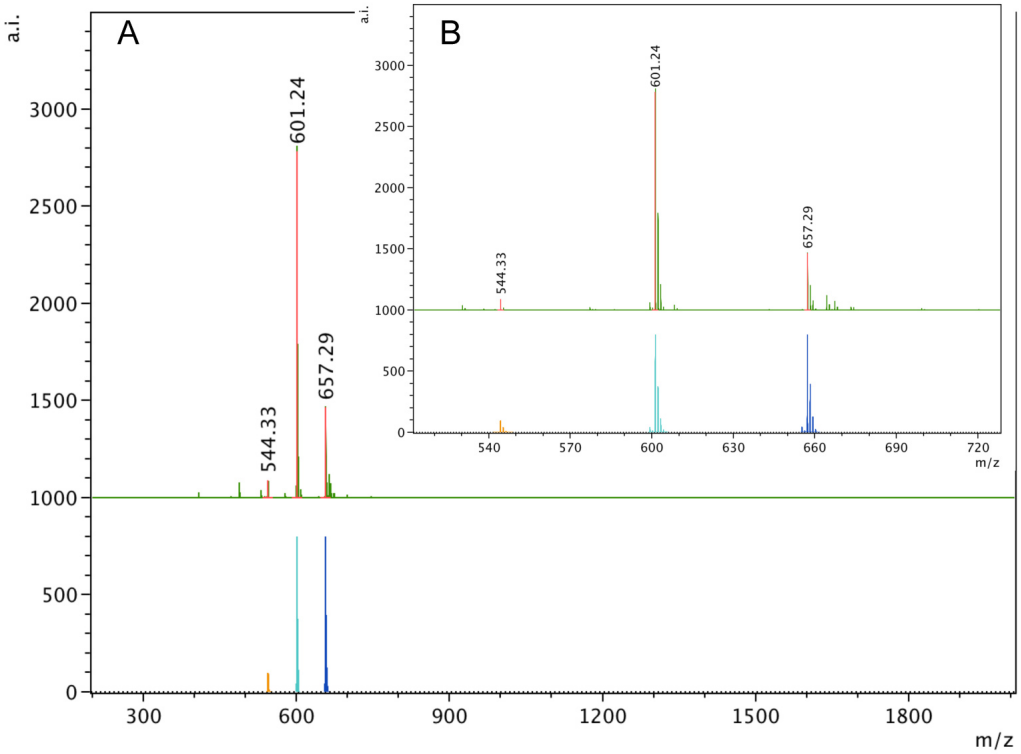

Figure 6.2 A) MALDI-TOF spectrum of **6.2** in *m/z* 200 to 2000 range. B) Expanded spectrum of the main peaks from *m/z* 500 – 700.

The ion at *m/z* 601.24 corresponds to the $[CrOAcL1]^{+\bullet}$ ion and the small peak at *m/z* 544.33 represents the complex after the acetate group is lost ($[CrL1]^{+}$). The

isotopic distribution of the experimental of $[CrOAcL1]^{+\bullet}$ (upper spectrum of Figure 6.3 A)) and $[CrL1]^{+}$ (upper spectrum of Figure 6.3 B)) are in good agreement with the calculated modeled peaks (lower spectra of Figure 6.3 A) and B)). The peak at *m/z* 657.29 most likely represents a $[CrAcL1(THF)]^{+\bullet}$ ion.

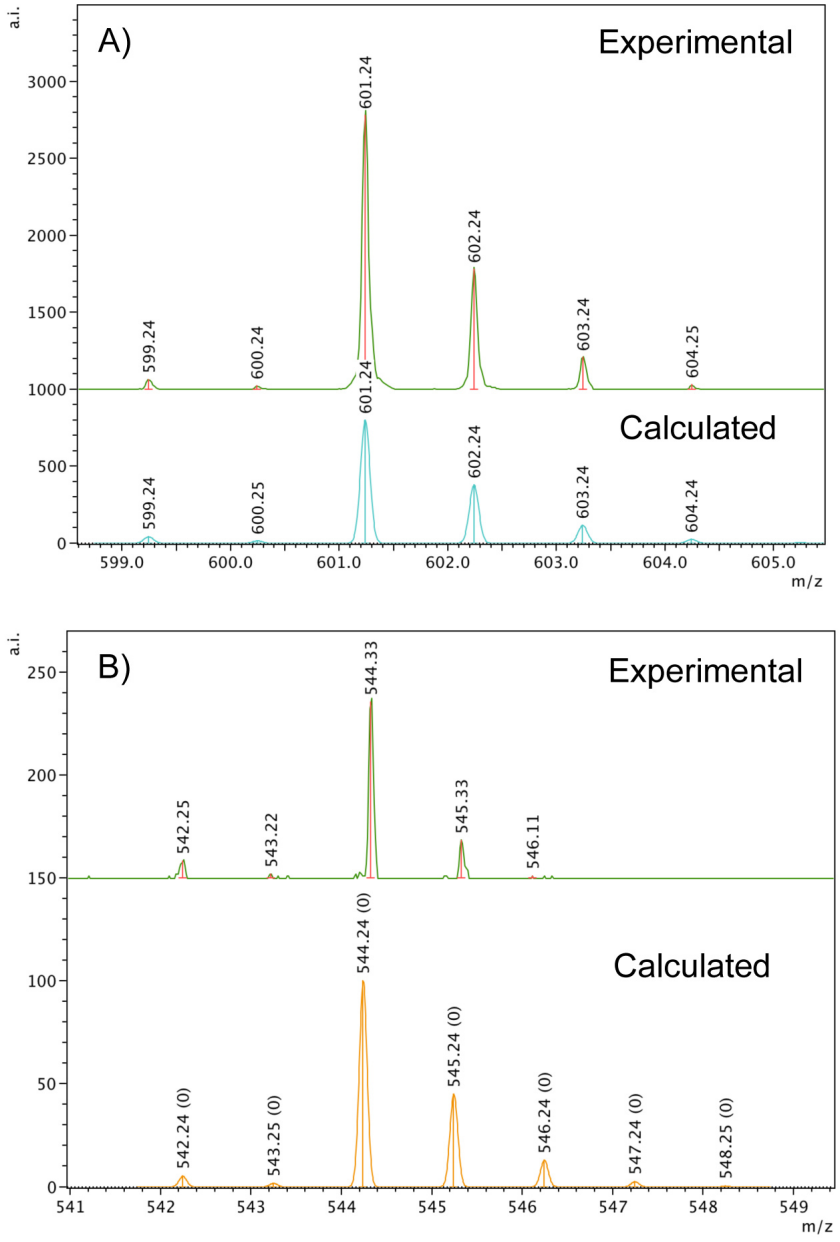

Figure 6.3 Expanded spectra of the peaks at *m/z* 601.24 and 544.33 with isotopic distribution patterns of the observed (experimental) and the calculated peaks.

The activity of **6.2** was tested in CHO/CO_2 copolymerization with DMAP as co-catalyst. The catalyst loading was kept at 0.2 mol%, and the conditions were 40 bar CO_2 and 60 °C for 24 h. ^{1}H NMR showed 79% conversion after the reaction and 61% yield of the polymer was isolated. It would be worth preparing the complex again and growing crystals to support the structure of **6.2**. Then, it would also be worth trying to perform the experiment without any co-catalyst added in order to see whether the chelating acetate group would be labile enough to act as a nucleophile and initiate ring opening of the epoxide. The lability of the acetate group could be enhanced with electron withdrawing groups on the acetate group. For example, using a trifluoroacetate group could result in a hemilabile ligand enhancing the catalytic activity of the complex.

6.3 Monomer screening with 2.1·THF and 2.1·DMAP

Copolymerization or coupling of limonene oxide and carbon dioxide was attempted with **2.1**·DMAP (0.2 mol% catalyst loading) at 40 bar pressure of CO_2, 60 °C for 24 h but no conversion of limonene oxide was observed. DMAP might be too big as a nucleophile for this coupling reaction because limonene oxide itself is bulkier than CHO and so, it is sensitive towards sterics in the ring opening step. The use of a chloride containing nucleophile, such as PPNCl with **2.1**·THF at higher catalyst loading (such as 1 mol%) and lower temperature (30 – 40 ºC) could be more favourable for this reaction.

Styrene oxide (SO) is typically poorly reactive to copolymerization with CO_2 and instead gives cyclic carbonates.[3,4] 65% conversion of styrene oxide to cyclic styrene carbonate (SC) was achieved previously with **1.21** (Figure 1.9, Chapter 1,

Section 1.1.5) and PPNCl when 45 bar CO_2 and 80 °C were applied for 18 h.[5] X. B. Lu and Darensbourg, however, were able to produce poly(styrene carbonate) (45% conversion) with a cobalt salen complex under 2 MPa CO_2, 25 °C and 3 h.[6,7] In order to see whether styrene oxide could be converted to polymer, **2.1**·THF (0.2 mol% catalyst loading) was used with $PPNN_3$ for 24 h at 40 bar CO_2 and 80 °C. Unfortunately, no polymer was formed and 59% conversion into cyclic styrene carbonate was observed (Figure C35 in Appendix C). The selectivity of polymer formation might be improved with PPNY [Y = 2,4-dinitrophenoxy] which was also utilized by Darensbourg and X. B. Lu. In fact, the selectivity toward poly(stryrene carbonate) was the highest, 99% when the complex was bearing a 2,4-dinitrophenoxy group. When the 2,4-dinitrophenoxy group was changed to chloride, polymer selectivity decreased to 58% and there was no polymer formed when the complex had a bromide group instead of the chloride.[6]

Copolymerization of propylene oxide (PO) with CO_2 usually results in polymer formation at lower temperatures and in cyclic carbonate at higher temperatures.[5,8-10] Therefore, experiments were performed at 25 °C and at 60 °C. Inconsistent with this, there was no polymer formed at 25 °C and 40 bar CO_2 after 24 h with **2.1**·DMAP (0.2 mol% catalyst loading). A mixture of poly(propylene carbonate) (PPC) (37%) and propylene carbonate (PC) (63%) was obtained at 60 °C when **2.1**·THF was used with 1 equiv. of DMAP and 40 bar CO_2 was applied for 24 h. Previously, product selectivity was established with **1.21** based on temperature,[5] so PO/CO_2 copolymerization with **2.1**·THF or **2.1**·DMAP was not investigated further. The ^{1}H NMR spectrum of an aliquot taken from the reaction mixture can be found as Figure C.36 in Appendix C.

6.4 Copolymerization attempts with 4.1

Di-magnesium compounds with macrocyclic ligands were reported to be capable of catalyzing CHO/CO_2 copolymerization.[11] The magnesium complex, **4.1**, that exhibited excellent activity in the ROP of *rac*-lactide[12] (also discussed in Chapter 4) was also tested in CHO/CO_2 copolymerizations in three trials.

6.4.1 CHO/CO_2 copolymerization with 4.1 and added nucleophiles

4.1 was used with 1 equiv. of DMAP under the typical conditions for CHO/CO_2 copolymerization, that is, 0.2 mol% catalyst loading, 40 bar CO_2 pressure and 60 °C for 24 h. When **4.1** dissolved in CHO, the colour of the solution became bright yellow, which stayed the same throughout the whole reaction as was revealed upon opening the reactor vessel. Consequently, no reaction occurred.

The ionic co-catalyst TBAB was used instead of the neutral DMAP under the same conditions described above but again, no activity was observed.

The third trial was attempted in two steps. First, no co-catalyst was added to the reaction but the catalyst loading was increased to 0.5 mol%, the temperature was increased to 90 °C and the CO_2 pressure to 50 bar. The reaction was left to run for 24 h. The next day, after opening the reactor vessel and taking a sample for NMR measurement, 1 equiv. of $PPNN_3$ was added to the solution and the mixture was subjected to a second experiment under 30 bar CO_2 pressure and 90 °C for another 24 h. Of course, for the second experiment, air free conditions could not be ensured as the sample was exposed to air after the first day of the reaction. No conversion was observed in either of the reactions as revealed by ^{1}H NMR.

The introduction of bulkier substituents on the pyridyl or the ethylene-dimethylamino group could favour monomeric Mg complex formation or help generating a vacant site easier for monomer coordination.

6.5 Experimental

6.5.1 General experimental conditions

Unless otherwise stated, all manipulations were performed under an atmosphere of dry oxygen-free nitrogen by using standard Schlenk techniques or using an MBraun Labmaster glove box. Cyclohexene oxide was purchased from Aldrich and freshly distilled from CaH_2 under N_2 atmosphere into an ampule. THF was purified by distillation from sodium/benzophenone ketyl under nitrogen. All other solvents were dried and degassed using an MBraun Manual Solvent Purification System. $CrCl_3(THF)_3$ and $PPNN_3$ were prepared via previously reported methods.[13,14] 99.998% (4.8 Supercritical fluid chromatography grade) CO_2 was supplied from Praxair in a high-pressure cylinder equipped with a liquid dip tube. All ^1H and $^{13}C\{^1H\}$ NMR spectra were obtained in $CDCl_3$ purchased from Cambridge Isotope Laboratories, Inc.

6.5.2 Instrumentation

^1H and $^{13}C\{^1H\}$ NMR spectra were recorded on a Bruker AVANCE III 300 MHz spectrometer. All copolymerization reactions were carried out in a 100 mL stainless steel Parr® 5500 autoclave reactor with a Parr 4836 controller. N.B. Caution should be taken when operating such high-pressure equipment. Elemental analysis was performed at Guelph Chemical Laboratories, Guelph, ON, Canada. MALDI-TOF

mass spectrometry was performed by using an Applied Biosystems 4800 MALDI-TOF/TOF Analyzer equipped with a reflectron, delayed extraction and high performance nitrogen laser (200 Hz operating at 355 nm). Anthracene was used as the matrix for analysis of **6.1**·THF. The matrix and complex were dissolved separately in toluene at concentrations of 10 mg/mL. The matrix and chromium complex solutions were combined in a 1:1 ratio and the mixture was spotted on the MALDI plate and left to dry. Samples were prepared in the glove box and sealed under nitrogen in a plastic bag for transport to the spectrometer.

6.5.3 Synthesis of compounds

H_2**[L4]**: 2-Aminomethyl-tetrahydrofuran (6.22 g, 0.0615 mol) was slowly added to a vigorously stirred mixture of 3-*tert*-butyl-5-hydroxyanisole (22.17 g, 0.123 mol) and formaldehyde (9.16 mL of a 37% aqueous solution, 0.123 mol) in deionized water (100 mL) in a round bottom flask equipped with a magnetic stir bar. This mixture was heated to reflux and stirred overnight. Upon cooling, a large quantity of orange solid formed. The solvent was decanted and the solid was washed with cold methanol then recrystallized from a chloroform/methanol solvent mixture to give 19.87 g of a beige crystalline powder. Yield = 67%. Anal. Calcd. For $C_{29}H_{43}NO_5$: C 71.72, H 8.92, N 2.88. Found: C 71.49, H 9.00, N 2.62. ^{1}H NMR (300 MHz, 298 K, $CDCl_3$, δ): 8.54 (br s, O*H*, 2H); 6.81 (dd, $^3J_{HH}$ = 3.1 Hz, Ar: C*H*CCH_2N, 2H); 6.47 (dd, $^3J_{HH}$ = 3.1 Hz, Ar: C*H*CMe_3, 2H); 4.21 (m, C*H*, 1H); 4.01 (m, C*H*HO, 1H); 3.89 (m, CH*H*O, 1H); 3.76 (m, NCH_2Ar, 4H); 3.74 (s, OCH_3, 6H); 2.56 (m, CH_2N, 2H); 1.88 (m, CH_2CH_2, 4H); 1.40 (s, C(CH_3)$_3$, 18H). ^{13}C{^{1}H} NMR (75 MHz, 298 K, $CDCl_3$, δ): 151.9 (Ar*C*OH); 149.5 (Ar*C*OMe); 138.6, (Ar*C*CMe_3); 122.9 (Ar*C*CH_2N);

113.4 (Ar*C*H); 112.5 (Ar*C*H); 68.5 (*C*H); 57.4 (*C*H_2O); 55.8 (N*C*H_2Ar); 55.8 (N*C*H_2CH) 35.1 (O*C*H_3); 29.6 (*C*H_2); 29.5 (*C*H_2); 25.3 (*C*H_3)$_3$.

6.1·THF: H_2[**L4**] (3.00 g, 6.20 mmol) was dissolved in THF (~50 mL) and cooled to -78 °C. ^{n}BuLi (1.6 M in hexanes, 8.52 mL, 13.64 mmol) was added dropwise to give a yellow solution, which was warmed to room temperature and further stirred for 2 h. This solution was transferred via cannula to a suspension of $CrCl_3(THF)_3$ (2.29 g, 6.20 mmol) in THF (~40 mL) cooled to –78 °C to give a dark green mixture. Upon warming to room temperature and stirring for 24 h the solids dissolved and the color darkened to deep dark green. The solvent was removed *in vacuo* and the solid residue was extracted into toluene. The solution was filtered through Celite and the solvent was removed *in vacuo*. The product was washed with pentane and dried to yield 3.50 g of green powder. Yield: 99%.

6.2: 0.5 g (0.87 mmol) **2.1**·THF was dissolved in ~ 30 mL dichloromethane in a Schlenk flask. 0.14 g (0.87 mmol) AgOAc was dissolved in dichloromethane in another Schlenk flask. The solution of **6.2** was cannula transferred to the flask containing the AgOAc. The flask was covered with aluminum foil to avoid Ag formation and left to stir at room temperature over the weekend for about 3 days. The solution was cannula filtered and the solvent was removed in vacuo. 0.28 g crystalline brown powder was obtained. Yield = 54%. Anal. Calcd for $C_{32}H_{41}CrN_2O_6$: C 63.88, H 6.87, N 4.66; Found: C 61.46, H 5.14, N 2.84.

6.6 References

1. R. K. Dean; S. L. Granville; L. N. Dawe; A. Decken; K. M. Hattenhauer; C. M. Kozak *Dalton Trans.* **2010**, *39*, 548-559.

2. H. Chen; L. N. Dawe; C. M. Kozak *Catal. Sci. Technol.* **2014**, *4*, 1547-1555.

3. J. Sun; S.-I. Fujita; F. Zhao; M. Arai *Green Chem.* **2004**, *6*, 613-616.

4. N. D. Harrold; Y. Li; M. H. Chisholm *Macromolecules* **2013**, *46*, 692-698.

5. R. K. Dean; K. Devaine-Pressing; L. N. Dawe; C. M. Kozak *Dalton Trans.* **2013**, *42*, 9233-9244.

6. G.-P. Wu; S.-H. Wei; X.-B. Lu; W.-M. Ren; D. J. Darensbourg *Macromolecules* **2010**, *43*, 9202-9204.

7. G. P. Wu; S. H. Wei; W. M. Ren; X. B. Lu; B. Li; Y. P. Zu; D. J. Darensbourg *Energy & Environmental Science* **2011**, *4*, 5084-5092.

8. D. J. Darensbourg; J. C. Yarbrough; C. Ortiz; C. C. Fang *J. Am. Chem. Soc.* **2003**, *125*, 7586-7591.

9. D. J. Darensbourg *Chem. Rev.* **2007**, *107*, 2388-2410.

10. Z. Q. Qin; C. M. Thomas; S. Lee; G. W. Coates *J. Am. Chem. Soc.* **2003**, *42*, 5484-5487.

11. M. R. Kember; C. K. Williams *J. Am. Chem. Soc.* **2012**, *134*, 15676-15679.

12. K. Devaine-Pressing; J. H. Lehr; M. E. Pratt; L. N. Dawe; A. A. Sarjeant; C. M. Kozak *Dalton Trans.* **2015**, *44*, 12365-12375.

13. J. H. So; P. Boudjouk *Inorg. Chem.* **1990**, *29*, 1592-1593.

14. K. D. Demadis; T. J. Meyer; P. S. White *Inorg. Chem.* **1998**, *37*, 3610-3619.

15. K. Ni; C. M. Kozak, *Unpublished results*.

Conclusions

Finding new, effective homogeneous catalysts for applications in novel polymer production is an ongoing area of research. Converting CO_2 into valuable products is another current research aim. The copolymerization of high free energy epoxides and CO_2 is a combination of both catalysis and CO_2 chemistry in the field of environmentally friendly polymer production. The first part of Chapter 1 presented a literature survey on both the advantages of catalysis and the conversion of carbon dioxide together with the array of existing chromium catalysts and their development toward cyclic and polycarbonate production. In addition, investigations and possibilities of the copolymerization reaction mechanism were also outlined based on the literature describing mainly three possibilities: a monometallic intramolecular, a monometallic intermolecular and a bimetallic pathway.

Utilization of renewable resources for biodegradable polymer production is an additional relevant field of study in order to avoid the exploitation of non-renewable petroleum resources and to ease the huge burden on the environment caused by non-degradable products. Lactide is an excellent example that can be derived from biomass and can be used for the production of the biodegradable and most importantly, biocompatible polylactide which finds numerous applications both in household objects and biomedical devices. Biocompatible metal complexes as catalysts are preferred over heavy metals, especially for polymer production toward biomedical applications. The second part of Chapter 1 introduced the beneficial aspects as well as the life cycle of polylactide, and a literature survey on appealing lithium-, sodium-, potassium-, magnesium- and calcium amine-bis(phenolate)

complexes that are capable of the ring opening polymerization of lactide. Additionally, mechanistic investigations of the ring opening reaction were also discussed based on the literature exploring two main possibilities: coordination insertion and activated monomer mechanisms.

Chapter 2 described three new chromium(III) amine-bis(phenolate) complexes bearing a more electron donating group at the *para* position of the phenolates with respect to the phenolate oxygens. Applying a methoxy group at this position resulted in electronically balanced chromium complexes (**2.1**·THF and **2.1**·DMAP) which were capable of selective poly(cyclohexene carbonate) production in consistently high yields (82%). In addition, **2.1**·THF and **2.1**·DMAP exhibited faster reaction rate compared to **1.21**. End group analysis of the polymers by MALDI-TOF MS was carried out in order to get insights into the initiation of the reaction. It revealed that epoxide ring opening is most likely initiated by the nucleophile of the added co-catalyst or the nucleophile dissociating from the complex. Based on this finding a monometallic intermolecular initiation pathway was proposed, which is depicted in Scheme 2.3 in Chapter 2, Section 2.3.

In order to underline the proposed monometallic intermolecular reaction mechanism in Chapter 2, further investigation of the initiation was performed using ATR-IR spectroscopy with the help of a React IR system and the results are summarized in Chapter 3. First, the reaction order on catalyst concentration was determined, resulting in a value of 0.96 meaning a reaction order of 1 on catalyst loading. Therefore, there is only one chromium complex per epoxide participating in the initiation, which further supports the monometallic intermolecular initiation pathway proposed earlier. However, the possibility of a monometallic intramolecular

initiation cannot be excluded especially with species **2.1**·DMAP that contains two nucleophilic groups. This possible initiation was depicted in Scheme 3-1 in Chapter 3. End group analysis of the polymers by MALDI-TOF MS supported this phenomenon where DMAP may initiate ring opening of a chromium bound epoxide intramolecularly resulting in the incorporation of DMAP in the polymer chain end(s) (Figure 3.5, 3.6 and 3.7).

Another finding of Chapter 3 was that even when 5 equiv. of DMAP there was no inhibition of the reaction observed which contradicts the behavior of a related chromium complex **1.57** where 2 equiv. of DMAP resulted in loss of activity. Furthermore, the initiation period of the reaction became longer but the reaction rate became faster when elevated amounts of DMAP were applied.

Mechanistic investigations of **2.1**·DMAP with CO_2 showed no reaction occurring between the two, which means a different behavior compared to the chromium(III) salen complex **1.9** where there was a weak interaction between the complex and CO_2 forming a carbamate species (Scheme 3.1 in Chapter 3, Section 3.3.2). There was no such an interaction found in the **2.1**·DMAP/CO_2 system, either because the flexibility of the amine-bis(phenol) and the salen ligand is different or the azide group of the salen complex complicated the observed resonances. Therefore, a control experiment with a chromium(III) salen complex without the azide group would be beneficial here.

Chapter 4 described the preparation of two new magnesium-bis(phenolate) complexes for the ring opening polymerization of *rac*-lactide. Magnesium is one of the metals that is biocompatible with the human body, and so, it is appealing to apply it in complex synthesis. **4.1** and **4.2** were capable of ROP under melt (125 °C) and

solution (90 °C in toluene) polymerization conditions. **4.1** and **4.2** proved to be more active than previously synthesized magnesium-bis(phenolate) complexes in the field. The inefficiency of previous complexes was attributed to the bulkiness of the ligand and the reluctant dissociation of the dimeric complexes. **4.1** and **4.2,** on the other hand, showed excellent polymerization control which was supported by the increase in polymer molecular weight with increasing time as well as the molecular weight decrease with elevated amount of alcohol added. The complexes remained active even under highly diluted conditions (0.1 mol% cat. loading). Mechanistic investigations were also carried out with the help of ^{1}H NMR and showed that the dimer did dissociate to monomeric species allowing for the monomer to bind to the metal. Based on the findings of the ^{1}H NMR studies a mechanism was proposed for both with and without an added alcohol (Schemes 4.2 and 4.3 in Chapter 4, Section 4.2.3), which showed closer relationship to a coordination insertion rather than an activated monomer mechanism. Based on this excellent activity of the magnesium complexes, other biocompatible alkali and alkaline earth metal complexes were synthesized and tested in the ROP of *rac*-lactide. The results were described in Chapter 5. Two lithium-, two sodium-, a potassium- and a calcium amine-bis(phenolate) complexes were synthesized and characterized. The crystal structures obtained for the lithium and the sodium complexes demonstrated partially hydrolyzed complex structures where one of the phenolate oxygens remained protonated resulting in a dimeric structure exhibiting intermolecular hydrogen bonding between two complex molecules. The tendency of such a behavior of lithium and sodium phenolate complexes was previously observed by other groups. Experimental studies showed that under melt phase polymerization, lithium complex **5.4** showed the best

activity, whereas sodium complex **5.4**·THF proved to be the best performing complex in solution. All six complexes were active at ambient temperature (25 °C), which meant an improvement compared to the magnesium complexes. This may be attributed to the monomeric nature of the complexes, where the dissociation of the hydrogen bonded dimers takes place easily allowing for monomer association. Based on the results of this study, the following order can be established among the activity of the alkali and alkaline earth complexes: Na > Li > K > Ca > Mg, which is consistent with previous observations by other groups.

Chapter 6 summarized the attempted experiments that were carried out but did not lead to significant results that were worth pursuing further. It discussed the synthesis of a new chromium(III) complex, **6.1**·THF, with an oxygen donor tetrahydrofurfuryl group, which proved to be inferior to the complexes bearing a nitrogen donor pyridyl group. Another chromium(III) complex, **6.2**, was also prepared which contained a chelating acetate group instead of the chloride and THF groups. Unfortunately, crystals suitable for X-ray diffraction were not obtained to support the structure of the complex. This complex, however, was active in CHO/CO_2 copolymerization with DMAP.

The chapter also gave information on trying other monomers than CHO but there were no improvements with them compared to earlier results in the field. In addition, the magnesium complex **4.2** was also tested in CHO/CO_2 copolymerization in order to check its activity but unfortunately it did not convert CO_2 into polymers or cyclic carbonates even though the co-catalyst was changed and the temperature and pressure were increased.

In summary, new highly active chromium(III) complexes were synthesized that were able to copolymerize CO_2 with CHO to selectively produce poly(cyclohexene carbonate). End group analysis of the polycarbonates and mechanistic studies pointed toward a monometallic intermolecular reaction mechanism where ring opening was initiated by either of an external nucleophile or the nucleophilic group of the complex. New alkali and alkaline earth complexes were also prepared for the ring opening polymerization of lactide. From among the eight new complexes, the magnesium complex **4.1** and **4.2** as well as the sodium complex **5.3**·THF exhibited the highest activity and the best control over the reaction.

APPENDIX A: Crystallographic and Structure Refinement Data

Table A-1 Crystallographic and Structure Refinement Data for **2.1**·THF, **2.2**·THF and **2.1**·DMAP

Compound	**2.1**·THF	**2.2**·THF	**2.1**·DMAP
Chemical formula	$C_{34}H_{46}CrN_2O_5Cl•(C_4H_8O)$	$C_{32}H_{50}CrN_2O_5Cl•(C_7H_8)$	$C_{37}H_{48}CrN_4O_4Cl•5(CH_2Cl_2)$
Colour	Green	Green	Green
Habit	Prism	Prism	Prism
Formula weight	722.30	722.35	827.66
Crystal system	Orthorhombic	Monoclinic	Triclinic
a [Å]	17.119(3)	14.615(10)	8.751(4)
b [Å]	11.4910(18)	16.834(12)	11.960(5)
c [Å]	37.818(6)	16.342(13)	20.098(9)
α [°]	90	90	95.039(7)
β [°]	90	112.456(8)	97.965(9)
γ [°]	90	90	92.325(3)
Unit cell *V* [Å^3]	7439(2)	3716(5)	2072.2(16)
Temperature [K]	163	123	163
Space group	$Pca2_1$ (#29)	$P2_1/c$ (#14)	*P*–1 (#2)
Z	8	4	2
D_c/g cm^{-3}	1.290	1.291	1.326
Radiation type	MoKα	MoKα	MoKα
μ (MoKα) [cm^{-1}]	4.26	4.25	5.76
F(000)	3080	1548	868
Reflections measured	63954	42817	17169
Unique refl's	14421	7619	8454
R_{int}	0.0455	0.0939	0.0296
R_1 (all)	0.0477	0.1168	0.0659
$wR(F_2)$ (all)	0.1177	0.2625	0.1535
R_1 ($I > 2\,\sigma(I)$)[a]	0.0446	0.0965	0.0616
$wR(F^2)$ ($I > 2\,\sigma(I)$) [b]	0.1133	0.2448	0.1496
Goodness of fit on F^2	1.068	1.082	1.059
CCDC Ref.	1408674	1408672	1408673

[a] $R_1 = \Sigma(|F_o| - |F_c|)/ \Sigma|F_o|)$; $wR_2 = [\Sigma(w(F_o^2 - F_c^2)^2)/ \Sigma w(F_o^2)^2]^{1/2}$.

Table A-2 Crystallographic and Structure Refinement Data for **4.2**

Compound	**4.2**
Empirical formula	$C_{56}H_{84}Mg_2N_4O_4$
Formula weight	925.89
Temperature/K	163(2)
Crystal system	monoclinic
Space group	C2/c
a/Å	31.345(14)
b/Å	9.706(5)
c/Å	25.551(12)
α/°	90
β/°	113.998(14)
γ/°	90
Volume/Å^3	7102(6)
Z	4
ρ_{calc}g/cm^3	0.866
μ/mm^{-1}	0.070
F(000)	2016.0
Crystal size/mm^3	0.20 × 0.20 × 0.20
Radiation	MoKα (λ = 0.71073)
2Θ range for data collection/°	4.432 to 52.876
Index ranges	-38 ≤ h ≤ 38, -12 ≤ k ≤ 10, -31 ≤ l ≤ 31
Reflections collected	31988
Independent reflections	7246 [R_{int} = 0.0748, R_{sigma} = 0.0820]
Data/restraints/parameters	7246/15/339
Goodness-of-fit on F^2	0.985
Final R indexes [I>=2σ (I)]	R_1 = 0.0784, wR_2 = 0.2128
Final R indexes [all data]	R_1 = 0.1222, wR_2 = 0.2416
Largest diff. peak/hole / e Å^{-3}	0.41/-0.38
CCDC Reference Number	1043113

[a] $R_1 = \Sigma(|F_o| - |F_c|)/ \Sigma|F_o|)$; $wR_2 = [\Sigma(w(F_o^2 - F_c^2)^2)/ \Sigma w(F_o^2)^2]^{1/2}$.

Table A-3 Crystallographic and Structure Refinement Data for **5.3** and **5.4**.

Compound	**5.3**	**5.4**
Chemical formula	$C_{30}H_{39}N_2NaO_4\cdot(C_4H_8O)$	$C_{30}H_{39}LiN_2O_4\cdot(C_7H_8)$
Colour	Colourless	Colourless
Habit	Prism	Prism
Formula weight	622.80	590.71
Crystal system	Monoclinic	Monoclinic
a [Å]	22.745(7)	17.399(7)
b [Å]	16.871(5)	12.202(5)
c [Å]	18.568(6)	19.503(10)
α [°]		
β [°]	104.513(4)	127.700(9)
γ [°]		
Unit cell *V* [Å^3]	6898(4)	3276(3)
Temperature [K]	123 ± 1	153 ± 2
Space group	C2/c (#15)	$P2_1/c$ (#14)
Z	8	4
D_c/g cm^{-3}	1.199	1.198
Radiation type	MoKα	MoKα
μ (MoKα) [cm^{-1}]	0.90	0.76
F(000)	2688	1272
Reflections measured	21786	8557
Unique refl's	7065	4562
R_{int}	0.0333	0.0904
R_1 (all)	0.0905	0.2006
$wR(F_2)$ (all)	0.2275	0.2396
R_1 ($I > 2\sigma(I)$)[a]	0.0789	0.1163
$wR(F^2)$ ($I > 2\sigma(I)$) [b]		
Goodness of fit on F^2	1.091	1.082
CCDC Ref.		

[a] $R_1 = \Sigma(|F_o| - |F_c|)/ \Sigma|F_o|)$; $wR_2 = [\Sigma(w(F_o^2 - F_c^2)^2)/ \Sigma w(F_o^2)^2]^{1/2}$.

Table A-4 Crystallographic and Structure Refinement Data for **6.1**·THF

Compound	**6.1**·THF
Empirical formula	$C_{36.5}H_{45}ClCrNO_6$
Formula weight	679.67
Temperature/K	148
Crystal system	monoclinic
Space group	C2/c
a/Å	25.670(20)
b/Å	16.836(12)
c/Å	16.352(12)
α/°	90
β/°	95.915(10)
γ/°	90
Volume/Å^3	7029(9)
Z	8
ρ_{calc}g/cm^3	1.287
μ/mm^{-1}	0.446
F(000)	2880.0
Crystal size/mm^3	0.205 × 0.167 × 0.05
Radiation	MoKα (λ = 0.71075)
2Θ range for data collection/°	5.644 to 54.206
Index ranges	$-27 \leq h \leq 32$, $-21 \leq k \leq 21$, $-20 \leq l \leq 20$
Reflections collected	32709
Independent reflections	7703 [R_{int} = 0.0499, R_{sigma} = 0.0387]
Data/restraints/parameters	7703/15/440
Goodness-of-fit on F^2	1.140
Final R indexes [I>=2σ (I)]	R_1 = 0.0578, wR_2 = 0.1434
Final R indexes [all data]	R_1 = 0.0608, wR_2 = 0.1456
Largest diff. peak/hole / e Å^{-3}	0.57/-0.62

[a] $R_1 = \Sigma(||F_o| - |F_c||)/ \Sigma|F_o|)$; $wR_2 = [\Sigma(w(F_o^2 - F_c^2)^2)/ \Sigma w(F_o^2)^2]^{1/2}$

APPENDIX B: MALDI-TOF Mass Spectra of Complexes and Polymers

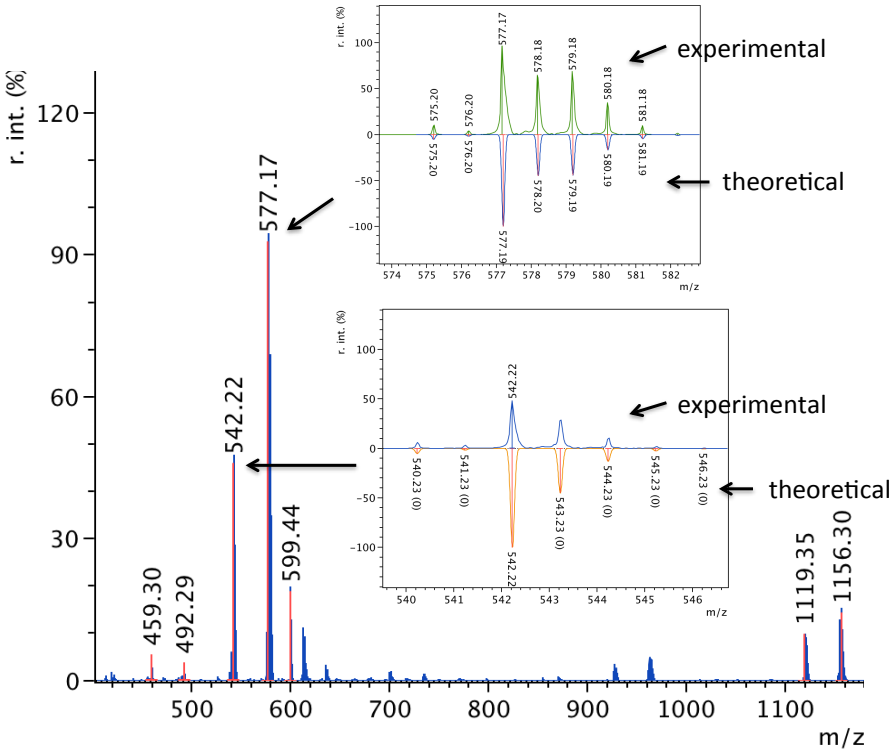

Figure B.1 MALDI-TOF mass spectrum of complex **2.1**·THF.

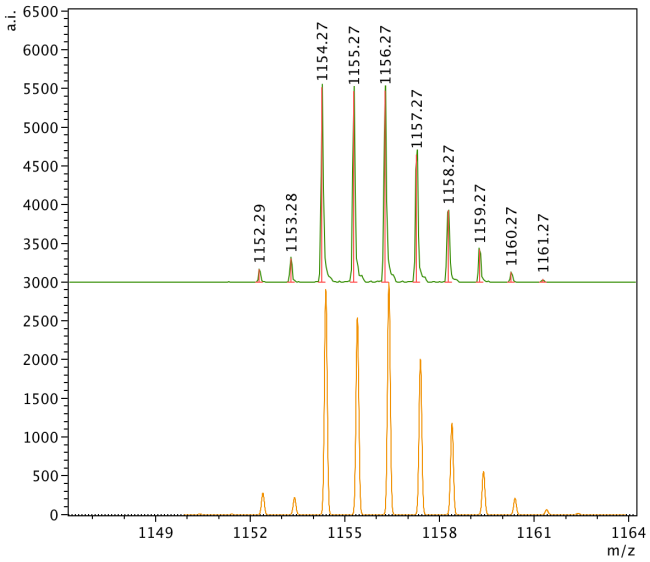

Figure B.2 MALDI-TOF mass spectrum of complex **2.1**·THF corresponding to $[Cr_2Cl_2[L1]_2]^{+\cdot}$

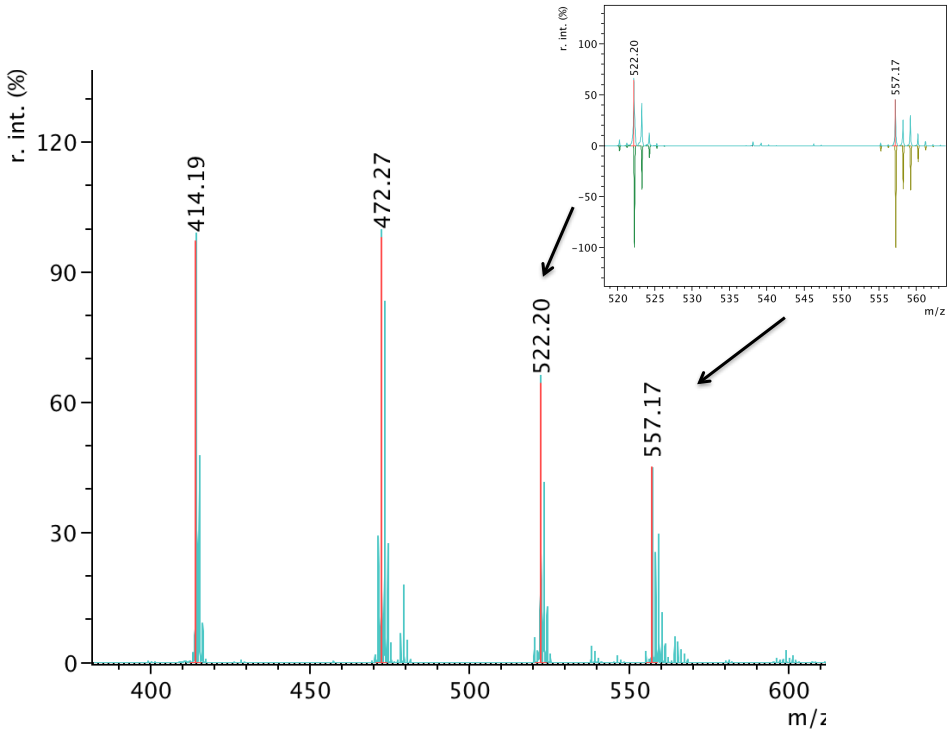

Figure B.3 MALDI-TOF mass spectrum of complex **2.2**·THF

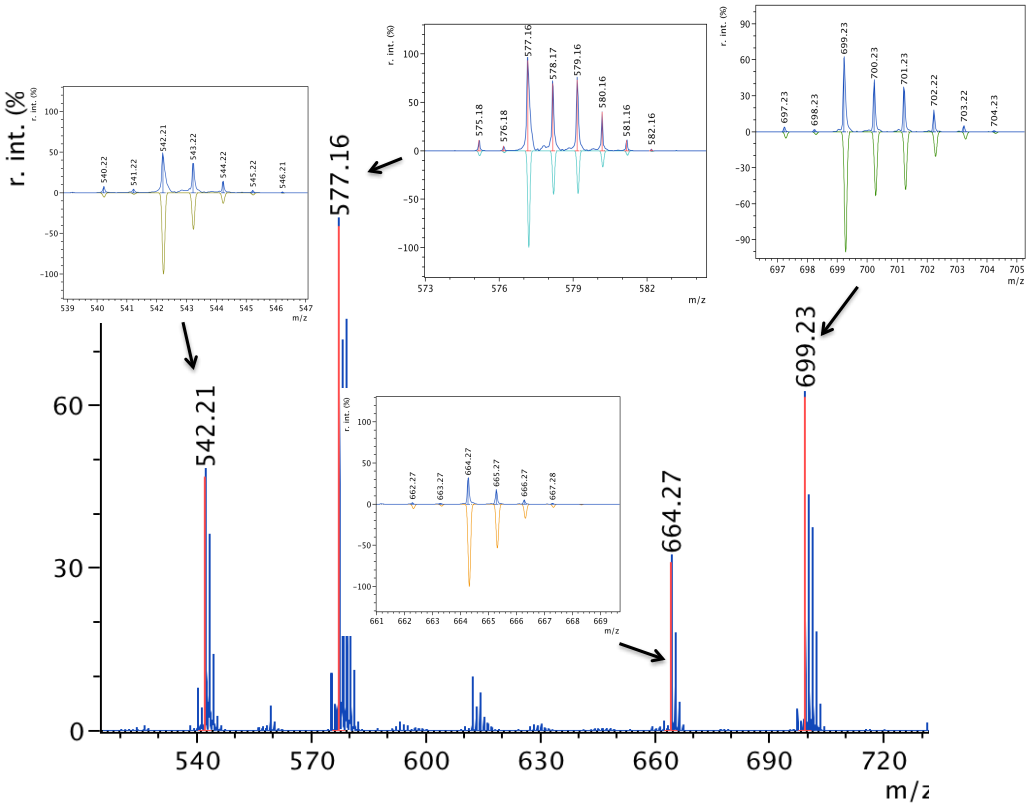

Figure B.4 MALDI-TOF mass spectrum of complex **2.1**·DMAP

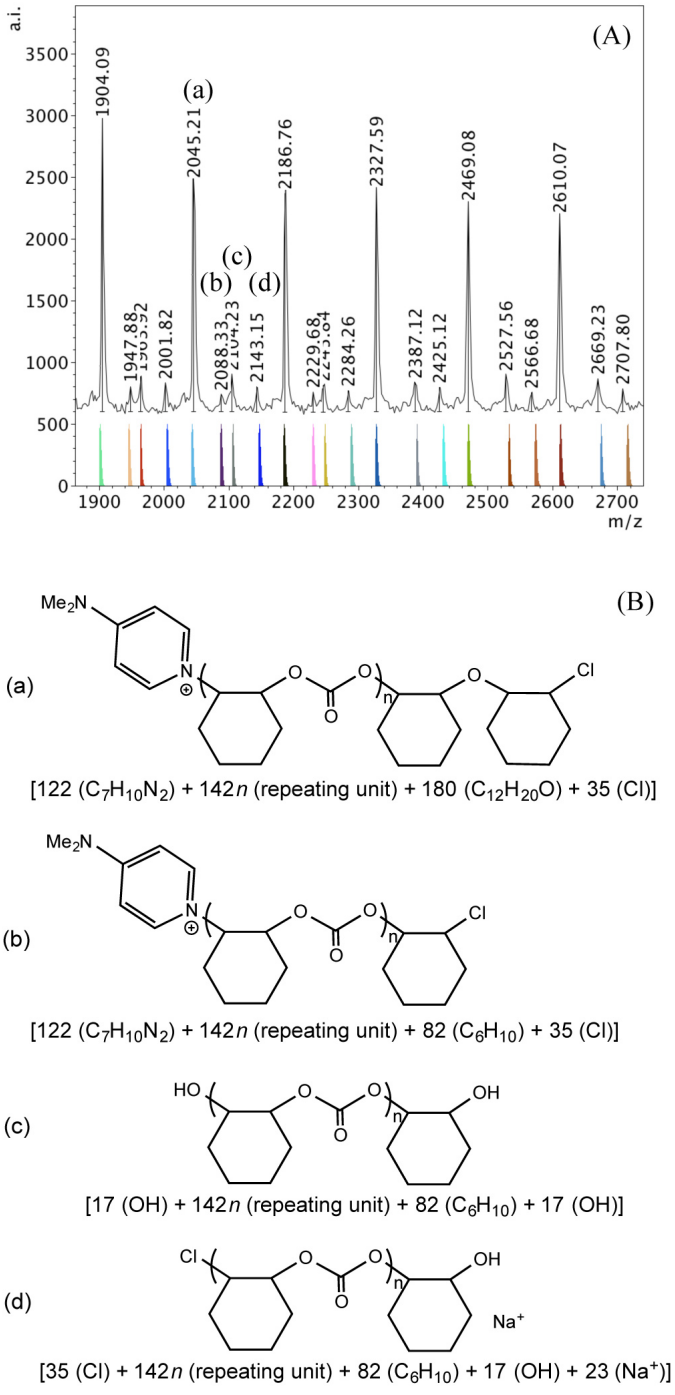

Figure B.5 (A) Lower mass region (*m/z* 1900 – 2700, n = 11 – 16) of the MALDI-TOF MS spectrum produced by **2.1**·THF according to Table 2-2, entry 3 with calculated masses of fragments shown beneath the observed spectrum. (B) Proposed structures of the lower mass range polymers (a), (b), (c) and (d).

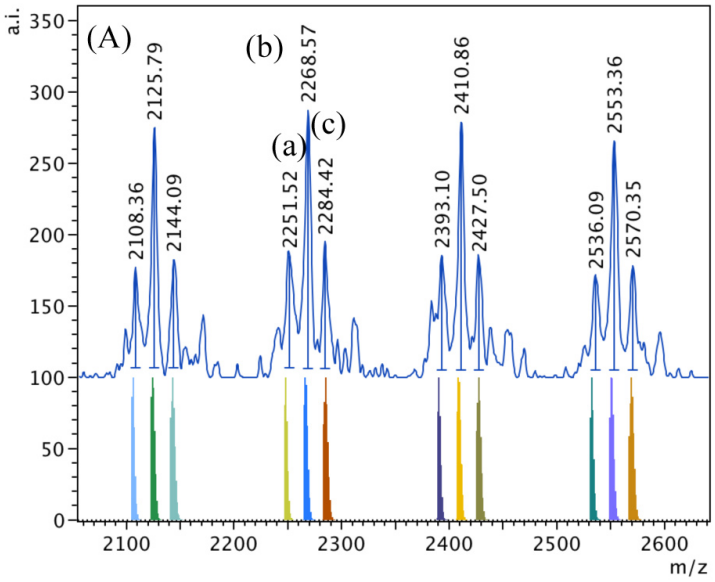

(B)

(a)

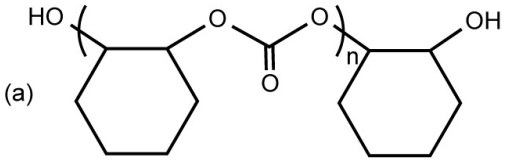

[17 (OH) + 142*n* (repeating unit) + 82 (C_6H_{10}) + 17 (OH)]

(b)

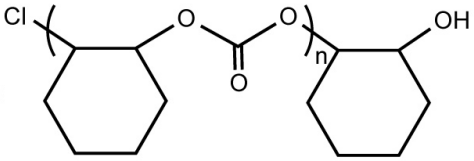

[35 (Cl) + 142*n* (repeating unit) + 82 (C_6H_{10}) + 17 (OH)]

(c)

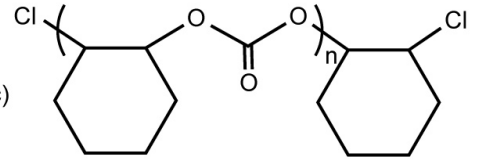

[35 (Cl) + 142*n* (repeating unit) + 82 (C_6H_{10}) + 35 (Cl)]

Figure B.6 (A) Lower mass region of the MALDI-TOF mass spectrum produced by **2.1**·THF according to Table 2-2, entry 5. (*m/z* 2100 – 2600, n = 14 – 17) of the spectrum with modelled polymer peaks. (B) Plausible structures of the polymers based on the calculations shown (a), (b) and (c).

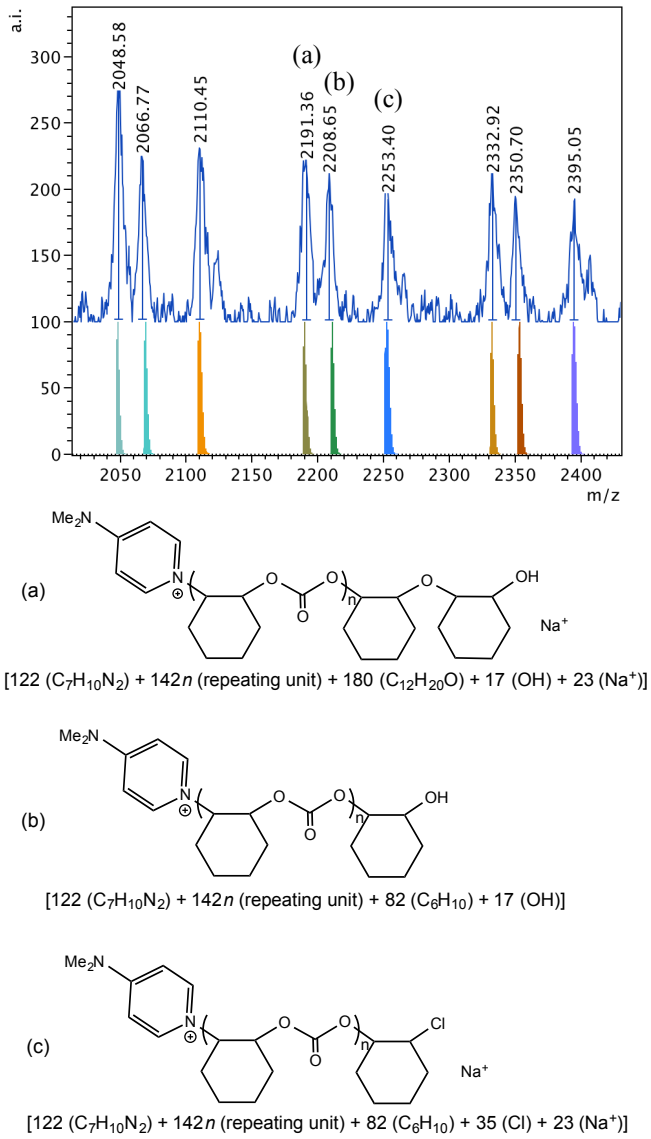

Figure B.7 Lower mass region (*m/z* 2000 – 2400, n = 13 – 16) of the MALDI-TOF MS spectrum produced by **2.1**·DMAP according to Table 2-2, entry 10, with calculated masses of fragments shown beneath the observed spectrum and the proposed structures of polymers (a), (b) and (c).

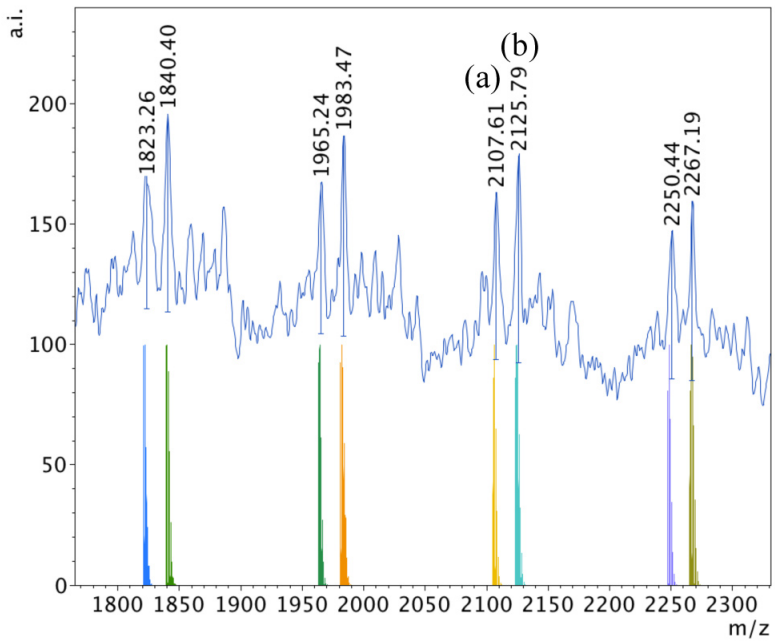

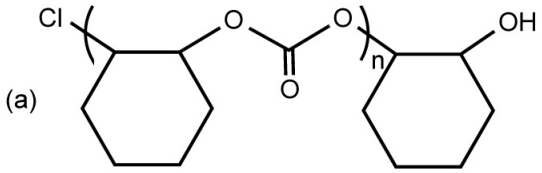

[35 (Cl) + 142*n* (repeating unit) + 82 (C_6H_{10}) + 17 (OH)]

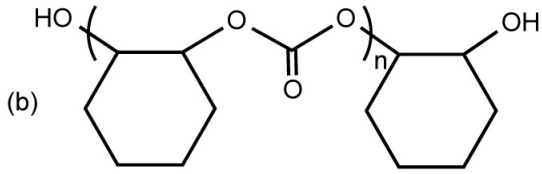

[17 (OH) + 142*n* (repeating unit) + 82 (C_6H_{10}) + 17 (OH)]

Figure B.8 Lower mass region (*m/z* 1800 – 2300, n = 13 – 16) of the MALDI-TOF MS spectrum produced by **2.1**·THF according to Table 2-2, entry 6., with modelled polymer peaks and the plausible structures of the different polymer chains (a) and (b).

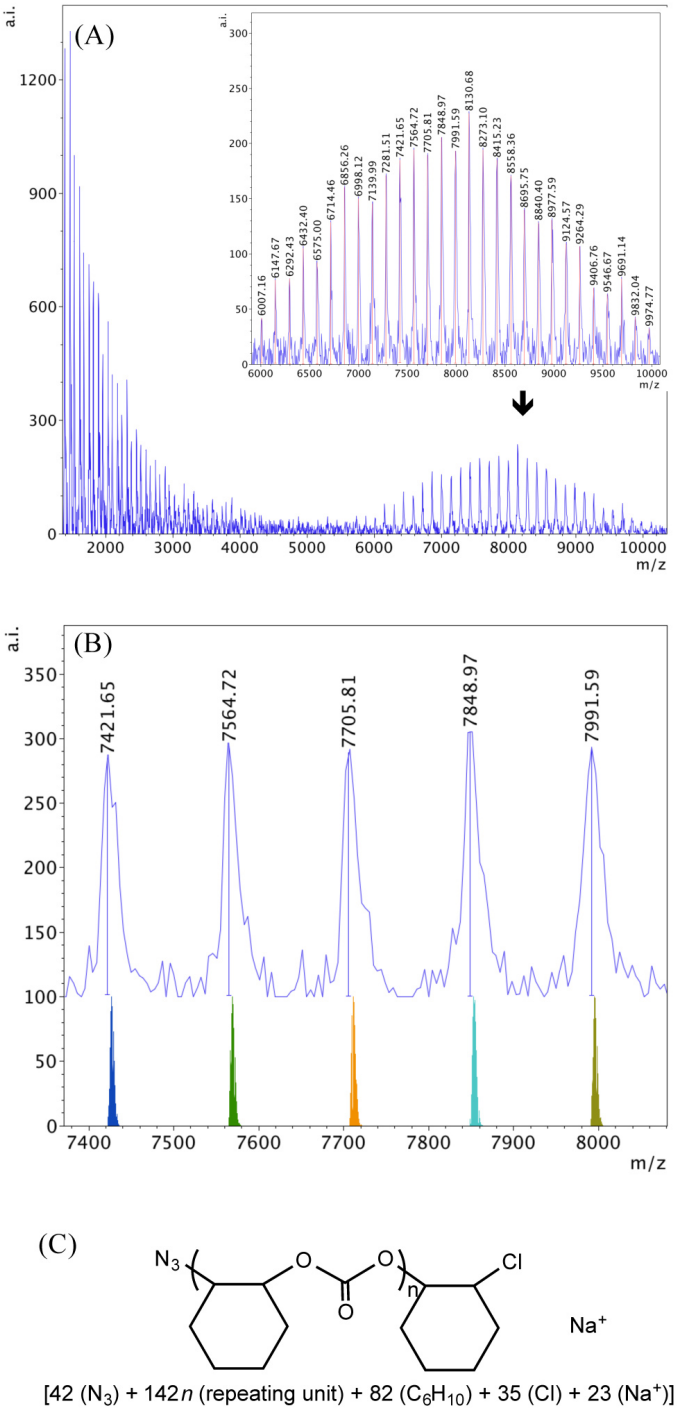

Figure B.9 A) MALDI-TOF MS spectrum produced by **2.1**·DMAP according to Table 2-2, entry 11. (B) Higher mass region (*m/z* 7400 – 8000, n = 51 – 55) of the spectrum with calculated masses of fragments shown beneath the observed spectrum. (C) Proposed structure of the high mass range polymer.

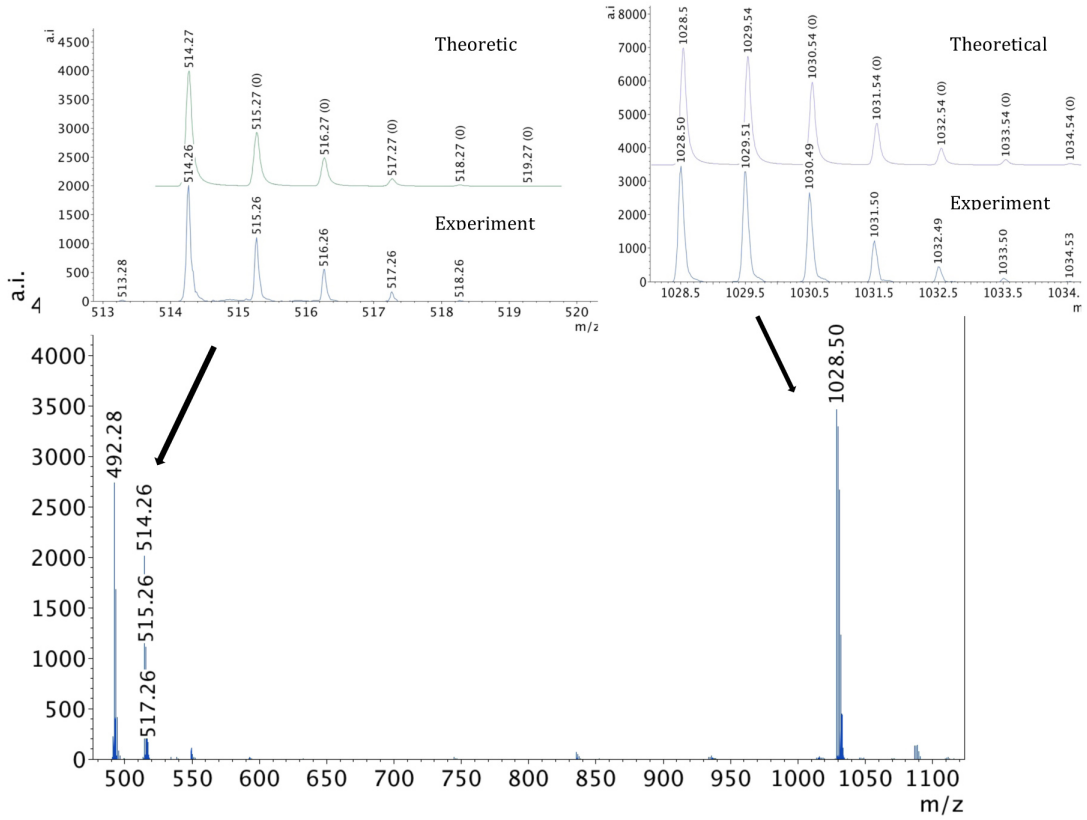

Figure B.10 MALDI-TOF mass spectrum of complex **4.1** with calculated and experimental representation of the isotopic distribution pattern of both the monomer and the dimer ions.

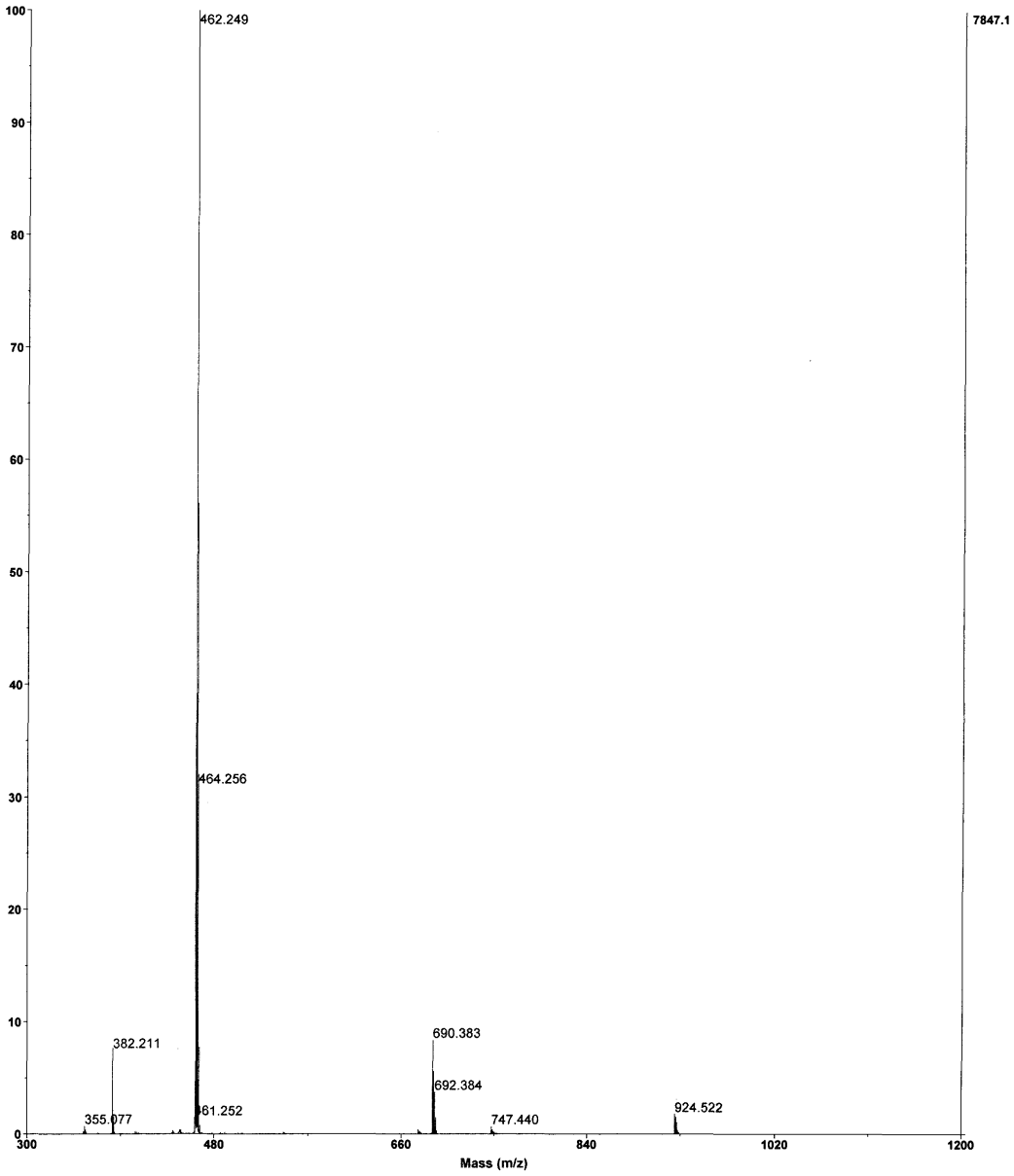

Figure B.11 MALDI-TOF mass spectrum of complex **4.2**.

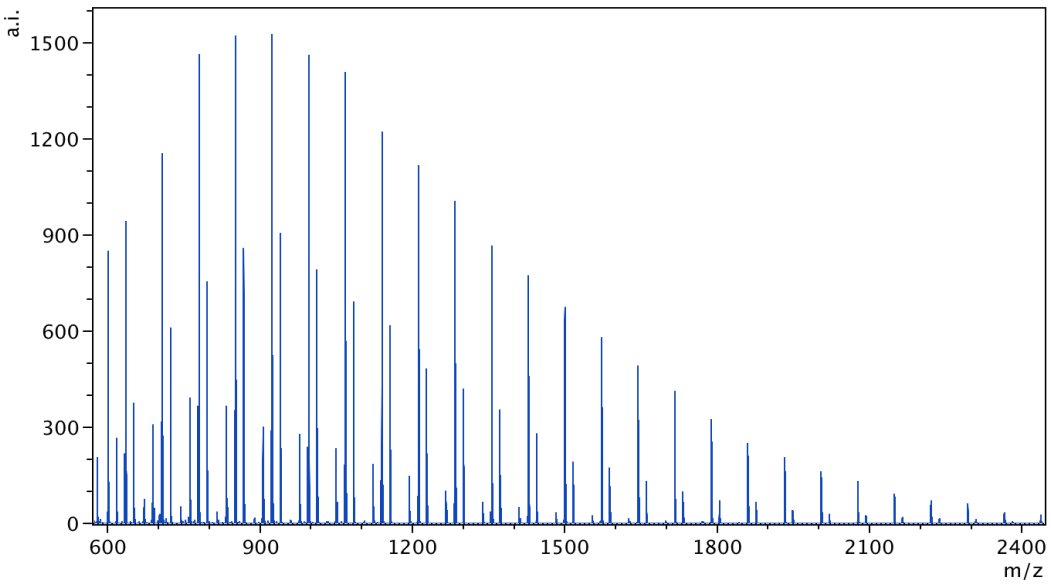

Figure B.12 MALDI-TOF mass spectrum of PLA produced by **4.1** according to Table 4-1, entry 1.

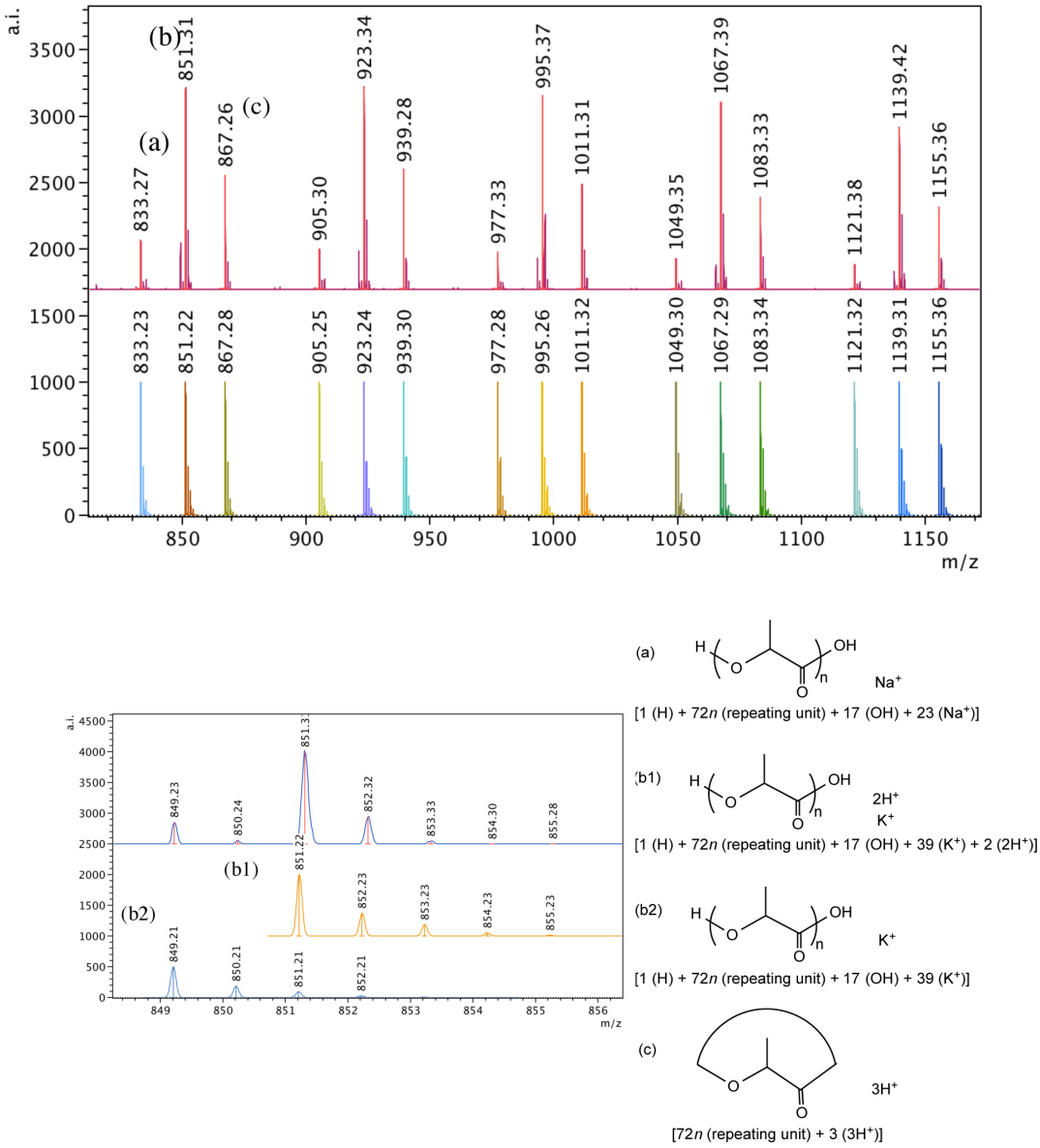

Figure B.13 Expanded region (*m/z* 830 – 1160, n = 54 – 61) of the spectrum in Figure B.12 with modelled calculated polymer peaks. Bottom: Expanded region of series (b) with modelled calculated polymer peaks and possible structures of the polymers based on the calculations shown.

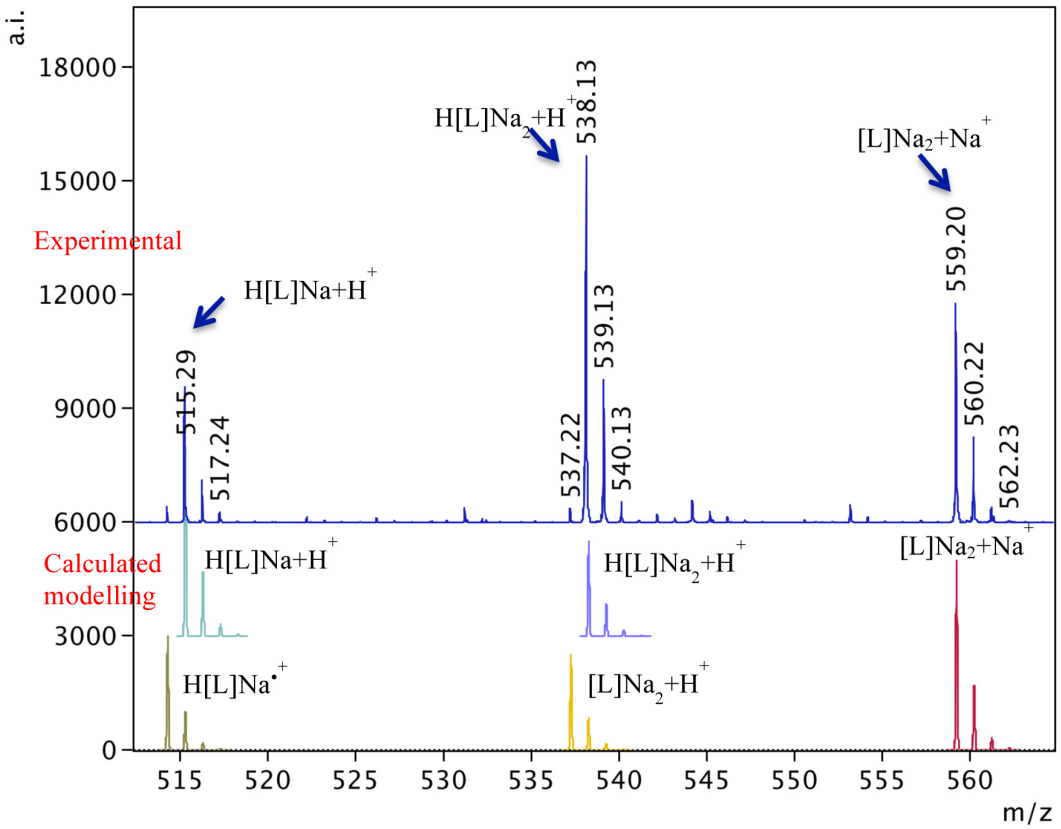

Figure B.14 MALDI-TOF mass spectrum of **5.1**·THF with modelled calculated isotopic distribution patterns.

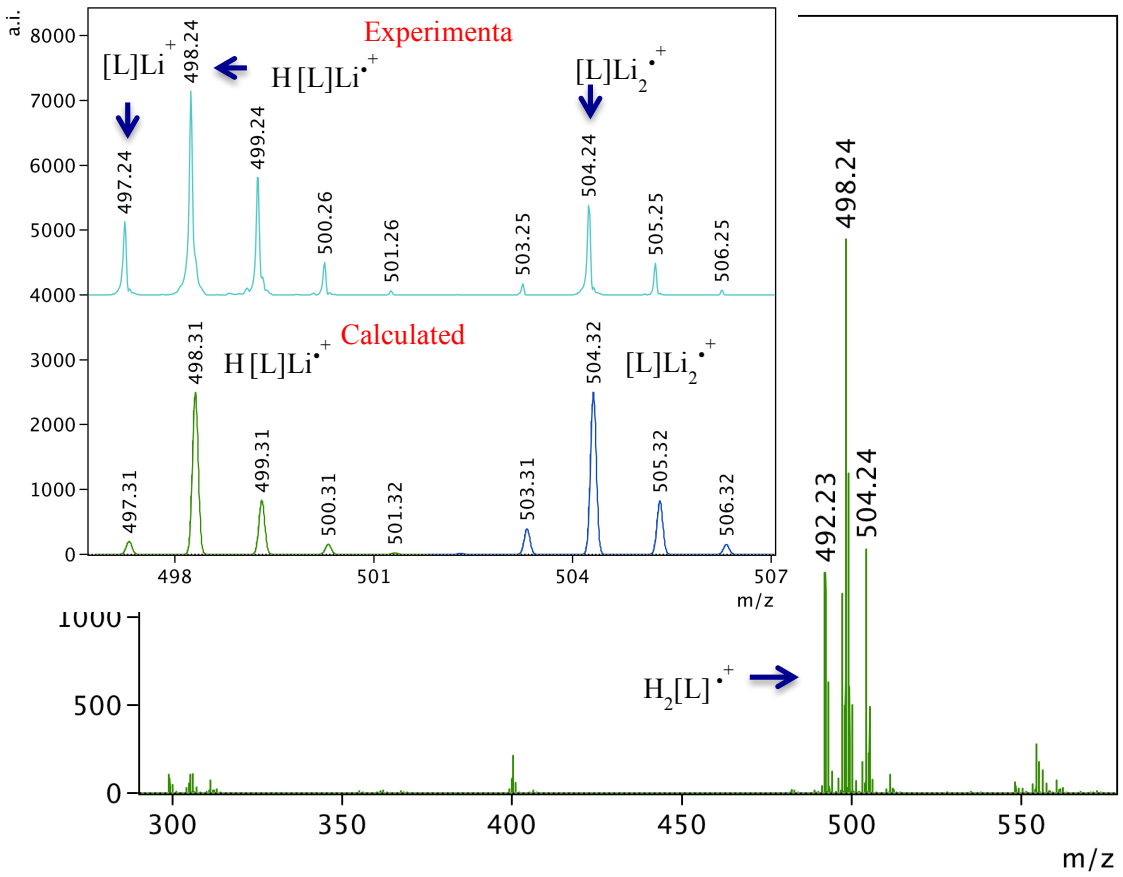

Figure B.15 MALDI-TOF mass spectrum of **5.2**. Inset shows the comparison of the experimental and the modelled calculated isotopic distribution patterns.

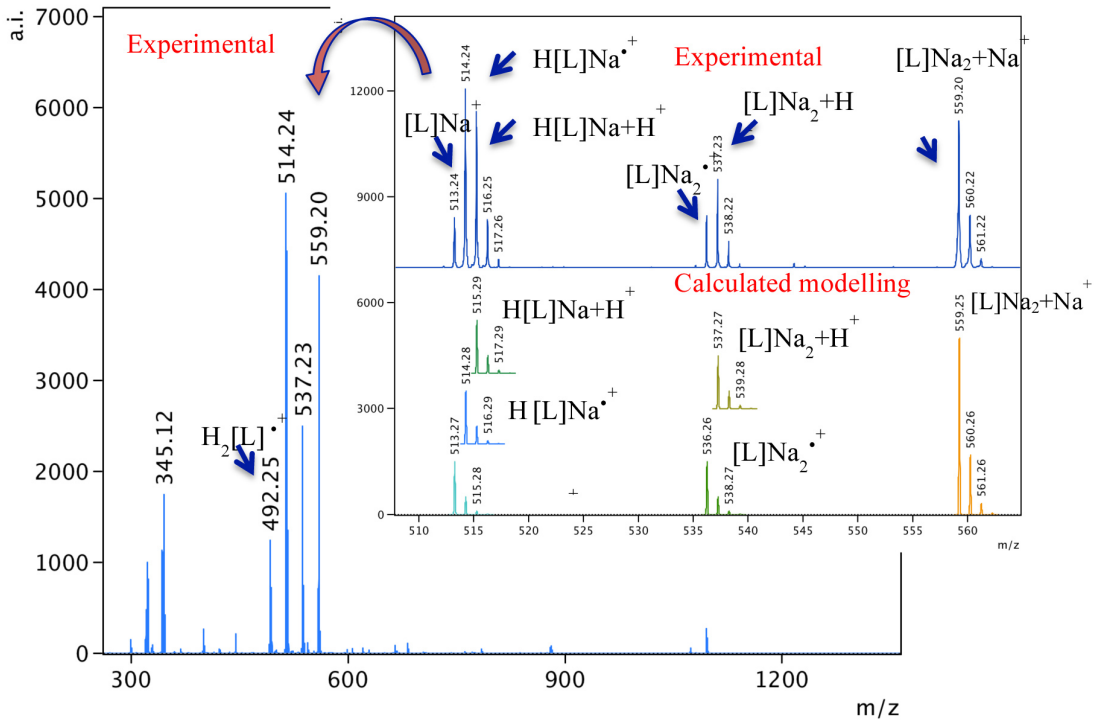

Figure B.16 MALDI-TOF mass spectrum of **5.3**. Inset: expanded region from *m/z* 510 – 565 and the calculated modelling of the isotopic distribution patterns of the peaks.

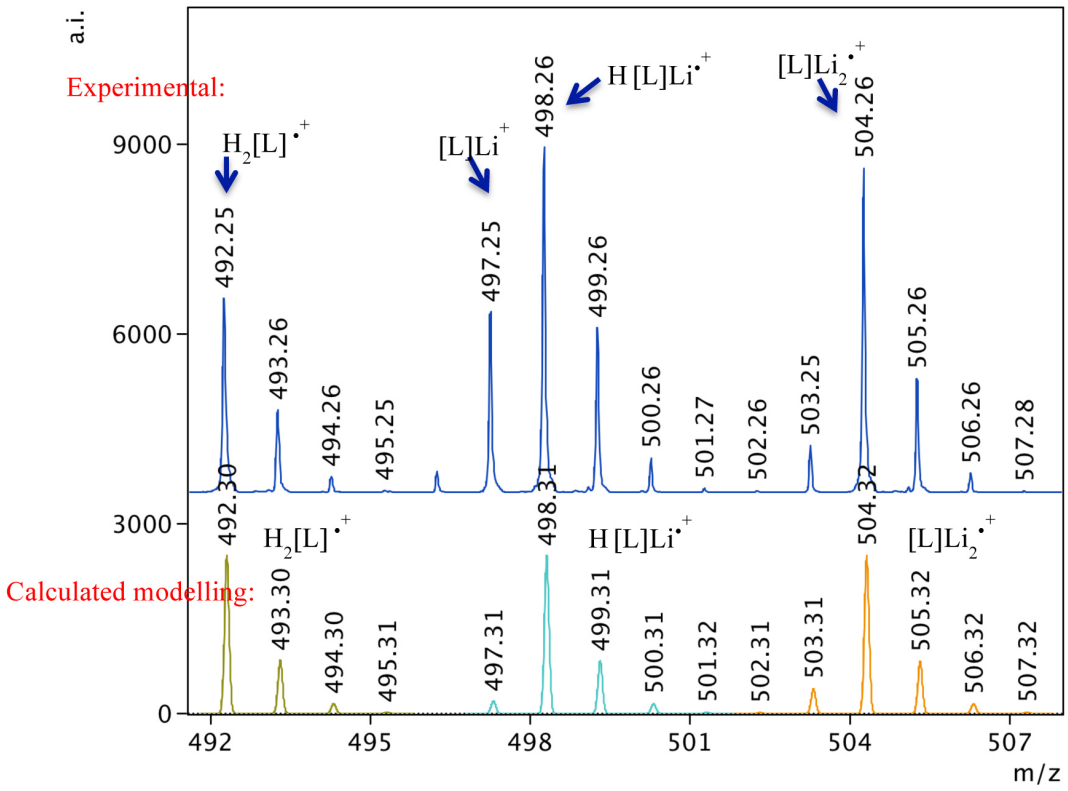

Figure B.17 MALDI-TOF mass spectrum of **5.4** with calculated modelling isotopic distribution patterns.

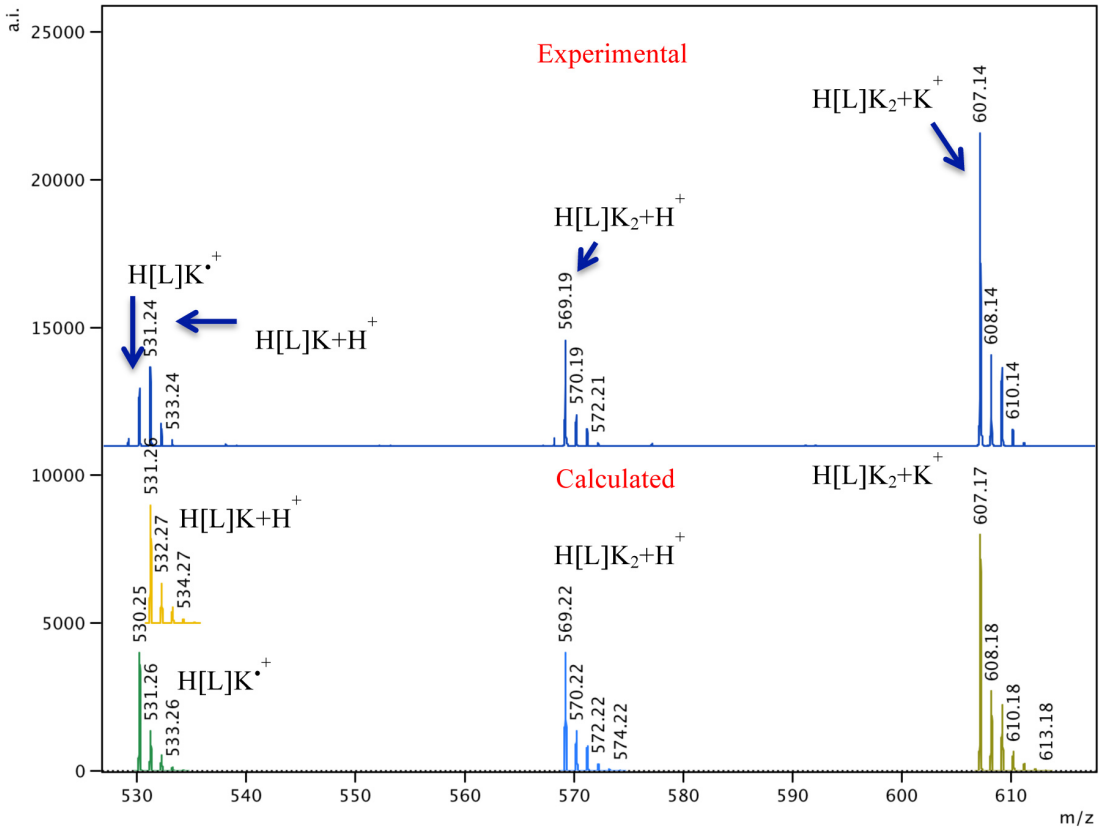

Figure B.18 MALDI-TOF mass spectrum of **5.5** with calculated modelling of the isotopic distribution patterns.

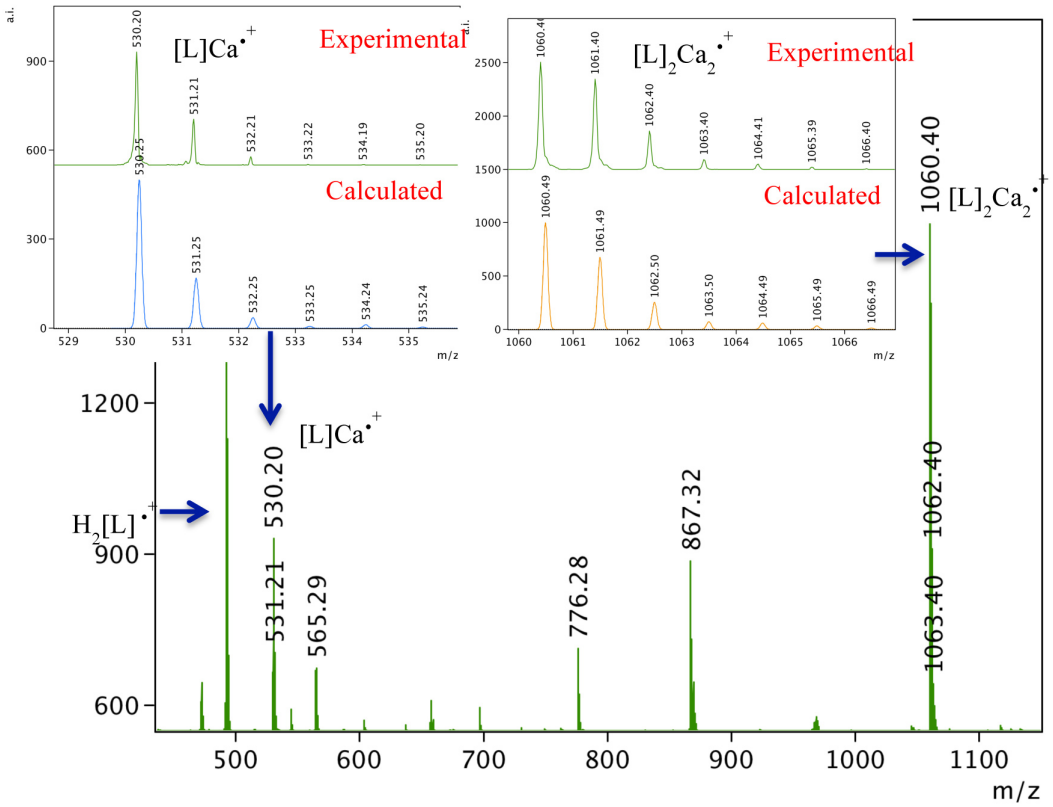

Figure B.19 MALDI-TOF mass spectrum of **5.6** with calculated modelling of the isotopic distribution patterns.

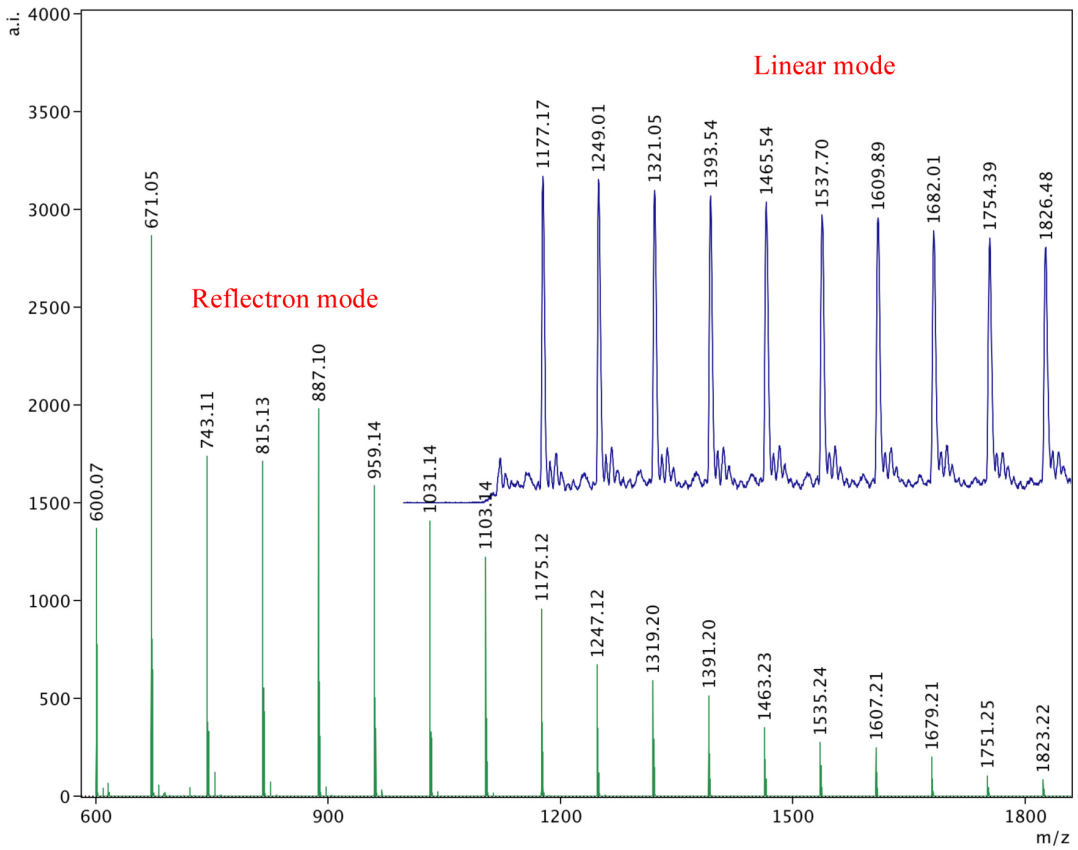

Figure B.20 MALDI-TOF mass spectrum of the polymer produced according to the conditions in Table 5-7, entry 3. Reflectron mode (green, lower) and linear mode (blue, upper) spectra are in good agreement with each other.

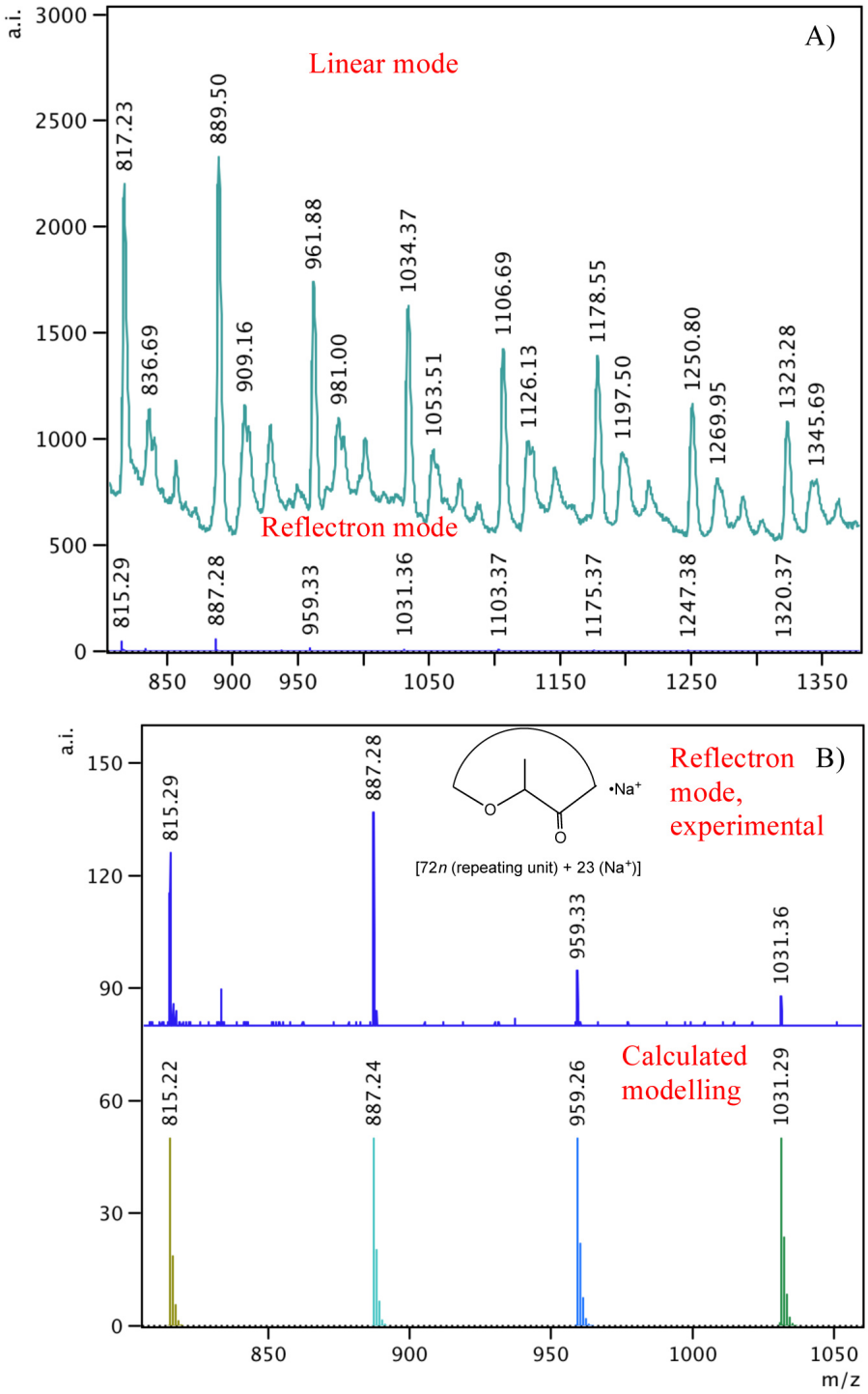

Figure B.21 MALDI-TOF mass spectrum of the polymer produced according to the conditions in Table 5-7, entry 6. A) Linear (upper) vs. reflectron (lower) mode. B) Expanded section, *m/z* 800 – 1050 with calculated isotopic patterns and the possible structure of the polymer based on the calculation shown.

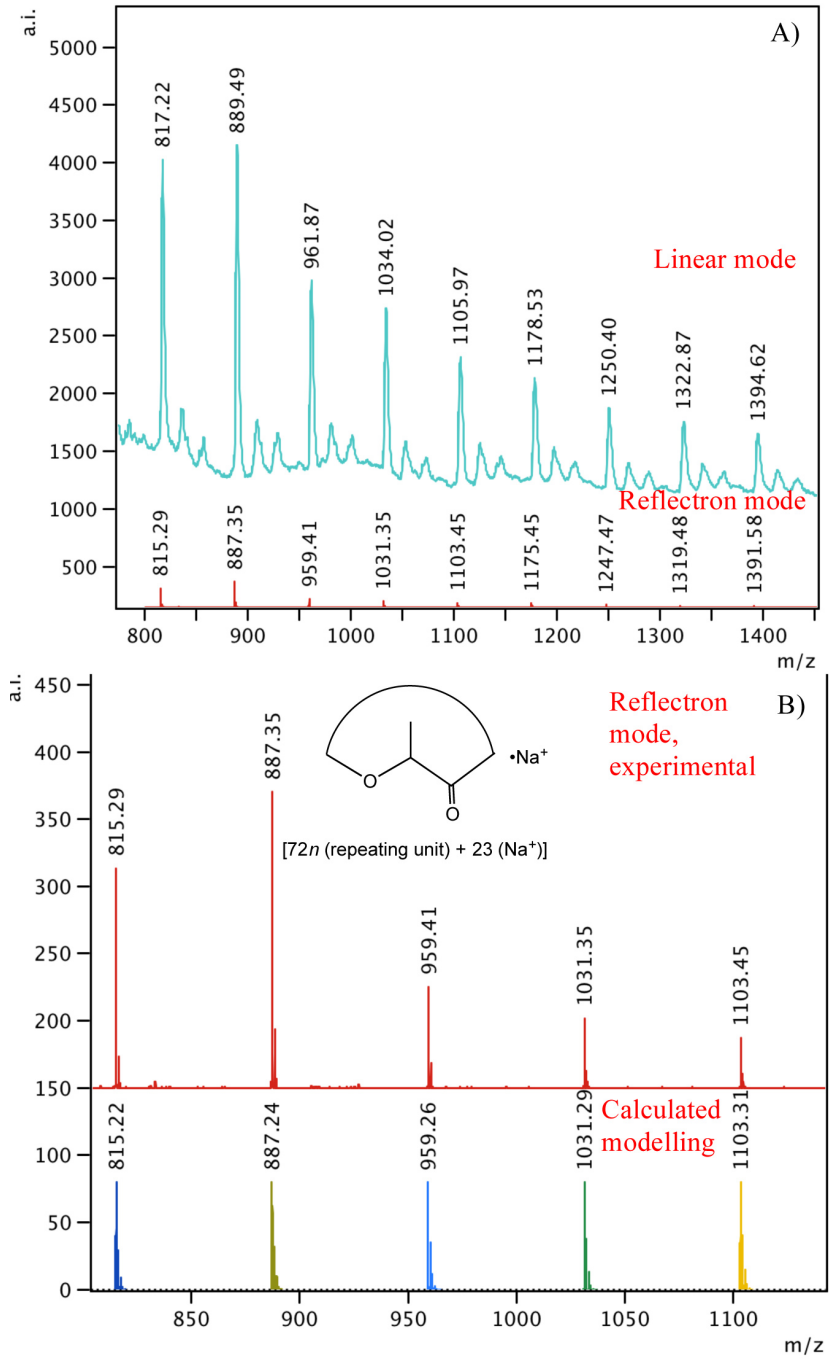

Figure B.22 MALDI-TOF mass spectrum of the polymer produced according to the conditions in Table 5-7, entry 7. A) Linear (upper) vs. reflectron (lower) mode. B) Expanded section, *m/z* 800 – 1150 (upper) with calculated isotopic patterns (lower) and the possible structure of the polymer based on the calculation shown.

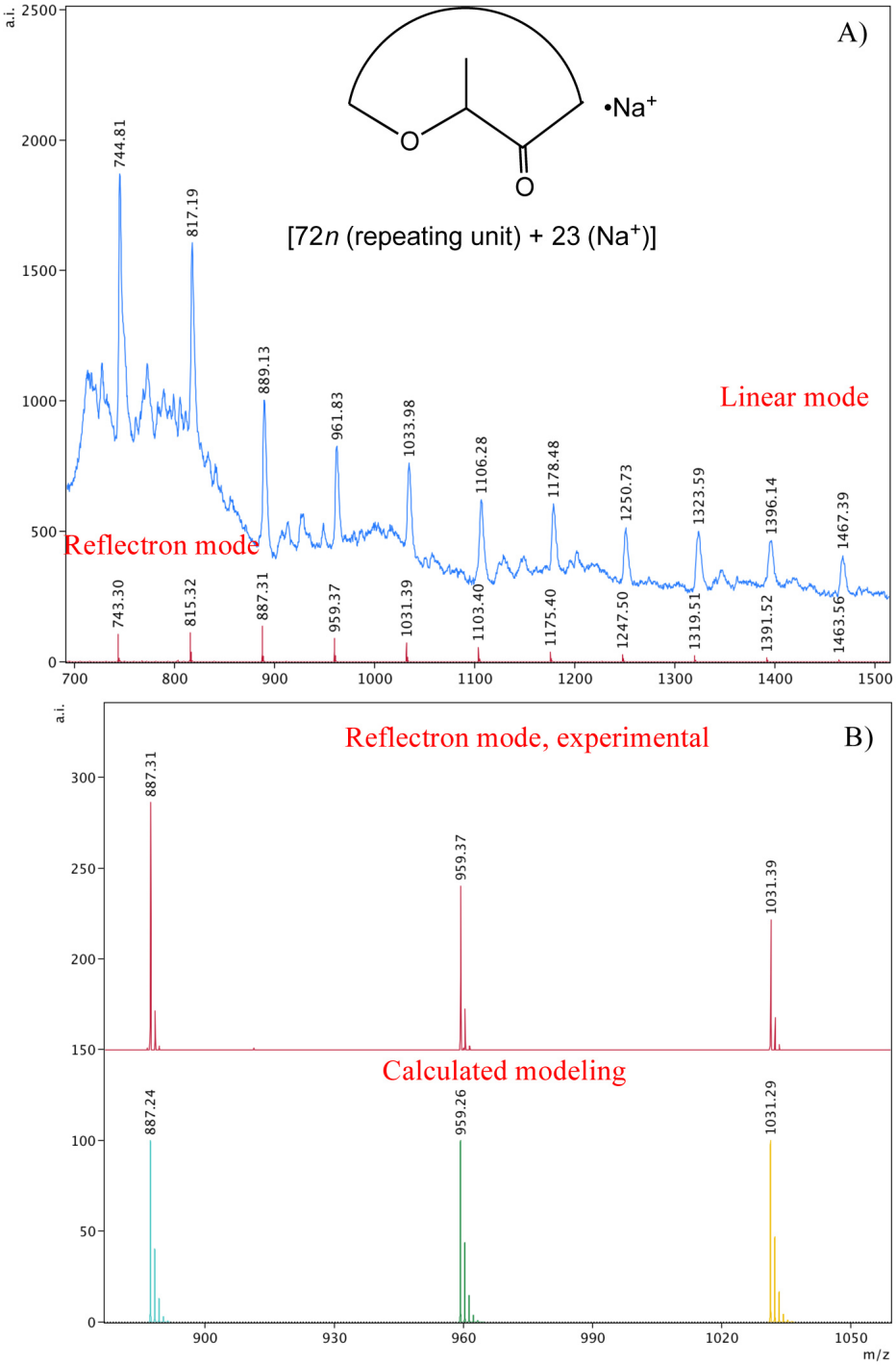

Figure B.23 MALDI-TOF mass spectrum of the polymer produced by **5.1** + H_2[**L1**] without BnOH, linear mode (upper) and reflectron mode (lower) with the possible structure of the polymer based on the calculation shown. B) Expanded section, *m/z* 800 – 1050 (upper) with calculated isotopic patterns (lower).

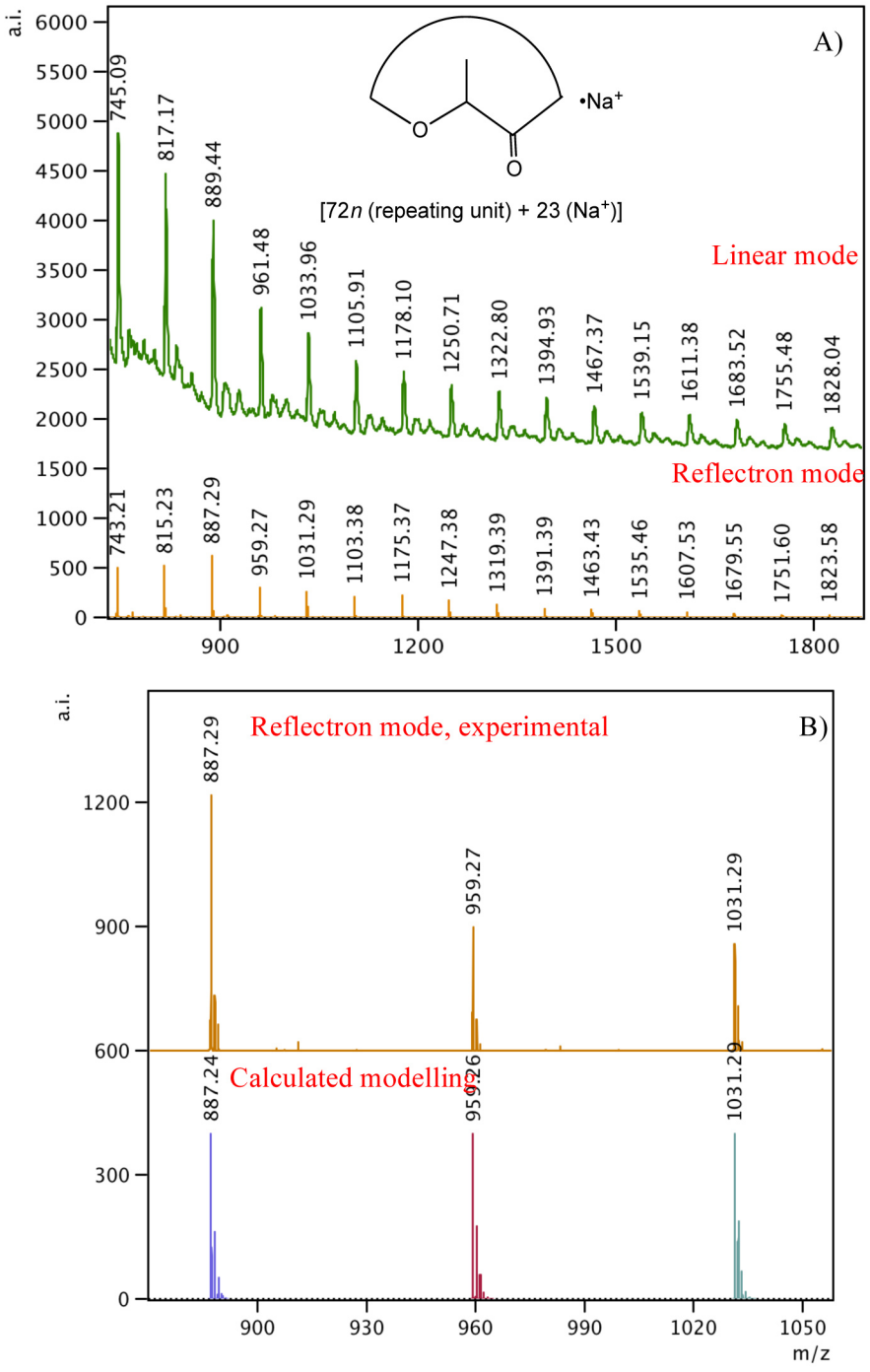

Figure B.24 MALDI-TOF mass spectrum of the polymer produced by **5.1** + H_2[**L1**] with BnOH, linear mode (upper) and reflectron mode (lower) with the possible structure of the polymer based on the calculation shown. B) Expanded section, *m/z* 800 – 1050 (upper) with calculated isotopic patterns (lower).

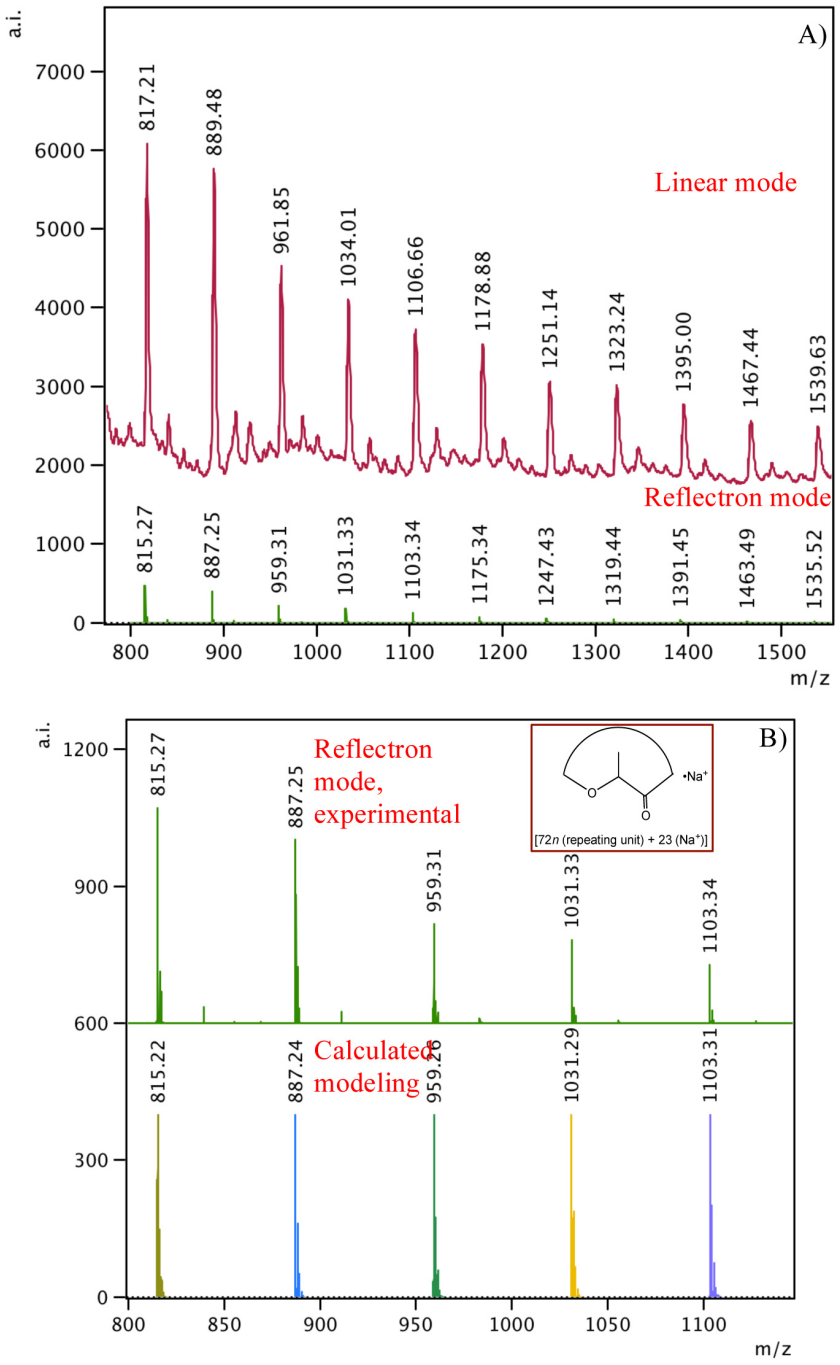

Figure B.25 MALDI-TOF mass spectrum of the polymer produced according to the conditions in Table 5-7, entry 11. A) Linear (upper part) vs. reflectron (lower part) mode. B) Expanded section, *m/z* 800 – 1150 (upper part) with calculated isotopic patterns (lower part) and the possible structure of the polymer based on the calculation shown.

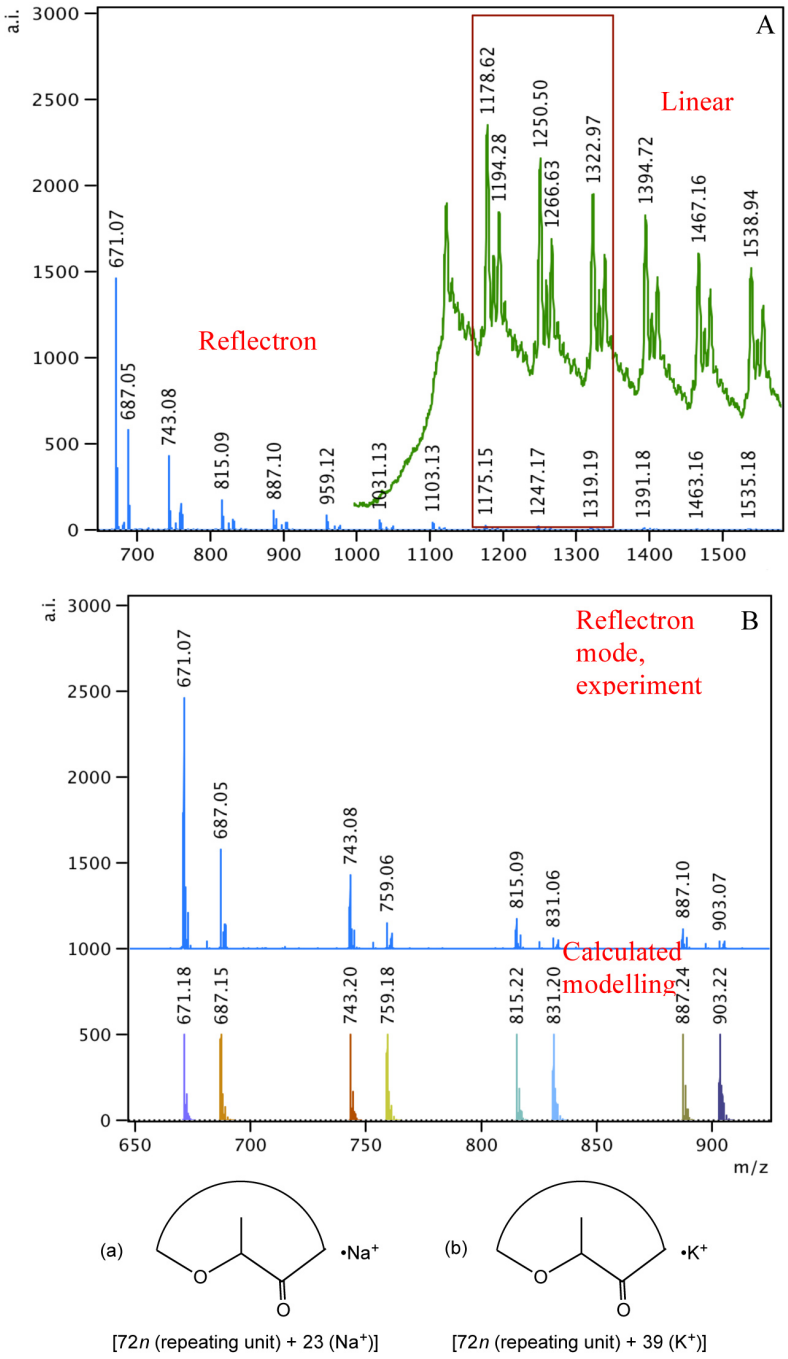

Figure B.26 MALDI-TOF mass spectrum of the polymer produced according to the conditions in Table 5-7, entry 13. A) Linear (upper part) vs. reflectron (lower part) mode. B) Zoomed in section, *m/z* 650 – 950 (upper part) with calculated isotopic patterns (lower part) and the possible structures of the polymers based on the calculations shown.

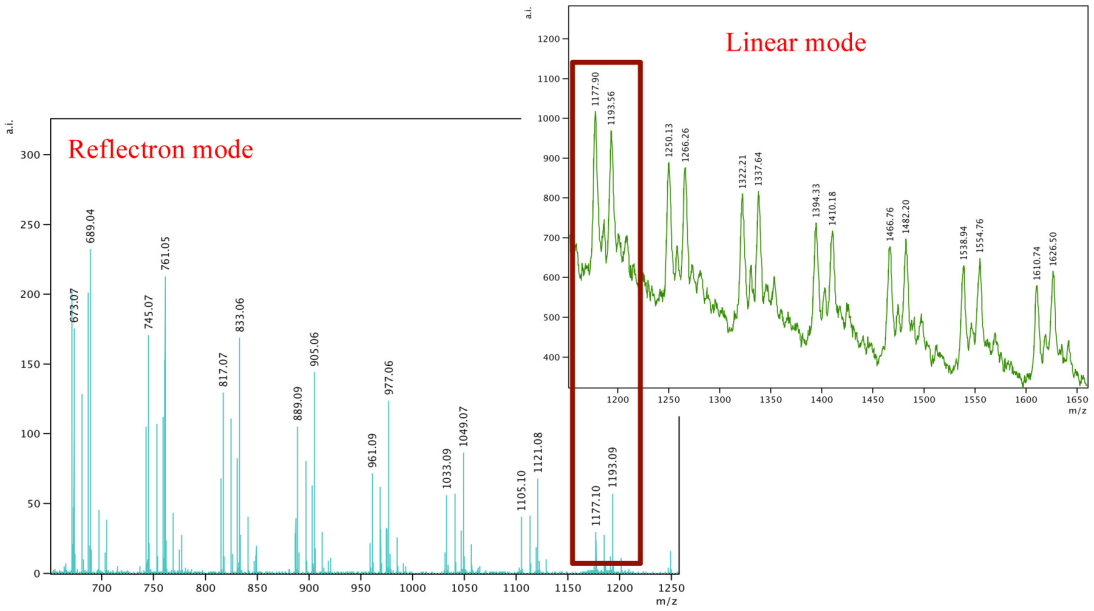

Figure B.27 MALDI-TOF mass spectrum of the polymer produced according to the conditions in Table 5-7, entry 14. Reflectron mode (left side) and linear mode (right side) spectra are in good agreement with each other.

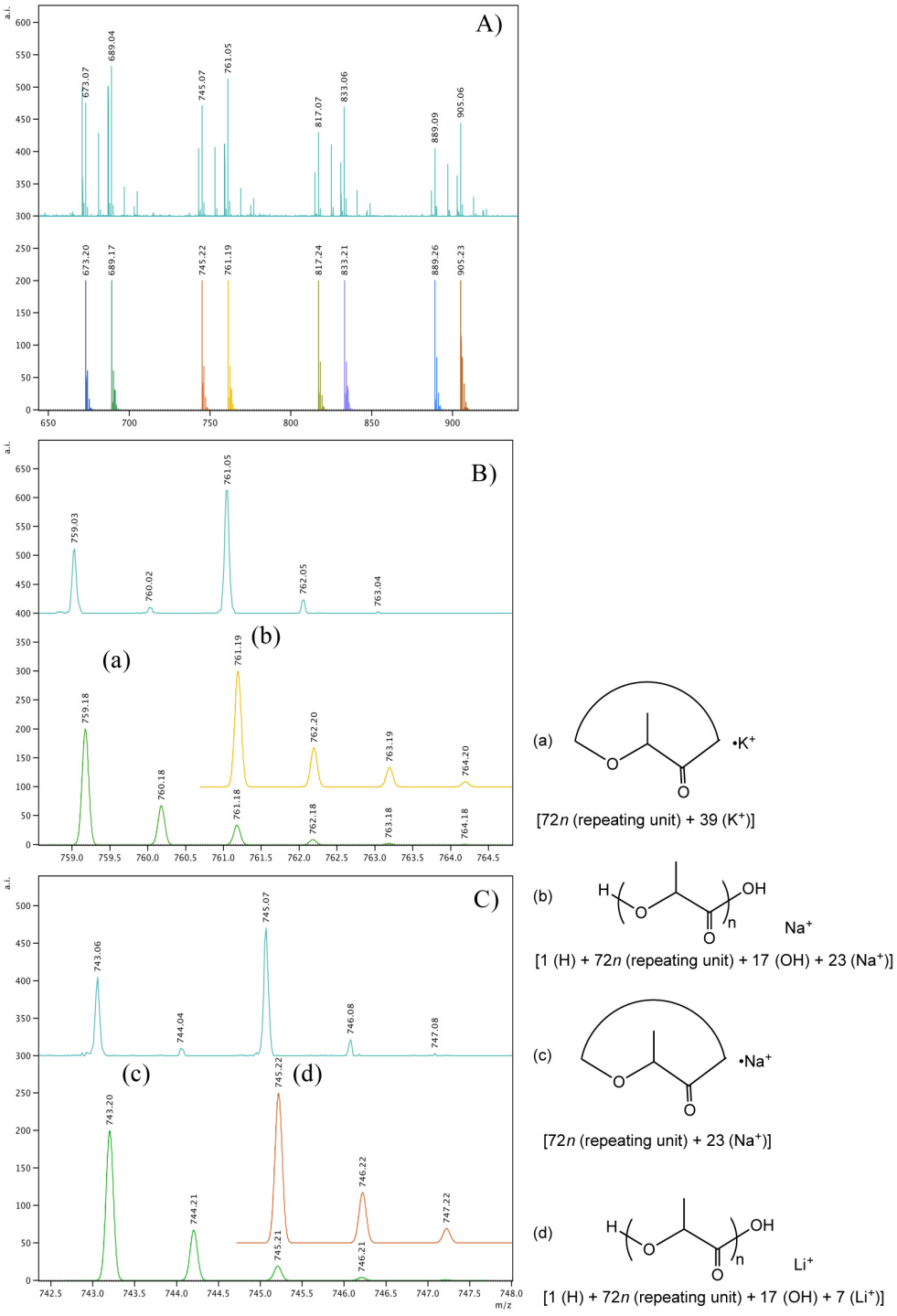

Figure B.28 A) Expanded section of Figure B.27, *m/z* 650 – 950. B) Calculated isotopic patterns for peaks *m/z* 759.03 (a) and 761.05 (b). C) Calculated isotopic patterns for peaks *m/z* 743.06 (c) and 745.07 (d) and the possible structures of the polymers based on the calculations shown.

APPENDIX C: ^{1}H and ^{13}C NMR Spectra

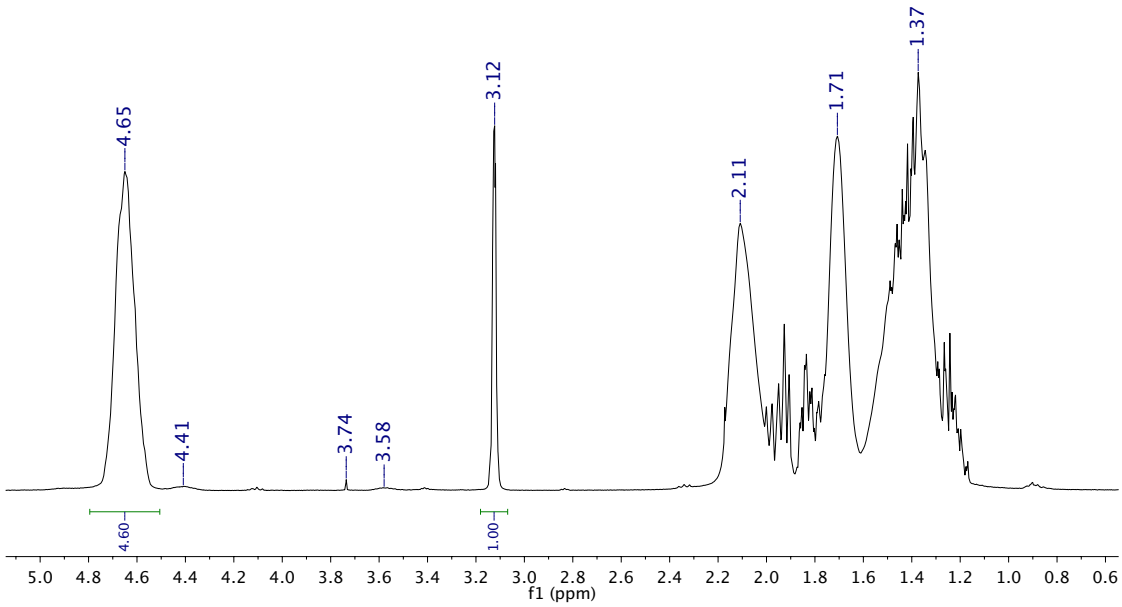

Figure C.1 ^{1}H NMR of the aliquot taken right after polymerization corresponding to Table 2-2, entry 3. %Conversion calculation = polymer peak integration (4.60 at 4.65 ppm) divided by the sum of the polymer (4.60 at 4.65 ppm) and monomer (1.00 at 3.12 ppm) peak integrations.

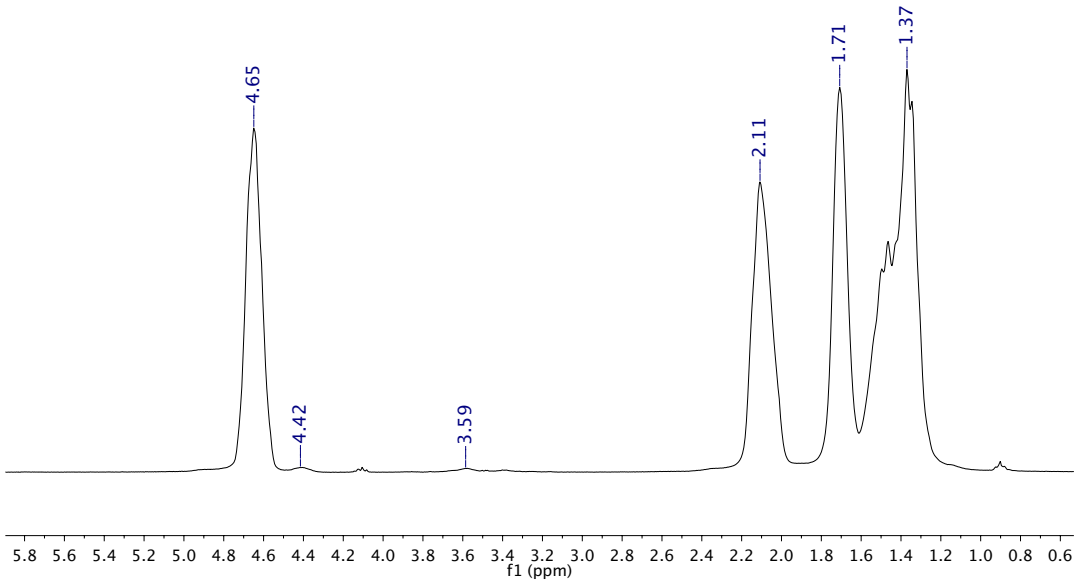

Figure C.2 ^{1}H NMR of the cleaned and dried polymer (Table 2-2, entry 3)

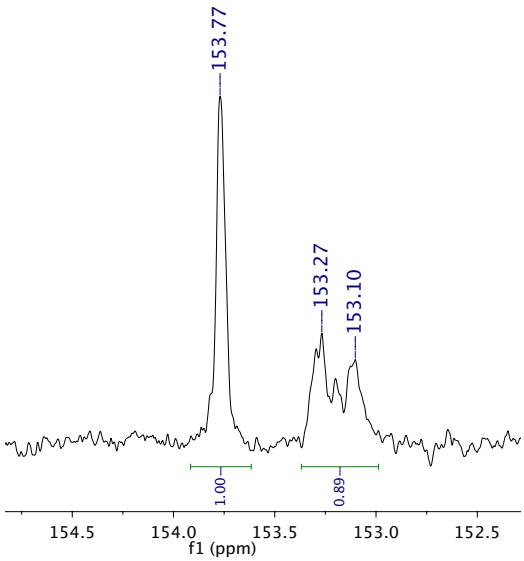

Figure C.3 Carbonyl region of the $^{13}C\{^{1}H\}$ NMR spectrum of a typical poly(cyclohexene) carbonate (Table 2-2, entry 3) showing the presence of both isotactic and syndiotactic isomers.

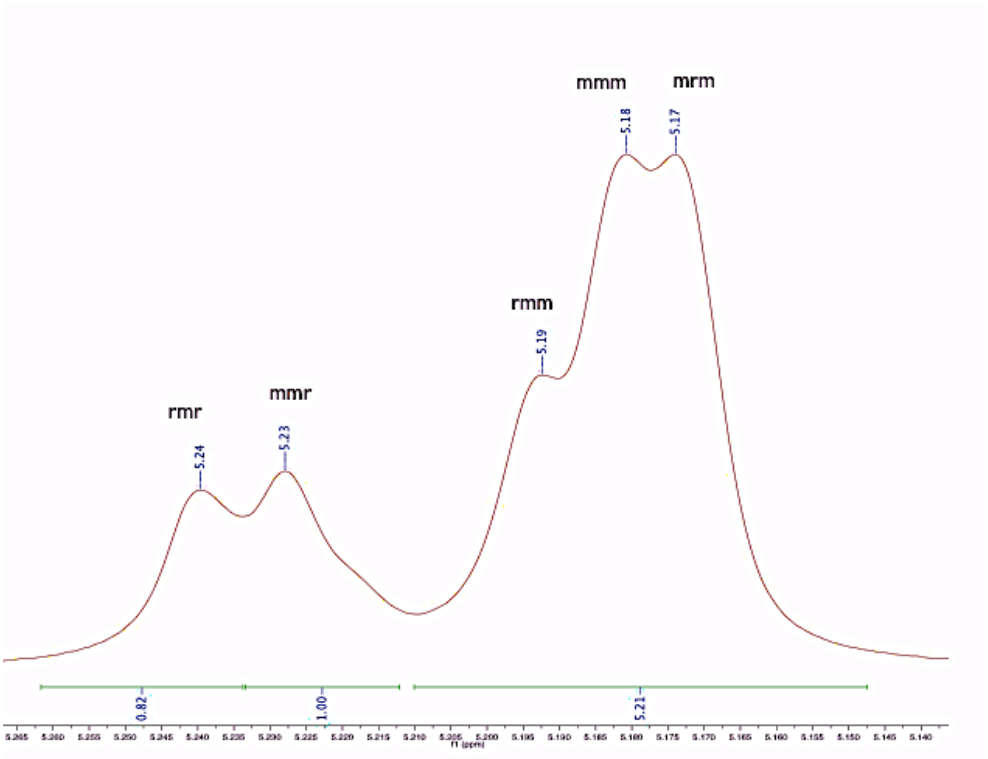

Figure C.4 $^{1}H\{^{1}H\}$-NMR spectrum of the PLA methine region obtained from *rac*-lactide catalyzed by **4.1** according to conditions in Table 4-1, entry 1

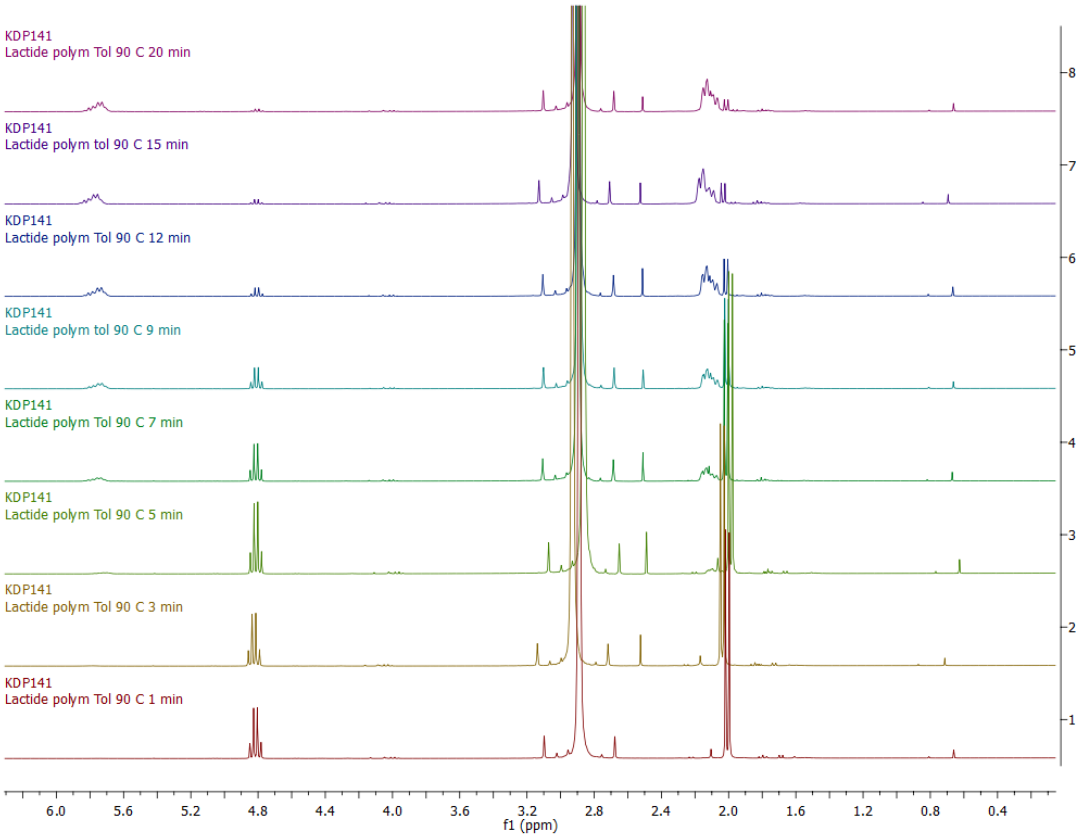

Figure C.5 Stacked ^{1}H NMR spectra of polymerization of *rac*-lactide by **4.2** in presence of *i*PrOH co-initiator ([LA]:[Mg]:[ROH] = 100:1:1) at 90 °C in toluene (Table 4-3, entry 1).

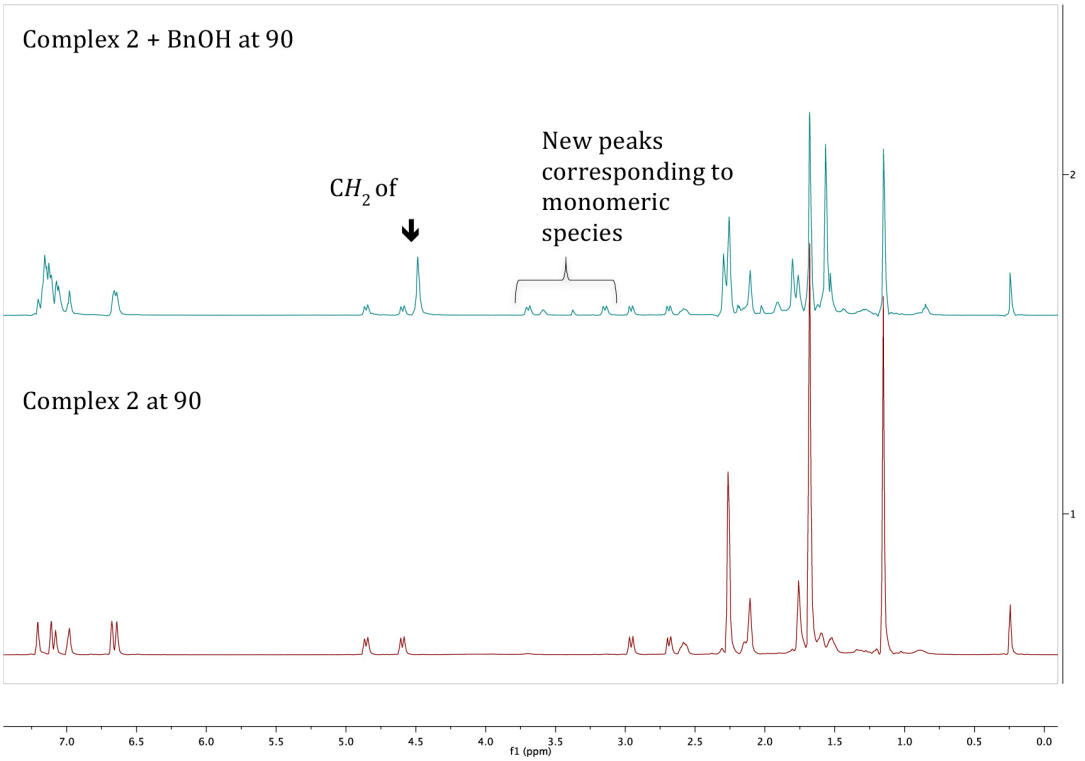

Figure C.6 ^{1}H NMR spectra of complex **4.2** (bottom) and 1:1 mixture of BnOH co-initiator with complex **4.2** (top) in toluene-d_8 at 363 K.

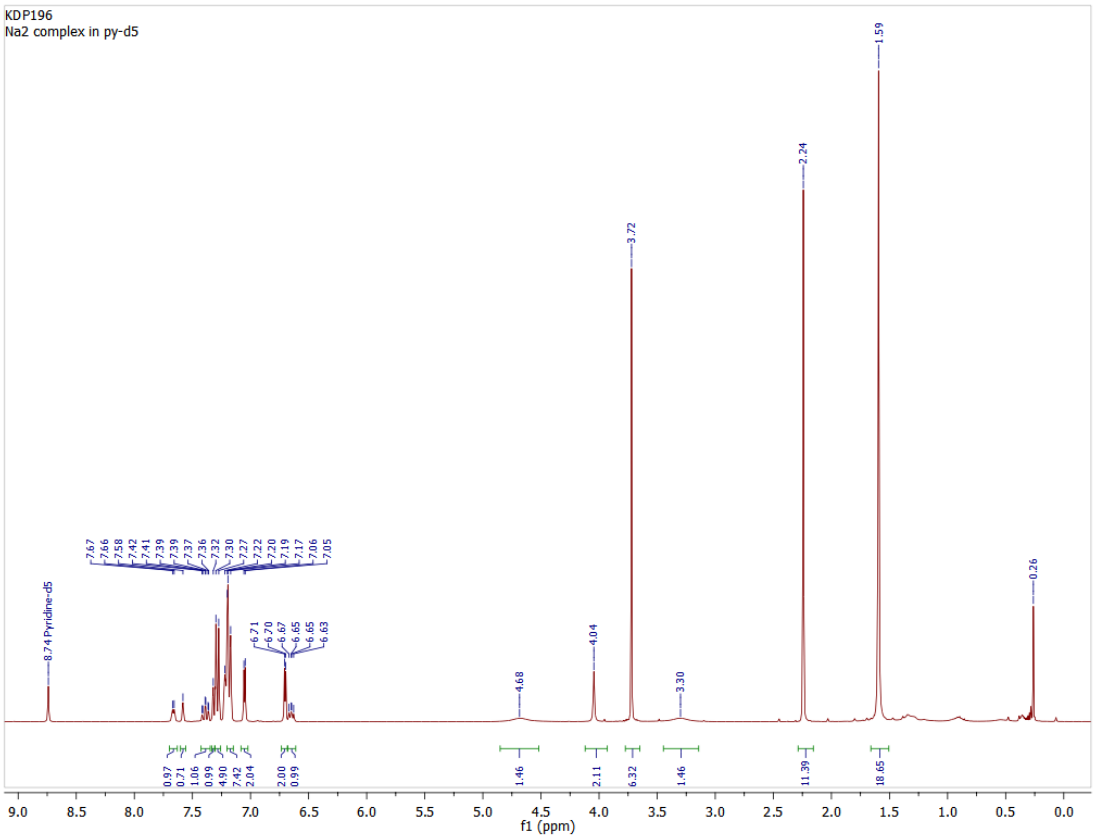

Figure C.7 ^{1}H NMR spectrum of **5.1** in py-d_5 (prepared in toluene).

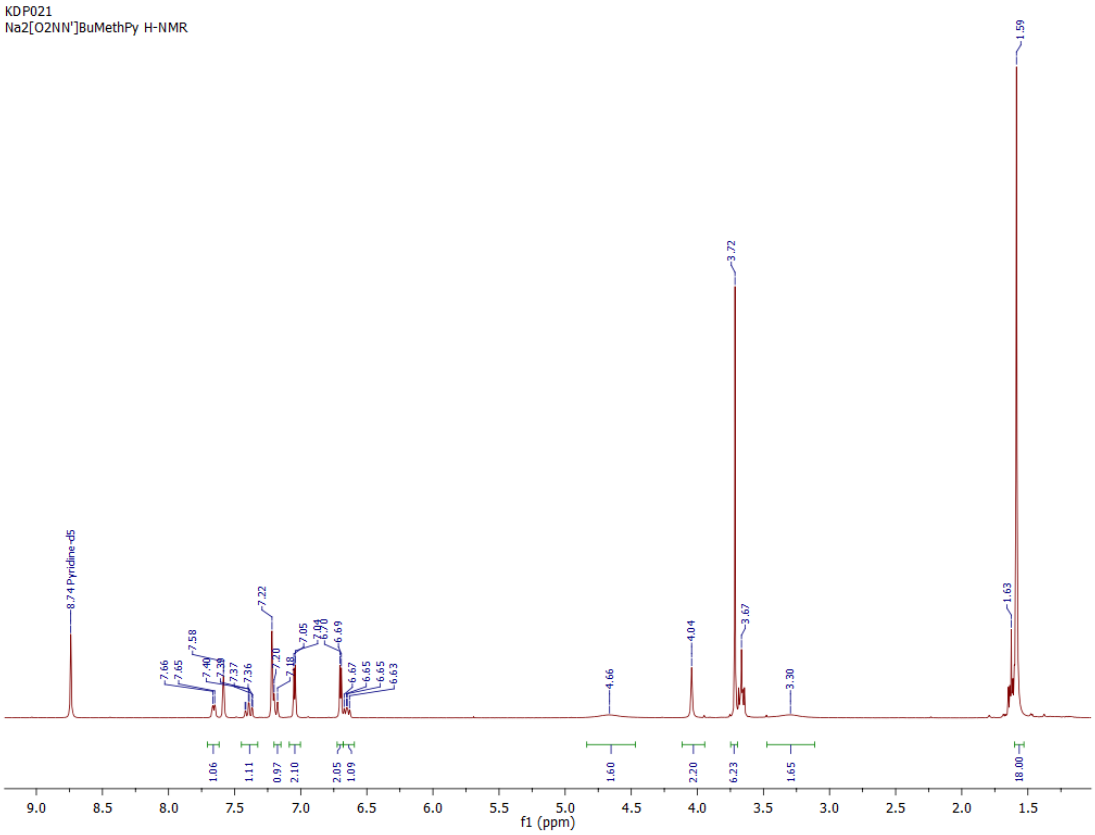

Figure C.8 ^{1}H NMR spectrum of **5.1** in py-d_5 (prepared in THF).

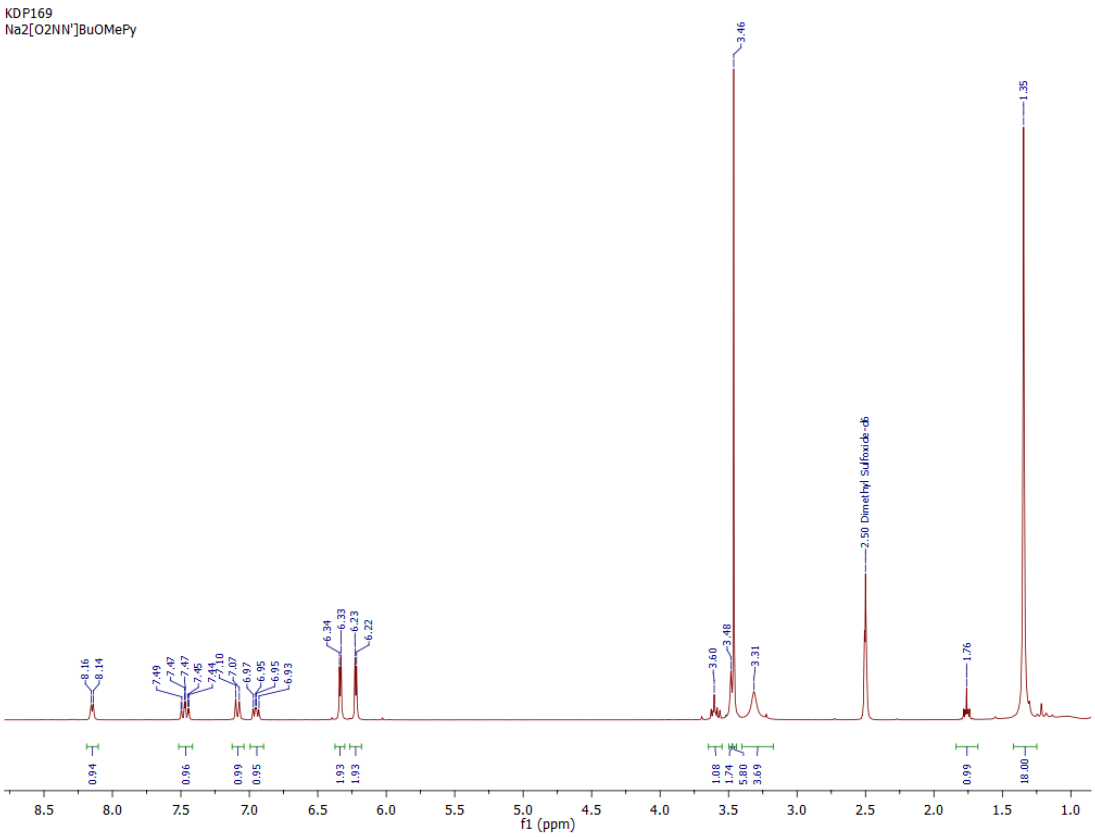

Figure C.9 ^{1}H NMR spectrum of **5.1** in DMSO-d_6.

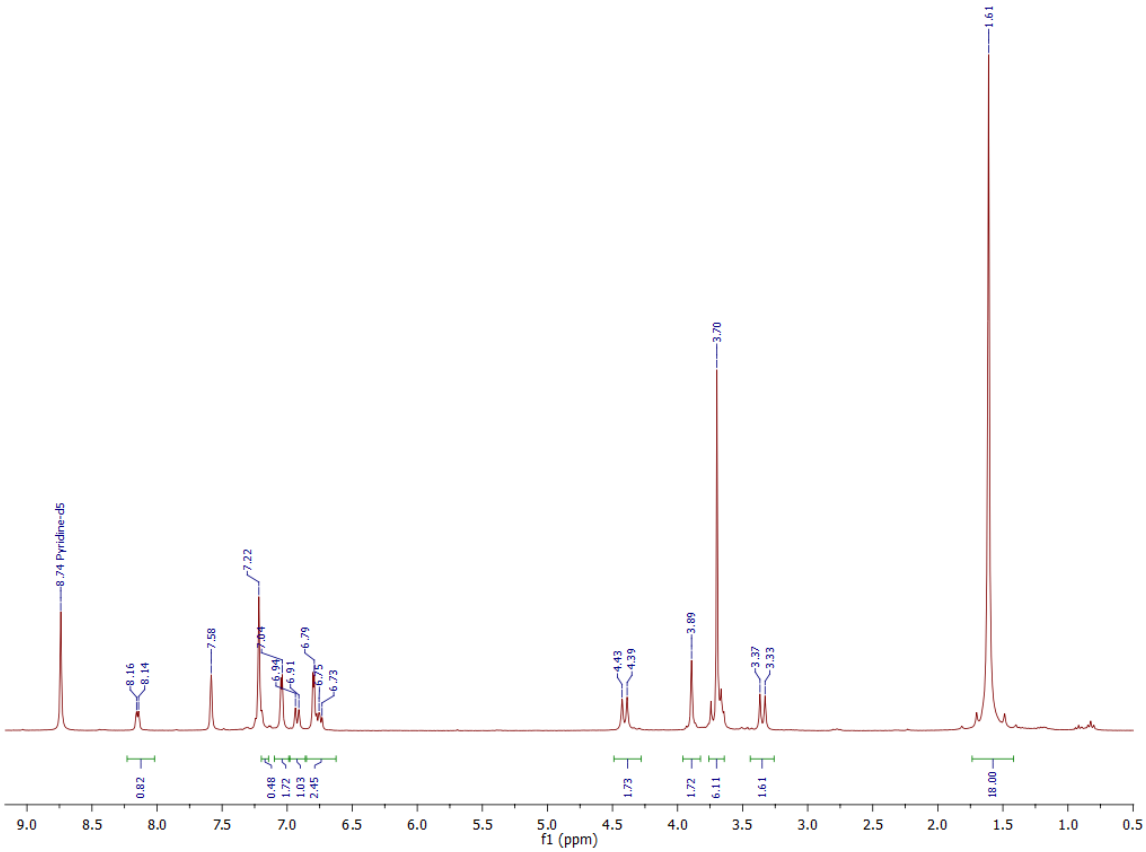

Figure C.10 ^{1}H NMR spectrum of **5.2** in py-d_5.

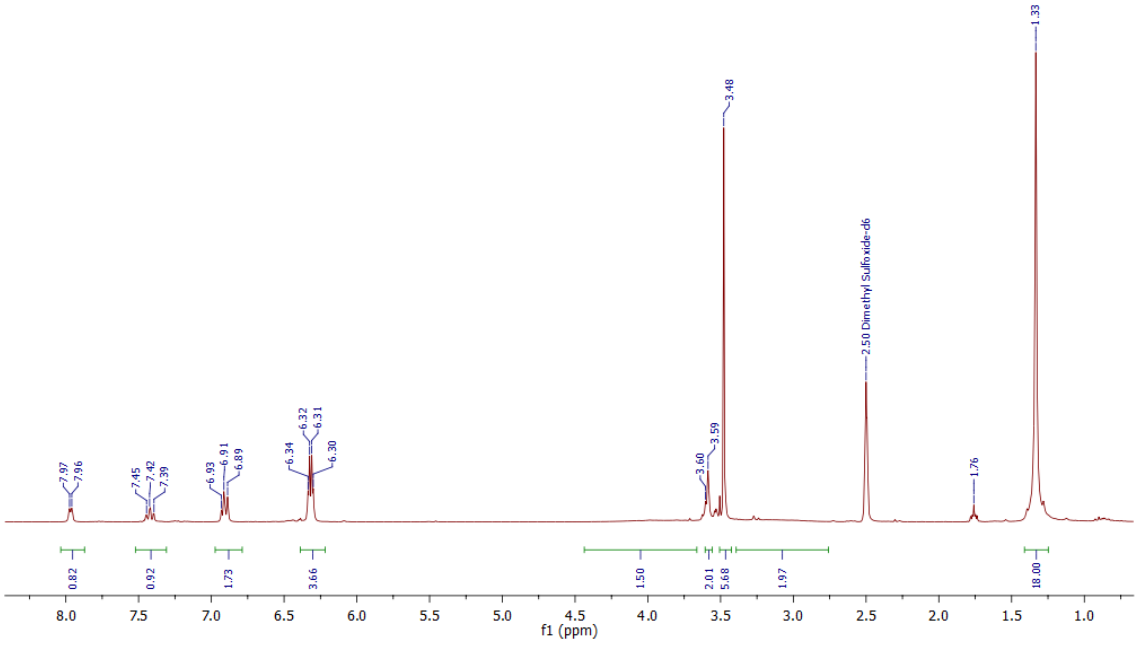

Figure C.11 ^{1}H NMR spectrum of **5.2** in DMSO-d_6.

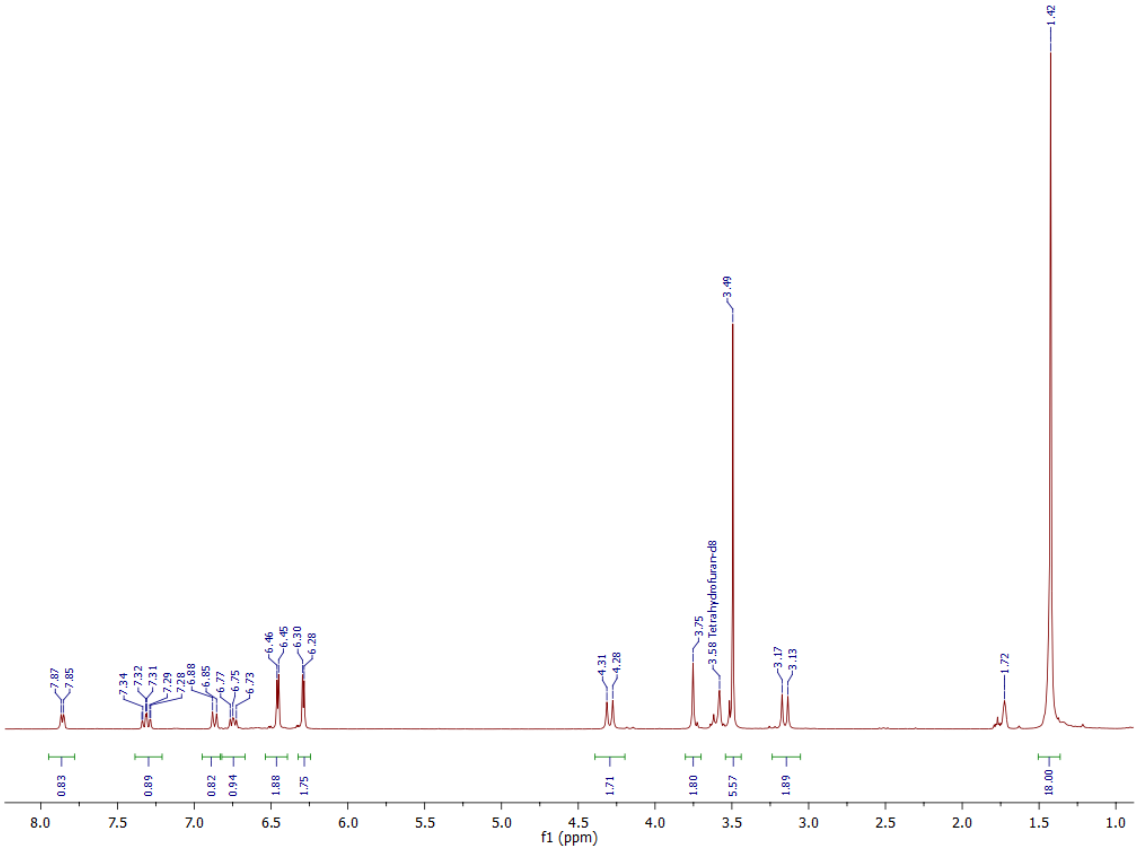

Figure C.12 ^{1}H NMR spectrum of **5.2** in THF-d_8.

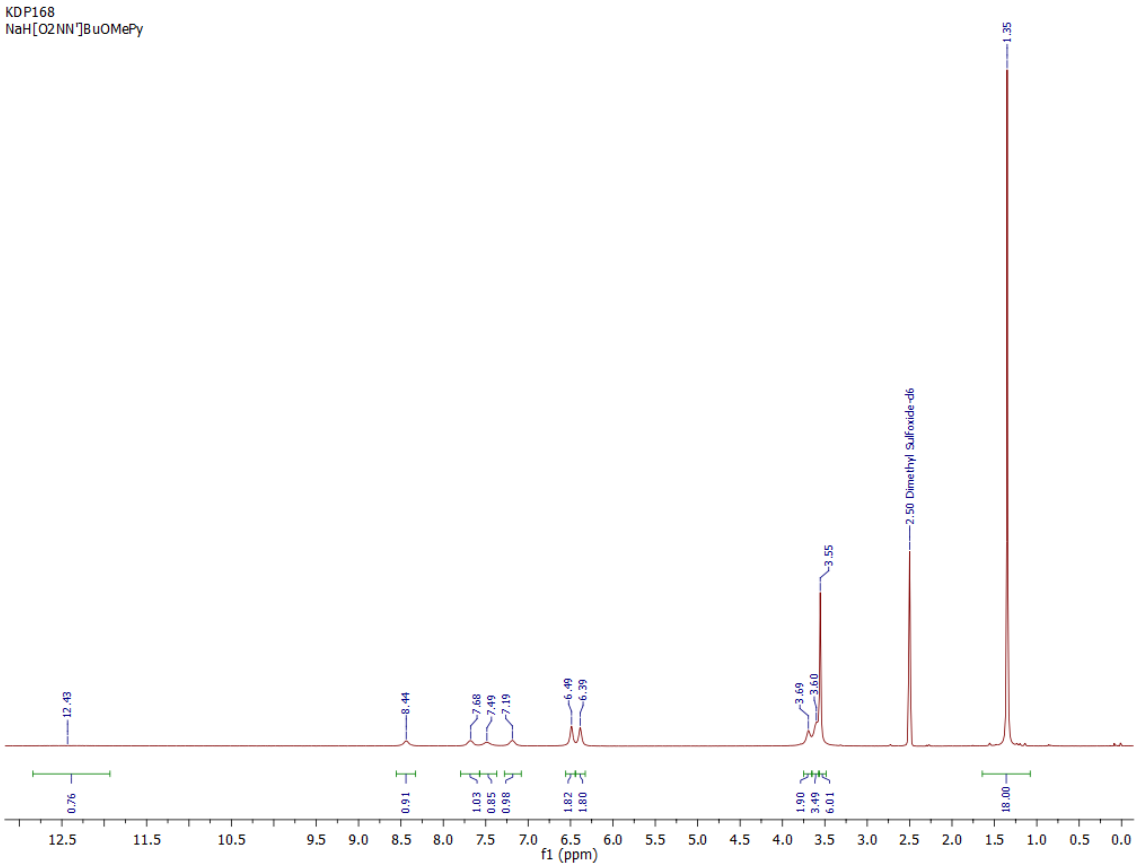

Figure C.13 ^{1}H NMR spectrum of **5.3** in DMSO-d_6.

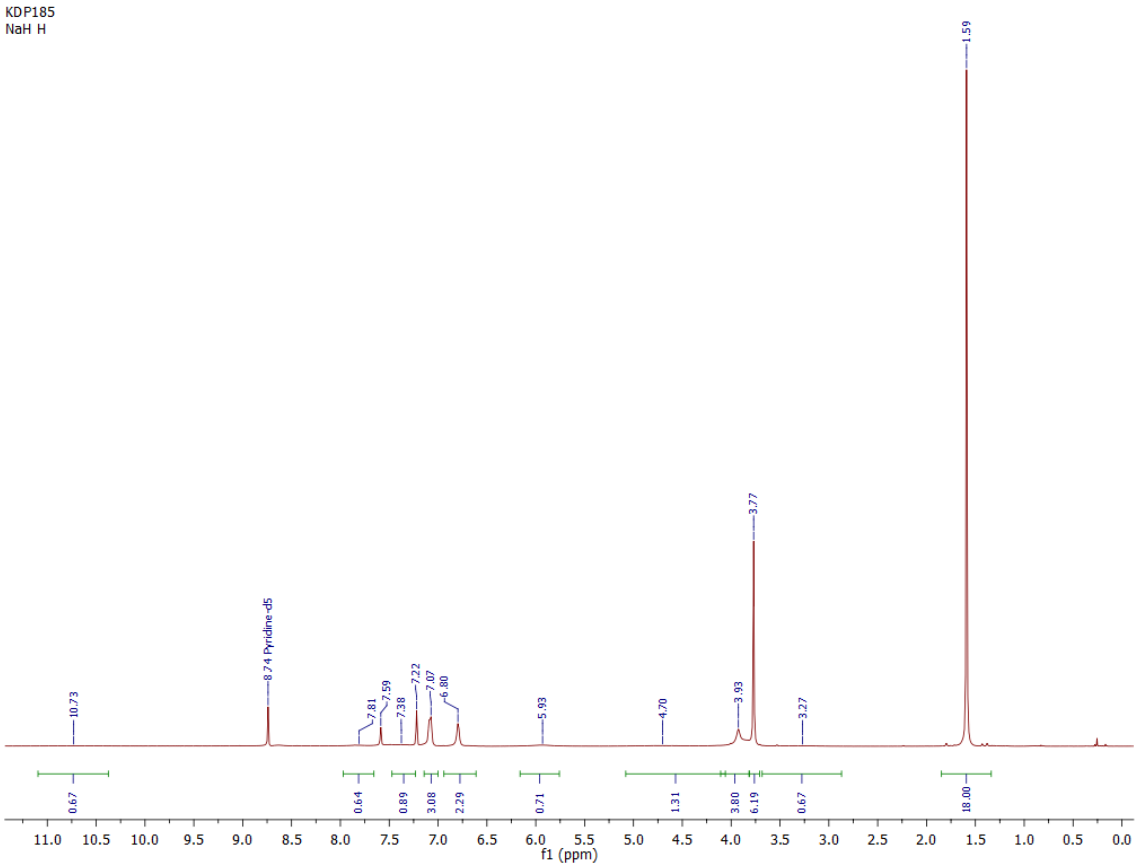

Figure C.14 ^{1}H NMR spectrum of **5.3** in py-d_5.

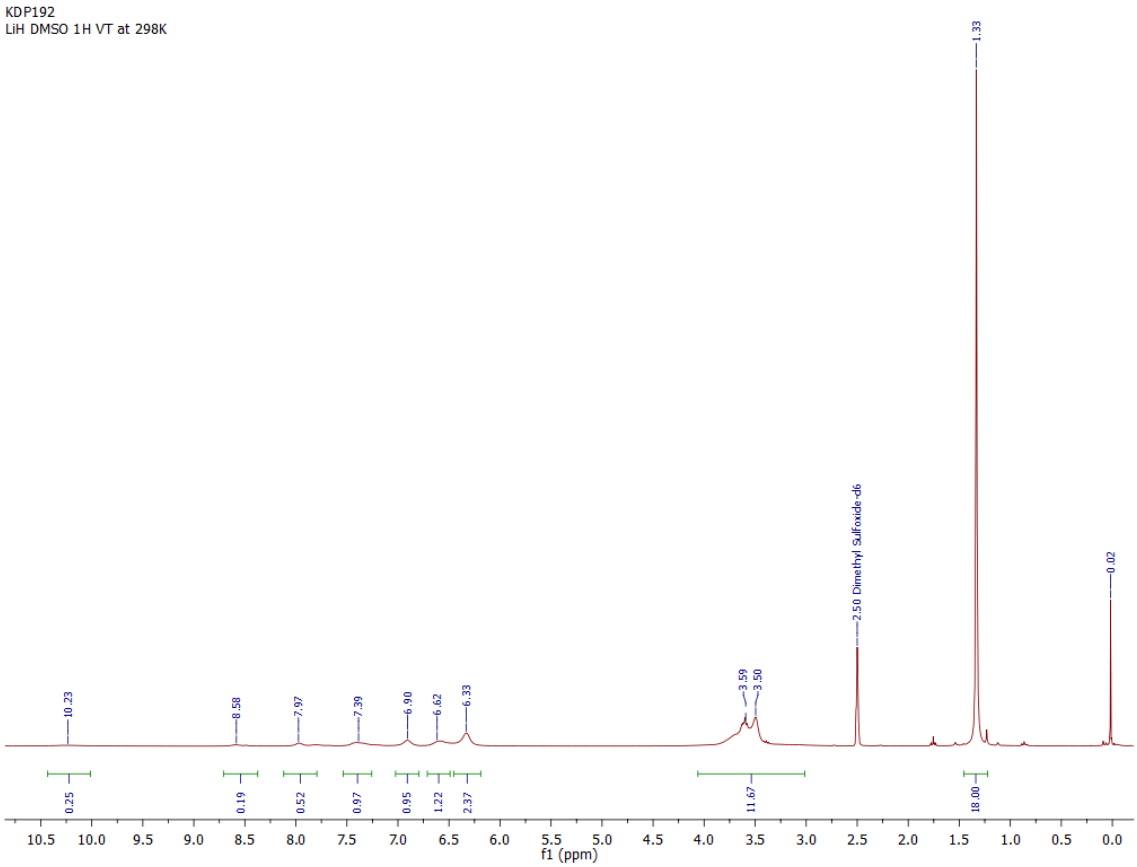

Figure C.15 ^{1}H NMR spectrum of **5.4** in DMSO-d_6.

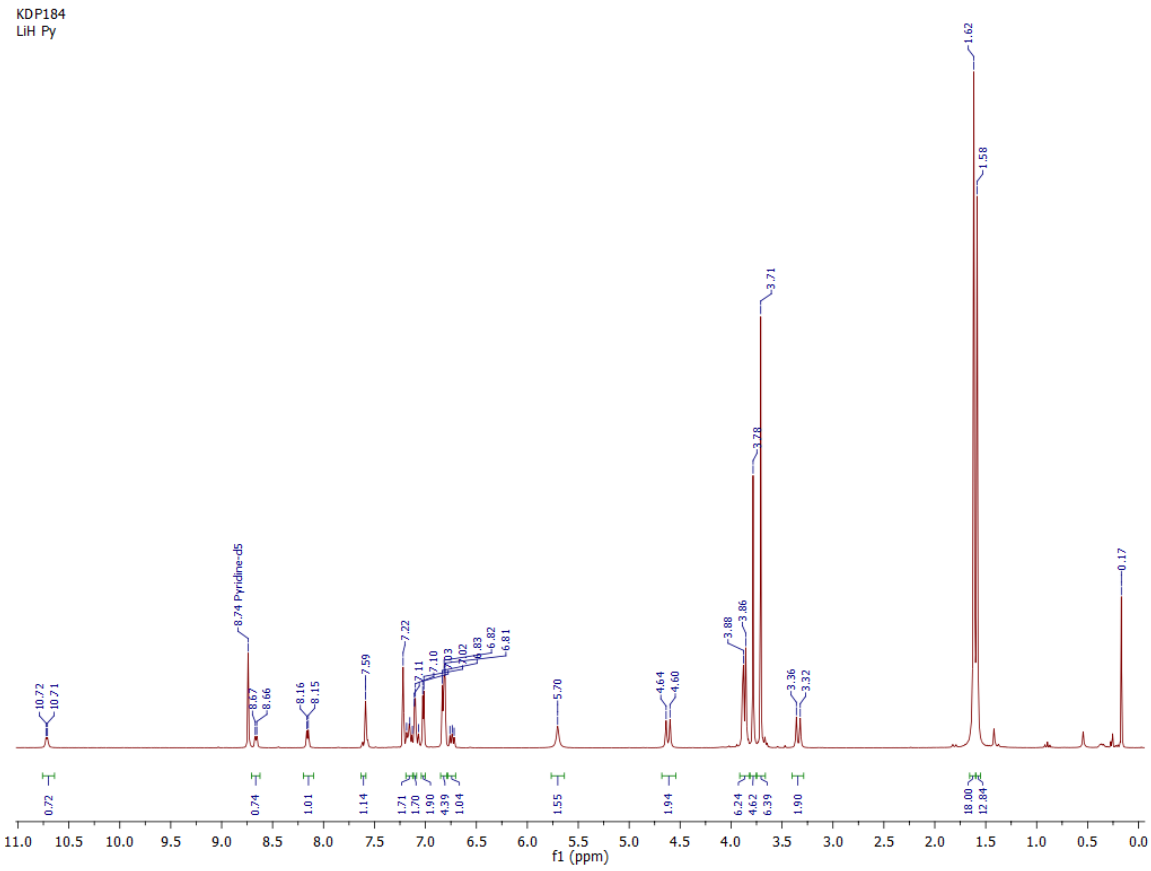

Figure C.16 ^{1}H NMR spectrum of **5.4** in py-d_5.

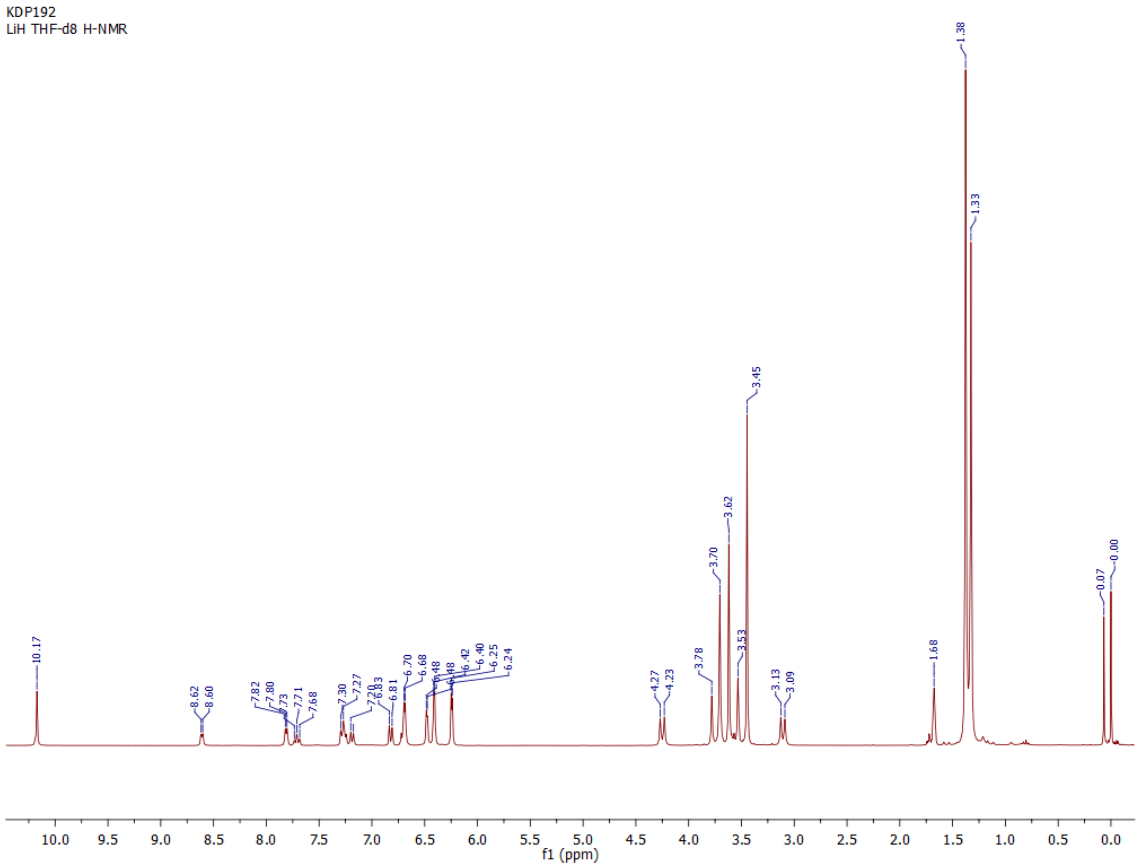

Figure C.17 ^{1}H NMR spectrum of **5.4** in THF-d_8.

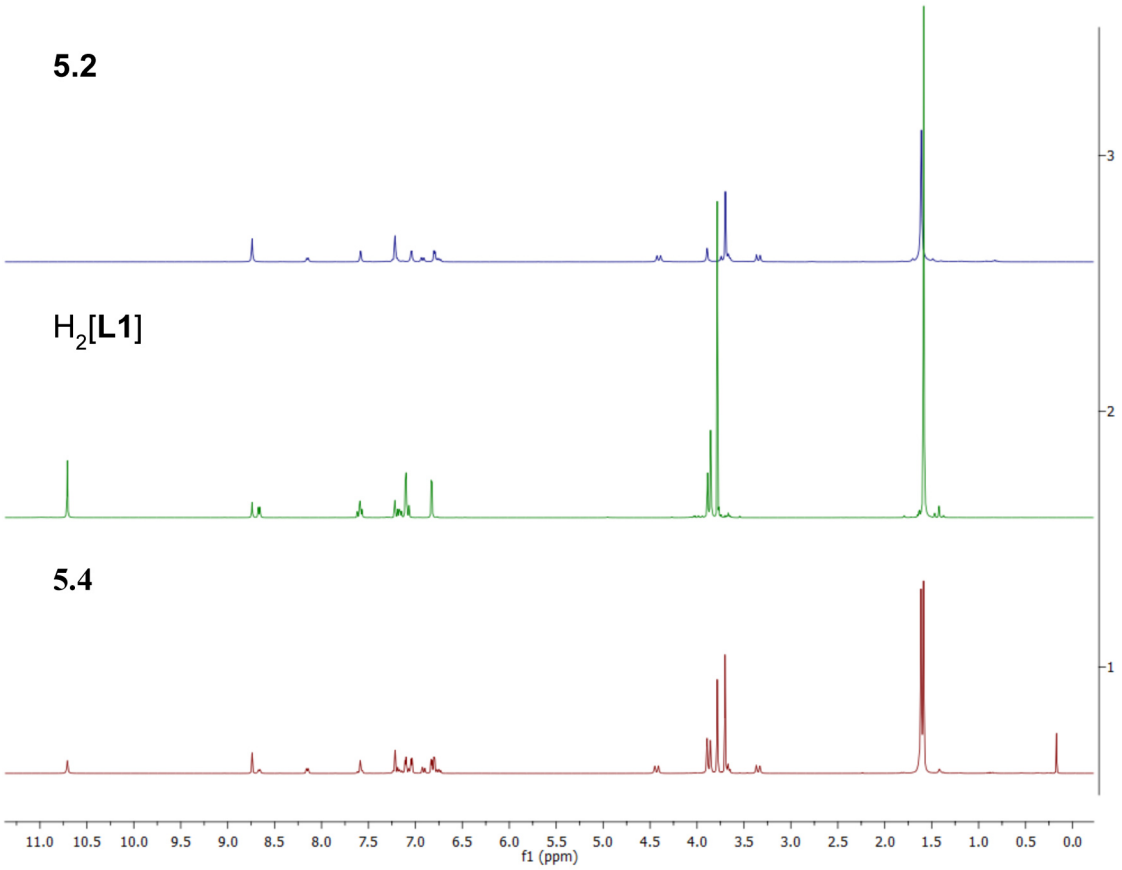

Figure C.18 ^{1}H NMR spectra of complexes **5.2** and **5.4** and H_2[**L1**] in py-d_5.

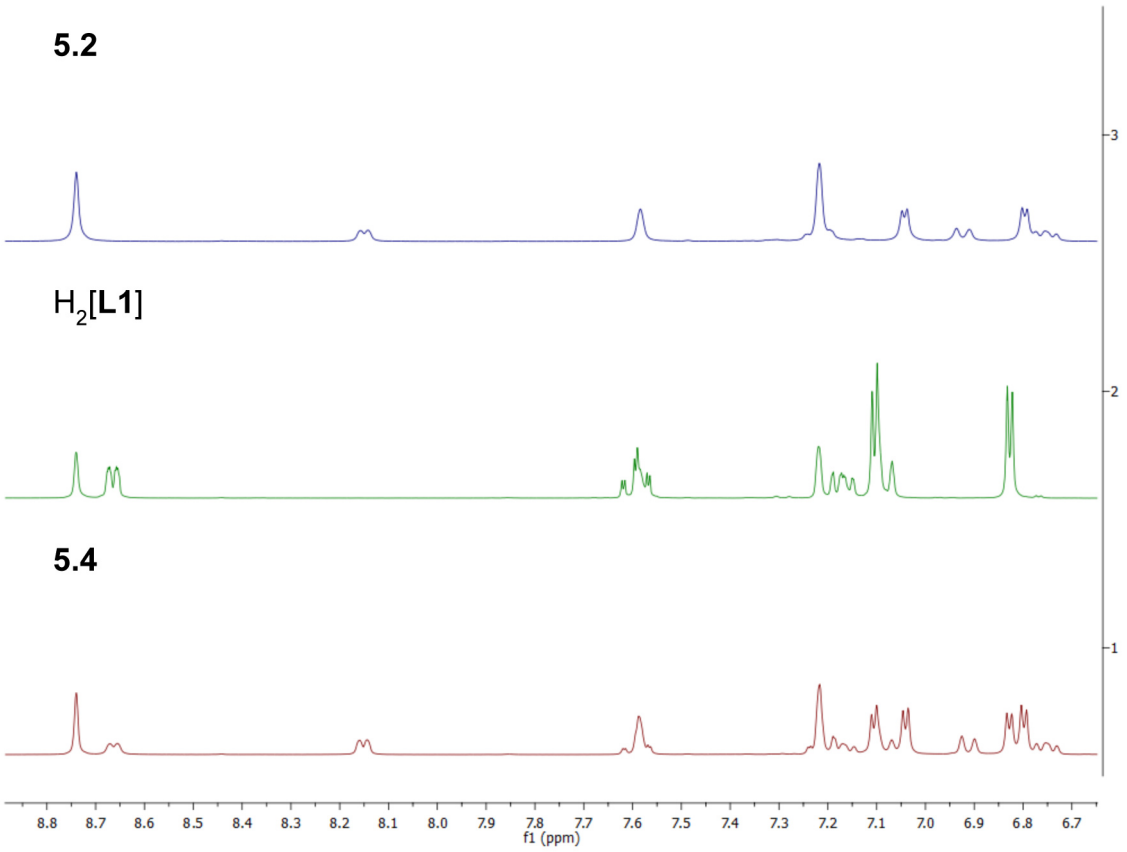

Figure C.19 Aromatic region of the ^{1}H NMR spectra of complexes **5.2** and **5.4** and H_2[**L1**] in py-d_5.

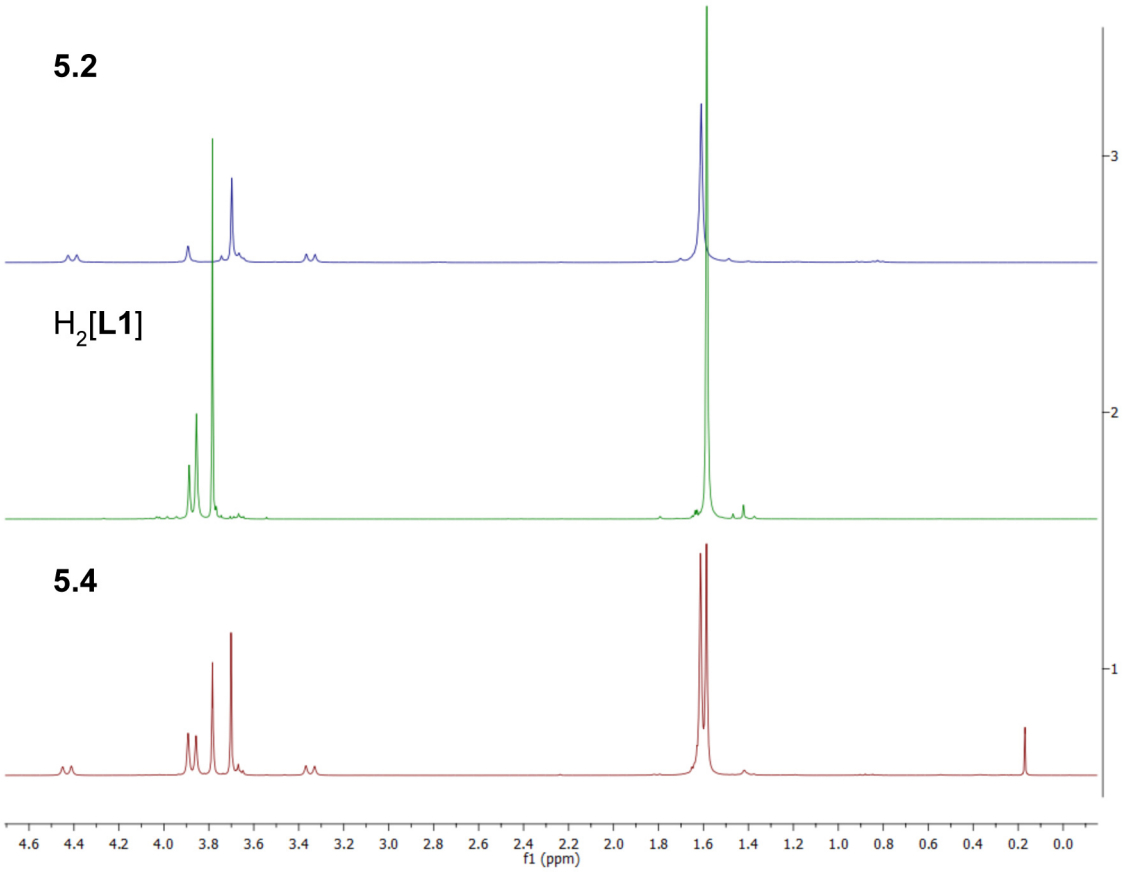

Figure C.20 Methylene and methyl region of the ^{1}H NMR spectra of complexes **5.2** and **5.4** and H_2[**L1**] in py-d_5.

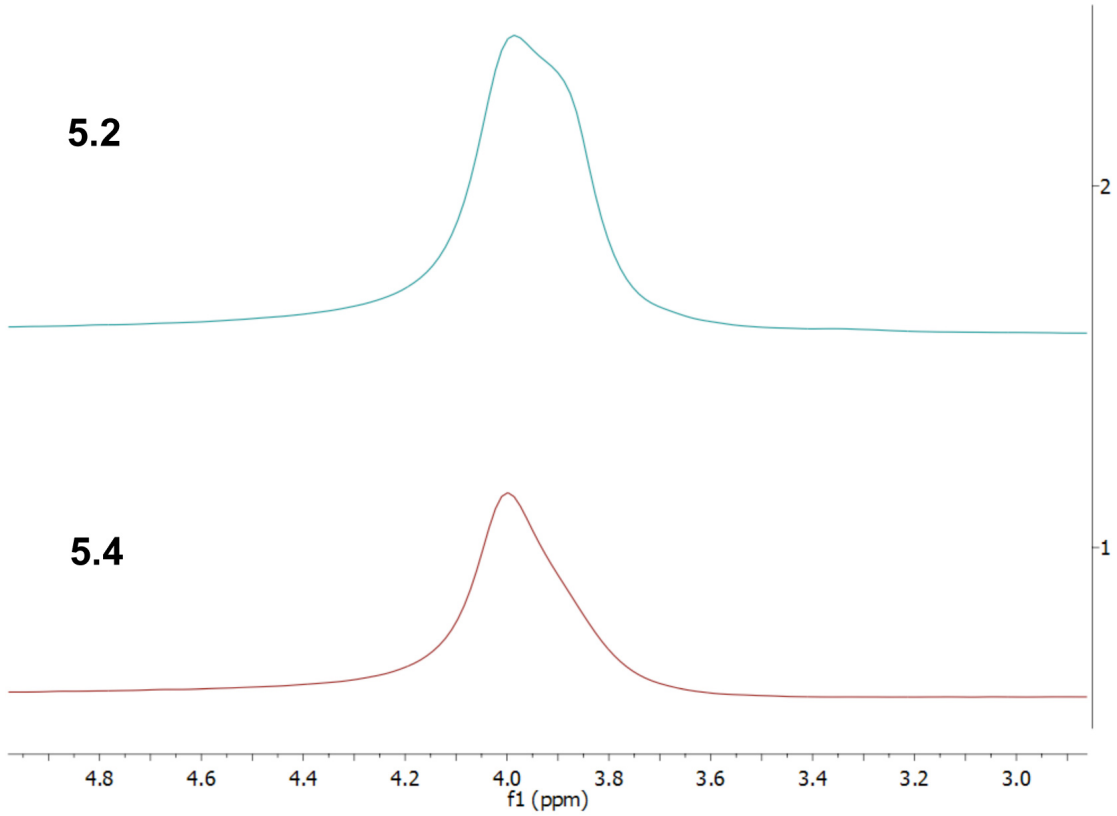

Figure C.21 Stacked ^{7}Li NMR spectra of **5.2** and **5.4** in py-d_5.

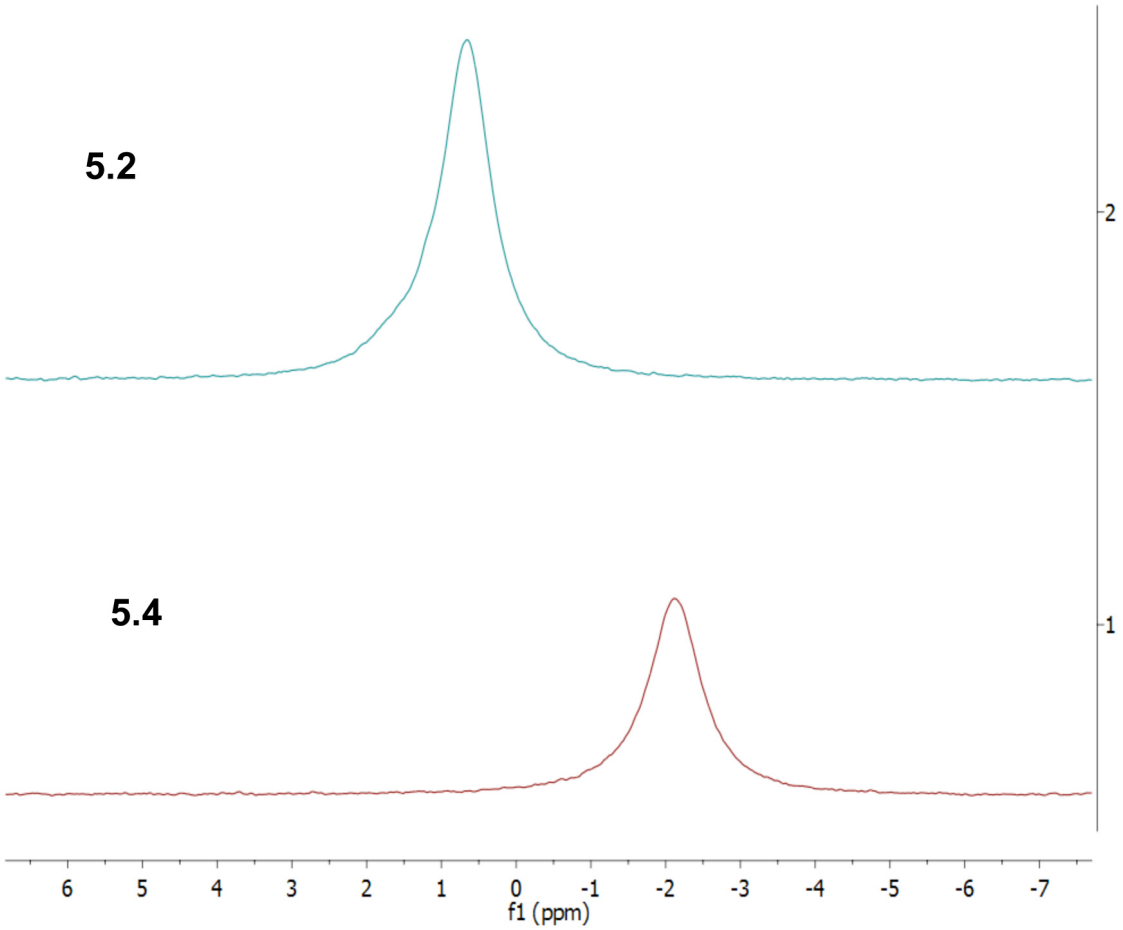

Figure C.22 Stacked ^{7}Li NMR spectra of **5.2** and **5.4** in DMSO-d_6.

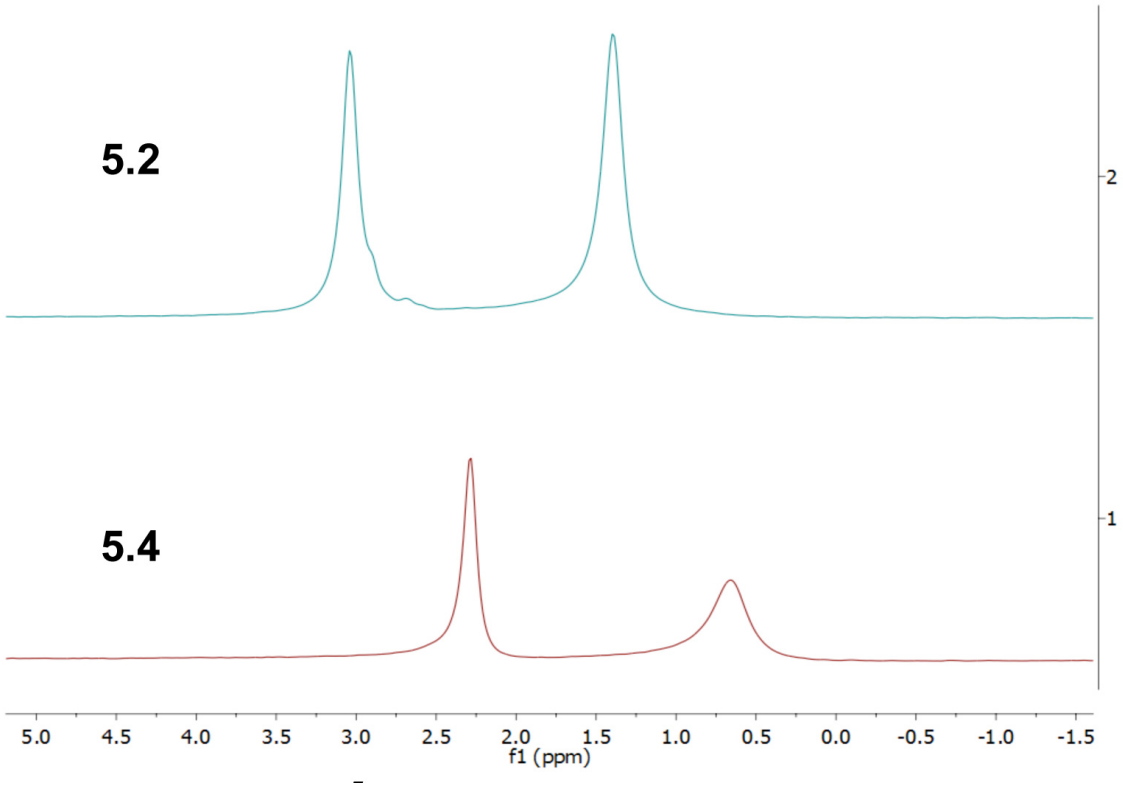

Figure C.23 Stacked ^{7}Li NMR spectra of **5.2** and **5.4** in THF-d_8.

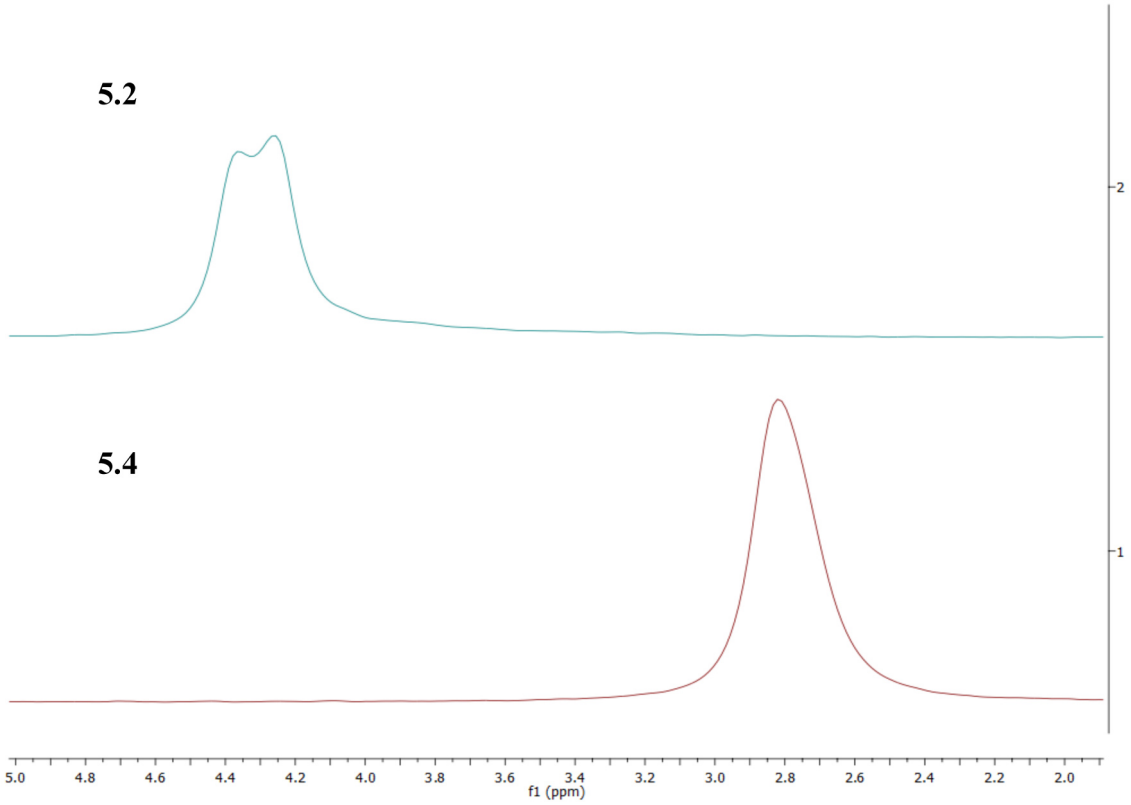

Figure C.24 ^{7}Li NMR spectra of **5.2** and **5.4** in py-d_5 (at a concentration of 0.0762 mol/L).

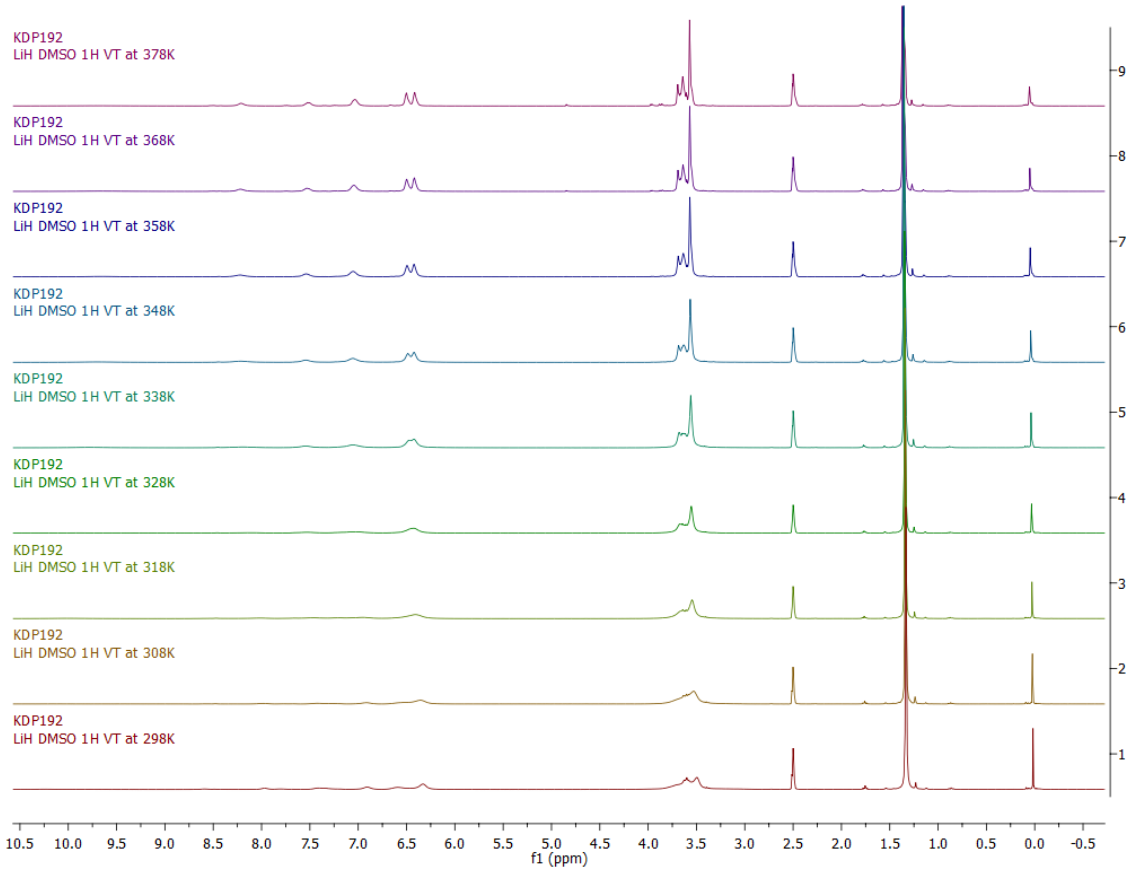

Figure C.25 Variable temperature ^{1}H NMR spectra for **5.4** in DMSO-d_6.

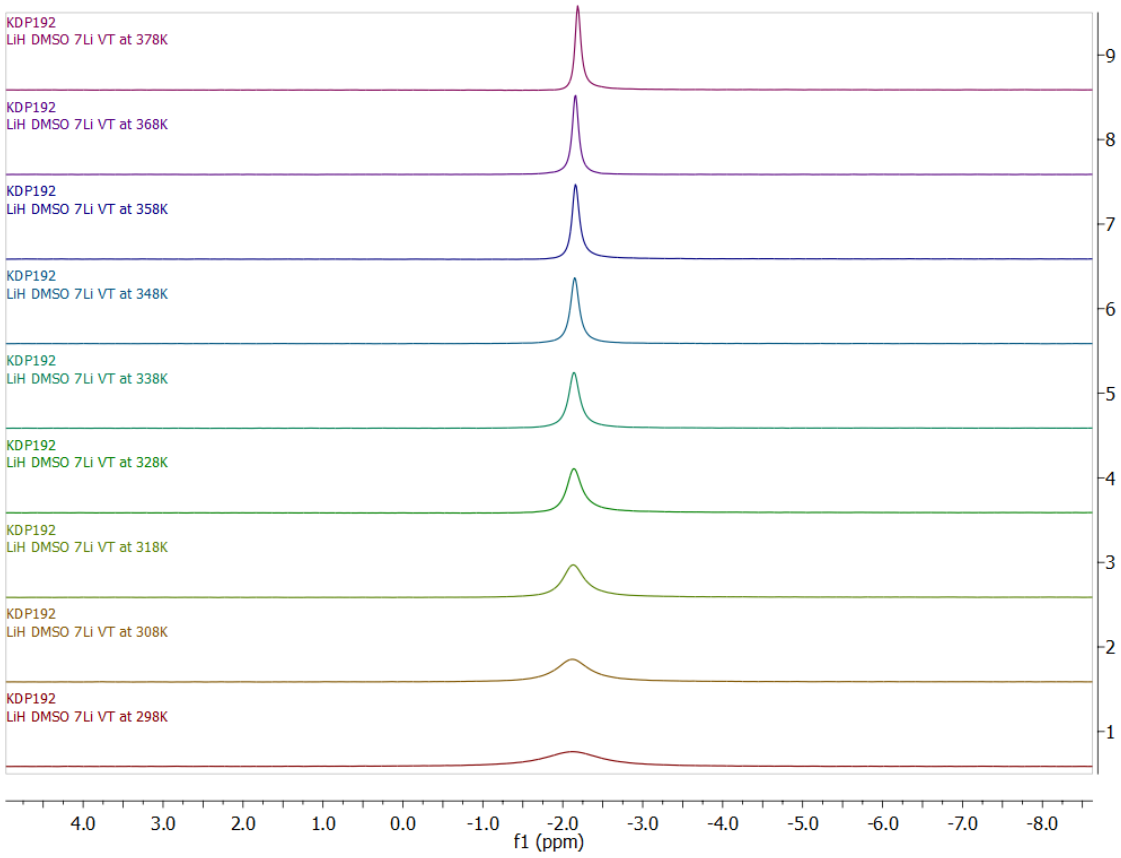

Figure C.26 Variable temperature ^{7}Li NMR spectra for **5.4** in DMSO-d_6.

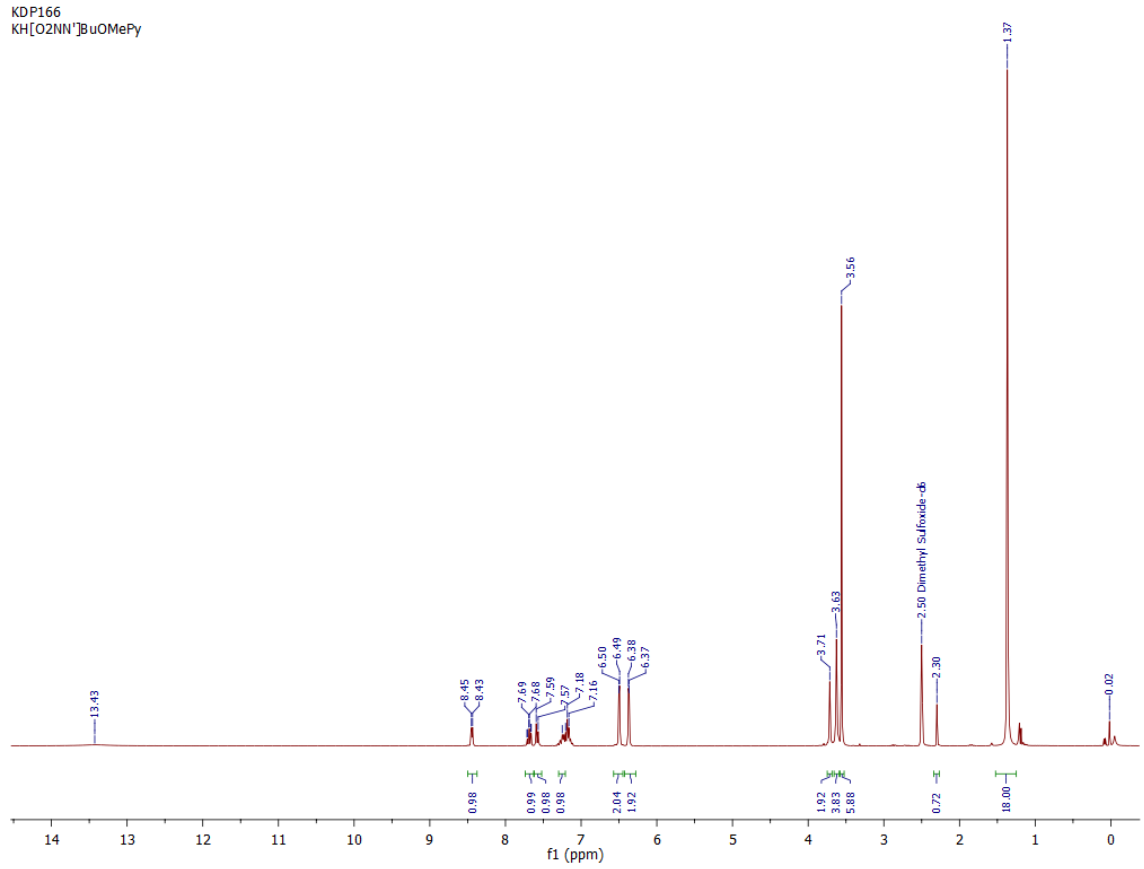

Figure C.27 ^{1}H NMR spectrum of **5.5** in DMSO- d_6.

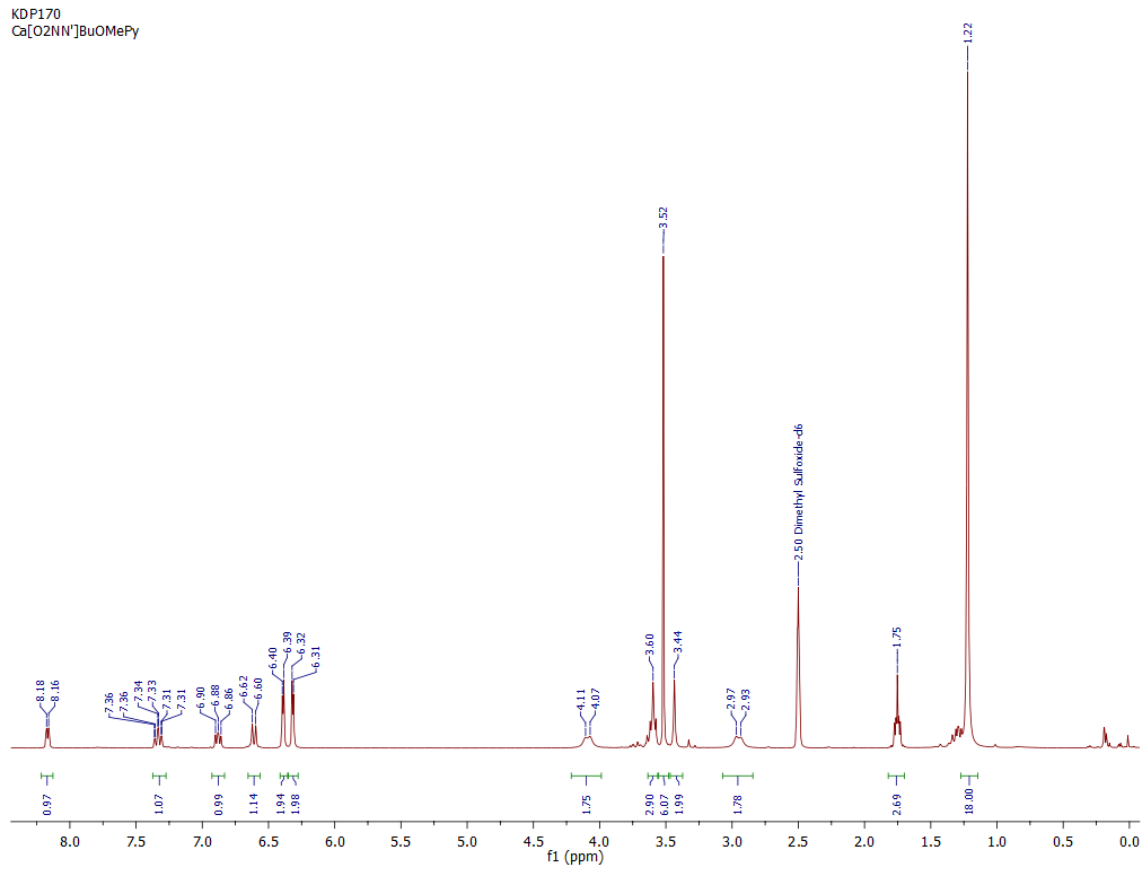

Figure C.28 ^{1}H NMR spectrum of **5.6** in DMSO-d_6 prepared via route A) in Scheme 5.1.

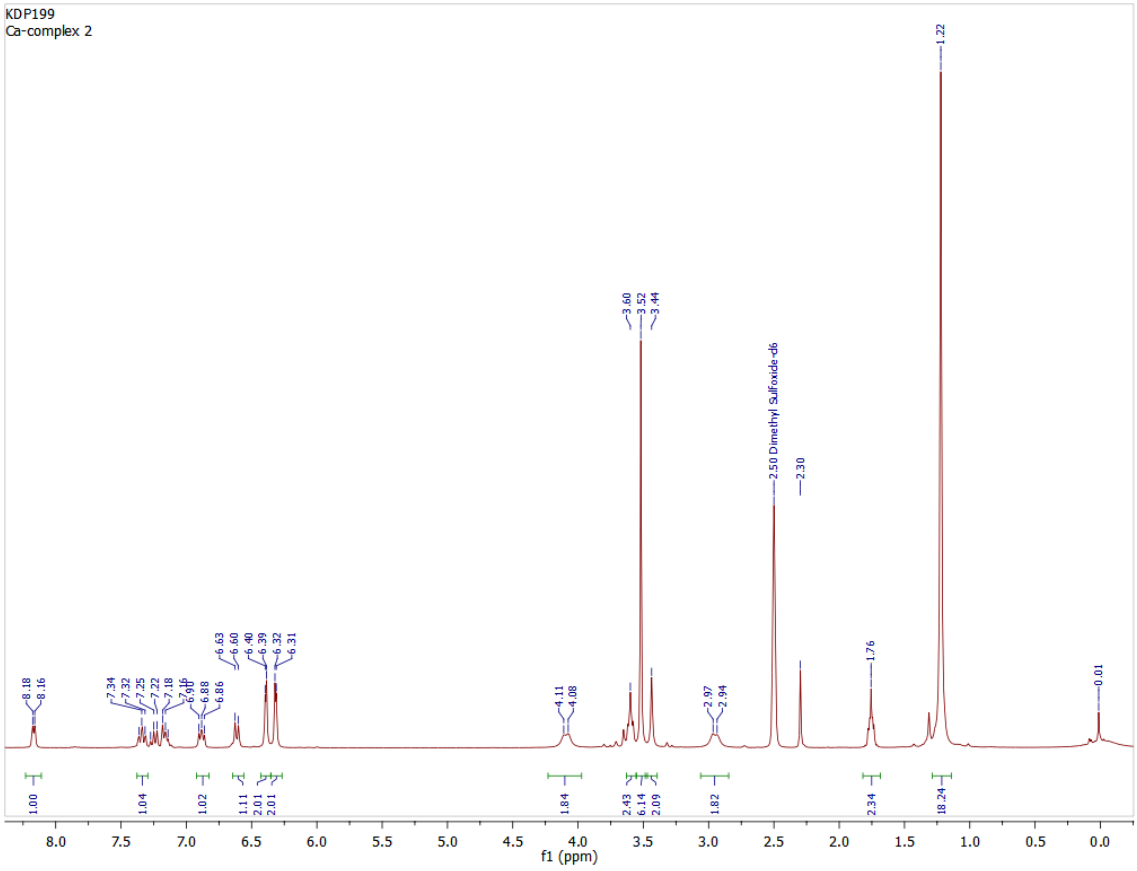

Figure C.29 ^{1}H NMR spectrum of **5.6** in DMSO-d_6 prepared via route B) in Scheme 5.1.

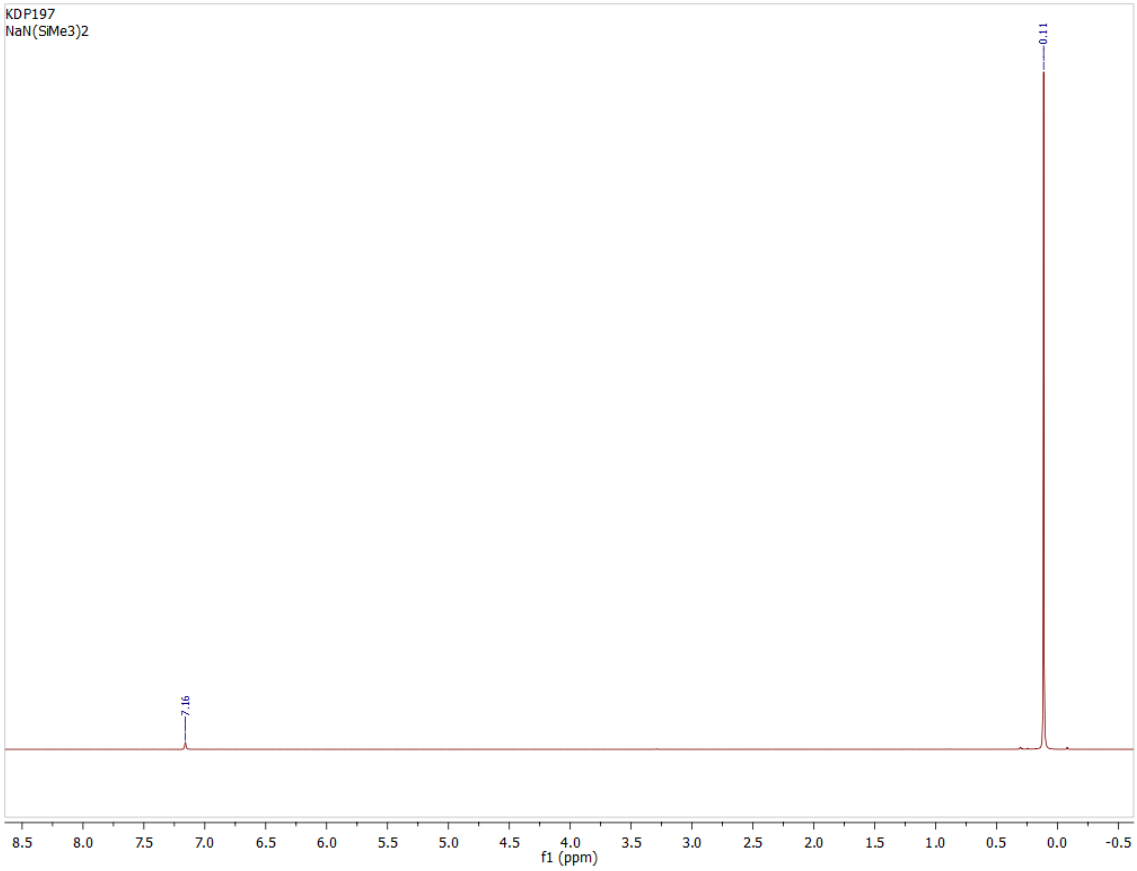

Figure C.30 ^{1}H NMR spectrum of freshly prepared $NaN(Si(CH_3)_3)_2$.

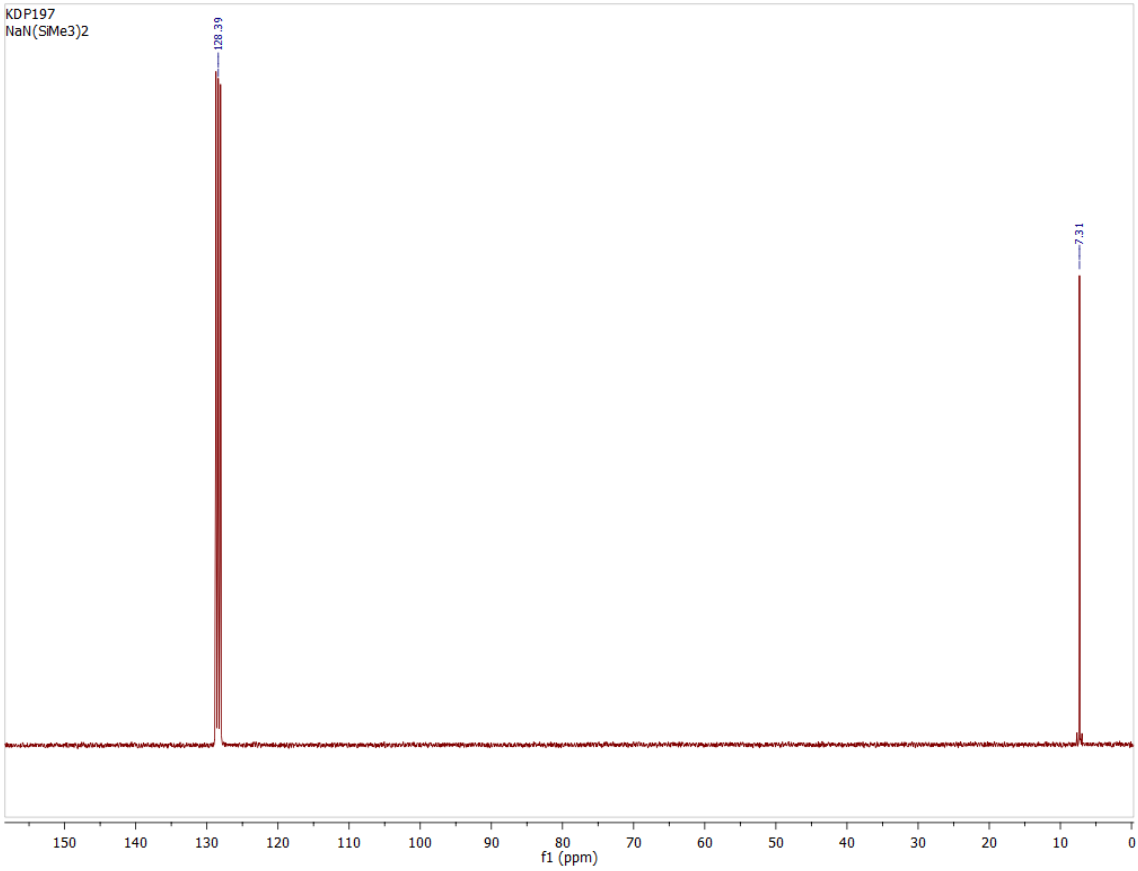

Figure C.31 ^{13}C NMR spectrum of freshly prepared $NaN(Si(CH_3)_3)_2$.

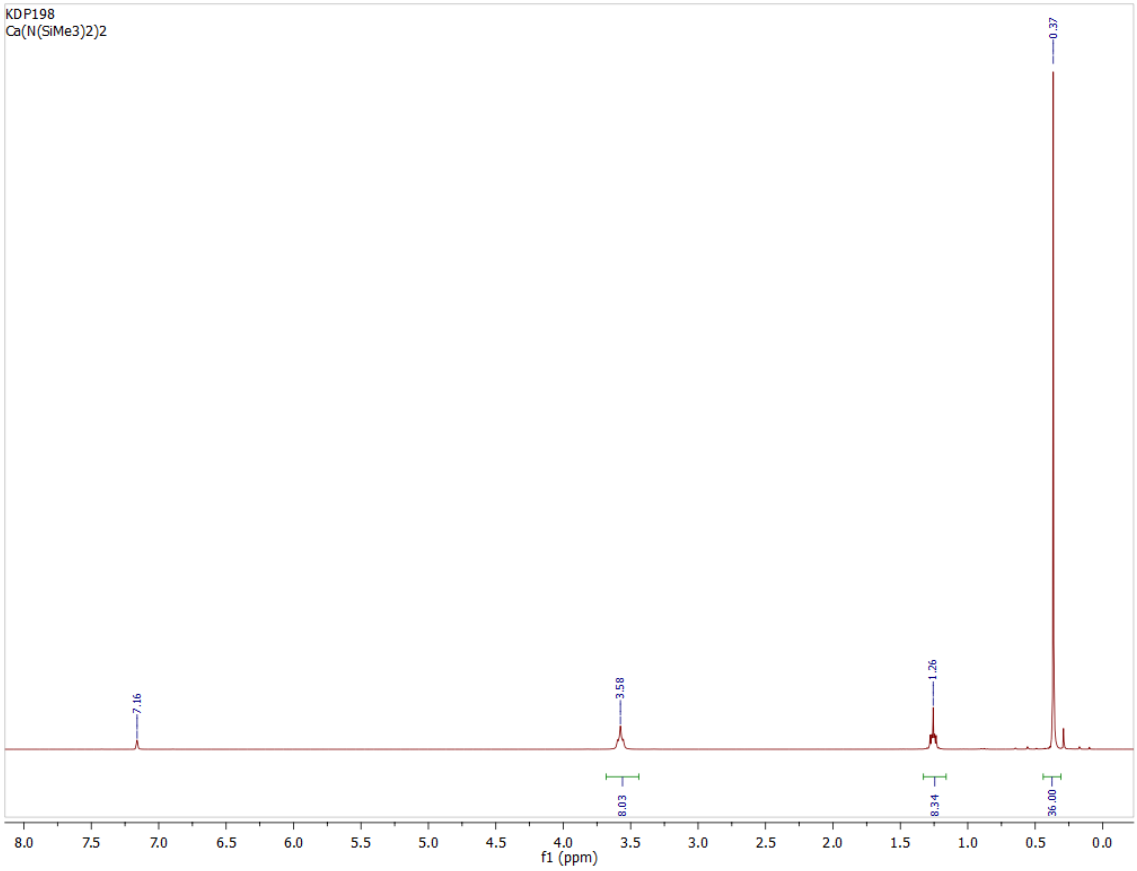

Figure C.32 ^{1}H NMR spectrum of $Ca\{N(Si(CH_3)_3)_2\}_2{\cdot}THF_2$.

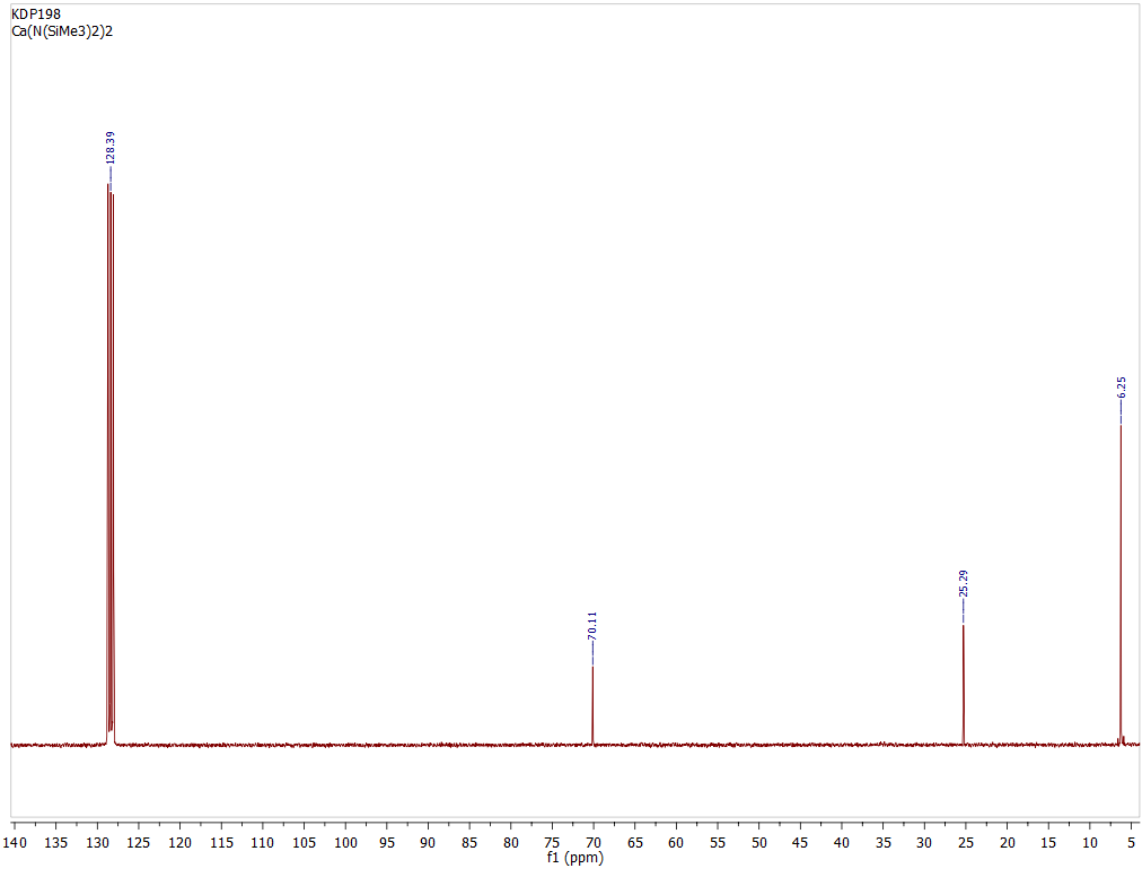

Figure C.33 ^{13}C NMR spectrum of $Ca\{N(Si(CH_3)_3)_2\}_2 \cdot THF_2$.

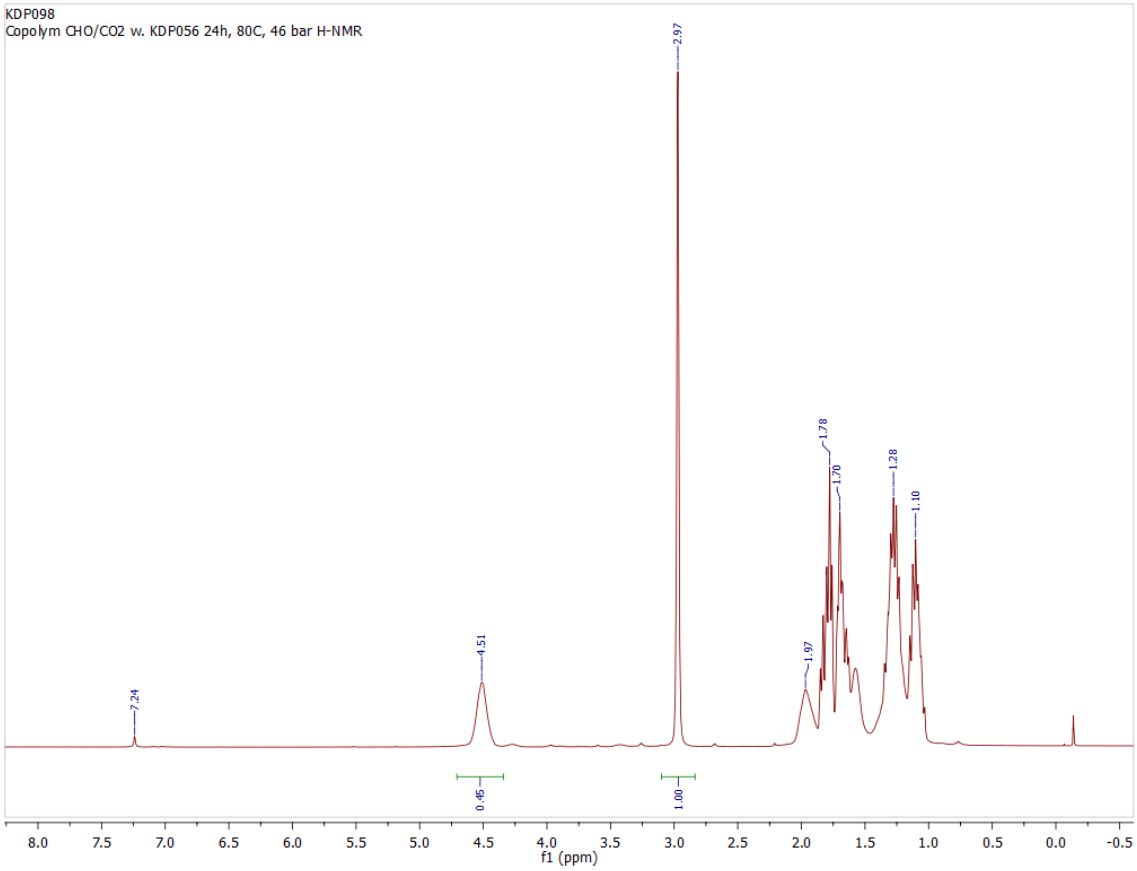

Figure C.34 ^{1}H NMR spectrum of the aliquot taken after the CHO/CO_2 copolymerization reaction with **6.1**·THF and DMAP.

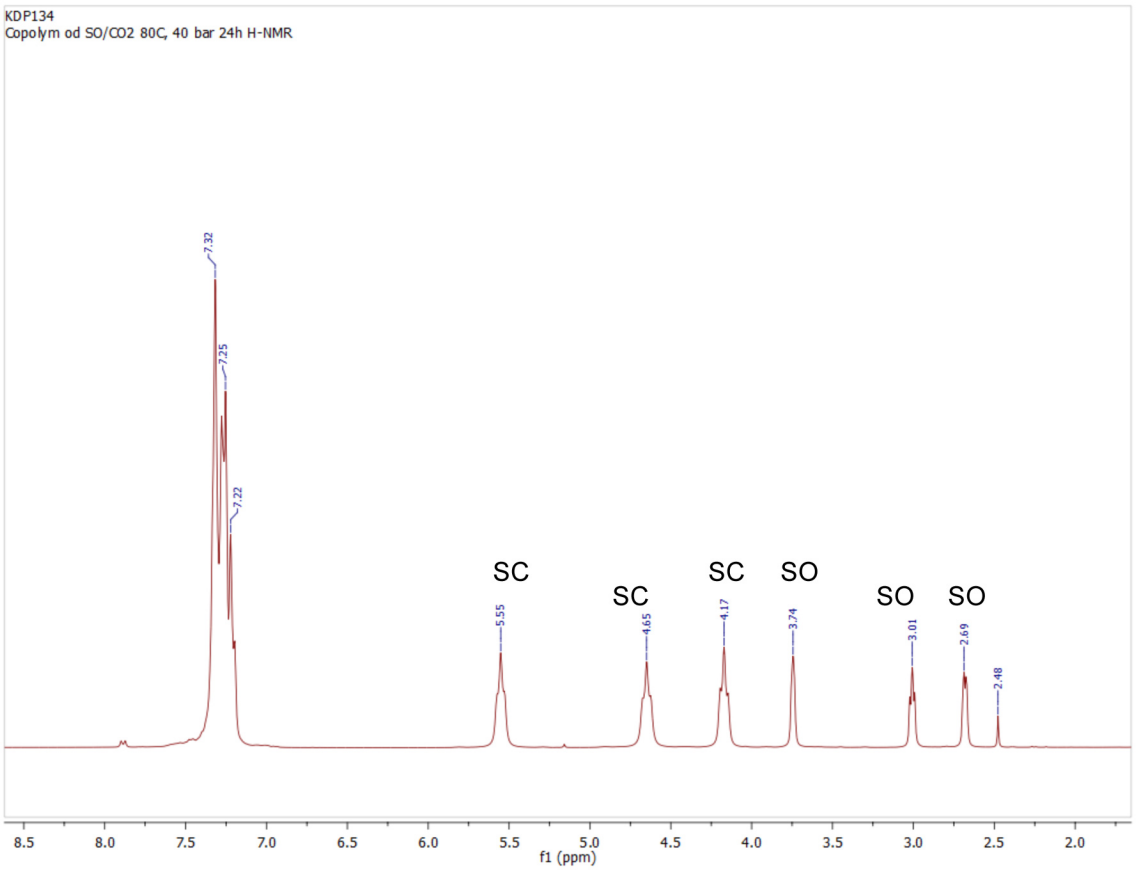

Figure C.35 ^{1}H NMR spectrum of the aliquot taken after the SO/CO_2 copolymerization reaction with **2.1**·THF and $PPNN_3$.

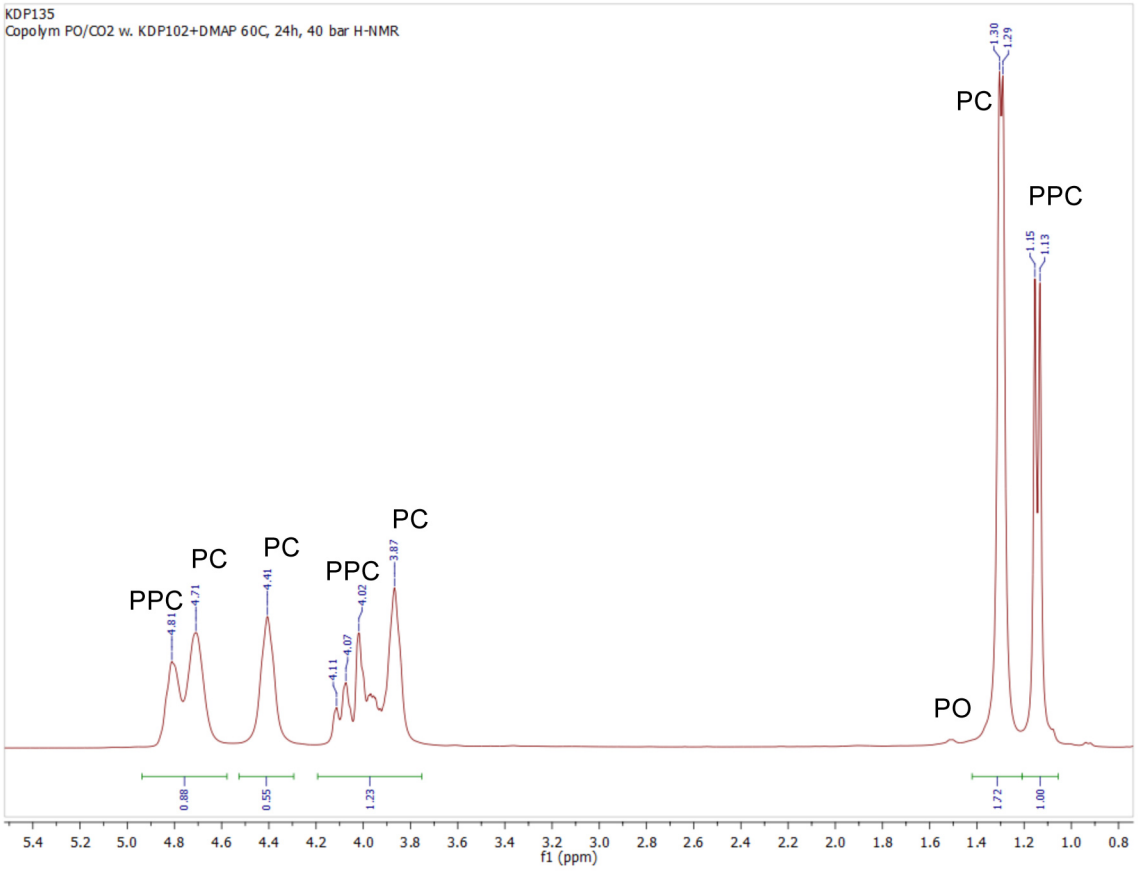

Figure C.36 ^{1}H NMR spectrum of the aliquot taken after PO/CO_2 copolymerization reaction with **2.1**·THF and DMAP.

APPENDIX D: Reaction Profiles, Trends, Surface Diagrams from Reactions Monitored via ATR-IR

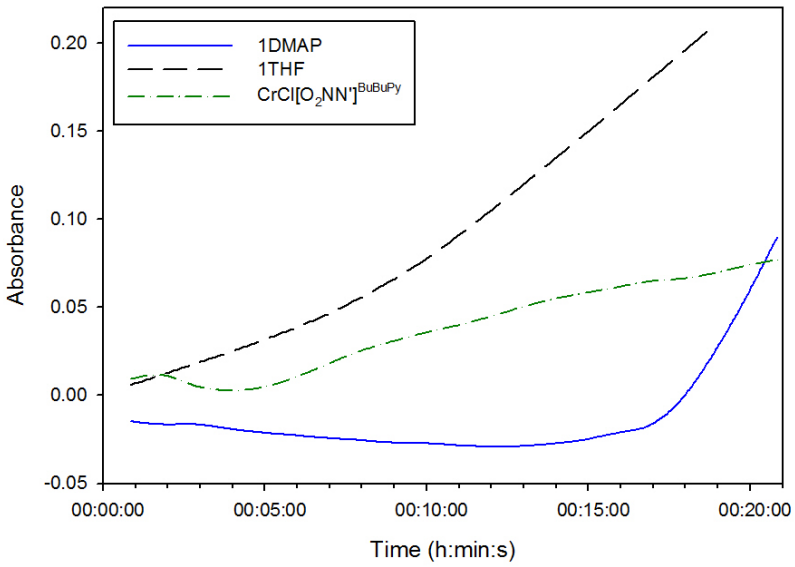

Figure D.1 The first 20 min of the reaction profile of the growth of the polycarbonate $\nu_{(C=O)}$ catalyzed by **2.1**·THF, **2.1**·DMAP and CrCl[O_2NN']^{BuBuPy} (**1.21** in Figure 1.7, Chapter 1). Reaction conditions: 40 bar CO_2, 60 °C, 24 h, [Cr]:[CHO]:[DMAP] = 1:500:1.

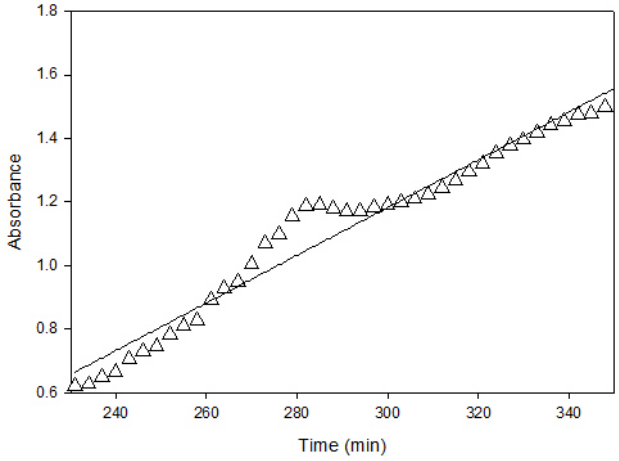

Figure D.2 The second stage of the propagation of the reaction catalyzed by **1.21** (Figure 1.7, Chapter 1). r_{obs} = 0.75 ± 0.024 x 10^{-2} min^{-1} (or 1.2 ± 0.04 x 10^{-4} s^{-1}).

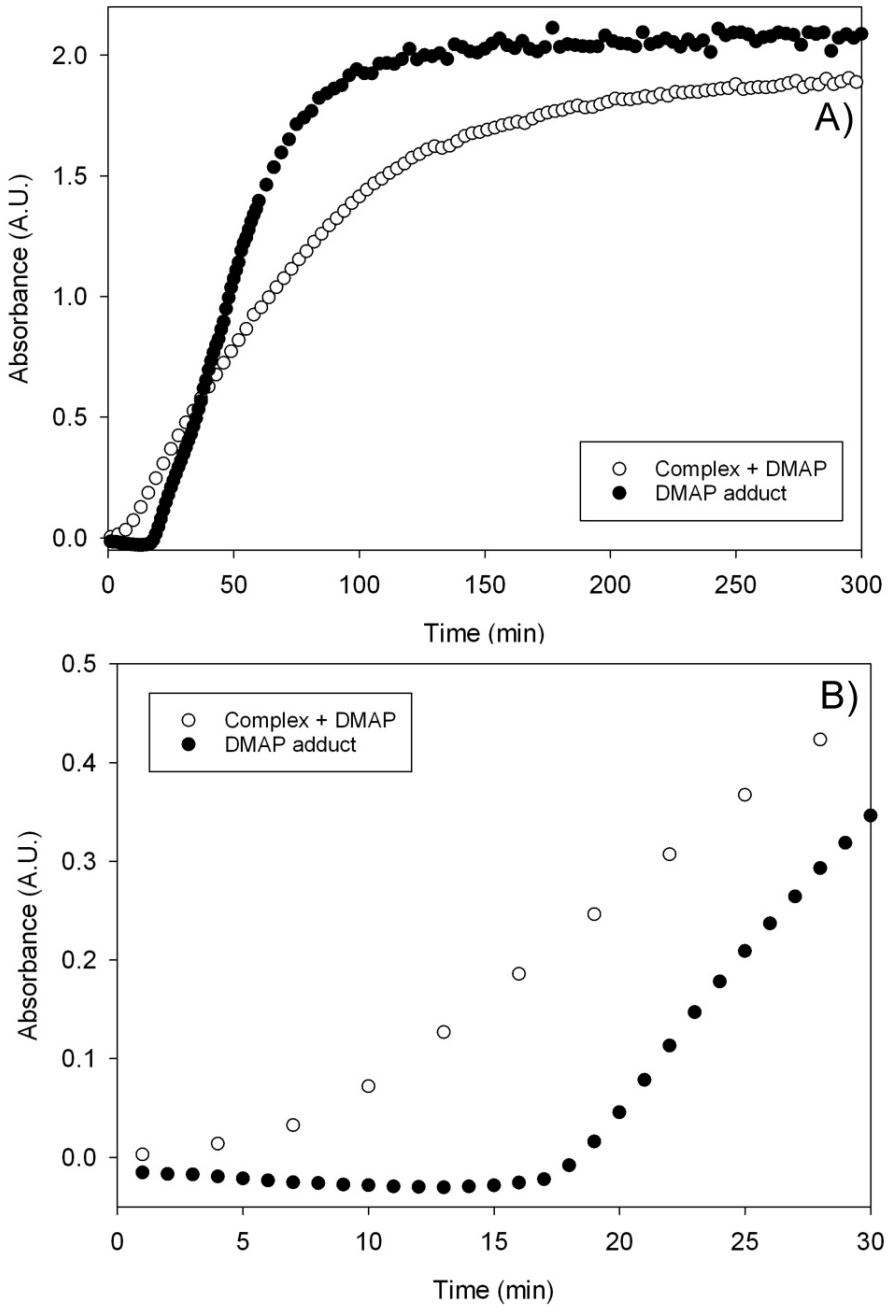

Figure D.3 A) First 5 h B) first 30 min of the reaction profiles showing the growth of the absorbance of the polycarbonate carbonyl C=O band at 1750 cm^{-1} catalyzed by **2.1**·DMAP (●) and **2.1**·THF + 1 equiv. DMAP (○). Reaction conditions: 40 bar CO_2, 60 °C, [Cr]:[CHO]:[DMAP] = 1:500:1.

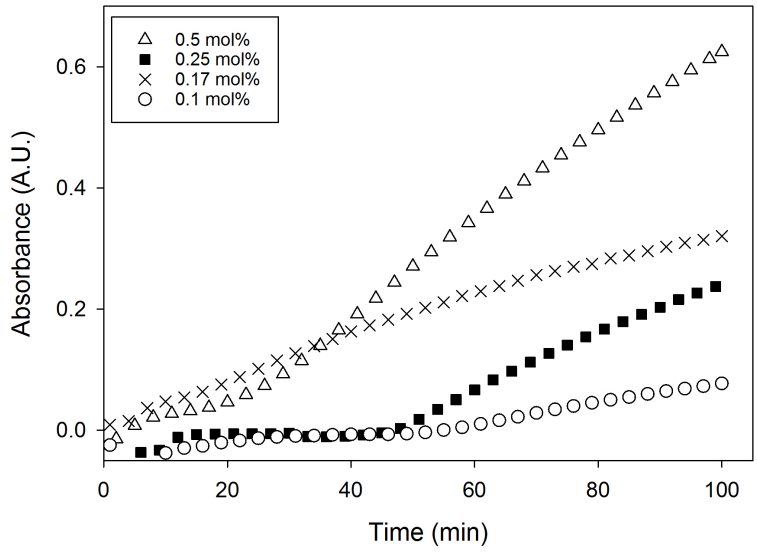

Figure D.4 First 100 min of the reaction profiles showing the growth of the absorbance of the polycarbonate carbonyl C=O band at 1750 cm^{-1} catalyzed by **2.1**·DMAP with different [cat]: 0.5 mol% (△), 0.25 mol% (■), 0.17 mol% (×), 0.1 mol% (○). (Reaction conditions: 40 bar CO_2, 60 °C, 24 h).

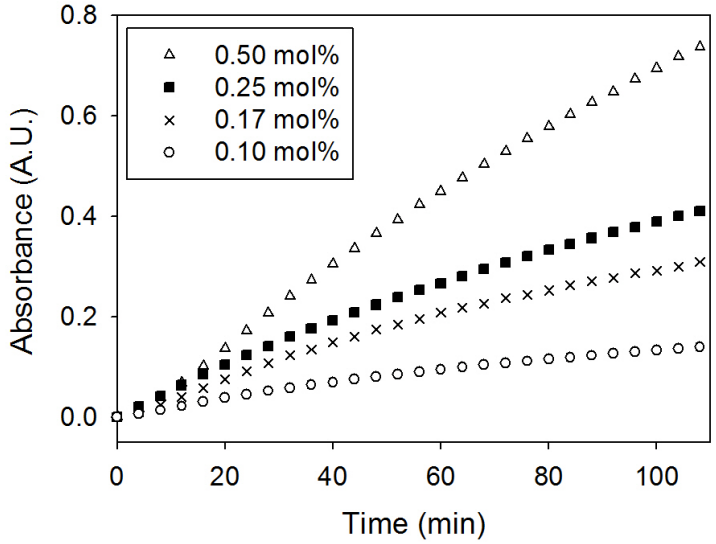

Figure D.5 Normalized absorbance vs time plots of Figure D.4, following the initiation periods for each catalyst loading study. Reaction conditions: 40 bar CO_2, 60 °C, 24 h. [cat]: 0.50 mol% (△), 0.25 mol% (■), 0.17 mol% (×), 0.10 mol% (○).

APPENDIX E: UV-Visible Spectra

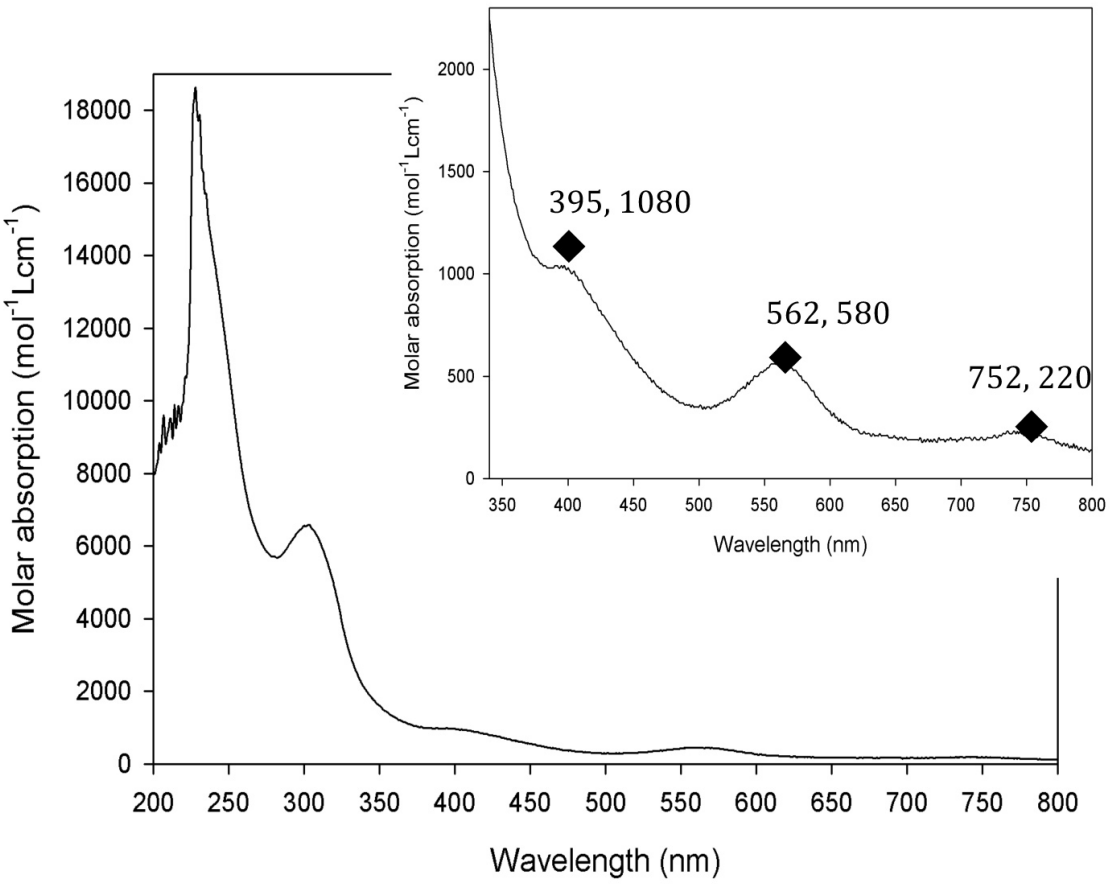

Figure E.1 UV-Vis absorption spectrum of **2.1**·THF. Expansion of the visible region shows peak wavelengths and molar extinction coefficients.

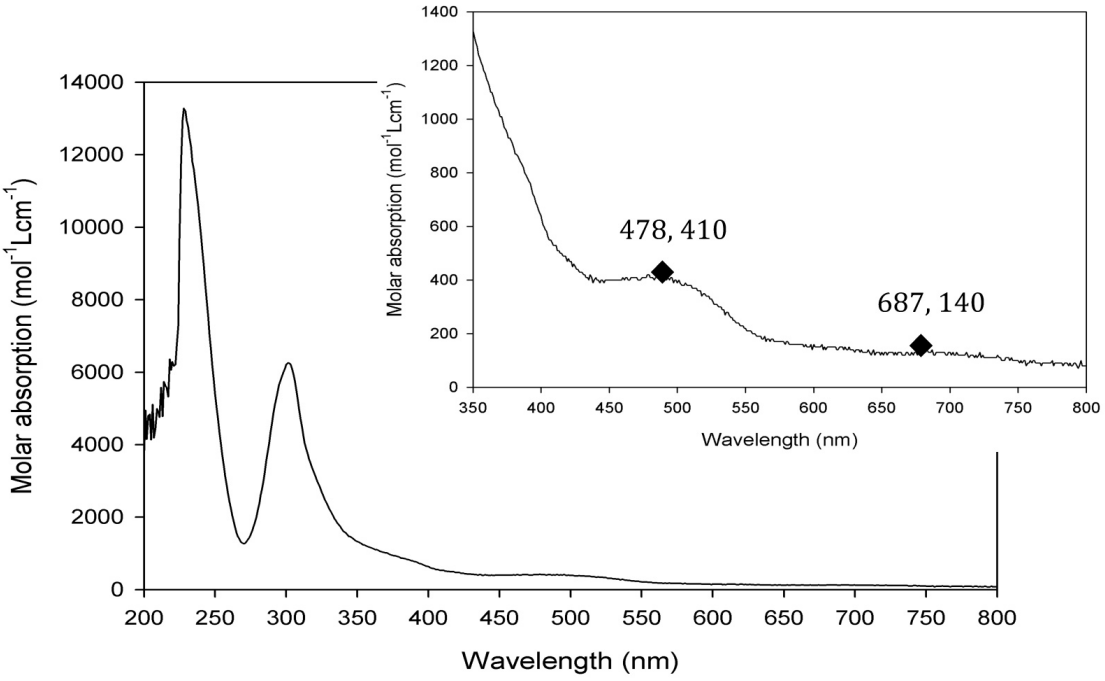

Figure E.2 UV-Vis absorption spectrum of **2.2**·THF. Expansion of the visible region shows peak wavelengths and molar extinction coefficients.

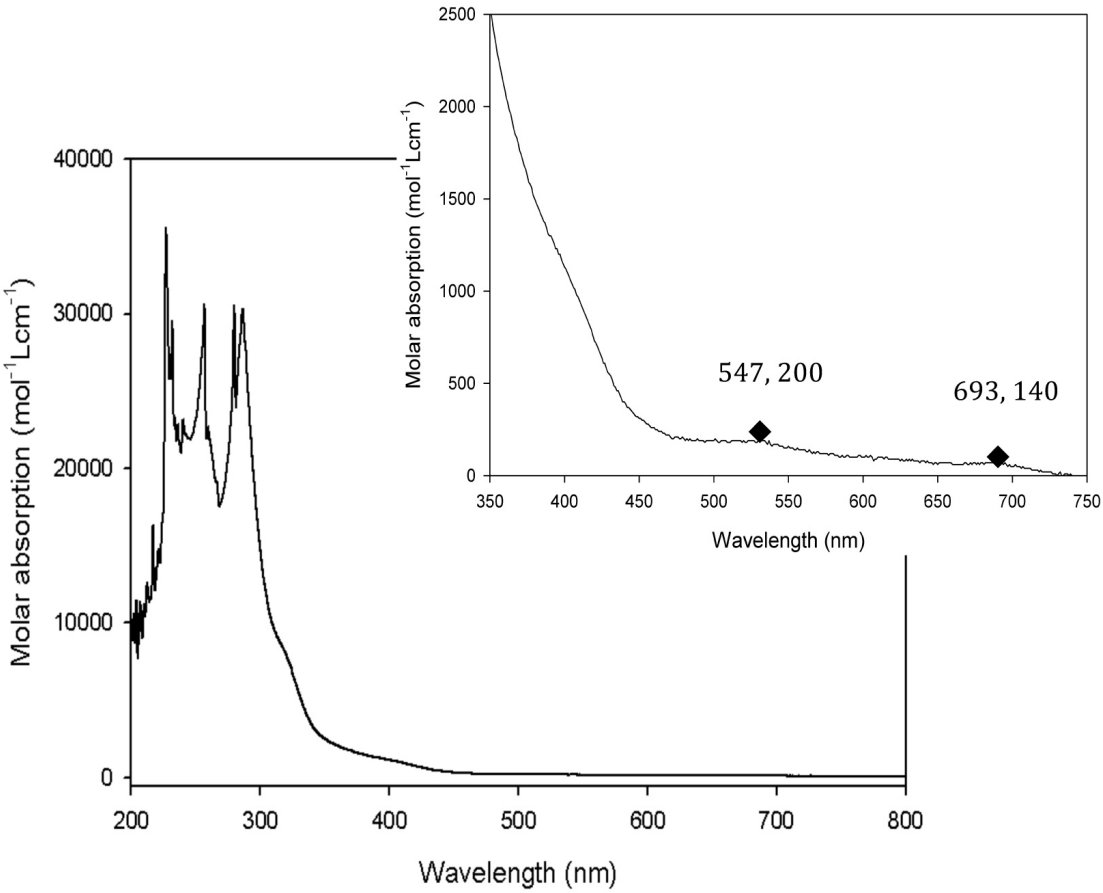

Figure E.3 UV-Vis absorption spectrum of **2.1**·DMAP. Expansion of the visible region shows peak wavelengths and molar extinction coefficients.

APPENDIX F: Infrared Spectra

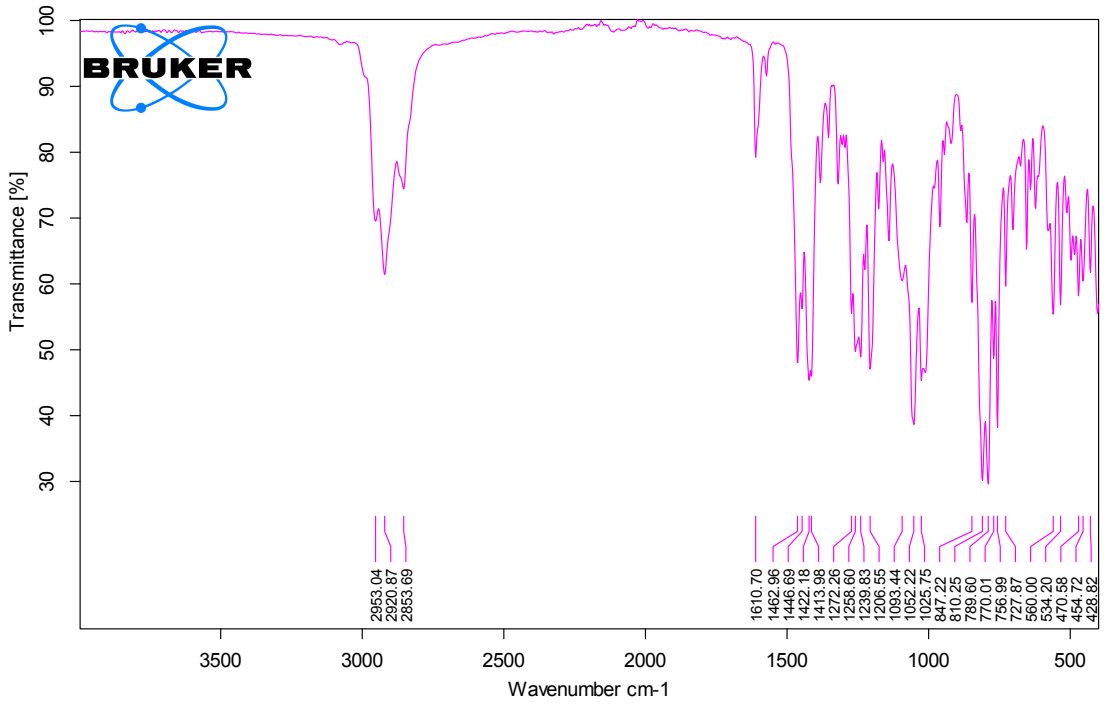

Figure F.1 IR spectrum of **2.1**·THF.

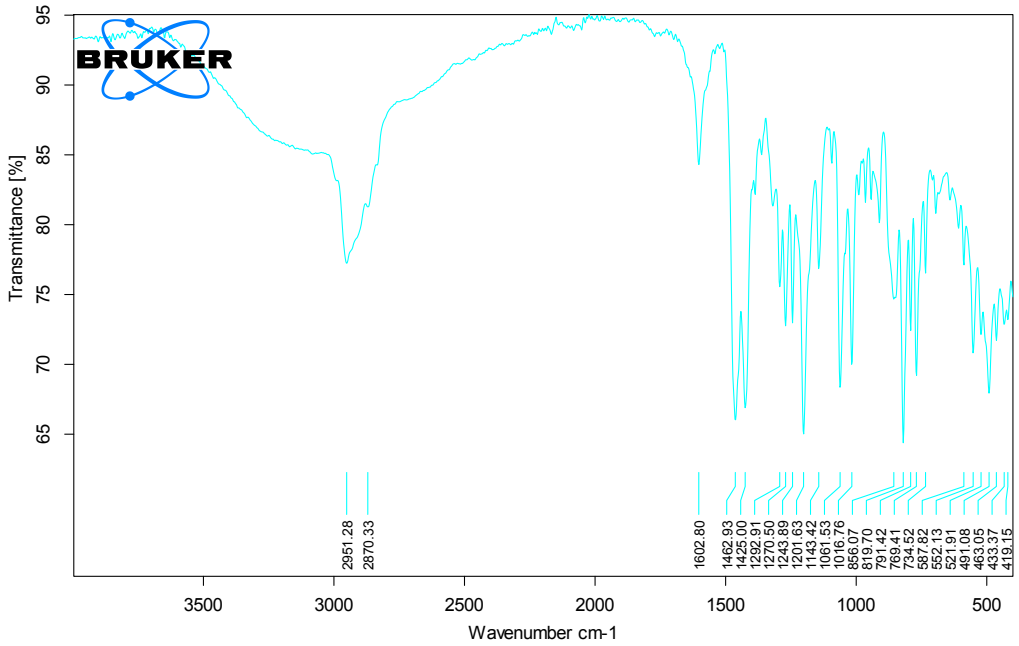

Figure F.2 IR spectrum of **2.2**·THF.

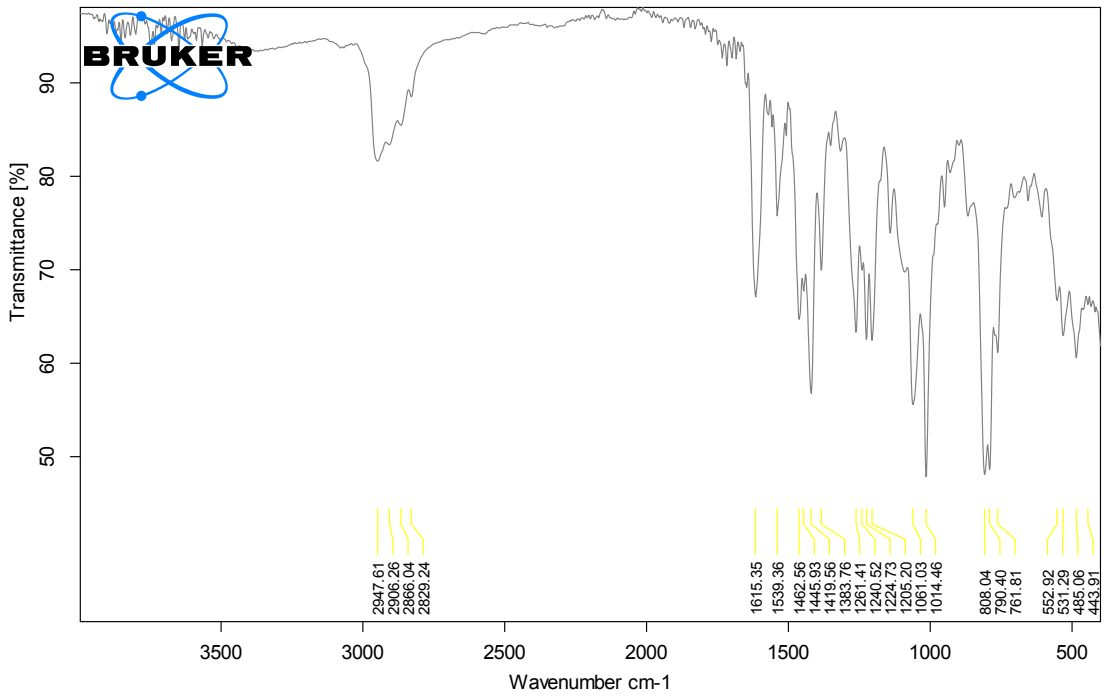

Figure F.3 IR spectrum of **2.1**·DMAP.

APPENDIX G: Polymerization Plots and Photos

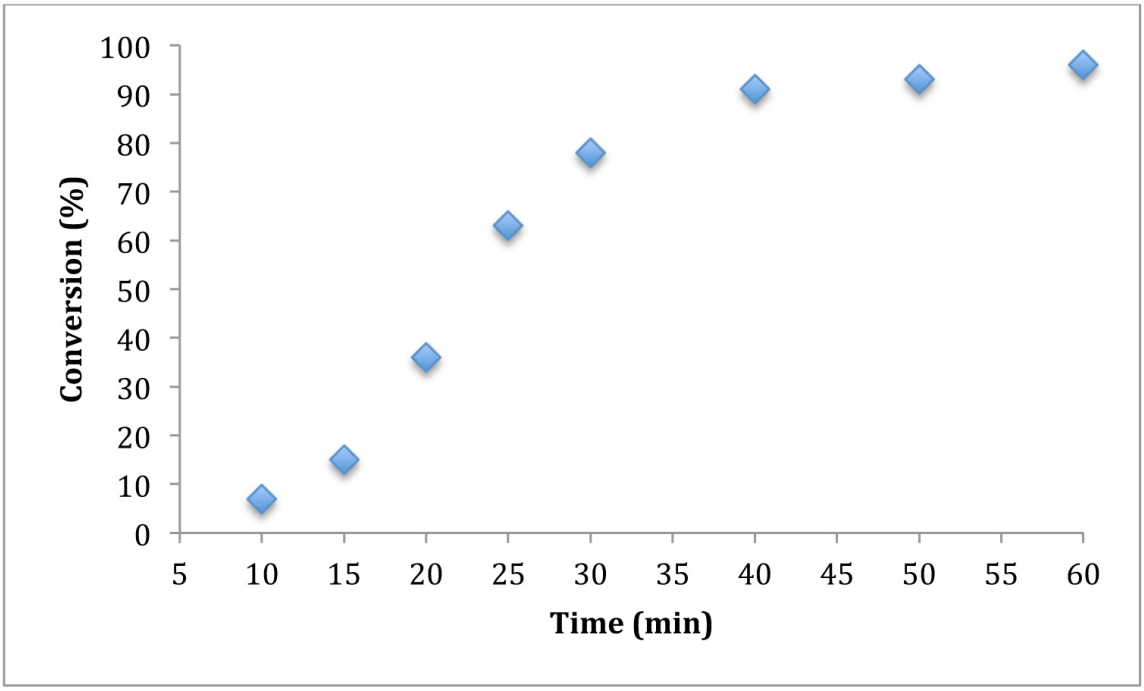

Figure G.1 Conversion (%) vs. time for the ROP of *rac*-LA initiated by **4.1** under the conditions described in Table 4-1, entry 3.

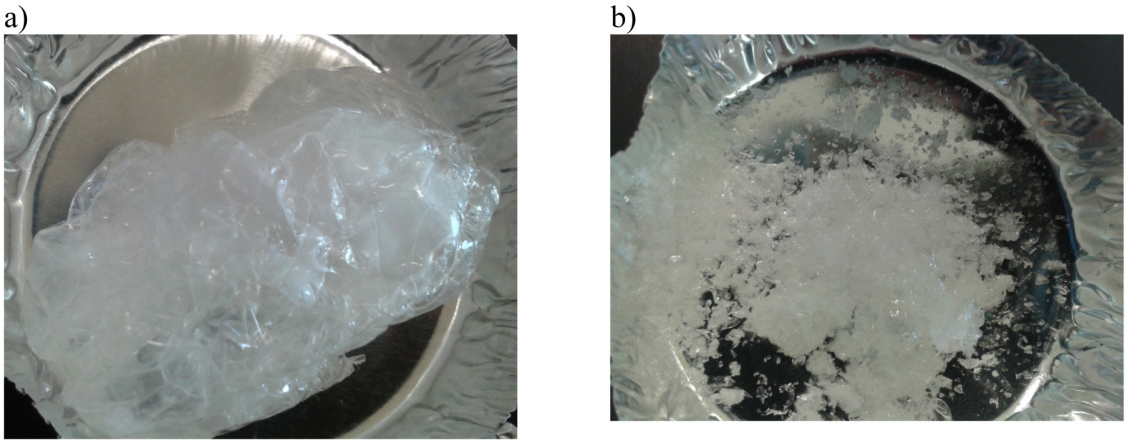

Figure G.2 Physical appearance of polylactide obtained (a) without BnOH, Table **4.1**, entry 3 and (b) with BnOH, Table 4-1, entry 4.

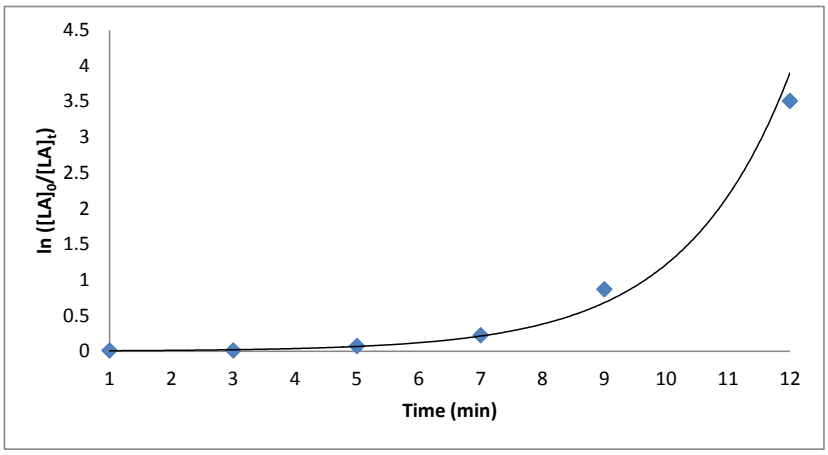

Figure G.3 Plot of $\ln[LA]_0/[LA]_t$ vs. time, $[LA]_0/[Mg]_0 = 100$, in toluene at 90 °C according to the conditions in Table 4-3, entry 1.

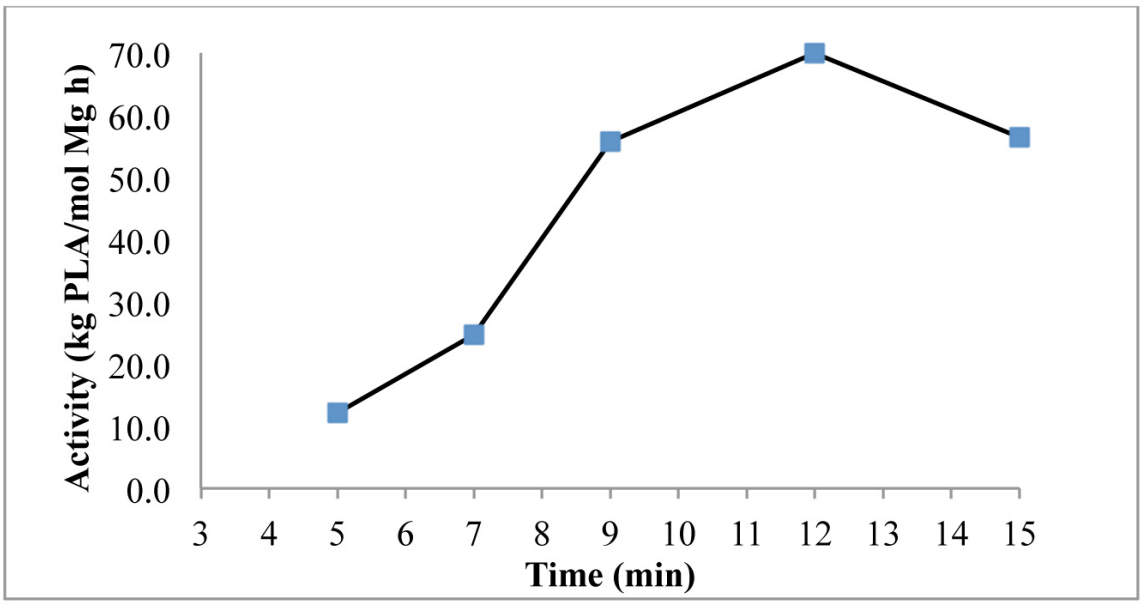

Figure G.4 Activity vs. *t* plot for *rac*-lactide ROP according to the conditions described in Table 4-3, entry 1.

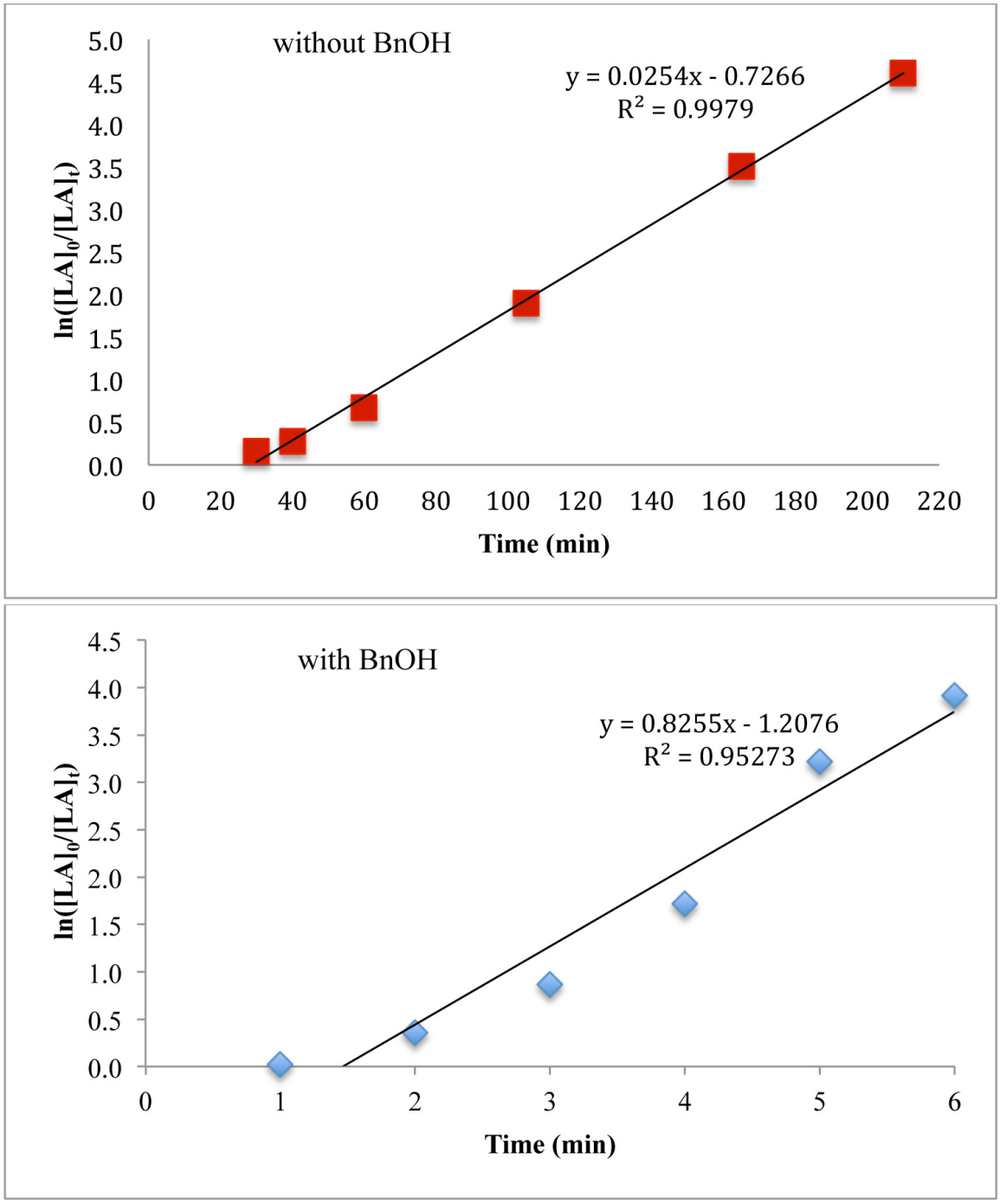

Figure G.5 Plot of $\ln[LA]_0/[LA]_t$ vs. time, $[LA]_0/[Mg]_0$ = 100, in toluene at 90 °C according to the conditions in Table 4-3, entries 3 (top) and 4 (bottom).

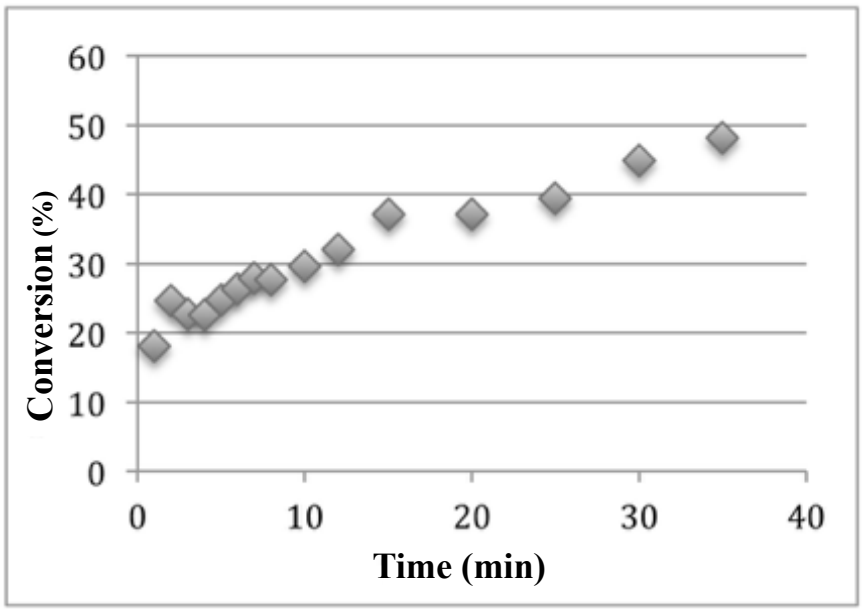

Figure G.6 Ring-opening polymerization of L-lactide with **5.4** at 125° C; [LA]:[Li]:[BnOH] = 100:1:0.

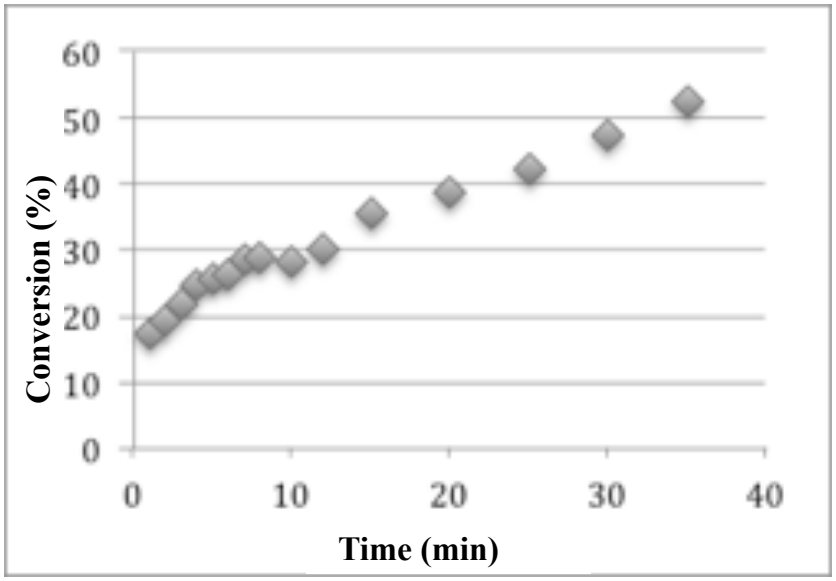

Figure G.7 Ring-opening polymerization L-lactide with **5.4** at 125° C; [LA]:[Li]:[BnOH] = 100:1:1.

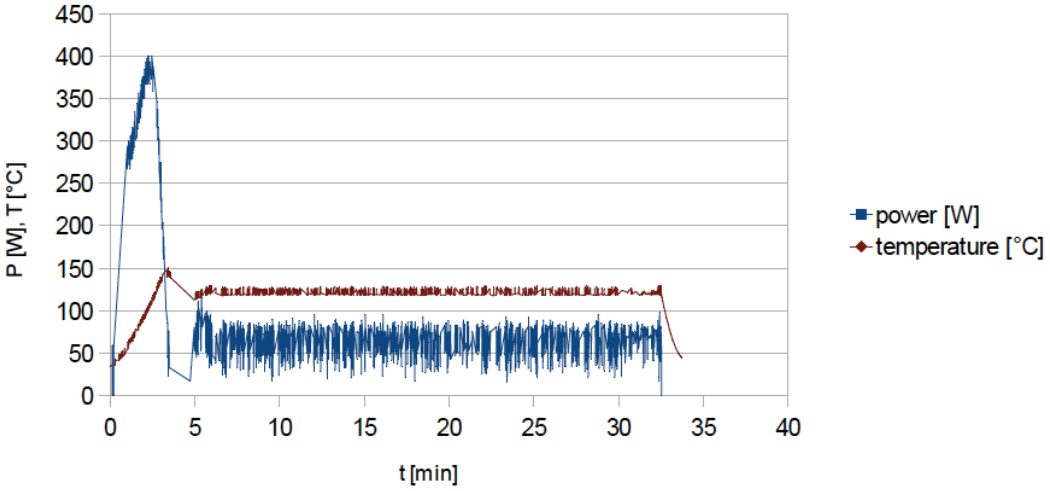

Figure G.8 Power vs. temperature graph during microwave assisted reactions (Chapter 5, Section 5.2.3).

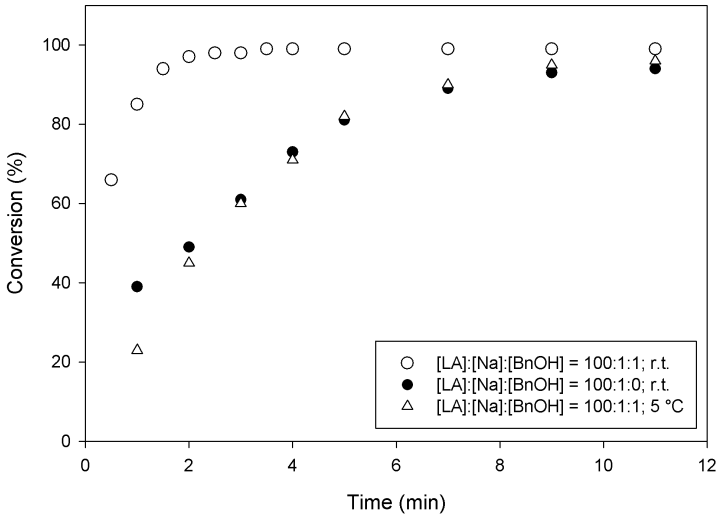

Figure G.9 Conversion vs. time plot of ROP of *rac*-lactide in toluene. Conditions: [LA]:[**5.4**]:[BnOH] = 100:1:1, 25 °C and 5 °C, and 100:1:0 at 25 °C.

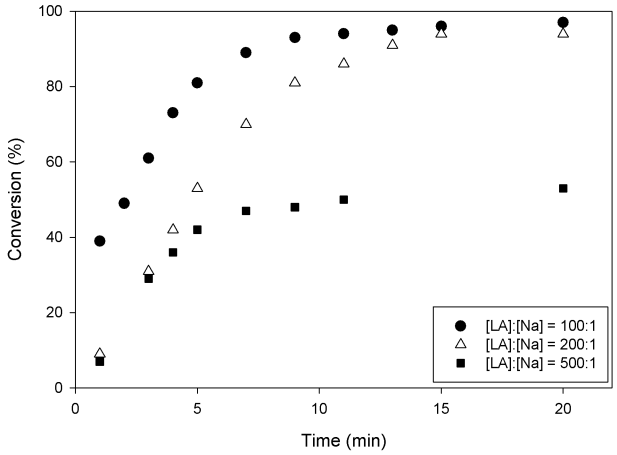

Figure G.10 Conversion vs. time plot, polymerization was carried out with complex **5.4** at different [LA]:[Na] ratios without BnOH at 25 °C in toluene.

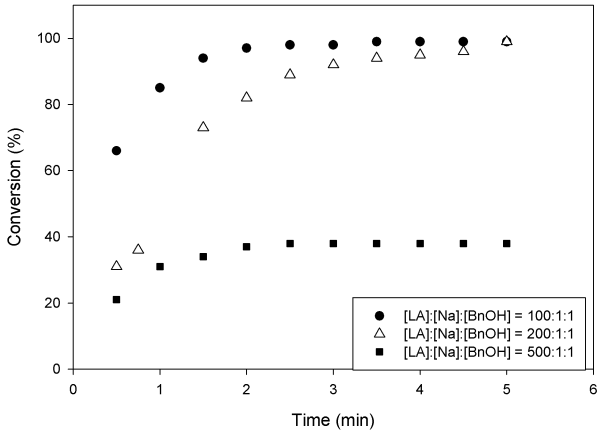

Figure G.11 Conversion vs. time plot, polymerization was carried out with complex **5.4** at different [LA]:[Na] ratios with BnOH at r.t. in toluene.

APPENDIX H: DSC and TGA Diagrams of Polymers

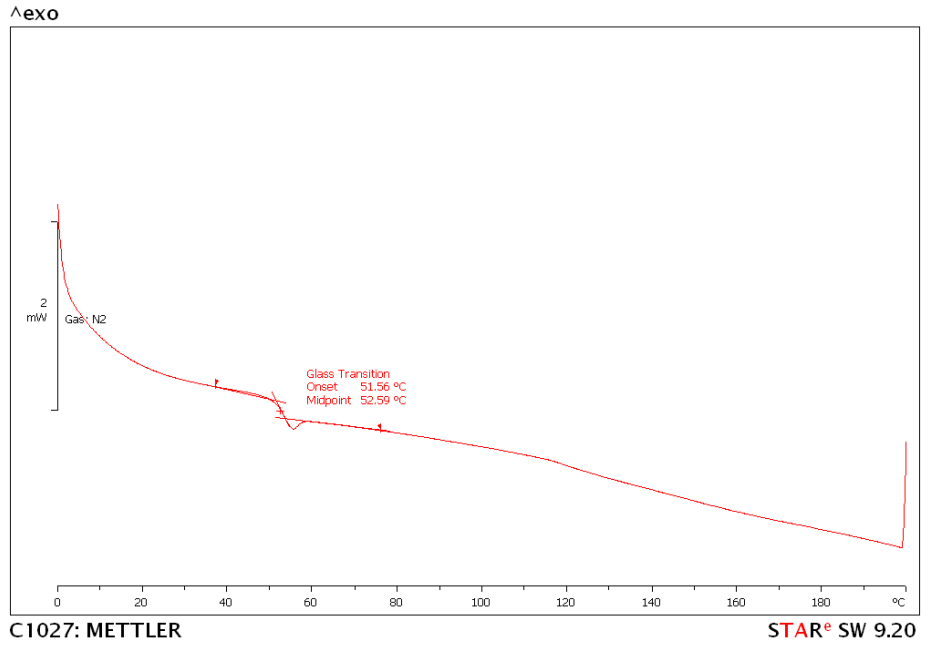

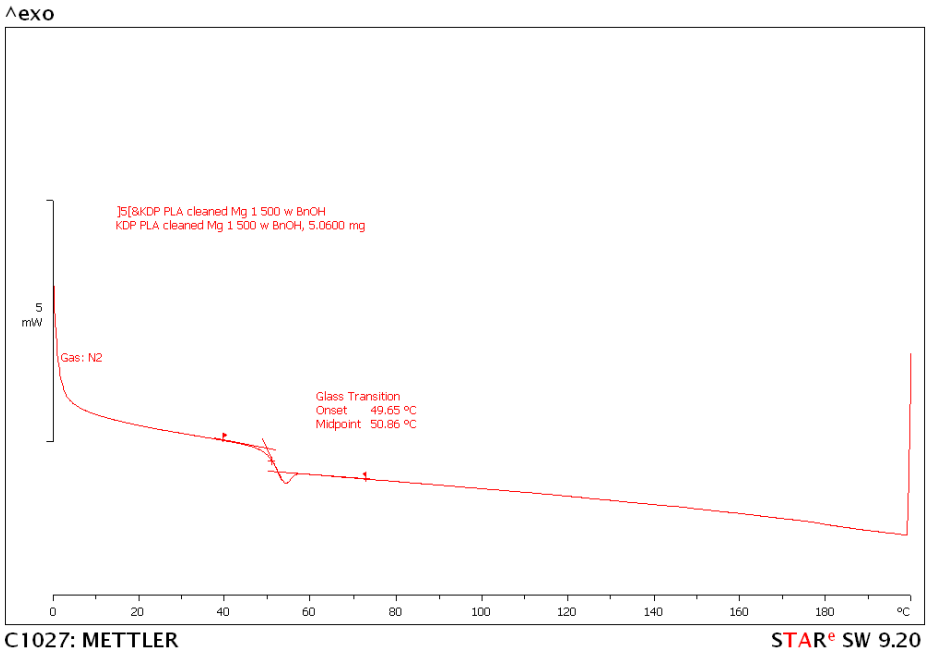

Figure H.1 Top: DSC third heating curve of the polymer obtained using the conditions of Table 4-1, entry 3 (without BnOH). Bottom: DSC third heating curve of the polymer obtained using the conditions of Table 4-1, entry 4 (with BnOH).

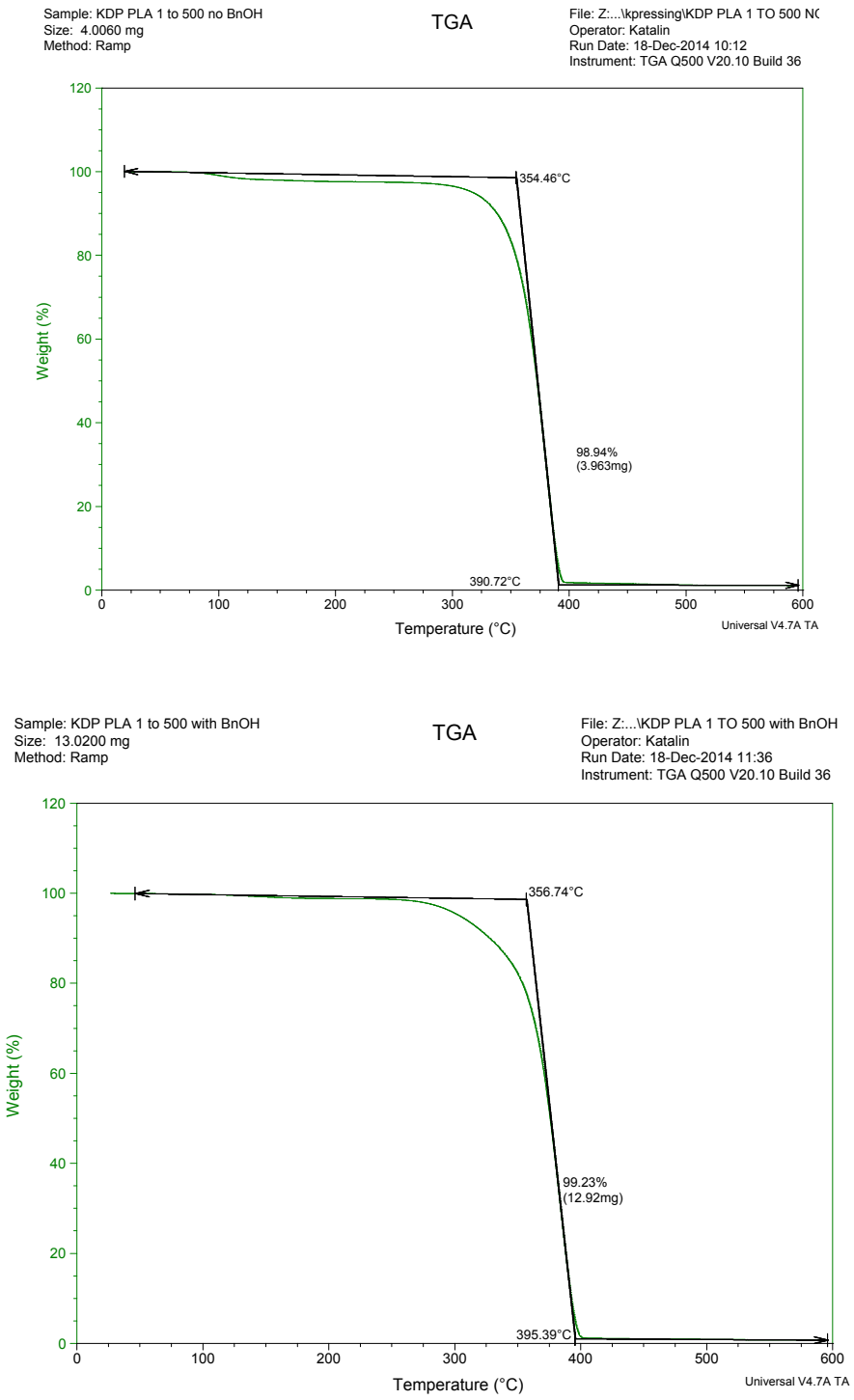

Figure H.2 TGA curves of polymers obtained, Top: without BnOH using the conditions of Table 4-1, entry 3. Bottom: With BnOH using the conditions of Table 4-1, entry 4. Scan rate of 10 °C/min.

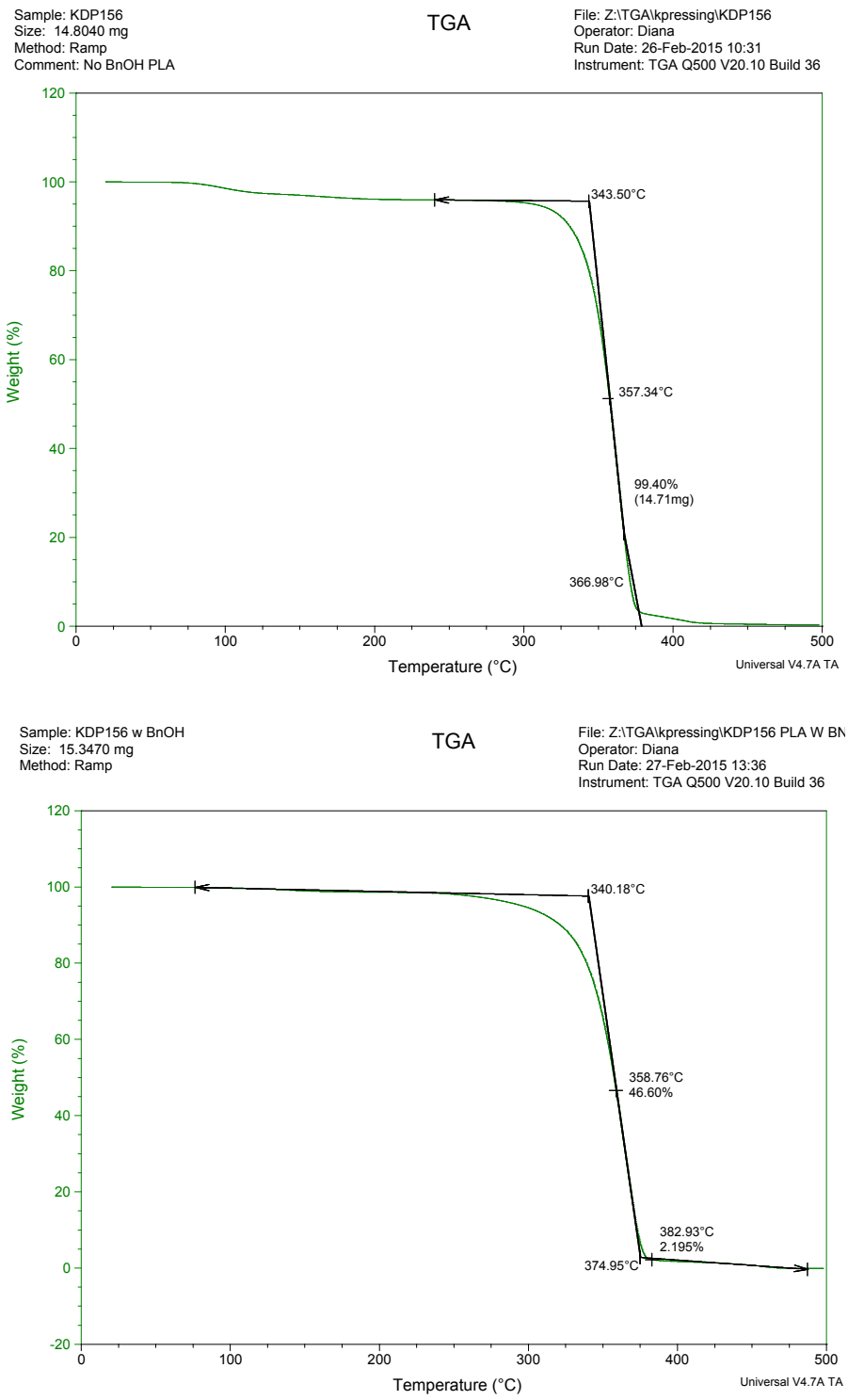

Figure H.3 TGA curves of polymers obtained, Top: without BnOH using the conditions of Table 4-1, entry 3. Bottom: With BnOH using the conditions of Table 4-1, entry 4.